

THERMAL CONTACT RESISTANCE  
IN A NON-IDEAL JOINT

Richard T. Roca  
Borivoje B. Mikic

Report No. DSR 71821-77

George C. Marshall Space Flight Center  
National Aeronautics and Space  
Administration  
Contract No. NAS 8-24867

Engineering Projects Laboratory  
Department of Mechanical Engineering  
Massachusetts Institute of Technology  
Cambridge, Massachusetts 02139

November 1971



N72-14946 (NASA-CF-12168) THERMAL CONTACT RESISTANCE  
IN A NON-IDEAL JOINT R.T. Roca, et al  
(Massachusetts Inst. of Tech.) Nov. 1971  
233 p CSCL 20M

Unclas  
11972

G3/33

FACIL (NASA CR OR TMX OR AD NUMBER)

(CATEGORY)

TECHNICAL REPORT NO. 71821-77

THERMAL CONTACT RESISTANCE

IN A NON-IDEAL JOINT

by

Richard T. Roca  
Borivoje B. Mikic

Sponsored by

George C. Marshall Space Flight Center  
National Aeronautics and Space Administration  
Contract No. NAS8-24867

November 1971

Department of Mechanical Engineering  
Massachusetts Institute of Technology  
Cambridge, Massachusetts 02139

## Thermal Contact Resistance in a Non-Ideal Joint

by Richard T. Roca

and Borivoje B. Mikic

### ABSTRACT

The contact conductance at an interface can be determined by knowing the material and surface properties and the interfacial pressure distribution. This pressure distribution can be influenced strongly by the roughness of the mating surfaces but until now this effect has been ignored in studies of joint conductance. This thesis considers this effect and shows the circumstances when it is an important factor. Furthermore, it is shown that one can either raise or lower the total resistance of a joint by changing the surface properties in the proper manner for the particular system being considered.

Specifically, this thesis deals with three systems: the contact of two rough, wavy surfaces; the contact of two rough but nominally flat plates pressed together over a concentrated area; and the contact of two rough but nominally flat plates bolted together. In each case the pressure distribution is calculated as a function of the surface properties. In the case of wavy surfaces it is found that all necessary information for any combination of parameters can be reduced to one master graph. In the other two cases one such graph is needed for each

geometry used. The resulting pressure distributions are used in a specific heat transfer example and the total joint resistance versus roughness is presented. It is shown how one can actually decrease the resistance by increasing the roughness - a seemingly contradictory phenomenon.

Heat transfer experiments performed by Joseph Pigott qualitatively confirmed the theoretical findings.

ACKNOWLEDGMENT

This project was sponsored by the National Aeronautics and Space Administration.

The heat transfer experiments included in this report were conducted by Joseph Pigott as part of his S.M. thesis.

We would like to thank Dr. Brandon Rightmire and Dr. Thomas Lardner for their suggestions and comments during the course of the research and in the preparation of the report. Mention must also be made of the various helpful conversations with colleagues at the Institute and the help of the various service organizations at M.I.T. The conversations held with Dr. L. S. Fletcher of Rutgers University concerning the literature already available were most helpful and are acknowledged.

<u>TABLE OF CONTENTS</u>	<u>PAGE NO.</u>
ABSTRACT	2
NOMENCLATURE	6
1. INTRODUCTION	10
1.1 Phenomena Description and Previous Work	10
1.2 Statement of Problem	14
1.3 Deformation of Asperities	22
1.4 Deformation of Spherical Surfaces	31
1.5 Deformation of Solid Disks	35
1.6 Deformation of Disks with Center Hole	36
2. MECHANICS	43
2.1 Contact of Two Wavy Surfaces	43
2.1.1 Model	43
2.1.2 Solution	47
2.1.3 Results	49
2.1.4 Discussion and Summary	57
2.2 Contact of Two Plates without Holes	64
2.2.1 Model	64
2.2.2 Midplane Stress	69
2.2.3 Solution	78
2.2.4 Results	79
2.2.5 Summary	92
2.3 Contact of Two Plates with Center Holes	93
2.3.1 Model	93
2.3.2 Midplane Stress	95

	<u>PAGE NO</u>
2.3.3 Solution	106
2.3.4 Results	107
2.3.5 Summary	118
2.4 Experimental Observations	120
3. HEAT TRANSFER EXAMPLE AND EXPERIMENTS	136
4. SUMMARY AND CONCLUSIONS	145
5. BIBLIOGRAPHY	149
6. APPENDIX	157
6.1 Deformation of Disks with and without Center Holes	157
6.1.1 Disk - No Hole - Midplane Stress	159
6.1.2 Disk - No Hole - Midplane Stress - Approximate Solution	170
6.1.3 Disk - No Hole - Variable Load	173
6.1.4 Disk - No Hole - Variable Load - Approximate Solution	178
6.1.5 Disk - Hole - Midplane Stress	179
6.1.6 Disk - Hole - Midplane Stress - Approximate Solution	183
6.1.7 Disk - Hole - Variable Load - Approximate Solution	184
6.1.8 Semi-Infinite Body - Finite Radius	187
6.2 Relationships for Hyperbolic and Cylindrical Functions	190
6.3 Truncation of Infinite Series	193
6.4 Computer Programs	201
6.4.1 Disk with No Hole	201
6.4.2 Disk with Hole	213
6.4.3 Auxiliary Programs	221
VITA	232

NOMENCLATURE

a	Radius of disk
$\bar{a}$	a/b
$a_h$	Radius of contact in Hertzian case
$A_a$	Apparent contact area
$A_c$	Actual contact area
b	Thickness of disk
c	Radius of hole in disk
$\bar{c}$	c/b
$E_1$	Young's Modulus of body 1
$\bar{E}$	$\left[ \frac{1-\nu_1^2}{\pi E_1} + \frac{1-\nu_2^2}{\pi E_2} \right]^{-1}$
E( )	Expected value
F	Load
$h_c$	Thermal contact conductance
H	Vicker's hardness
$\bar{H}$	H/p <sub>0</sub>
H*	$\bar{E} \tan \theta / \pi 2\sqrt{2}$
$I_{0,1}$	Modified Bessel function of the first kind of order zero, one
$J_{0,1}$	Bessel function of the first kind of order zero, one
$k_1$	Thermal conductivity of body 1
k	$2k_1 k_2 / (k_1 + k_2)$

$K_{0,1}$	Modified Bessel function of the second kind of order zero, one
$n$	Number of contact points per unit area
$N$	Number of terms used in infinite series
$p$	Pressure
$p_0$	For spherical surfaces - average Hertzian stress for disks - average load stress
$\bar{p}$	$p/p_0$
$q/A$	Heat flux
$r$	Radial coordinate
$\bar{r}$	$r/b$ for disk; $r/a_h$ for spheres
$r_c$	Radius of contact at interface
$\bar{r}_c$	$r_c/b$ for disks; $r_c/a_h$ for spheres
$r_o$	Radius of applied load
$\bar{r}_o$	$r_o/b$ for disks; $r_o/a_h$ for spheres
$R_1$	Radius of curvature for body 1
$\bar{R}$	$R_1 R_2 / (R_1 + R_2)$
$R_c$	Contact resistance
$t_n$	Truncation factor
$\tan \theta$	Mean of absolute slope of profile
$T$	Temperature
$w$	Deflection of surface with respect to coordinate origin

$\bar{w}$	$wE/bp_0$
$y$	Distance from mean surface of body
$y_0$	Distance between mean surfaces of two bodies in contact
$\bar{y}_0$	$y\bar{E}/a_n p_0$ for spheres; $yE/bp_0$ for disks
$Y_{0,1}$	Bessel function of the second kind of order zero, one
$z$	Axial coordinate
$\theta_n$	Zero of $J_1(\theta_n) = 0$
$\nu$	Poisson's ratio
$\sigma_1$	rms roughness of surface on body 1
$\sigma$	$\sqrt{\sigma_1^2 + \sigma_2^2}$
$\bar{\sigma}$	$\sigma\bar{E}/a_n p_0$ for spheres; $\sigma E/bp_0$ for disks
$\sigma_r$	Radial normal stress
$\sigma_z$	Axial normal stress
$\sum_1$	Parametric representation for force-deflection relationships (see Appendix for particular values)
$\tau_{rz}$	Shear stress

## 1. INTRODUCTION

### 1.1 Phenomenon Description and Previous Work

The concept that there is a resistance to the flow of heat at the interface of two materials has been acknowledged for some time but it has only been within the last few decades with the advent of modern electronics and nuclear power that this resistance has had importance.

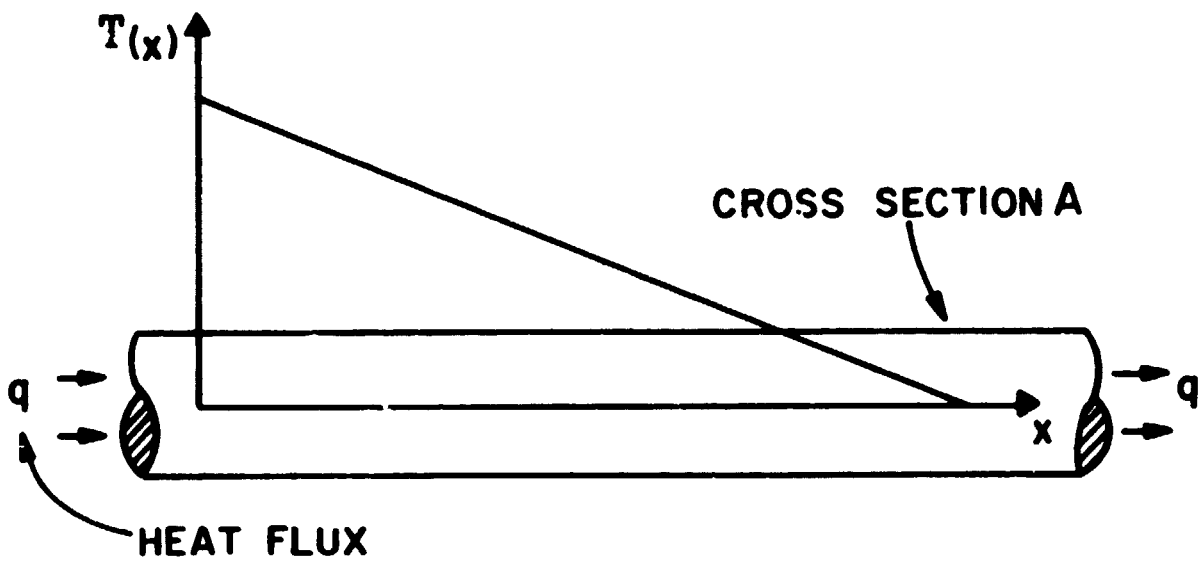
It has been observed that if a heat flux is passed through a body, a linear temperature change will occur as shown in Figure 1a. If, however, this body has an interface, the temperature change will not be linear in the neighborhood of the interface as shown in Figure 1b. The additional resistance to heat flow caused by the presence of the interface is the contact resistance. It is defined as

$$R_c = \frac{\Delta T}{q/A} \quad (1)$$

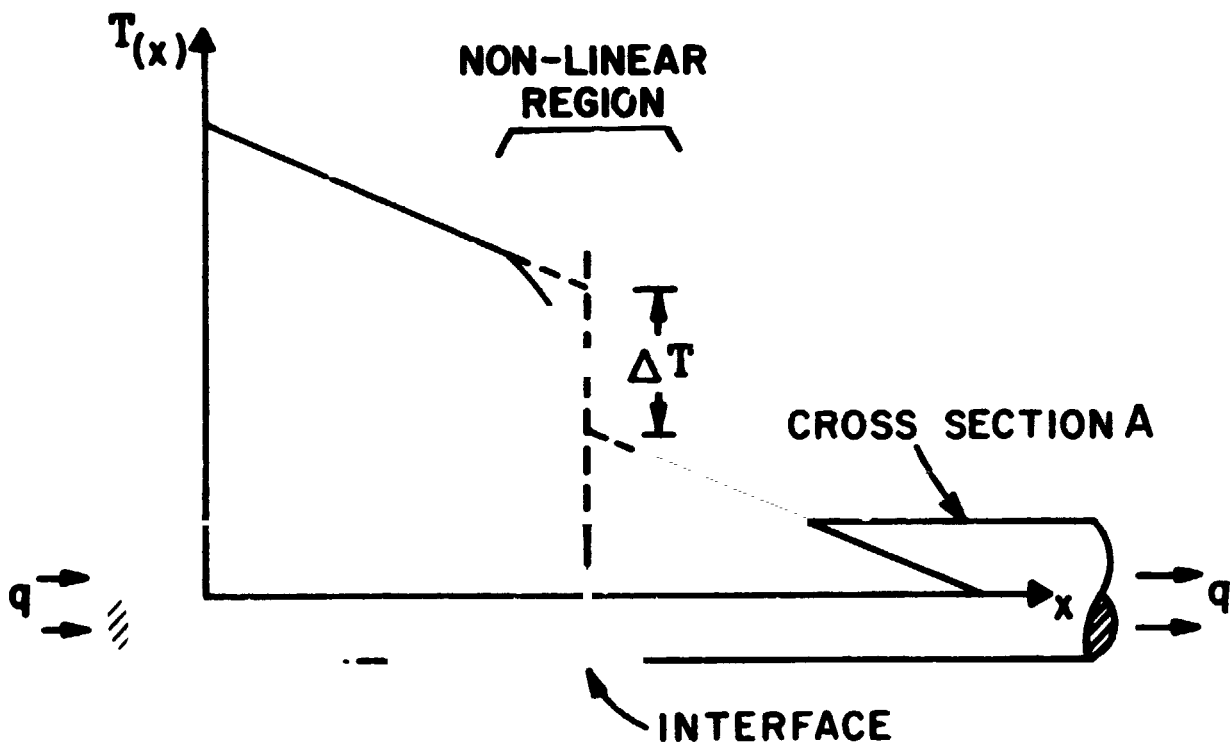
where  $\Delta T$  is the temperature difference at the interface between the extended linear profiles. The reciprocal of the resistance, the thermal contact conductance is, therefore,

$$h_c = \frac{1}{R_c} = \frac{q/A}{\Delta T} \quad (2)$$

The reason for this interfacial resistance has been attributed to various phenomena including quantum effects due



(a)-NO INTERFACE



(b) INTERFACE WITH RESISTANCE

FIG. 1

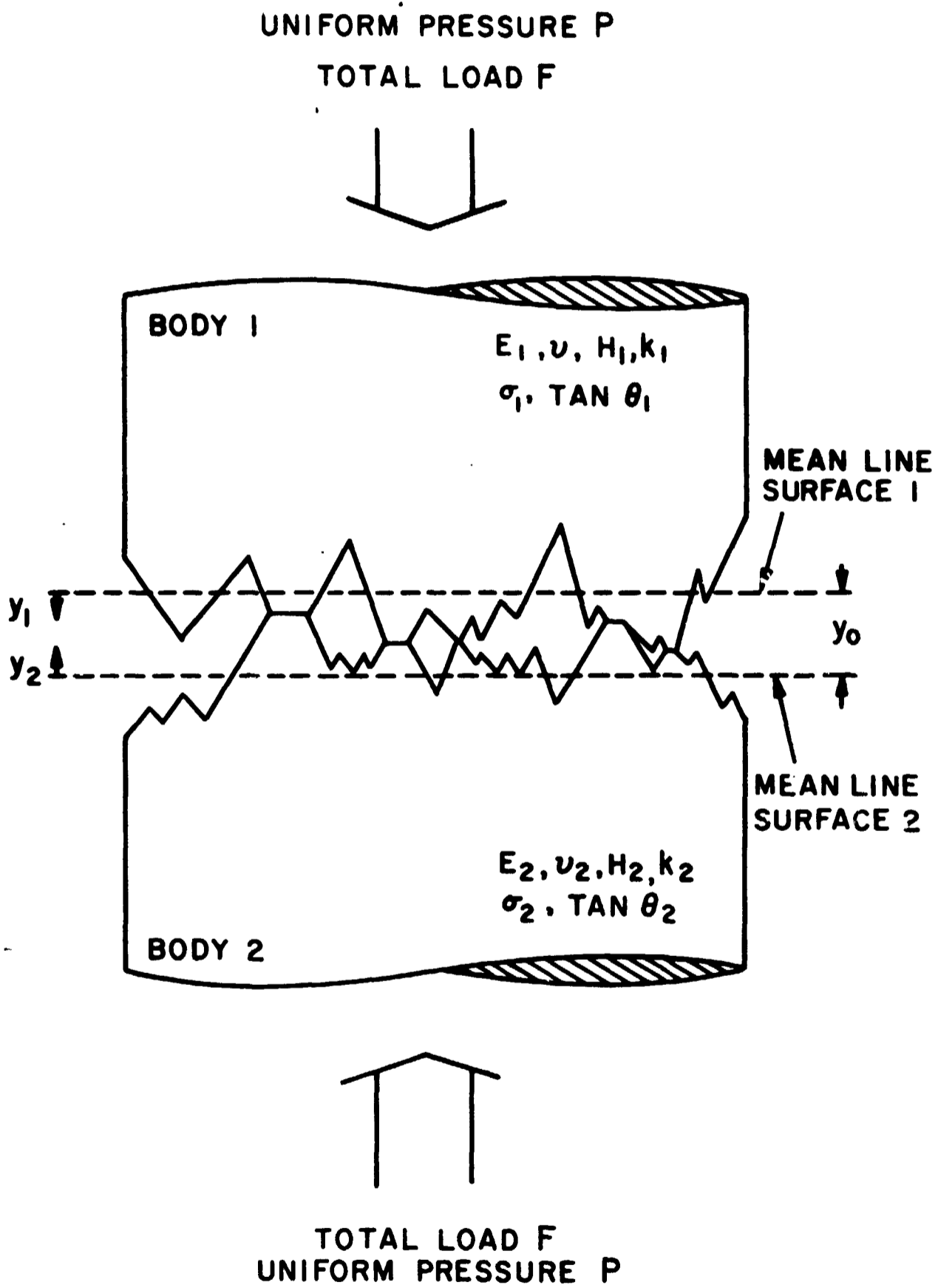
to mis alignment of the crystal lattices, [1-5]\*; surface films (oxide and other contaminants), [6]; and heat flow constriction. While the former two may apply in certain specific occasions, the predominant effect by far is the latter, the constriction resistance.

Because real surfaces are not smooth (in the microscopic sense) but are made up of asperities, two surfaces in contact will not touch over 100% of the apparent area in contact but only where the asperities touch. The actual area of contact may be of the order of 0.1% of the apparent area. Since heat will only flow through the actual area in contact, the constriction of heat flow and, hence, the added resistance will be present. The other parameter of prime importance influencing the contact resistance other than the roughness is the pressure which directly affects the actual to apparent area ratio.

There is extensive literature dealing with contact resistance, both experimental [7-30] and analytical [31-36]. All of the latter realize the importance of surface roughness but most use a rather cumbersome manual technique to predict the contact conductance. In [36], however, advantage is taken of the statistical nature of the problem and expected values for the conductance are arrived at. Based on the model shown in Figure 2 it is found that

---

\* Numbers in brackets denote references listed at the end.



MODEL USED IN [36]  
FIG.2

$$h_c = 1.45 \frac{k \tan(\theta)}{\sigma} \left( \frac{p}{H} \right)^{.985} \quad (3)$$

This was developed for contact in a vacuum (i.e., heat passing only through asperities in contact and not through the gaps), Gaussian distribution of surface heights above a mean plane, and contact between two nominally flat surfaces - uniform  $p$ . If the surfaces are not flat and contact pressure varies with a particular coordinate, say radius  $r$  in an axially-symmetric system, then  $h_c$  is modified to  $h_c(r)$ . Relationship (3) has been substantiated independently in [29].

Other phenomena connected with thermal contact conductance which have been investigated over the past years are: the directional effect [37-43]; the effect of previous loading [44]; the effect of plating [45]; the effect of interstitial materials [27,46,47]; specific surface geometries and materials [28,48-52]; specific systems such as bolted or riveted joints [53-60]; and nonuniform pressure distribution [61,62]. Additional references can be found in the bibliographies given in [27,28,48,51] and in [63-65].

It should be noted that it is impossible to develop a general relationship for the resistance of an interface,  $R_c$ , regardless of the system of which the interface is a part. Contact resistance is a constriction resistance and can only be described by distributed system parameters such as  $h_c$  as a function of surface location. To take

advantage of a succinct lumped parameter such as  $R_c$  is to limit its use only to the specific case for which it was developed. Therefore, while there is much experimental work available as mentioned before, much of it is applicable only to the specific case studied by the experimenter. The best that can be done is to investigate trends and give general relationships for the behavior at the interface, such as equation (3).

### 1.2 Statement of the Problem

In the contact of certain systems such as bolted or riveted plates, clamped disks, wavy plates, etc., there is contact in certain areas and narrow gaps between the surfaces in others. See, for example, Figure 3. Heat which is to flow from one body to another must first be constricted to the areas of large scale contact and then, once in these areas, must be constricted still further to the actual areas of contact at the roughness asperities.\* From (3) one sees that

$$h_c(r) \propto \frac{p(r)}{\sigma}$$

---

\* It is assumed that no heat is transferred across the gaps. In the case of radiation this is a warranted assumption at the temperatures usually considered. For conduction through a gas which might be in the gap this assumption is weak. However, if the assumption is made and the gas ignored - the case of a vacuum - the resulting relationship can be combined later with the parallel flow of heat through the gap for an overall result. See [29,36]. Since the gap is so narrow, convection is justifiably ignored.

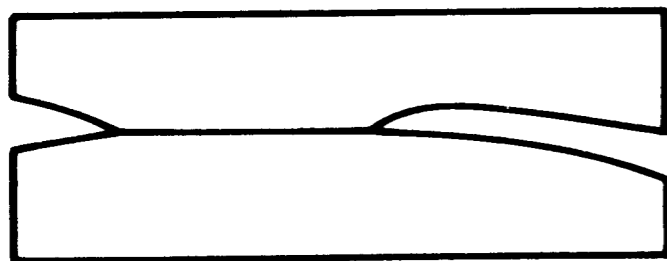


FIGURE 3a CONTACT OF BODIES WITH WAVY SURFACES

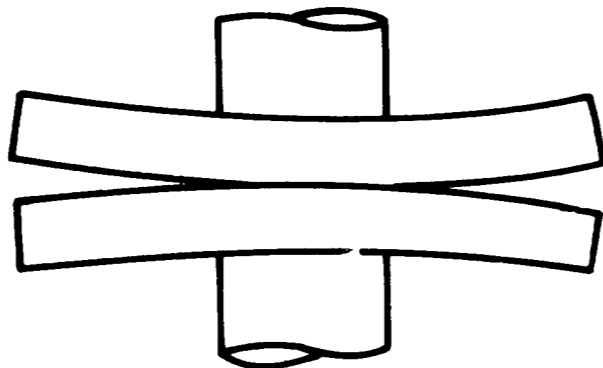


FIGURE 3b CONTACT OF TWO PLATES UNDER EXTERNAL LOAD

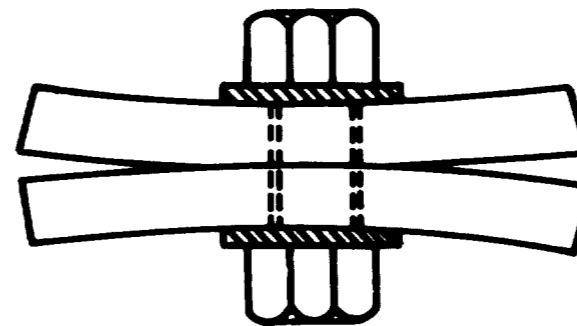


FIGURE 3c CONTACT OF BOLTED JOINT

where it is assumed that one is dealing with an axially-symmetric system and is allowing for radial variations in pressure. If  $p(r)$  were not affected by the roughness, then increasing the roughness would directly decrease the contact conductance. However, if one increases the roughness in a case where there is a narrow gap, the asperities may touch in this gap and  $p(r)$  will then be affected. See Figure 4. Since the tendency will be to enlarge the large-scale area of contact, that constriction will be lessened. However, since the roughness is being increased, the small-scale constriction, that due to the asperities, will increase. These two trends, both due to an increase in  $\sigma$ , run opposite to each other. It is the purpose of this thesis to investigate the combined effect.

There are three immediate reasons to do this: to explain previously unexplainable experimental observations where the resistance at an interface decreased when the roughness was increased, e.g. [48,66]; to determine if it is necessary, as it is now assumed, to go through the expensive process of smoothing a surface to a mirror finish in order to enhance the contact conductance; and to see if one can control more accurately the contact resistance of an overall system by varying the roughness.

The specific cases investigated here are those shown in Figure 3: two wavy surfaces, two externally clamped plates, and two bolted plates. The cases and models, all assumed to be axially-symmetric, are as follows:

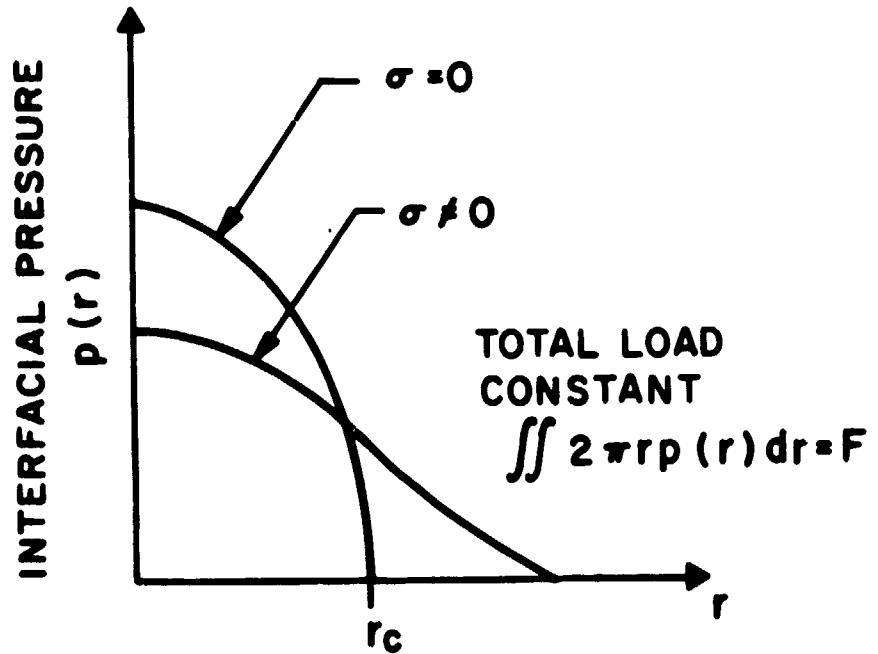
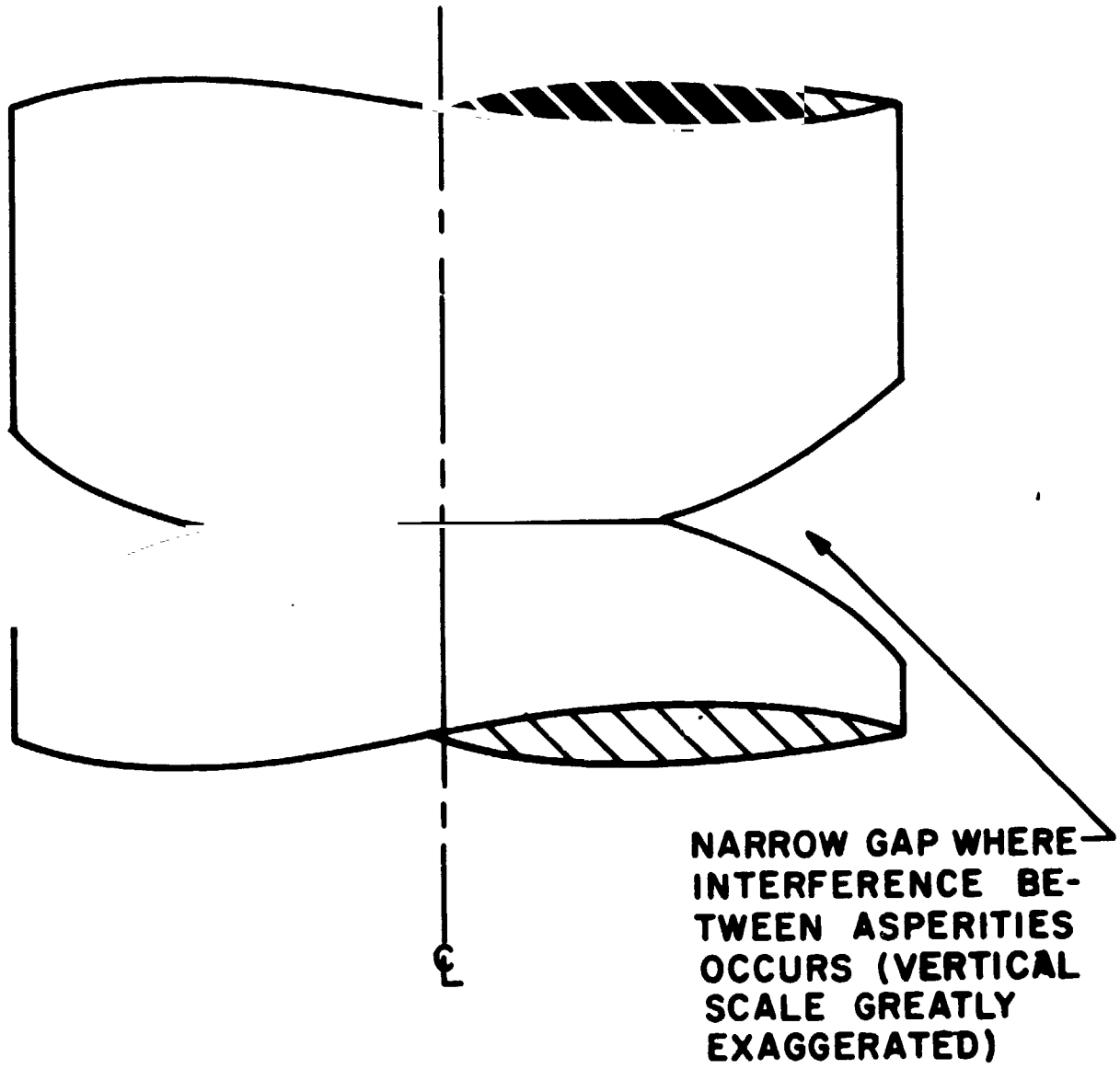
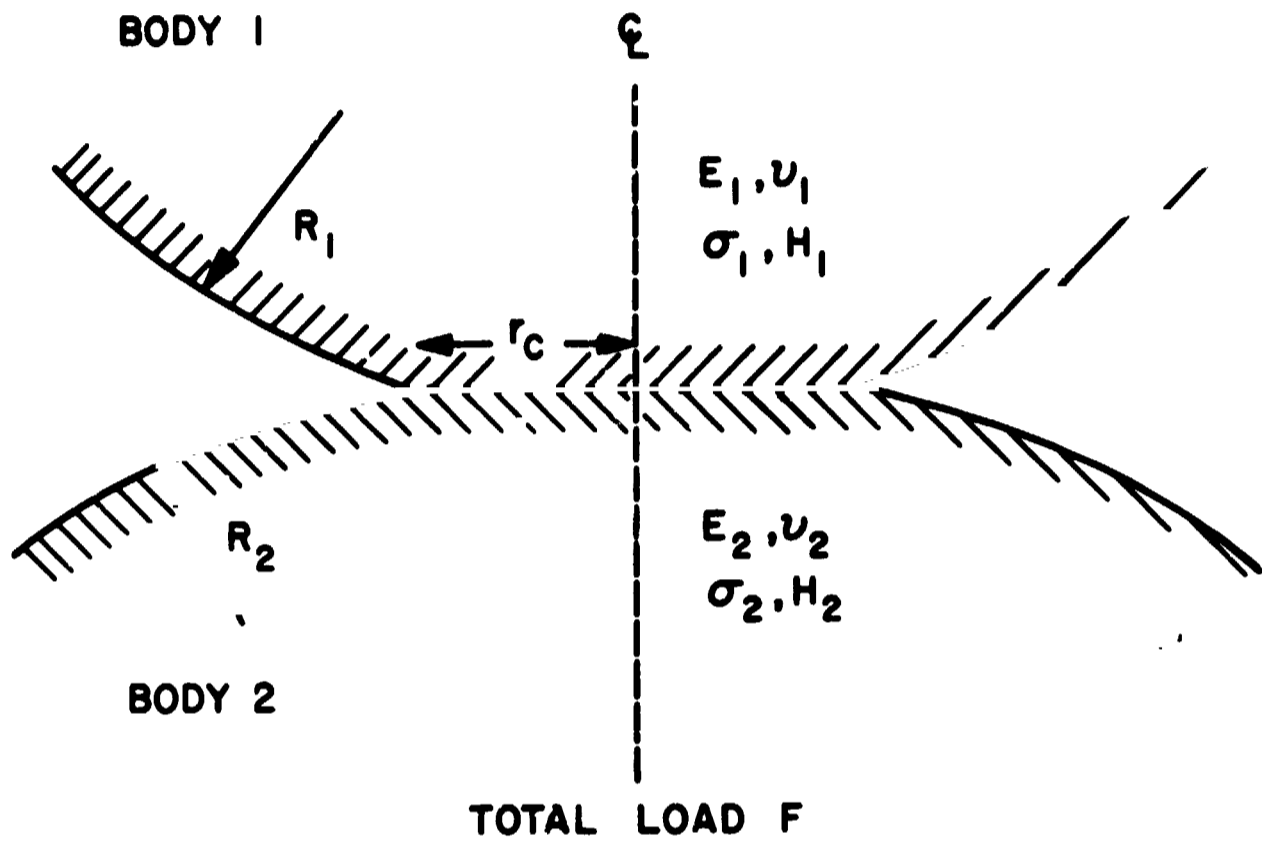


FIG. 4

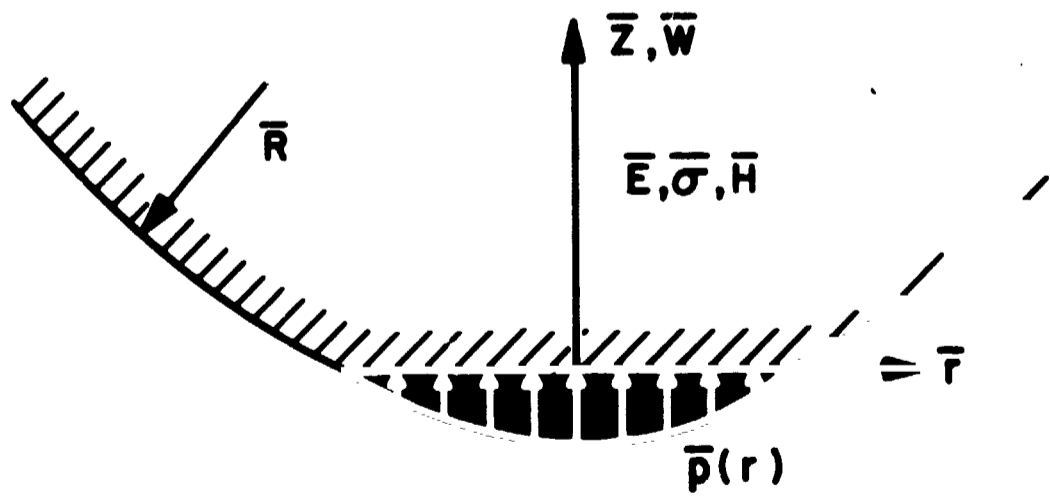
- (1) Wavy surface - Figure 5 - The wavy surfaces (Figure 3a) are modeled as two semi-infinite elastic bodies with non-flat surfaces of uniform (but not necessarily equal) radii of curvature. The radius of contact is assumed to be much less than the radius of curvature. For  $\sigma = 0$  this is the hertzian problem.
- (2) Clamped plates - Figure 6 - The externally clamped plates (Figure 3b) are modeled as two adjoining elastic disks of finite radius and thickness. They are forced together under a uniform load over a prescribed area. There are no other shear or normal loads on any face or edge.
- (3) Bolted joint - Figure 7 - The bolted (or riveted) plates (Figure 3c) are modeled as two adjoining elastic disks with center holes. These disks of finite radius and thickness are forced together under a uniform load over a prescribed annular area. There are no other shear or normal loads on any face or edge.

The required information is  $h_c(r)$  for each model.

From equation (3) one sees that in order to obtain the conductance it is necessary and sufficient to obtain the interfacial pressure distribution,  $p(r)$ . (The other parameters in (3) are functions of the materials.) The main goal of the thesis is to calculate  $p(r)$  for each of the three models and incorporate the result in thermal contact resistance behavior.

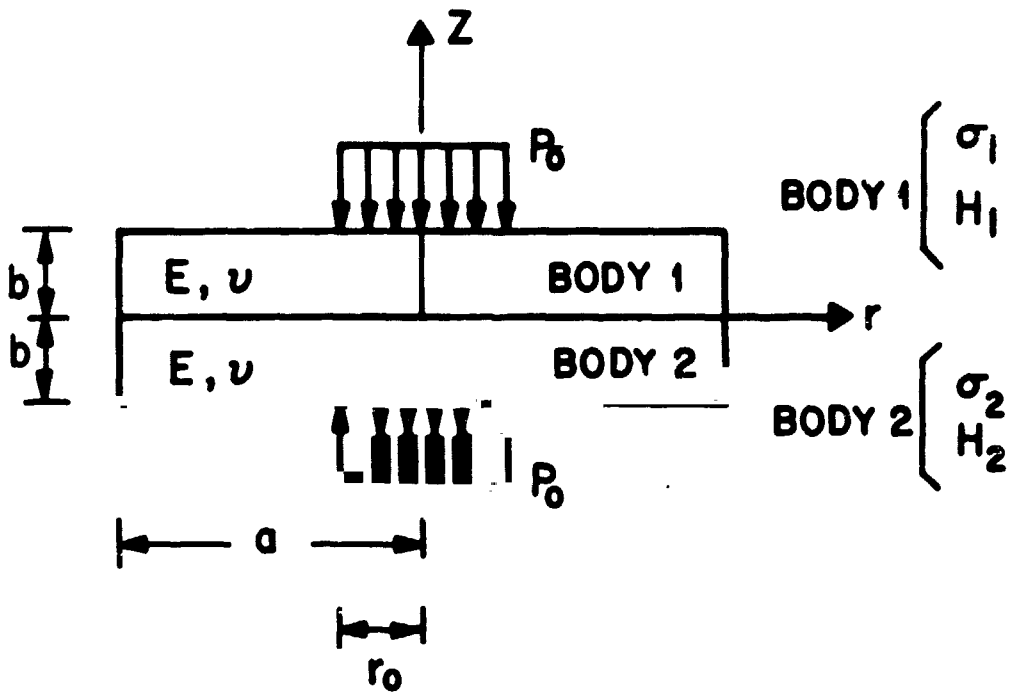


(a) - PHYSICAL MODEL FOR CONTACT OF TWO WAVY SURFACES

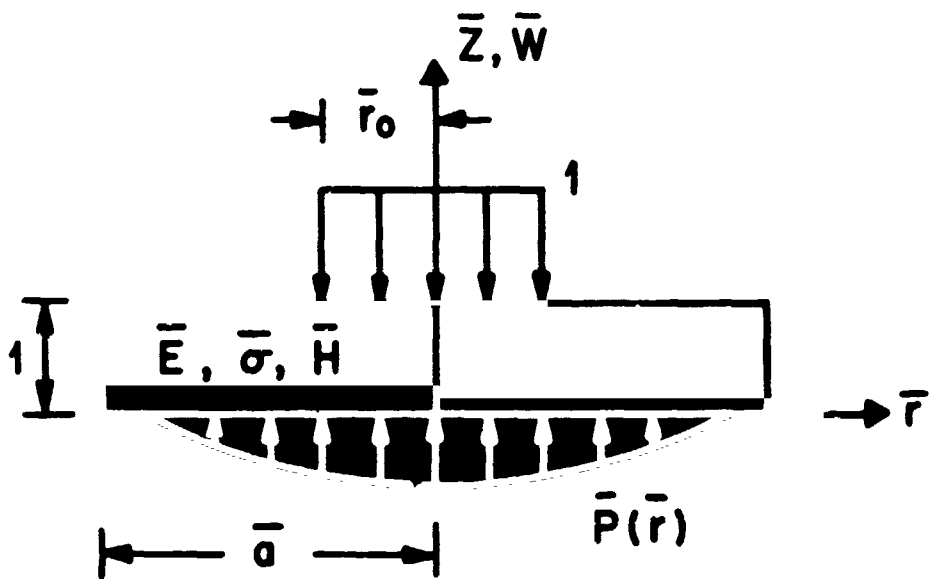


(b) - MODEL USED IN ITERATION SCHEME (IN NONDIMENSIONAL TERMS)

FIG. 5

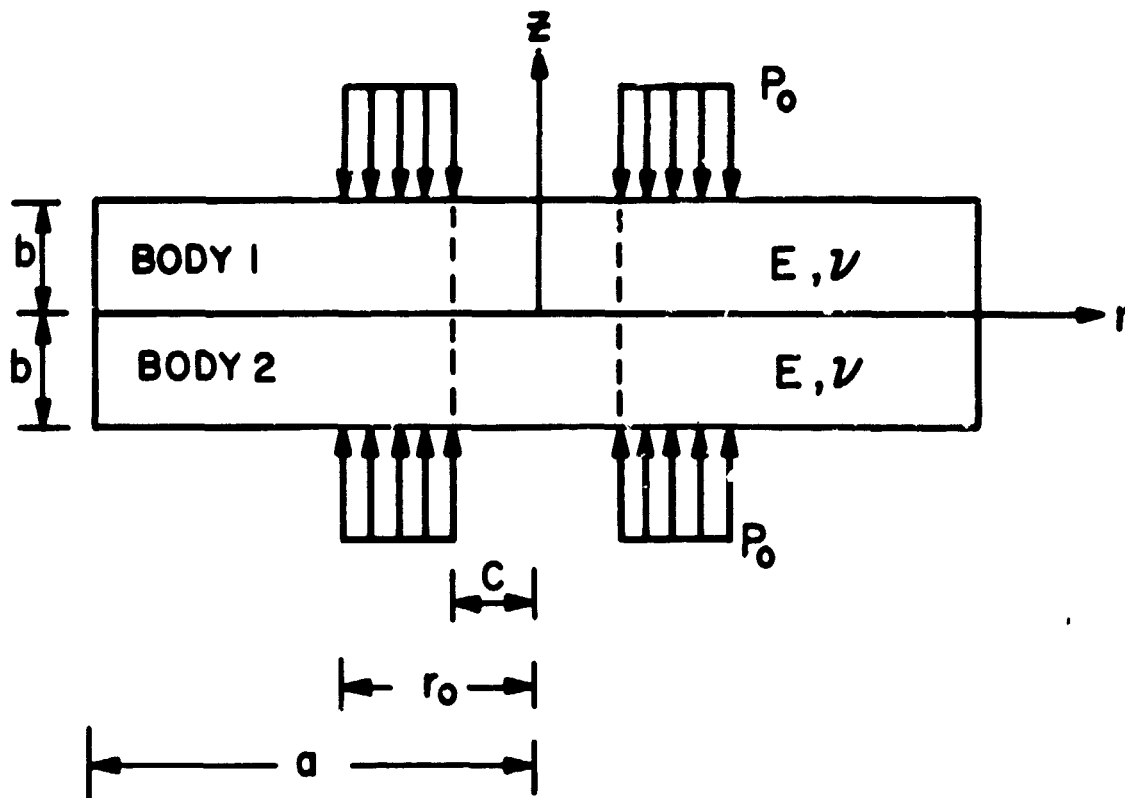


(a) PHYSICAL MODEL USED FOR CONTACT BETWEEN TWO PLATES

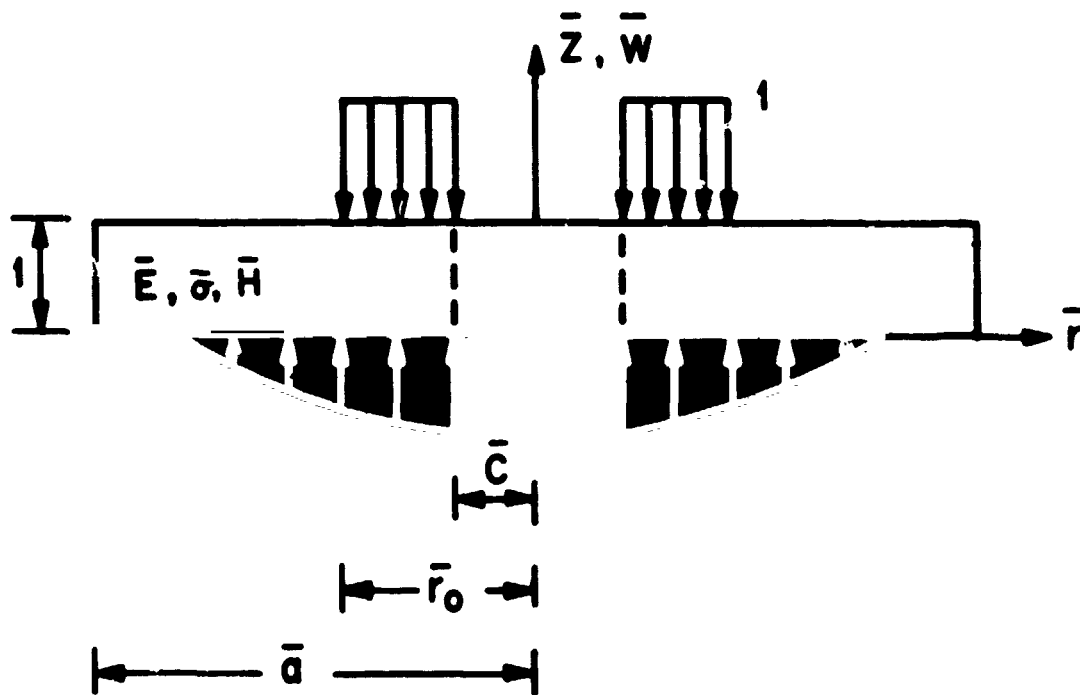


(b) MODEL USED IN ITERATION SCHEME (WITH NONDIMENSIONAL VARIABLES)

FIG.6



(a) - PHYSICAL MODEL USED FOR CONTACT AT BOLTED JOINT



(b) - MODEL USED IN ITERATION SCHEME (WITH NON DIMENSIONAL VARIABLES)

FIG. 7

The overall method of solution is straightforward. It is assumed that an asperity experiences the same load that the part of the main body directly under it experiences. It is further assumed that the asperities will "ride" on the mean surface of the body in addition to being deformed. The problem is then separated into two parts: deformation of the asperities and the deformation of the large body. The latter is solved using classical techniques of mechanics. Figure 8 illustrates the above.

The final result is arrived at through an iterative procedure utilizing three constraints:

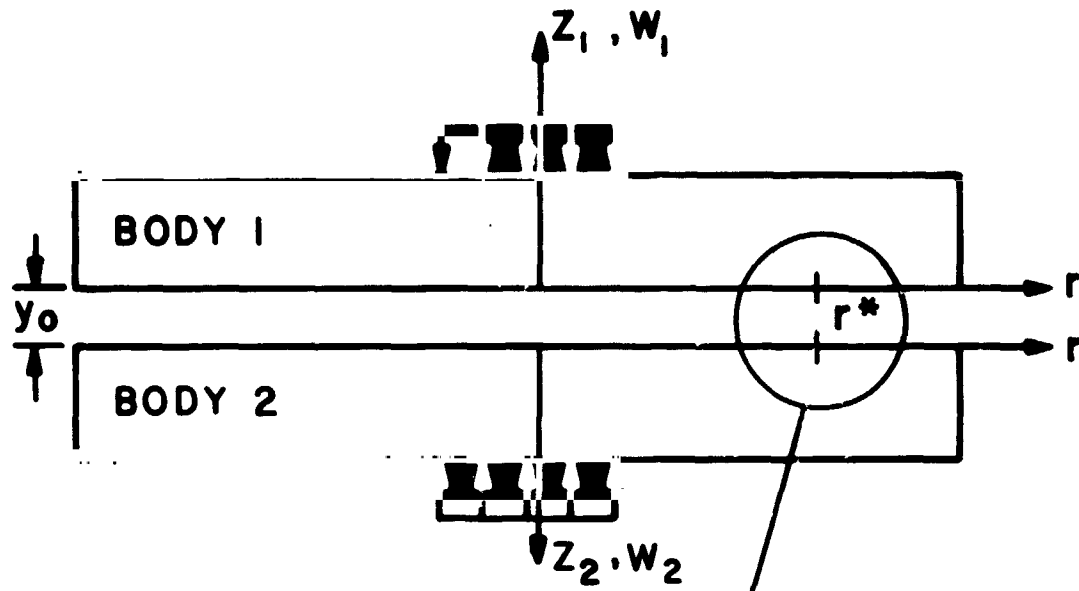
- (1) the elastic deformation of a body must conform to the pressure distribution it experiences;
- (2) the deformation of the asperities must conform to the pressure distribution they experience;
- (3) the total load applied to the elastic body is equal to the sum of the loads applied to the asperities.

This technique is not new with this paper and has been used before by various investigators [62,67,68].

To solve the problem for these three models, therefore, general force-deflection relationships for asperities, semi-infinite bodies, and finite disks with holes are needed. Previous work done in these areas will now be discussed.

### 1.3 Deformation of Asperities

It has been shown [69-71] that the behavior of a real surface can be described using the Gaussian distribution.



$W(r)$  = DEFLECTION (ON PLANE  $Z=0$ ) AT  $r$   
WITH RESPECT TO DEFLECTION AT  $r=0$   
i.e.  $w(0)=0$ .

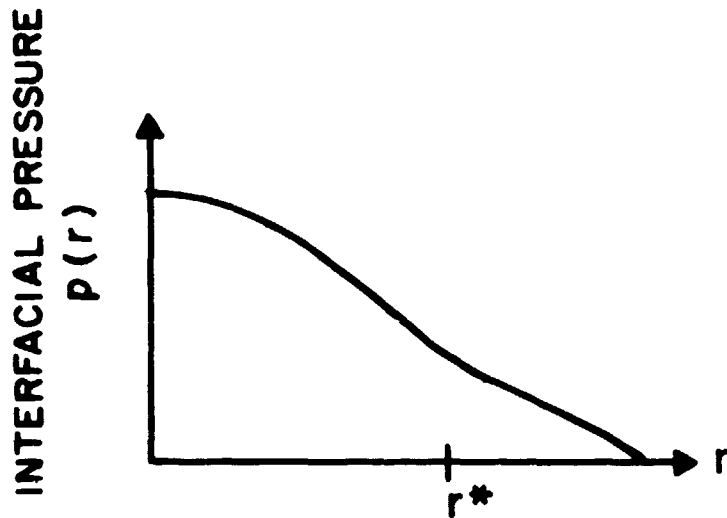
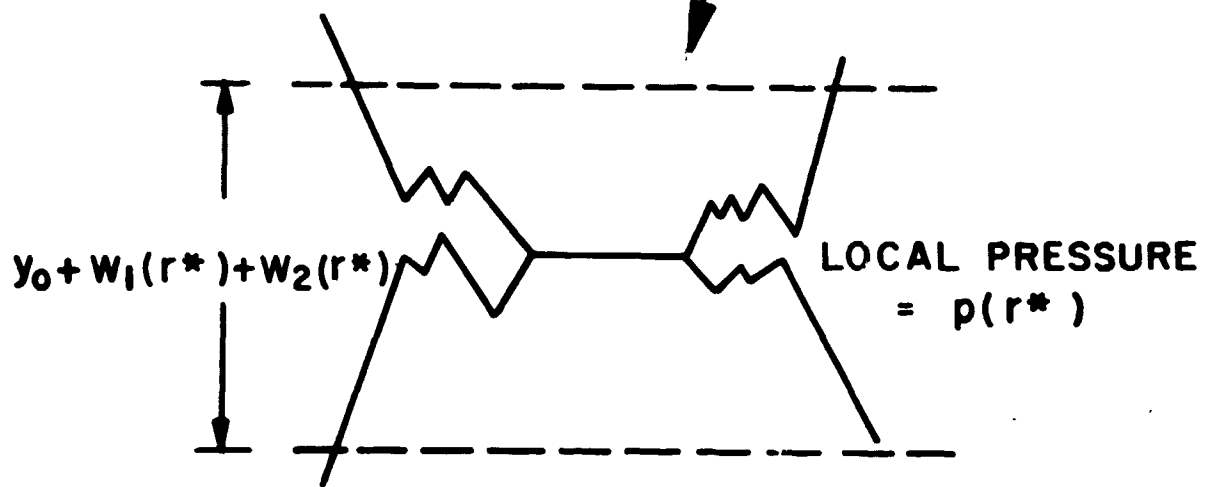


FIG. 8

For complete identification of a surface for our purposes one needs two statistical parameters: the standard deviation and the average mean slope. In this section the salient results developed by Mikic [36,72,73] are presented for such a Gaussian model. Both plastic and elastic deformation of the asperities are considered.

The model shown in Figure 2 illustrates a typical contact between two real surfaces. The mean lines are what are normally called the "surfaces" of the bodies. The actual contact between these two bodies is at discrete points where the asperities overlap. A statistical description of the surface is necessary and as mentioned before the distribution of heights of the surface above the mean line has been found to be Gaussian. That is

$$\text{probability (y)} = \frac{1}{\sqrt{2\pi}} \frac{e^{-y^2/2\sigma^2}}{\sigma}$$

In the work done by Greenwood [70,71] it is not the height of the surface which is considered but the heights of the peaks. This forces one to assume an asperity shape in order to account for the remainder of the surface. While Greenwood has shown that the choice is not particularly critical [71], the model in [36] is less restrictive.

In using a Gaussian model it should be noted that,

$$E(y) = 0$$

$$E\left(\sqrt{y^2}\right) = \sigma$$

$$E(|y|) = \sqrt{\frac{2}{\pi}} \sigma$$

where  $E(\ )$  is the expected value. The first is the mean value of  $y$  which is defined to be zero since  $y$  is measured from the mean plane. The second is the rms value and is equal to the standard deviation. The third is the center line average, or CLA, and is that value usually measured by such instruments as a Talysurf.

The other parameter needed to describe the surface is the average absolute value of the slope,  $\tan(\theta)$ , where

$$\tan(\theta) = \frac{1}{L} \int_L \left| \frac{dy}{dx} \right| dx$$

This has been found experimentally to be in the neighborhood of (0.1).

Besides a Gaussian distribution of asperity height above a mean plane, the other experimentally observed criterion to be met is Amonton's Law: the frictional force between two bodies is dependent on contact load only and independent of apparent area. This implies that the actual contact area,  $A_c$ , is proportional only to load,  $F$ ,

$$A_c \propto F$$

but since  $F = pA_a$  then,

$$p \propto \frac{A_c}{A_a} \quad (4)$$

By assuming that each asperity is a small hardness indenter and that the asperities deform plastically, one can remove the proportionality from (4) with use of the experimentally obtained hardness,  $H$ . Since  $F = HA_c$  then

$$p = H \frac{A_c}{A_a} \quad (5)$$

Using the model in Figure 2 one can find the probability that the surfaces intersect,  $p(y_1 + y_2 > y_0)$ ; and, from that, predict the area in contact [36]. The result is

$$\frac{A_c}{A_a} = 1/2 \operatorname{erfc} \left( \frac{y_0}{\sigma\sqrt{2}} \right) \quad (6)$$

where

$$\operatorname{erfc}(x) = \frac{2}{\sqrt{\pi}} \int_x^{\infty} e^{-t^2} dt$$

Therefore from (5) and (6),

$$p = \frac{H}{2} \operatorname{erfc} \left( \frac{y_0}{\sigma\sqrt{2}} \right) \quad (7)$$

Equation (7) is, then, the required force-deflection relationship needed in the eventual solution if one assumes that the asperities deform plastically.

Another result of interest is the number of contacts per unit area,  $n$ . To derive this one must also use the second statistical parameter mentioned,  $\tan(\theta)$ . The final result given in [72] is

$$n = \frac{\tan^2(\theta)}{16\sigma^2} \frac{e^{-y_0^2/\sigma^2}}{\operatorname{erfc}\left(\frac{y_0}{\sigma\sqrt{2}}\right)} \quad (8)$$

The only additional assumption needed is that the radius of curvature of the asperities before deformation is the same for all contacts which started at the same distance from the mean plane.

If the asperities deform elastically rather than plastically then (5) is no longer applicable. In [73] it is shown that for elastic deformation of the asperities,

$$\frac{A_c}{A_a} = 1/4 \operatorname{erfc}\left(\frac{y_0}{\sigma\sqrt{2}}\right) \quad (9)$$

and

$$p = 1/4 \frac{\bar{E} \tan(\theta)}{\pi\sqrt{2}} \operatorname{erfc}\left(\frac{y_0}{\sigma\sqrt{2}}\right) \quad (10)$$

where

$$\frac{1}{\bar{E}} = \frac{(1 - \nu_1^2)}{\pi E_1} + \frac{(1 - \nu_2^2)}{\pi E_2} \quad (11)$$

This is the force-deflection relationship which one uses if the asperities are assumed to yield elastically. Except for this, the same assumptions are made here as before. The number of contacts per unit area is the same, equation (8). If one considers  $H^*$  to be an equivalent hardness,

$$H^* = \frac{\bar{E} \tan(\theta)}{\pi 2\sqrt{2}} \quad (12)$$

then for the elastic case

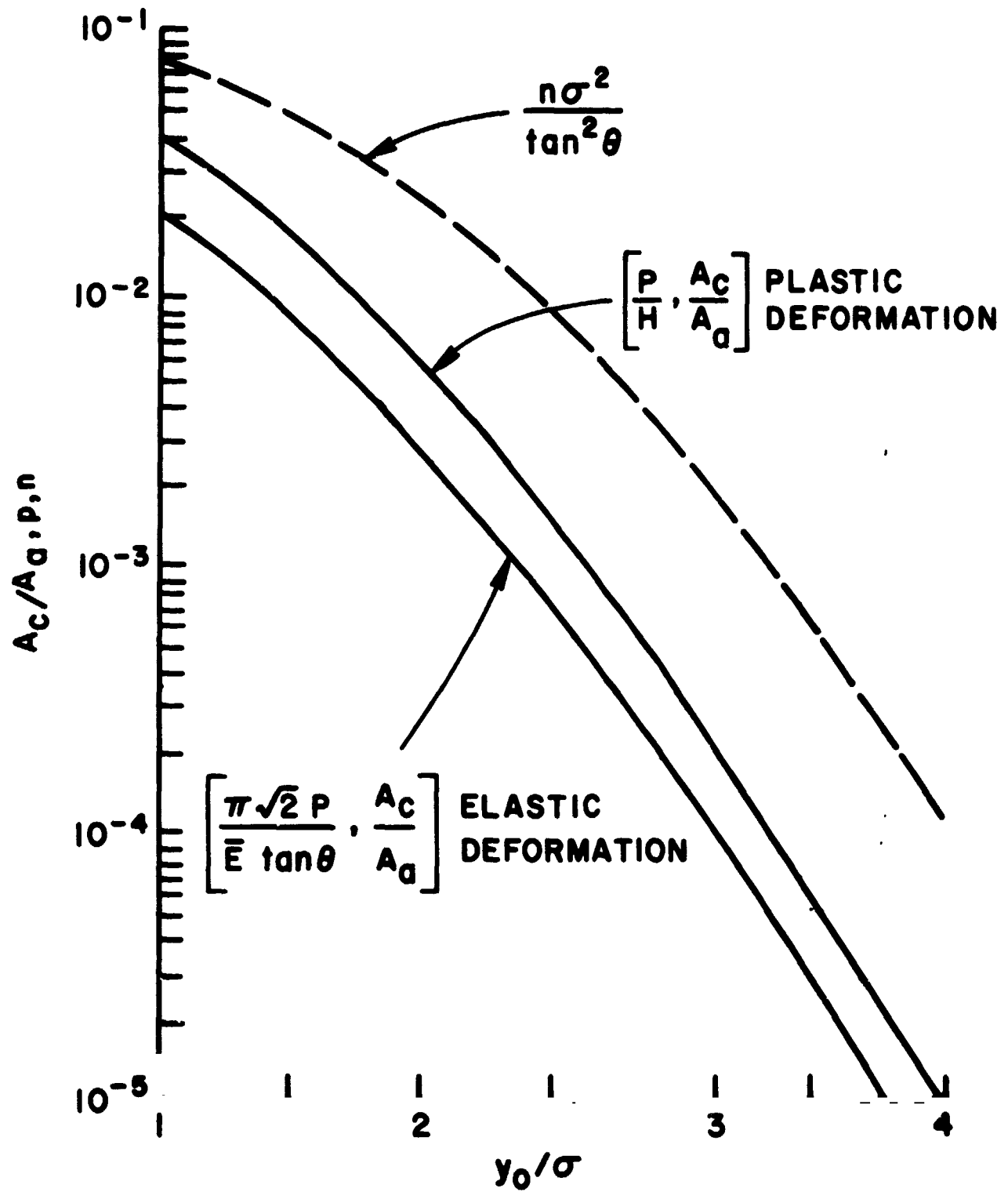
$$p = \frac{H^*}{2} \operatorname{erfc} \left( \frac{y_0}{\sigma\sqrt{2}} \right)$$

It is obvious from (9) and (10) that Amonton's Law is satisfied since

$$p = \frac{\bar{E} \tan(\theta)}{\pi\sqrt{2}} \frac{A_c}{A_a}$$

Figure 9 illustrates the behavior of the various parameters versus  $y_0/\sigma$  and Figure 10 summarizes the results.

In brief, then, regardless of whether or not the asperities deform plastically or elastically one has a force-deflection expression in the form



EXPECTED VALUES OF VARIOUS  
PARAMETERS VERSUS SEPARATION  
OF MEAN PLANES

FIG. 9

	PARAMETER	PLASTIC DEFORMATION OF ASPERITIES	ELASTIC DEFORMATION OF ASPERITIES
n	NUMBER OF CONTACTS PER UNIT AREA	$\frac{\text{TAN}^2\theta}{16\sigma^2} \frac{e^{-y_0^2/\sigma^2}}{\text{erfc}\left(\frac{y_0}{\sigma\sqrt{2}}\right)}$	$\frac{\text{TAN}^2\theta}{16\sigma^2} \frac{e^{-y_0^2/\sigma^2}}{\text{erfc}\left(\frac{y_0}{\sigma\sqrt{2}}\right)}$
$\frac{A_c}{A_d}$	<u>ACTUAL AREA IN CONTACT</u> APPARENT AREA IN CONTACT	$\frac{1}{2} \text{erfc}\left(\frac{y_0}{\sigma\sqrt{2}}\right)$	$\frac{1}{4} \text{erfc}\left(\frac{y_0}{\sigma\sqrt{2}}\right)$
p	PRESSURE AS FUNCTION OF SEPARATION	$\frac{H}{2} \text{erfc}\left(\frac{y_0}{\sigma\sqrt{2}}\right)$	$\frac{\bar{E} \text{TAN}\theta}{\pi 4\sqrt{2}} \text{erfc}\left(\frac{y_0}{\sigma\sqrt{2}}\right)$

SUMMARY OF RESULTS FOR ASPERITY DEFORMATION

FIG. 10

$$p = \frac{H}{2} \operatorname{erfc} \left( \frac{y_0}{\sigma\sqrt{2}} \right)$$

For plastic deformation  $H$  is the Vickers hardness. For elastic deformation  $H$  is that given in (12),  $H^*$ .

#### 1.4 Deformation of Spherical Surfaces

The previous section showed that there was sufficient information already existing in the literature concerning the deformation of asperities to satisfy the needs of this paper. The next three sections will review previous work done on the models given in Figures 5-7. In all three of these models two facts are needed: What is the interfacial pressure distribution for zero roughness when the two bodies are pressed together? What is the deflection at the surface for an arbitrary interfacial pressure distribution? The latter is needed in the iteration procedure when the roughness is non-zero.

In the case of two bodies with spherical surfaces (Figure 5), the first question has been answered by the work of Hertz [74]. For the model shown in Figure 5, with  $\sigma = 0$ , the interfacial pressure distribution is

$$p(r) = \frac{3}{2} \frac{F}{\pi a_h^2} \left( 1 - r^2/a_h^2 \right)^{1/2} \quad (13)$$

where the radius of the contact area,  $a_h$ , is

$$a_h = \left( \frac{3\pi}{4} \frac{F\bar{R}}{E} \right)^{1/3} \quad (14)$$

It is assumed that each body is a semi-infinite elastic body, that the radii are of constant curvature (before deformation) within the area of contact, and that  $\bar{R} \gg a_h$ .

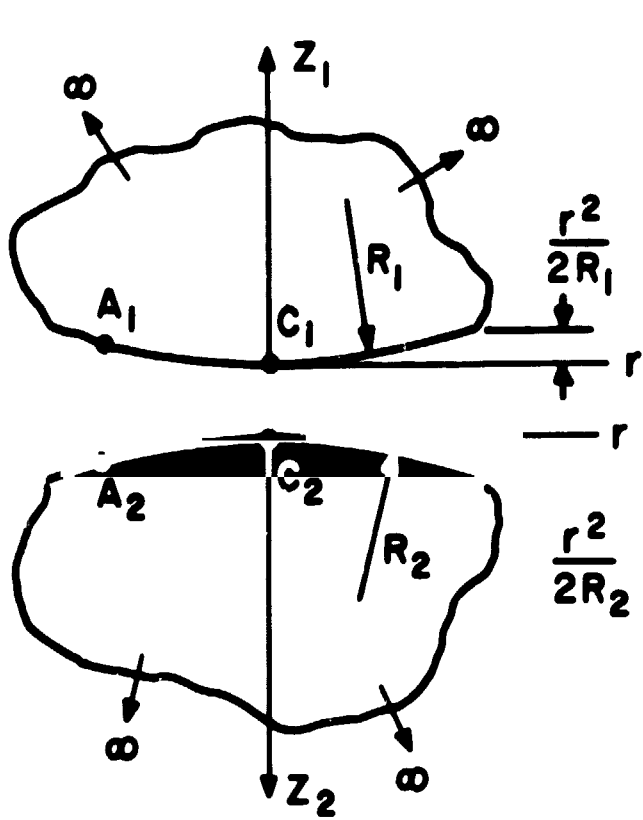
There are two ways to solve the second problem of a variable pressure distribution. The first is to superimpose point load solutions [74], the second is to use Hankel transforms (Terezawa's solution) [76]. The point load solution is difficult to use because of the point of discontinuity which arises. To avoid this difficulty the Hankel transform solution is used here instead. The procedure is to take the solution for a flat semi-infinite body and add to it the original curvature. This gives the overall distance between two opposing points on the two bodies.

Using the notation given in Figure 11, the deflection at the surface of a semi-infinite body  $w(r)$  due to a load,  $p(r)$  is [76]

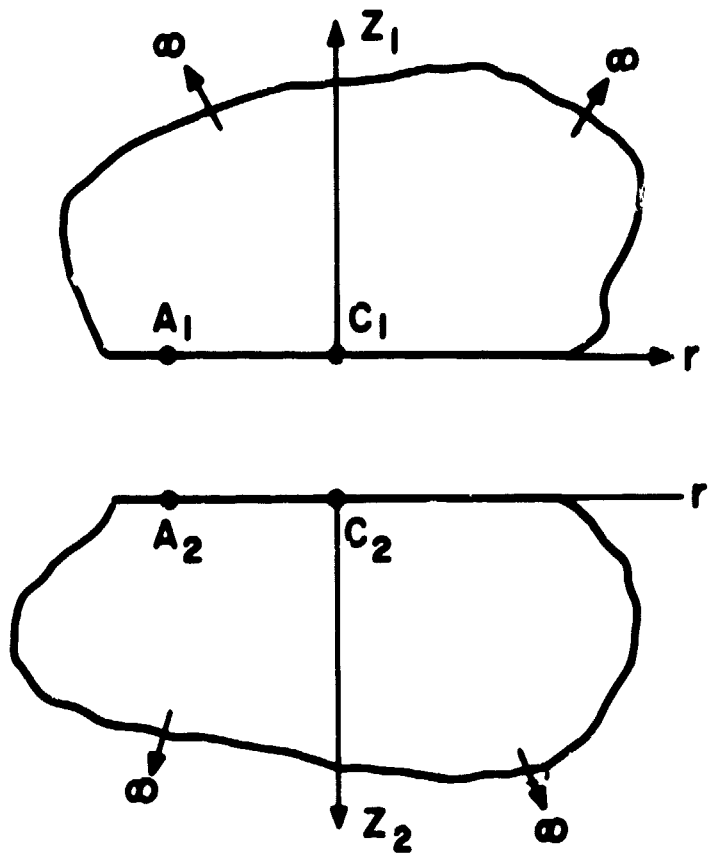
$$w(r) = \frac{2(1-\nu^2)}{E} \int_0^{\infty} P(\rho) J_0(\rho r) d\rho \quad (15)$$

where

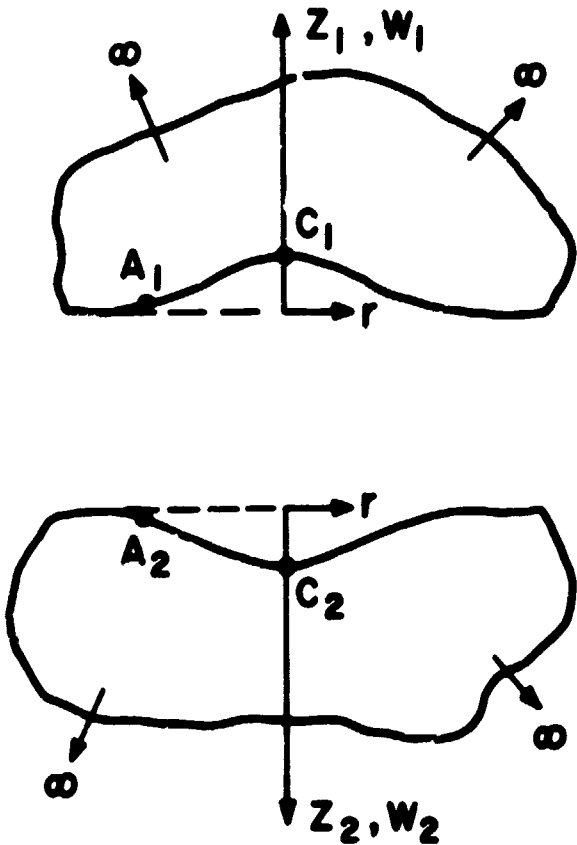
$$P(\rho) = \int_0^{\infty} r p(r) J_0(\rho r) dr \quad (16)$$



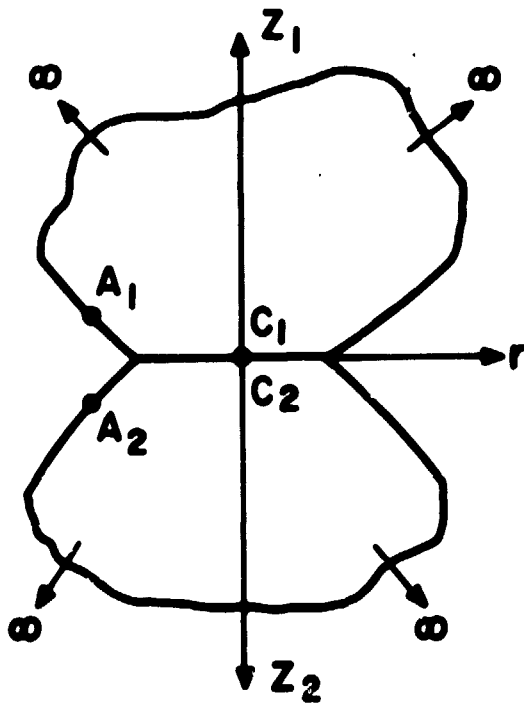
(a) ORIGINAL PROBLEM BEFORE CONTACT



(b) BEFORE CONTACT, CURVATURE IGNORED



(c) AFTER CONTACT, CURVATURE IGNORED



(d) AFTER CONTACT ( $\sigma = 0$ )

CONTACT OF TWO SPHERICAL SURFACES

FIG. II

The distance, then, between two points opposing each other (Figure 11) without considering the curvature is

$$\left( w_{A_1} - w_{C_1} \right) + \left( w_{A_2} - w_{C_2} \right)$$

Superimposing the curvature of the bodies gives the total distance between the two points  $A_1$  and  $A_2$

$$\overline{A_1 A_2} = \left( w_{A_1} - w_{C_1} \right) + \left( w_{A_2} - w_{C_2} \right) + \frac{r^2}{2} \left( \frac{1}{R_1} + \frac{1}{R_2} \right)$$

or, from (15)

$$\overline{A_1 A_2} = \frac{2\pi}{E} \int_0^{\infty} P(\rho) J_0(\rho r) d\rho - \frac{2\pi}{E} \int_0^{\infty} P(\rho) d\rho + \frac{r^2}{2R} \quad (17)$$

The above assumes that the bodies touch at  $C_1$  and  $C_2$ . When the roughness is considered, a constant term,  $y_0$ , will be added to (17) to account for the separation of the two reference points.

Using a procedure similar to the above but using the superposition method rather than Hankel transforms, Greenwood [75], Flengas [68], and McMillan [62] all investigated the effect of roughness on the interfacial pressure distribution and arrived at similar conclusions. Because of an unfortunate choice of non-dimensional variables, however, the results published were not general and could be

used only for the specific cases presented. The main contribution here is to show that by proper non-dimensionalizing, all pertinent data regarding this problem can be reduced to one compact graph. This will be done in section 2.1.

To recapitulate: as was done for asperities, a basic force-deflection relationship for spherical surfaces has been presented, equation (15). It is not in as simple a form as that for the asperities and will generally require numerical integration for a particular  $p(r)$ .

#### 1.5 Deformation of Solid Disks

Unlike the case of contact between two spherical surfaces, there is no exact solution available for the contact of two solid disks with zero surface roughness. The expected behavior is intimate contact with finite pressure and zero deflection (symmetrical loading assumed) within a certain radius of contact,  $r_c$ , and zero pressure and finite deflection outside of  $r_c$ . Of interest is both the nature of the pressure distribution,  $p(r)$ , and the value of  $r_c$ .

In lieu of an exact solution, the midplane stress of a single plate of thickness  $2b$  (rather than two plates each of thickness  $b$ ) has been used [73-80]. Even though the midplane stress becomes tensile a certain distance from the centerline it has been assumed that this can be ignored. From this it is estimated [79] that the radius of contact for  $r_0/b > 0.5$  is

$$r_c = r_0 + b \quad (18)$$

It will be shown later that this relationship can be improved.

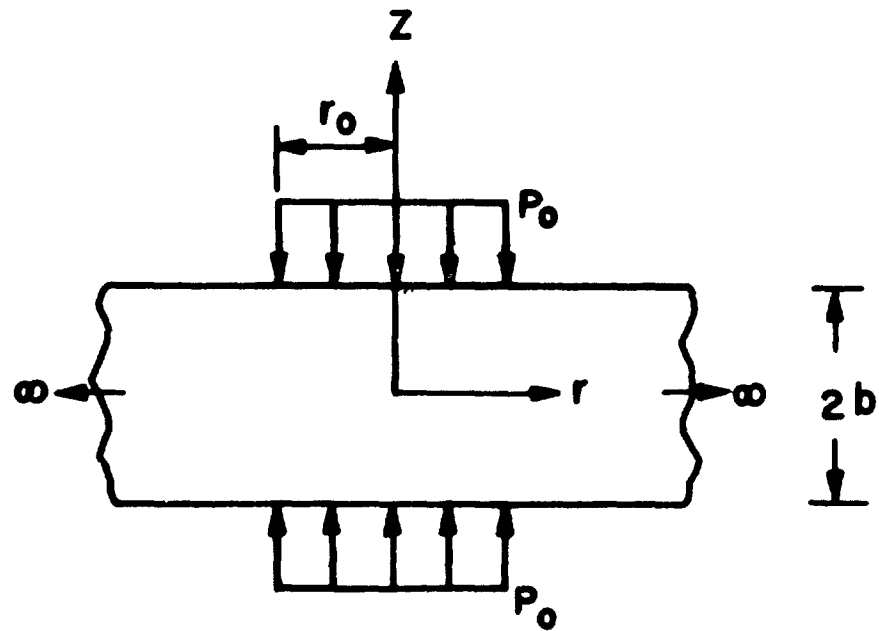
Figure 12 gives published results for the midplane stress. These are from [79] but the results of the other references cited agree with them.

As was mentioned before, besides the contact pressure between two smooth disks, the force-deflection relationship for a single disk of thickness  $b$  is needed (Figure 6). No solution exists in the literature for a disk of finite radius but does exist for one of infinite radius [77,79]. The solution to the finite radius problem will be presented later in this paper. It is found using a method suggested by Pickett [81] in solving the similar problem of a cylinder under a compressive load from two rigid bodies. The method, which uses Fourier-Bessel series, is explained in the Appendix. With this solution, comparison to the existing one will be made and the accuracy in using the midplane stress for the contact pressure (at zero roughness) will be examined.

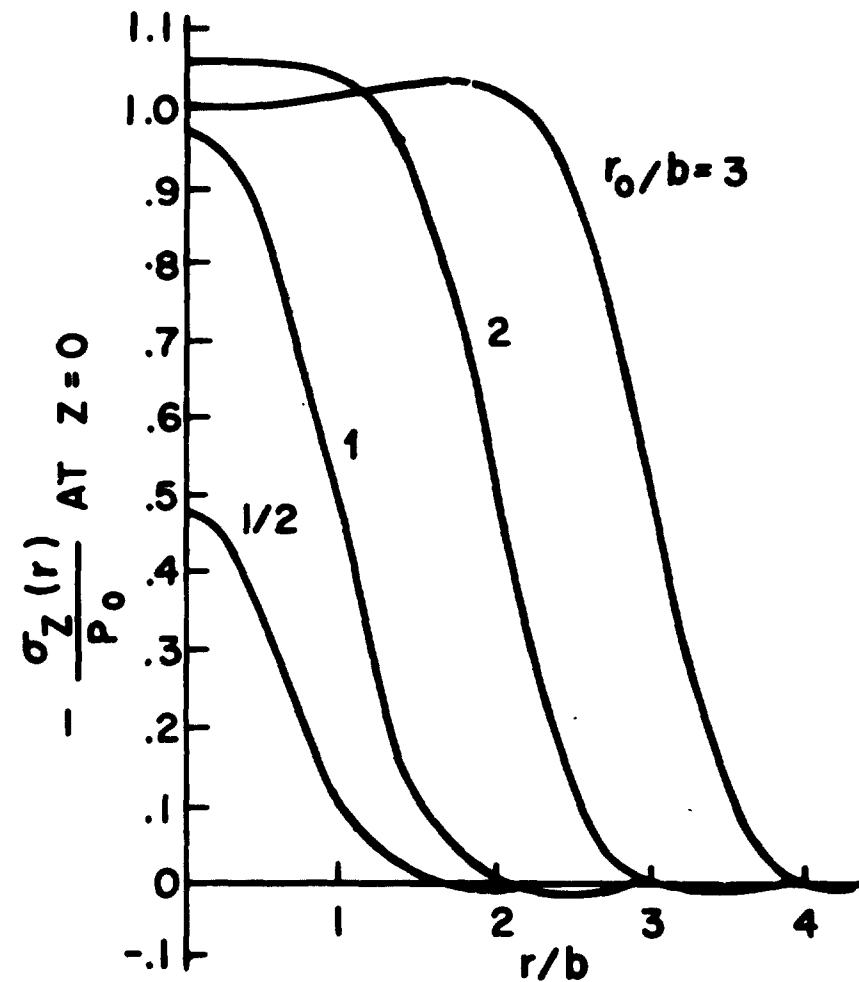
Therefore, as was done with spherical surfaces, a force-deflection relationship for disks will be presented and used along with that for the asperities in order to examine the effect of varying roughness.

#### 1.6 Deformation of Disks with Center Holes

While no exact closed-form solution exists for the contact of two disks with center holes, a numerical one



(a) APPROXIMATE MODEL FOR CONTACT OF TWO PLATES OF THICKNESS  $b$  EACH [79]



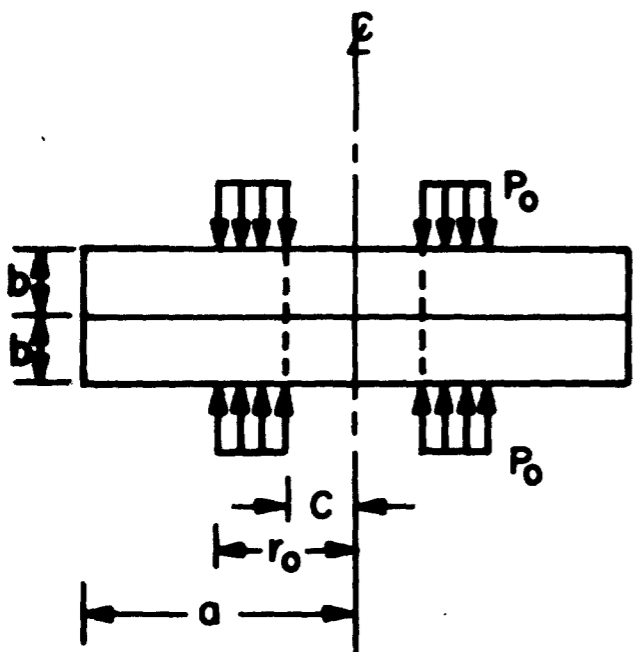
(b)- MIDPLANE STRESS OF DISK OF INFINITE RADIUS AND THICKNESS  $2b$ .

FIG. 12

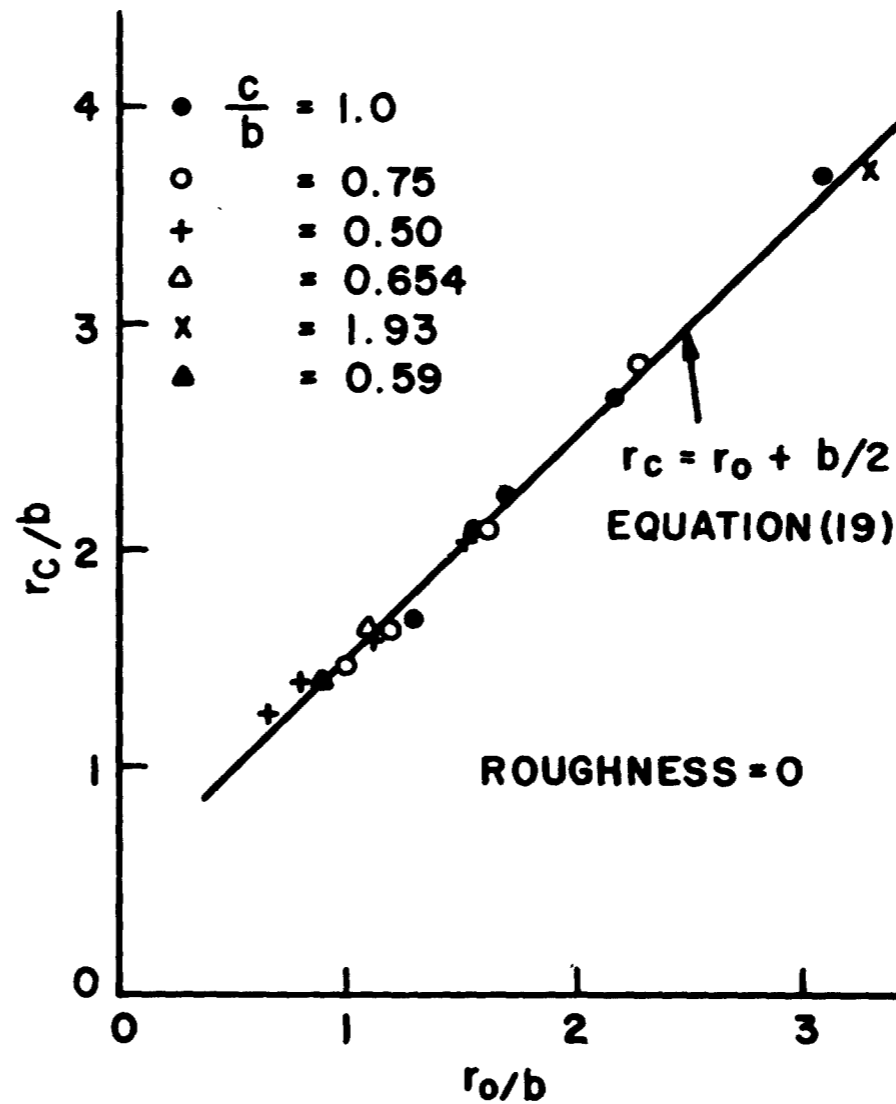
does [83]. This finite-element solution solves the mixed boundary value problem of zero deformation up to  $r_c$  and zero pressure beyond  $r_c$  by a trial and error technique of locating  $r_c$ . The results are found to be independent of hole radius. The relationship given for  $r_c$  is,

$$r_c = r_0 + 0.5b \quad (19)$$

The model, data on which (19) is based, and an example of the pressure distribution for contact between two smooth plates are given in Figures 13 and 14. It should be noted from the latter that the midplane distribution is not a good estimate of the interfacial contact pressure. Not only is the negative pressure zone not found in the correct solution (as is expected), but the rate of decrease of  $p(r)$  beyond  $r_0$  is much steeper than that predicted by the midplane stress curve. However, if one extends the tangent to the midplane stress curve at  $r_0$  to the  $r$  axis it will intersect at, or close to, the value of  $r_c$  predicted by the numerical solution. It seems reasonable then to extend this approximation to the previous section where there was no center hole. If this is done it is seen that equation (19) can be used there also for predicting  $r_c$ . One expects (19) to decrease in accuracy as  $r_0$  decreases, in either case.

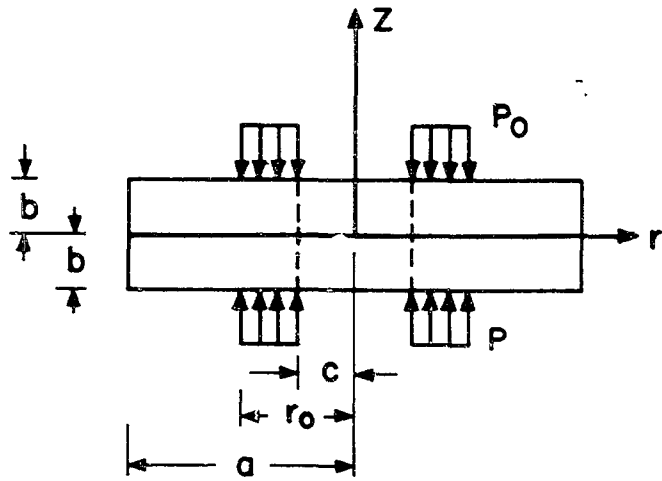


(a)-MODEL USED IN [83]

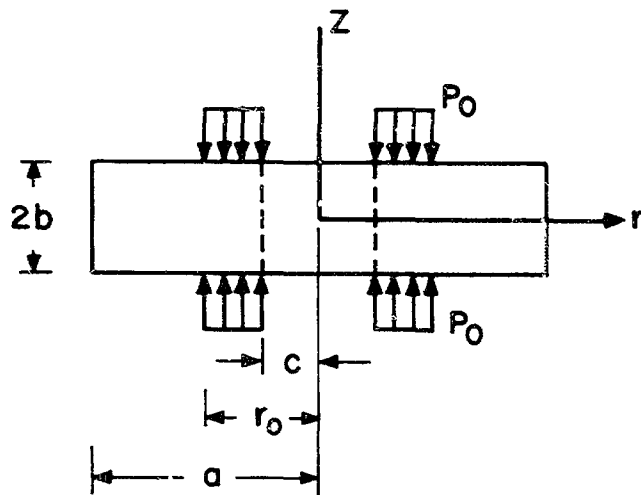


(b)-NUMERICAL RESULTS FROM RADIUS OF CONTACT [83]

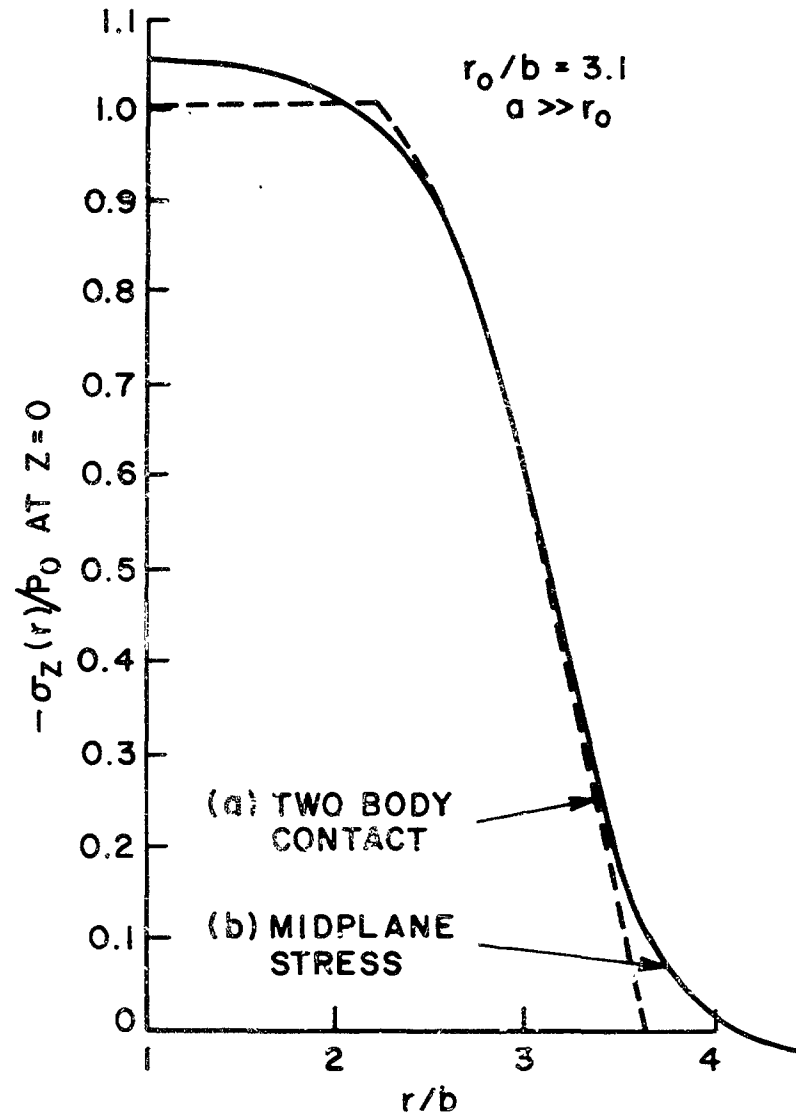
FIG. 13



(a) - MODEL FOR TWO BODY CONTACT



(b) - MODEL FOR MIDPLANE STRESS



(c) - NUMERICAL SOLUTION [83]

FIG. 14

There have also been approximate solutions for  $p(r)$  developed through the use of thin plate theory [84,85].

The form used is

$$p(r) = p^* \left[ 1 - \left( \frac{r}{r_c} \right)^m \right] \quad 0 < r < r_c$$
$$= 0 \quad r > r_c$$

The constants  $p^*$ ,  $m$ , and  $r_c$  are unknown and are evaluated using various boundary conditions and assumptions. The critical boundary condition that the deflection is zero within the radius of contact cannot be met, however. Thin plate theory assumes uniform stress through the narrow dimension of the plate (here the  $z$  axis). The essence of the contact problem considered here is the change in the stress through this thin section. To meet the requirement of changing  $p(r)$  with  $z$  and zero deflection for  $r < r_c$  is impossible.

At large values of  $r_0/b$  one can use the approximation

$$r_c \cong r_0$$

and, therefore,

$$p(r) \cong p_0$$

Experimental results [83,85] bear out the analytical work done in [83].

Like the case with the spherical surfaces, there exists a solution for the contact of two smooth disks with center holes. There is, however, no general force-deflection relationship which can be used in the more general problem of contact between two rough disks. Subsequent work will yield such a relationship.

In the subsequent section the force-deflection relationship for asperities, (7) or (10), will be coupled with that for the spherical surfaces, disks without center hole, and disks with center hole in turn to arrive at the interfacial pressure distribution for a rough contact. Knowing  $p(r)$ , one can use (3) to determine the local contact conductance  $h_c(r)$ . With this knowledge one can, for example, find the resistance of a given configuration. This will be done in section 3 for a particular bolted joint.

## 2. MECHANICS

### 2.1 Contact of Two Wavy Surfaces

#### 2.1.1 Model

It is assumed that the behavior of the contact between two wavy surfaces can be determined by investigating the behavior of the contact between two spherically shaped surfaces. It is further assumed that

- (a) the spherically shaped bodies deform elastically;
- (b) the radius of contact,  $r_c$ , is small compared to the radii of curvature of the two surfaces;
- (c) asperities deform plastically;
- (d) asperity height distribution above a mean line is Gaussian;
- (e) asperity contact is normal with no tangential component;
- (f) the contact (i.e., pressure distribution and deformation) will be symmetric about an axis through the center of the area in contact.

Using these assumptions and the model given in Figure 5, one can arrive at the following set of equations (see sections 1.3 and 1.4) for the

- (a) deformation of spherical surfaces

$$w(r) = \frac{2\pi}{E} \int_0^{\infty} P(\rho) J_0(\rho r) d\rho - \frac{2\pi}{E} \int_0^{\infty} P(\rho) d\rho + \frac{r^2}{2R} \quad (20)$$

where

$$P(\rho) = \int_0^{\infty} r p(r) J_0(\rho r) dr$$

(b) pressure distribution at asperities

$$p(r) = \frac{H}{2} \operatorname{erfc} \left( \frac{y_0 + w(r)}{\sqrt{2}} \right) \quad (21)$$

(c) and for the load, F

$$F = \int_0^{\infty} 2\pi r p(r) dr \quad (22)$$

There are three unknowns:  $p(r)$ ,  $w(r)$ , and  $y_0$  where  $y_0$  is the separation between the two mean lines of the surfaces. One can numerically iterate using equations (20), (21), and (22) to arrive at a solution for the particular set of variables used. It can be shown that for the special case of perfectly smooth surfaces ( $\sigma = 0$  - Hertz's problem) that the solution is

$$y_0 = 0$$

$$p(r) = \frac{3}{2} \frac{F}{\pi a_h^2} \left( 1 - \frac{r^2}{a_h^2} \right)^{1/2} \quad (13)$$

where  $a_h$  is the Hertzian radius of contact and is

$$r_c |_{\sigma=0} = a_h = \left( \frac{3\pi F R}{4\bar{E}} \right)^{1/3} \quad (14)$$

When  $\sigma \neq 0$ , one does not have a closed-form solution like (13).

Non-dimensionalize equations (20), (21), and (22) with the average Hertzian pressure,  $p_0$ , where

$$p_0 = \frac{F}{\pi a_h^2}$$

and with the Hertzian radius of contact,  $a_h$ . The variables become

$$\bar{w} = \frac{w\bar{E}}{a_h p_0} \quad \bar{y}_0 = \frac{y_0 \bar{E}}{a_h p_0}$$

$$\bar{p} = \frac{p}{p_0} \quad \bar{H} = \frac{H}{p_0}$$

$$\bar{r} = \frac{r}{a_h} \quad \bar{r}_c = \frac{r_c}{a_h}$$

$$\bar{\sigma} = \frac{\sigma \bar{E}}{a_h p_0}$$

One has, then, from (20)

$$\bar{w}(\bar{r}) = \frac{2\pi}{E} \int_0^{\infty} \bar{P}(\bar{\rho}) J_0(\bar{\rho}\bar{r}) d\bar{\rho} - \frac{2\pi}{E} \int_0^{\infty} \bar{P}(\bar{\rho}) d\bar{\rho} + \frac{3\pi^2}{8} \bar{r}^2 \quad (23)$$

where

$$\bar{P}(\bar{\rho}) = \int_0^{\infty} \bar{r}\bar{p}(\bar{r}) J_0(\bar{\rho}\bar{r}) d\bar{r}$$

from (21)

$$\bar{p}(\bar{r}) = \frac{\bar{H}}{2} \operatorname{erfc} \left( \frac{\bar{y}_0 + \bar{w}(\bar{r})}{\bar{\sigma}\sqrt{2}} \right) \quad (24)$$

and from (22)

$$\int_0^{\infty} \bar{r}\bar{p}(\bar{r}) d\bar{r} = 0.5 \quad (25)$$

Thus the non-dimensional force is 0.5 and remains fixed regardless of the choice of  $\bar{\sigma}$  and  $\bar{H}$ , the only free parameters for the problem in its new non-dimensional form. Using these particular variables one sees that for the Hertzian problem of contact between two smooth spherical bodies ( $\bar{\sigma}=0$ ), the

pressure distribution also is not a function of  $\bar{\sigma}$  and  $\bar{H}$ .

$$p(r) = \frac{3}{2} (1-\bar{r}^2)^{1/2} \quad \bar{r} \leq 1 \quad (26)$$

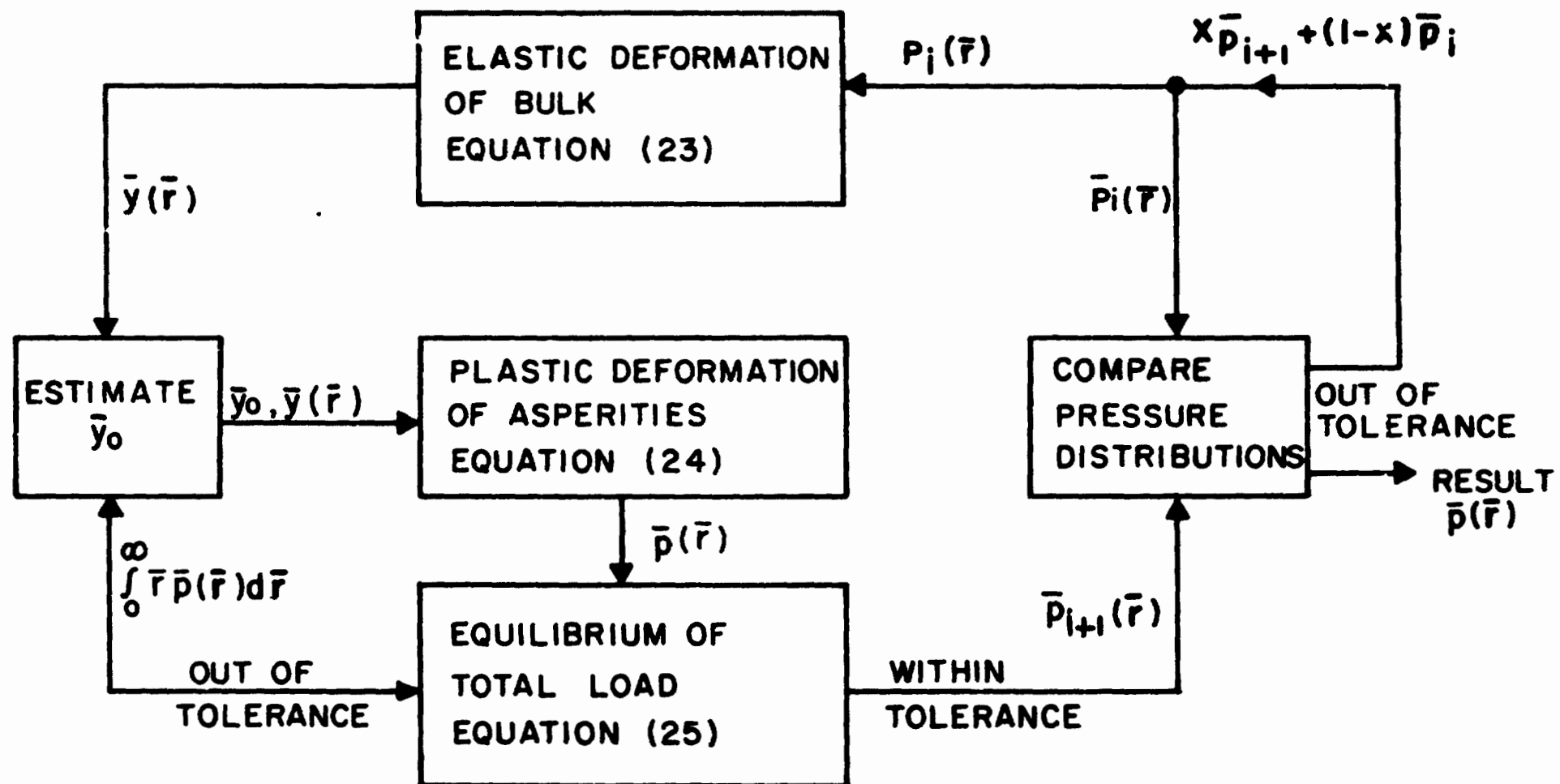
The radius of contact in this case is

$$\bar{r}_c = 1$$

Thus by choosing this particular method to non-dimensionalize the problem, one fixes the solution to the Hertzian problem regardless of load, radius of curvature, etc. and then is able to examine departures from this one curve due to the presence of asperities.

### 2.1.2 Solution

The solution is as follows: A first guess is made of  $\bar{p}(\bar{r})$  and placed into (23). This first guess is the Hertzian distribution (26). The resultant  $\bar{y}(\bar{r})$  is substituted into (24) along with a guess for  $\bar{y}_0$ . The calculated  $\bar{p}(\bar{r})$  is placed into (25) and  $\bar{y}_0$  is adjusted until the integration yields a load equal to 0.5. The accepted tolerance is one percent. This final  $\bar{p}(\bar{r})$  is compared to the first guess and if they do not agree within a prescribed range (1%) a new guess of  $\bar{p}(\bar{r})$  is made which is a weighted average of the original estimate and the result from (24). A flow diagram is given in Figure 15.



FLOW CHART FOR ITERATIVE SCHEME

FIG. 15

It was found that a particularly efficient way of converging on the correct value of  $\bar{y}_0$  was to use the following:

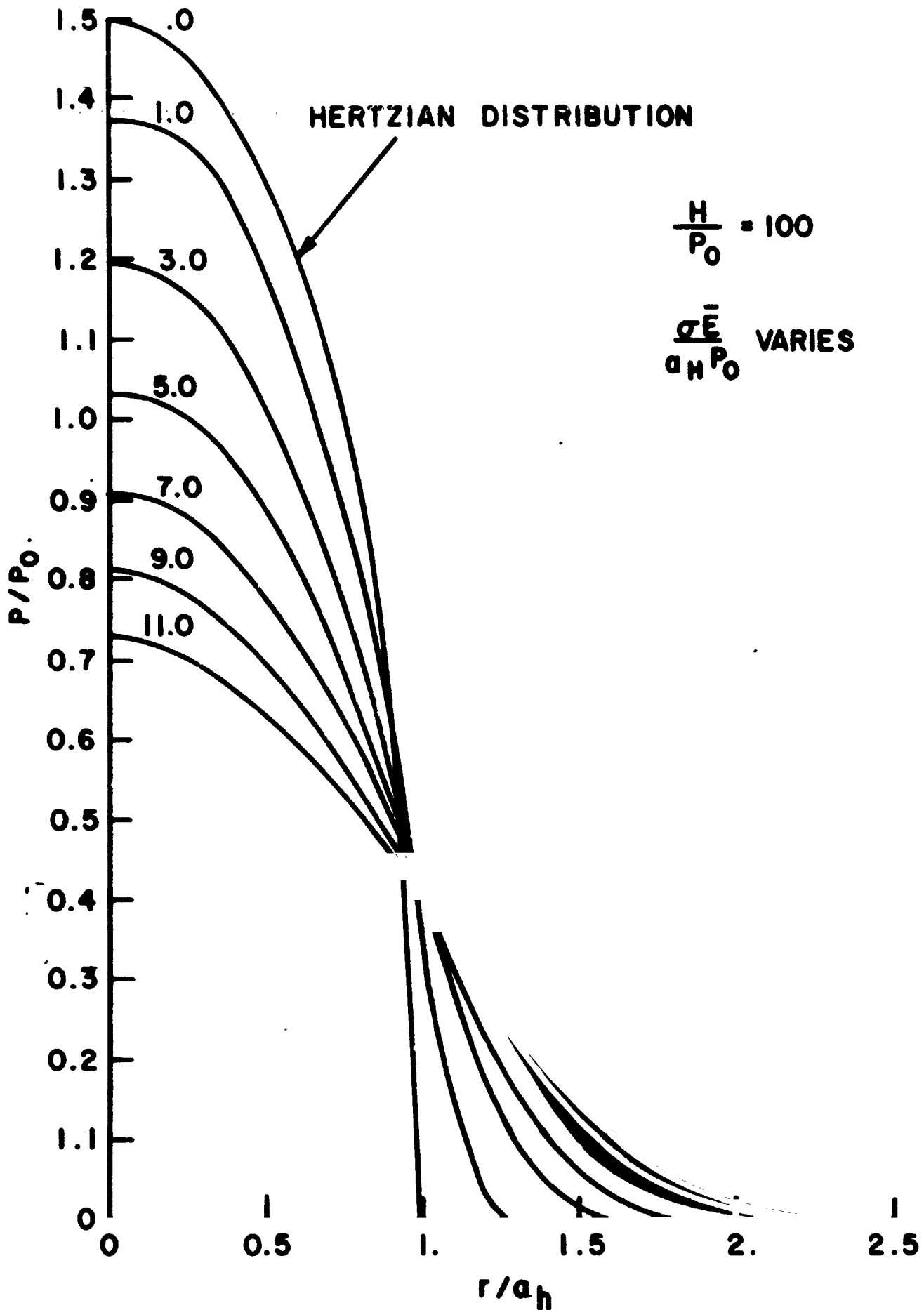
$$\begin{aligned} (\bar{y}_0)_{i+1} &= (\bar{y}_0)_i + \frac{\bar{\sigma}}{2} \left\{ \log_e \left[ \frac{\text{load calculated}}{\text{using } (\bar{y}_0)_i} \right] - \log_e(\text{true load}) \right\} \\ &= (\bar{y}_0)_i + \frac{\bar{\sigma}}{2} \left[ \log_e \left( \int_0^{\infty} \bar{r} \bar{p}(\bar{r})_i d\bar{r} \right) - \log_e(.5) \right] \end{aligned}$$

The above iterative scheme was incorporated into a FORTRAN IV program and run on an IBM 360/65. Convergence was achieved, if at all, within five complete iterations.

### 2.1.3 Results

An example of the results that one can achieve is shown in Figure 16 where  $\bar{p}(\bar{r})$  is given against  $\bar{r}$  for various values of  $\bar{\sigma}$  at one particular  $\bar{H}$ . A different choice of  $\bar{H}$  would produce a different family of curves. It should be noted that the behavior that was predicted by Figure 4 is substantiated and one finds an increase in  $\bar{r}_c$  and subsequent decrease in  $\bar{p}(0)$  with an increase in  $\bar{\sigma}$ . Presumably this will affect  $h_c(r)$  and, consequently, the overall thermal resistance of the interface.

A natural question to ask is: if various pressure distributions, resulting from different pairs of  $\bar{\sigma}$  and  $\bar{H}$ ,



**PRESSURE DISTRIBUTION AS FUNCTION OF  
ROUGHNESS AND HARDNESS FOR SPHERICAL SURFACES  
FIG. 16**

are compared, how close will the distributions be to each other throughout the range of  $\bar{r}$  if they are chosen so as to agree at  $\bar{r} = 0$ ? That is, given that

$$\bar{p}_1(0) = \bar{p}_2(0)$$

then will

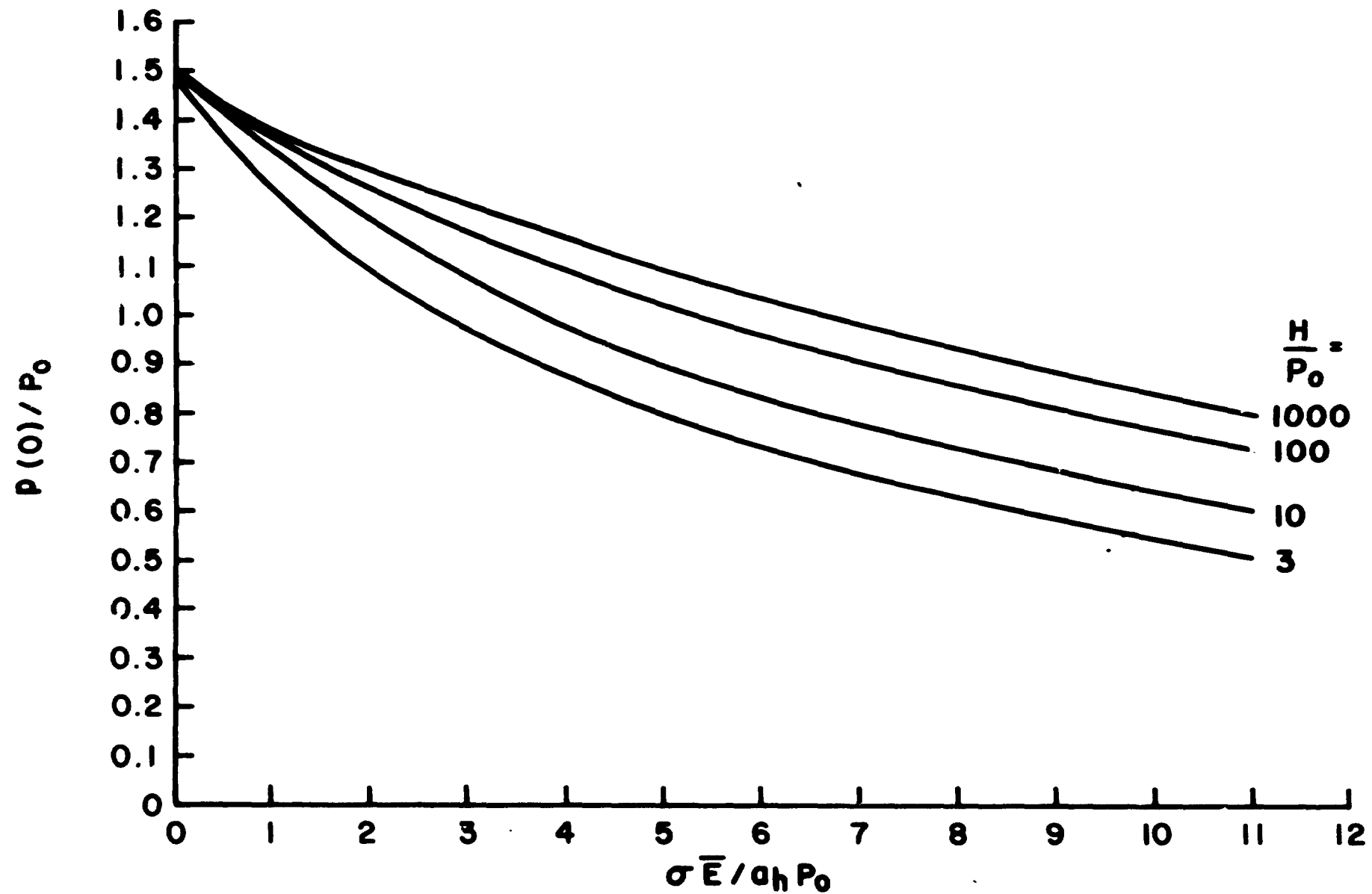
$$\bar{p}_1(\bar{r}) \stackrel{?}{=} \bar{p}_2(\bar{r})$$

Intuitively one expects the agreement to be good since the curves start at the same level at  $\bar{r} = 0$ , have the same slope at  $\bar{r} = 0$  (symmetry of the problem), have the same area underneath them (equation (25)), and probably have the same general shape (an exponential-type decay as opposed to a sharp cut-off). No attempt was made to determine if they agree in a precise mathematical sense, but through observations of various sets of solutions it was found that the pressure distributions do indeed agree with each other over their range if their centerline values agree. An example is shown in the table below. It was somewhat difficult to pick a priori a set of  $\bar{\sigma}$  and  $\bar{H}$  which would precisely yield a particular  $\bar{p}(0)$ , so some tolerance was accepted for comparison.

$\bar{\sigma}$	6.60	9.3	11.0
$\bar{H}$	10.	100.	1000.
$\bar{r}$	$\bar{p}(\bar{r})$	$\bar{p}(\bar{r})$	$\bar{p}(\bar{r})$
0	.801	.806	.801
.2	.788	.792	.787
.4	.736	.737	.731
.6	.656	.652	.644
.8	.547	.540	.530
1.0	.408	.406	.395
1.2	.283	.280	.271
1.4	.168	.169	.163
1.6	.082	.087	.085
1.8	.031	.037	.037
2.0	.009	.013	.014

Considering the allowed tolerances during the iterative solution, the agreement is excellent.

The above allows one to conclude that all one needs to determine  $\bar{p}(\bar{r})$  is  $\bar{p}(0)$  which is, in itself, uniquely determined from  $\bar{\sigma}$  and  $\bar{H}$ . The relationship between  $\bar{\sigma}$ ,  $\bar{H}$ , and  $\bar{p}(0)$  can be determined from the iterative procedure mentioned above. Figures 17 and 18 show this relationship in two different ways. It should be noted that either graph could be used to reconstruct the other.



CENTERLINE PRESSURE FOR SPHERICAL SURFACES  
AS A FUNCTION  $\bar{\sigma}$  AND  $\bar{H}$

FIG. 17

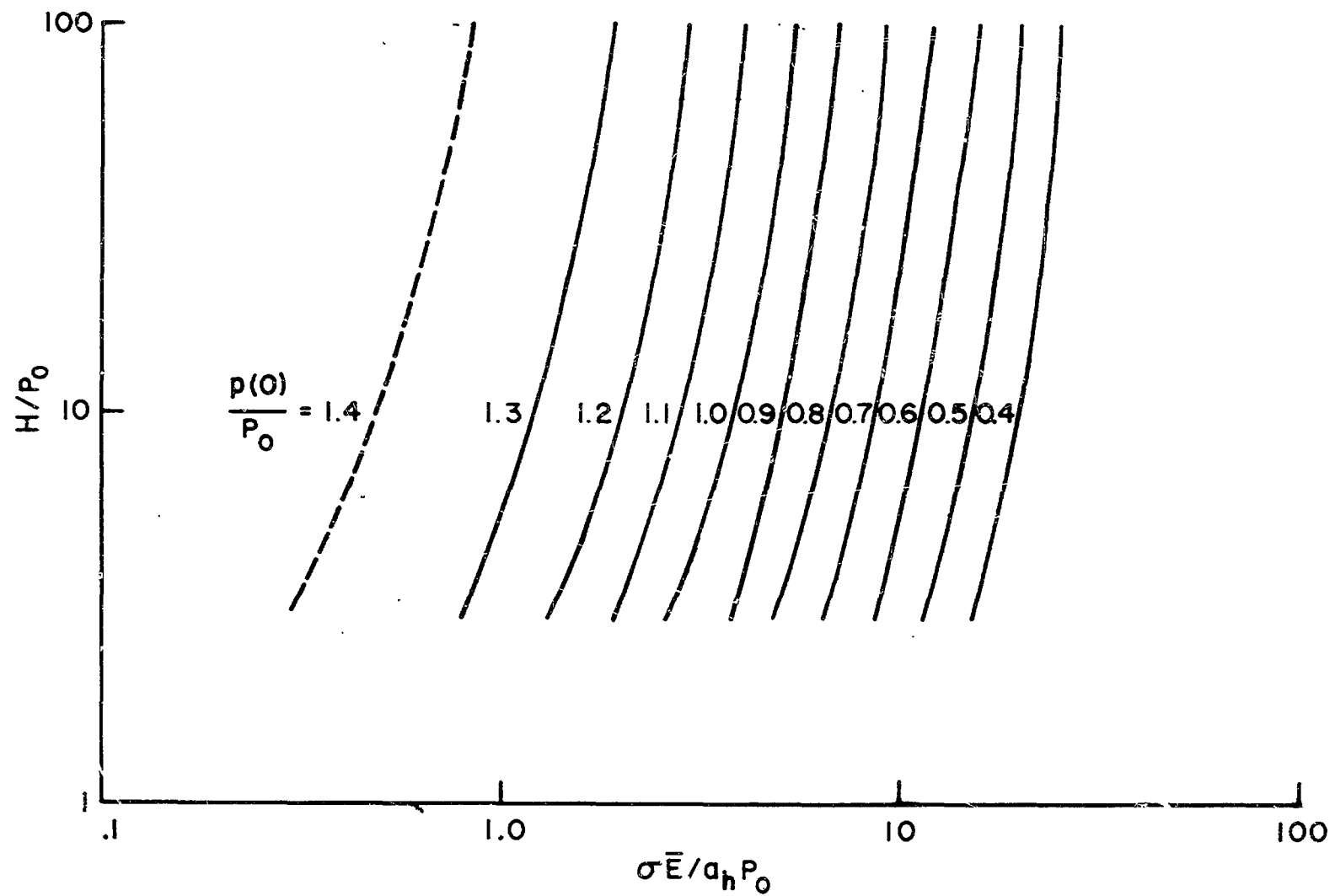


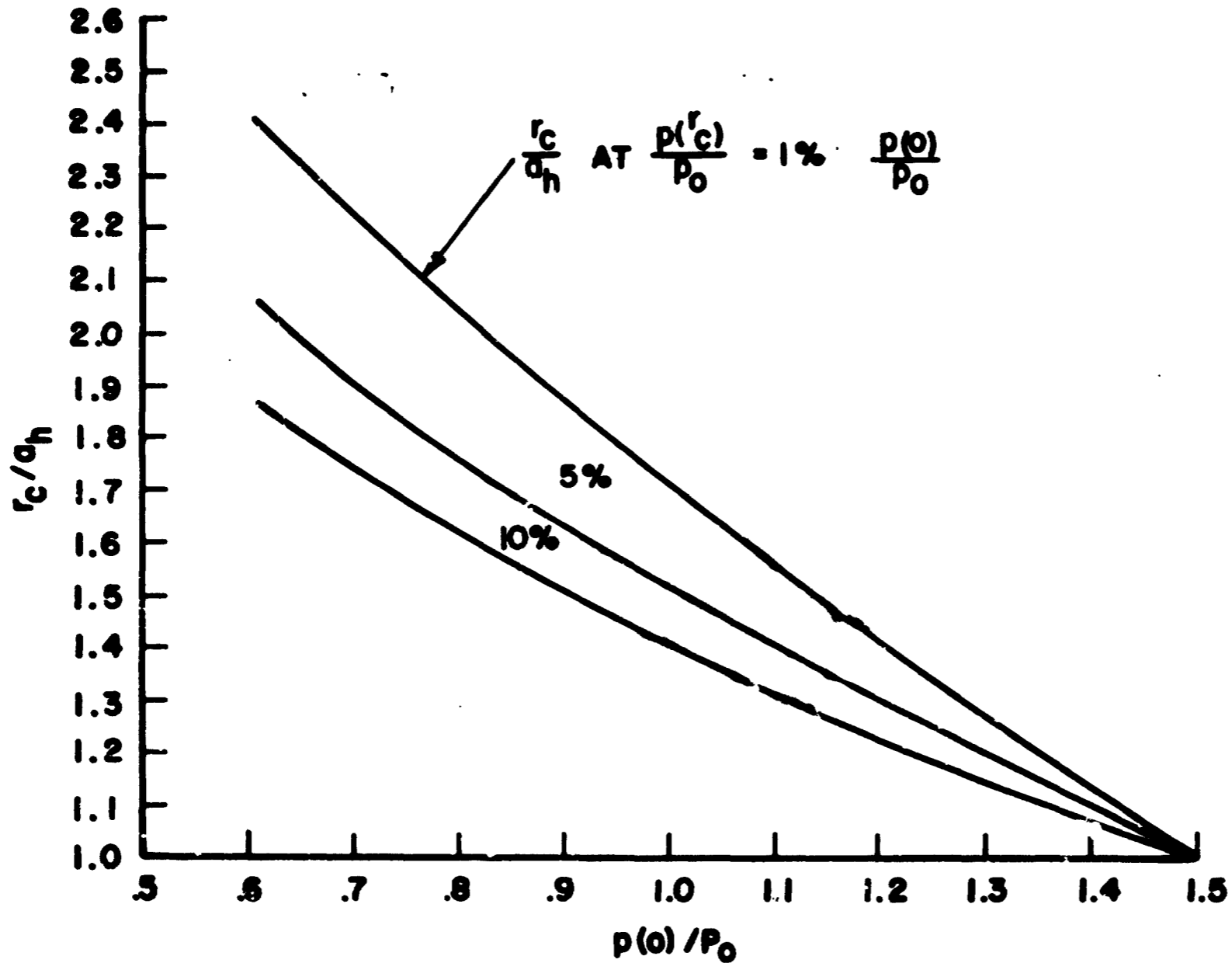
FIG. 18

A reasonable choice of physical variables indicate that the expected range of  $\bar{H}$  (or  $\bar{H}^*$ ) is

$$100 < \bar{H} < 1000$$

and from Figures 17 and 18 it can be seen that in this range  $\bar{p}(0)$  is a strong function of  $\bar{\sigma}$  and a weak function of  $\bar{H}$ . Therefore a further conclusion might be that the hardness ( $H$  or  $H^*$ ) of the asperities has little effect on the final pressure distribution and the assumption that the asperities deform plastically is not a critical one.

A variable of interest is the radius of contact,  $\bar{r}_c$ . Because of the conclusions drawn above, the radius of contact can be considered a function of the centerline pressure,  $\bar{p}(0)$ , only. The minimum value of  $\bar{r}_c$  is when the roughness is zero or when  $\bar{p}(0) = 1.5$ . At this value  $r_c = a_h$  and  $\bar{r}_c = 1$ . Since the pressure distribution for  $\bar{\sigma} \neq 0$  falls off in an exponential-like decay rather than in a sharp drop as it does for  $\bar{\sigma} = 0$ , there is no definite point where one can say that  $\bar{p}(\bar{r}_c) = 0$ . One must, instead, define the radius of contact in an arbitrary manner much like that in which the thickness of a boundary layer is defined. The criterion used here is to define the radius of contact as the radius at which the pressure is a certain percentage of the centerline pressure. Three levels are considered: ten, five, and one percent. In Figure 19 the relationship between  $\bar{r}_c$  and



**RADIUS OF CONTACT AT DIFFERENT PRESSURE LEVELS**

**FIG. 19**

$\bar{p}(0)$  is shown for these three levels. One sees that a fifty percent drop in  $\bar{p}(0)$  leads to an eighty percent increase in  $\bar{r}_c$  (at the 5% level) and, therefore, over a two hundred percent increase in the area of contact.

#### 2.1.4 Discussion and Summary

In the introduction it was mentioned that the problem of a rough spherical contact had been considered before [62,75,68]; but, because of the non-dimensional variables which were chosen, the published results could not be used for any arbitrary set of parameters. While the effect was demonstrated, each change in governing parameters required a new solution. The main contribution here is that all necessary information is reduced to two figures: one such as Figure 17 or 18 which shows the relationship between  $\bar{p}(0)$  and  $\bar{\sigma}$  and  $\bar{H}$ , and one such as Figure 20 which is a "master" graph and which shows the relationship between  $\bar{p}(\bar{r})$  and  $\bar{p}(0)$ . By choosing the proper  $\bar{p}(0)$  from Figure 17 or 18 for a prescribed  $\bar{\sigma}$  and  $\bar{H}$ , one can determine the rest of the pressure distribution,  $\bar{p}(\bar{r})$ , from Figure 20.

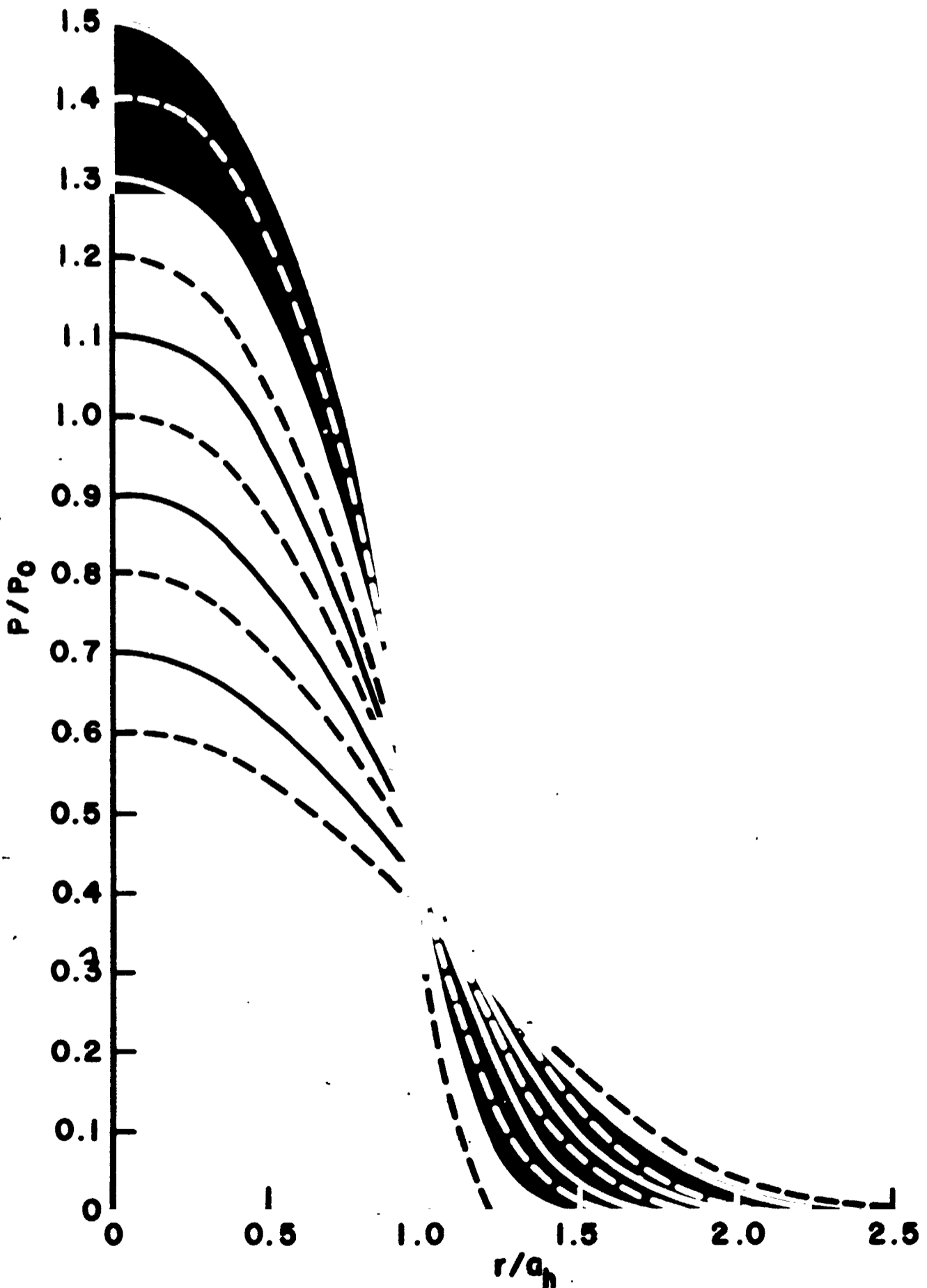
Consider the following example:

Assume a wavy surface in the shape of a sinusoid of the form

$$y = A \sin(fx)$$

The radius of curvature at a summit is

$$R = \frac{1}{2f^2}$$



MASTER GRAPH FOR SPHERICAL SURFACES  
FIG. 20

Furthermore assume that the peak-to-trough height is  $50 \cdot 10^{-6}$  inches/inch or

$$A = 25 \cdot 10^{-6} \text{ inches}$$

$$f = 2\pi \text{ cycles/inch}$$

In this case  $R = 10^3$  inches and

$$\bar{R} = \frac{R_1 R_2}{R_1 + R_2} = 500 \text{ inches}$$

If the material is steel, then

$$E = 30 \cdot 10^6 \text{ psi}$$

$$\nu = .3$$

$$H = 3 \cdot 10^5 \text{ psi}$$

and

$$\bar{E} = 51.7 \cdot 10^6$$

If the applied load is 1000 pounds then

$$a_h = .283 \text{ inches}$$

$$p_0 = 4000 \text{ psi}$$

$$\bar{H} = 75$$

If  $\sigma = 32 \cdot 10^{-6}$  inches, then

$$\bar{\sigma} = 1.46$$

and if  $\sigma = 150 \cdot 10^{-6}$  inches, then

$$\bar{\sigma} = 6.85$$

From Figure 17 we see that

$$\bar{p}(0) = 1.3 \quad \text{at} \quad \bar{\sigma} = 1.46$$

$$\bar{p}(0) = .9 \quad \text{at} \quad \bar{\sigma} = 6.85$$

We can, therefore, predict the pressure distribution,  $\bar{p}(\bar{r})$ , using Figure 20. For example we see that

$\sigma$	$32 \cdot 10^{-6}$ in.	$150 \cdot 10^{-6}$ in.
$\bar{\sigma}$	1.46	6.85
$\bar{r}$	$\bar{p}(\bar{r})$	$\bar{p}(\bar{r})$
0.	1.3	.9
.5	1.13	.78
1.0	.39	.44
1.5	0	.10
2.0	0	0

We can use Figure 19 to find that

$\bar{\sigma}$	$\bar{p}(0)$	$\bar{r}_c$ 1%	$\bar{r}_c$ 5%	$\bar{r}_c$ 10%
1.46	1.3	1.28	1.20	1.14
6.85	.9	1.87	1.63	1.50

It is seen from the above that the effect of the roughness is significant for values of waviness and roughness which are common in manufactured products.

Although the non-dimensional variables used here present, for the most part, a clear and general picture of the problem, it is difficult with them to immediately see the effect that the changing of the load has on the pressure distribution, radius of contact, etc. One observes that

- 62 -

$$a_h \propto F^{1/3}$$

$$p_c \propto F^{1/3}$$

$$\bar{\sigma} \propto \frac{1}{F^{2/3}}$$

$$\bar{H} \propto \frac{1}{F^{1/3}}$$

A change in  $F$  will produce a weak change in  $\bar{H}$ . Since the results here are not strongly dependent on  $\bar{H}$  in the first place, one can ignore any effect of  $F$  on  $\bar{H}$  without too much error in the final result. Then, from Figure 17, a decrease in  $F$  which causes an increase in  $\bar{\sigma}$ , brings about a decrease in  $\bar{p}(0)$ . From either Figure 19 or 20 one sees that the original decrease in  $F$  which causes a decrease in  $\bar{p}(0)$  also increases  $\bar{r}_c$ . But since

$$r_c = a_h \bar{r}_c$$

and since a decrease in  $F$  causes a decrease in  $a_h$  it is uncertain how the product of these two variables changes and, therefore, how the actual radius of contact changes.

This section has shown

- (a) how in the contact of two rough spherically shaped surfaces the behavior can be described by two parameters,  $\bar{\sigma}$  and  $\bar{H}$ ;
- (b) how the centerline pressure,  $\bar{p}(0)$ , determines the remainder of the pressure curve  $\bar{p}(\bar{r})$  with good engineering accuracy;
- (c) how  $\bar{p}(0)$  is a strong function of  $\bar{\sigma}$ , a weak function of  $\bar{H}$ , and not a function of any other parameter;
- (d) and how for reasonable values of material properties and loads the effect of roughness on the pressure distribution can be significant.

In the following sections the above procedure will be repeated for disks with and without center holes. After this is done the resulting information on pressure distributions for the different models will be converted into data on contact conductance and the total thermal resistance of certain joints will be presented.

## 2.2 Contact of Two Plates without Holes

### 2.2.1 Model

The model used for the contact of two plates which do not have a center hole is the contact of two disks of finite radius and finite thickness as shown in Figure 6. It is assumed that

- (a) the disks deform elastically;
- (b) asperities deform plastically;
- (c) asperity height distribution above a mean plane is Gaussian;
- (d) asperity contact is normal with no tangential component;
- (e) the contact (i.e., pressure distribution and deformation) will be symmetric about an axis through the center of the area in contact;
- (f) both disks have the same dimensions, material characteristics and loading distribution.

As mentioned before, no solution to the elastic deformation of a disk with finite radius exists in the literature. The method used here to find such a solution is an infinite Fourier-Bessel series technique. A detailed description is given in the Appendix and only a brief outline of the procedure is presented below to indicate the general nature of the solution.

Fourier series analysis is used successfully in the solution of the Laplacian

$$\nabla^2 T = 0$$

in potential field problems because it is relatively easy to pick the final solution, save for constants, out of the family of possible solutions. This is largely because there is only one condition to satisfy at any boundary. A problem in elasticity, however, requires the solution to a biharmonic equation,

$$\nabla^4 \phi = 0$$

The biharmonic not only introduces a larger family of solutions from which to choose, but it also requires two conditions to be satisfied at each boundary. The sum effect is to make it difficult if not impossible for one to choose out of the available solutions the particular one which will satisfy the given boundary conditions, of which there are eight in an axially-symmetric problem. It is not difficult, however, to choose a solution which will satisfy four boundary conditions, two of which are on the same axis and are a homogeneous pair. The technique used with multiple Fourier-Bessel series is to divide the problem into parts where only four boundary conditions are required. By superposition the sections are reunited into the original problem. Further explanation and an example are found in the Appendix along with the solutions to various problems used in this paper.

Suffice it to say that one can obtain solutions in the form

$$\sigma_z = a_0 + \sum_{n=1}^{\infty} a_n f_1(r, z) + \sum_{m=1}^{\infty} b_m f_2(r, z) + \dots$$

The first term,  $a_0$ , is the zeroeth term and is the average value of the unknown (e.g.,  $\sigma_z$ ). The remaining series are the Fourier-Bessel expansions which have an average value of zero in the homogeneous direction. In the body of this report, the solutions are presented in shortened parametric forms, the full expansions of which can be found in the Appendix.

There are two possible areas of difficulty in using an infinite series solution to the elastic problem: if convergence is not rapid a numerical result will be difficult and expensive to get; and, since the infinite series used here are superpositions of oscillating functions, a numerical result will be in the form of an oscillation superimposed on the average value. The larger the number of terms, the greater the frequency of oscillation. A deflection calculated with such an infinite series, for example, would not predict a smooth continuous surface but a wavy one. Thus when one introduced the presence of asperities, the mathematics would not recognize the waviness as a spurious oscillation but would consider it as a true representation of the surface.

Both these problems can be overcome by using truncation terms,  $t_n$ , in a finite series so that one would have

$$\sigma_z = a_0 + \sum_{n=1}^N t_n a_n f_1(r, z) + \dots$$

instead of the original infinite series. Since the average value of each term in the series is zero in the homogeneous direction, the truncation term does not alter the average value,  $a_0$ , of the variable - here  $\sigma_z$ . The truncation term allows one to use only  $N$  terms in the series and dampens out the oscillations by decreasing the effect of higher frequency terms. The net result is to make the predictions as smooth and continuous mathematically as they are physically. The truncation terms are discussed further in the Appendix and in [88].

With the above in mind, one can state that for the problem shown in Figure 6, the governing equations are:

(a) deformation of solid disks

$$\bar{w}(\bar{r}) = \sum_7 [\bar{r}, \bar{a}, \bar{r}_0, \bar{p}(\bar{r})] - \sum_8 [\bar{r}, \bar{a}, \bar{r}_0, \bar{p}(\bar{r})] - \sum_9 [\bar{r}, \bar{a}, \bar{r}_0, \bar{p}(\bar{r})] \quad (27)$$

(b) pressure distribution at asperities

$$\bar{p}(\bar{r}) = \frac{\bar{H}}{2} \operatorname{erfc} \left[ \frac{\bar{y}_0 + 2\bar{w}(\bar{r})}{\bar{\sigma}\sqrt{2}} \right] \quad (28)$$

(c) and for load

$$\int_0^{\bar{a}} \bar{r}\bar{p}(\bar{r})d\bar{r} = \frac{\bar{r}_0^2}{2} \quad (29)$$

The above are written directly in non-dimensional form. The variables are

$$p_0 = \frac{F}{\pi r_0^2} \quad \bar{H} = \frac{H}{p_0} \quad \bar{\sigma} = \frac{\sigma E}{bp_0}$$

$$\bar{p} = \frac{p}{p_0} \quad \bar{y}_0 = \frac{y_0 E}{bp_0}$$

$$\bar{r}_c = \frac{r_c}{b} \quad \bar{w} = \frac{wE}{bp_0}$$

$$\bar{r} = \frac{r}{b} \quad \bar{r}_0 = \frac{r_0}{b}$$

The difference in the non-dimensional variables between the above and that used before is that the radial variables are

divided by the disk thickness rather than the contact radius. Also, in equation (28) the factor "2" appears because  $\bar{w}(\bar{r})$  is the deflection for one plate only.

The above set of equations is solved in exactly the same way as was done for the spherical surfaces. However, rather than present the solutions at this point as was done in the previous section, the midplane stress of a disk, the classical solution to the contact problem, will be discussed.

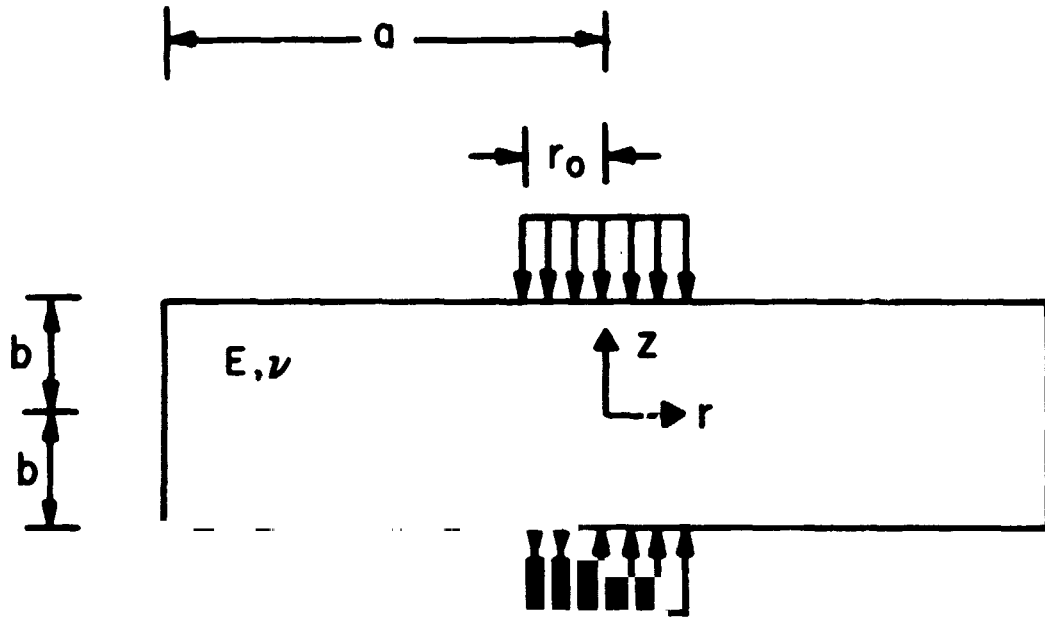
### 2.2.2 Midplane Stress

The midplane stress of a disk of thickness  $2b$  has been used before as the interfacial pressure distribution for the contact of two smooth disks of thickness  $b$  each [79,80]. It was shown by Gould [83] that this approximation overestimates the actual radius of contact. It is useful, however, to examine the midplane stress distribution so that one can compare published results with those calculated here, thus indicating the accuracy of the methods used here. One can also investigate behavior common to the contact problem without the complexity of the contact problem since an effect that is appreciable to one should be appreciable to the other.

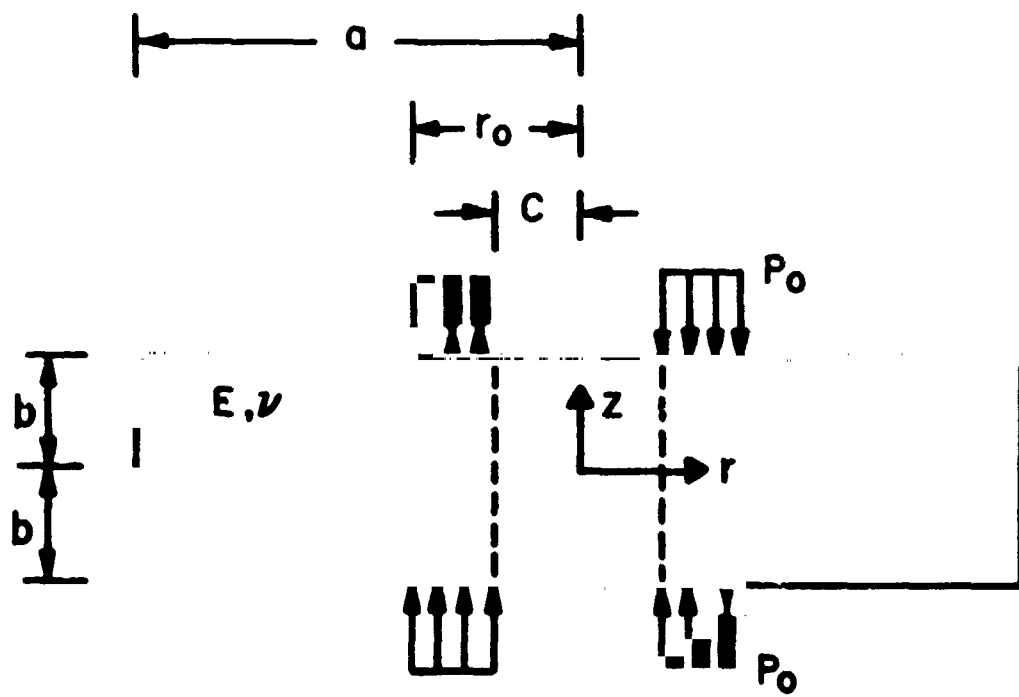
For the model shown in Figure 21a and the boundary conditions

$$\text{at } z = \pm b \quad \sigma_z = -p_0 \quad 0 < r < r_0$$

$$\sigma_z = 0 \quad r_0 < r < a$$



MODEL FOR MIDPLANE STRESS  
IN DISK WITHOUT HOLE



MODEL FOR MIDPLANE STRESS  
IN DISK WITH HOLE

FIG. 21

$$\tau_{rz} = 0$$

$r = 0$  stresses finite

$$r = a \quad \sigma_r = 0$$

$$\tau_{rz} = 0$$

the midplane stress is

$$\left. \frac{\sigma_z}{p_0} \right|_{\bar{z}=0} = - \frac{\bar{r}_0^2}{\bar{a}^2} + \sum_1 (\bar{r}, \bar{a}, \bar{r}_0) + \sum_2 (\bar{r}, \bar{a}, \bar{r}_0) \quad (30)$$

If one neglects the boundary condition

$$\text{at } r = a \quad \sigma_r = 0$$

the midplane stress then becomes

$$\left. \frac{\sigma_z}{p_0} \right|_{\bar{z}=0} = - \frac{\bar{r}_0^2}{\bar{a}^2} + \sum_3 (\bar{r}, \bar{a}, \bar{r}_0) \quad (31)$$

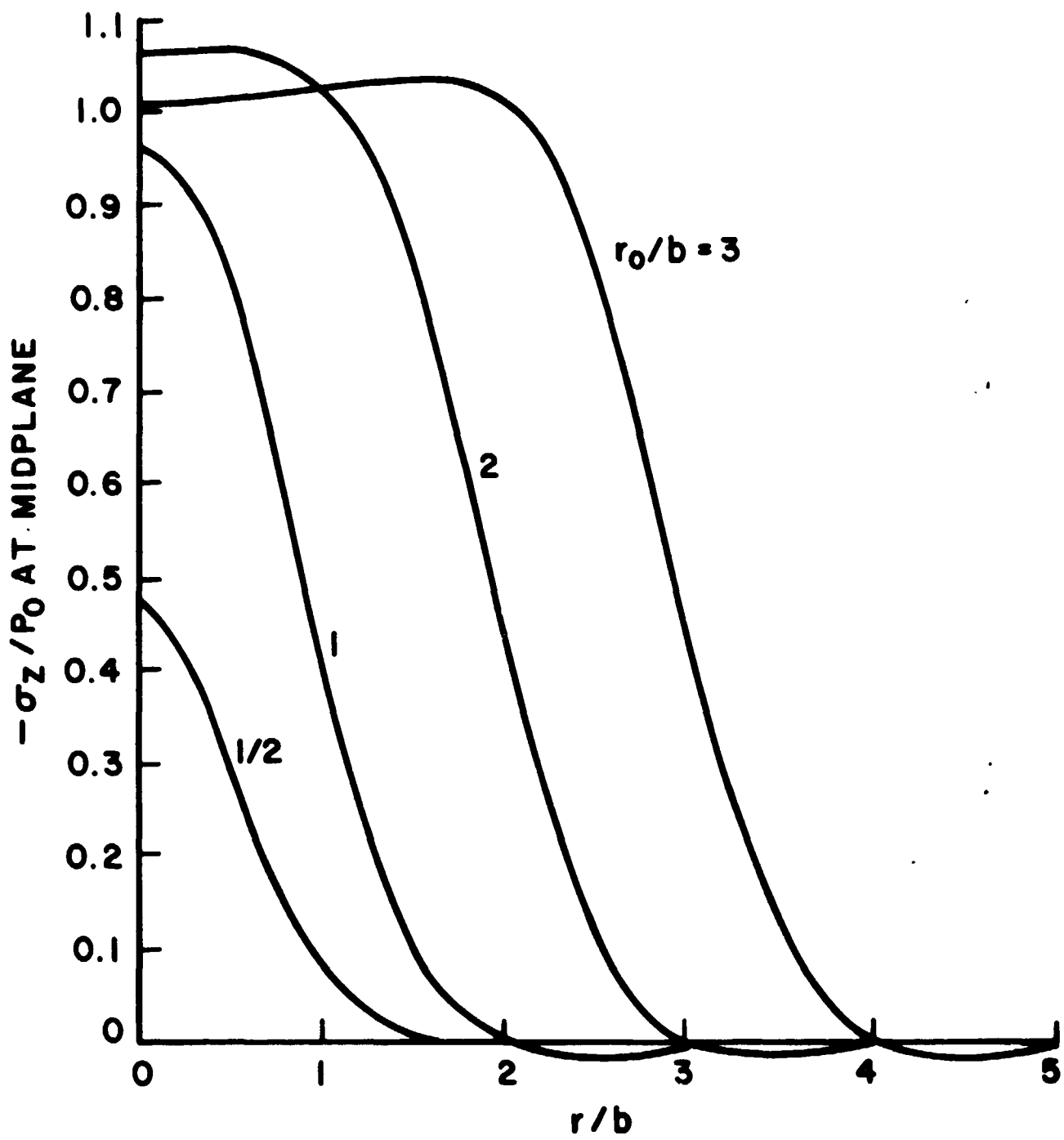
As is shown in the Appendix, at large  $\bar{a}$  equation (31) is equivalent to those equations used in [79,80] which were derived using Hankel transforms for a disk of infinite radius.

If one compares the results for large  $\bar{a}$  from (30) or (31) to those published, one can estimate the accuracy of the multiple series method used in this report. Fortunately, access was had to the computed numerical output used in [80]. The agreement between (30) and the data from [80] is excellent. This is, of course, to be expected since at large  $\bar{a}$  (30) is equivalent to the formula used in [80]. Figure 22 shows the midplane stress distribution for various values of  $\bar{r}_0$  when  $\bar{a}$  is sufficiently larger than  $\bar{r}_0$  as to be considered infinite. Just how much larger this must be will be discussed later.

An immediate observation made from Figure 22 is that the curves for  $\bar{r}_0 = 2$  and  $\bar{r}_0 = 3$  are remarkably similar and seem to be linear translations of each other over a wide range. It was found by comparing different numerical solutions that for  $\bar{r}_0 > 2$  the curves for different  $\bar{r}_0$  are similar for  $\bar{r} > \bar{r}_0 - 1$ . The stress distribution in this range is shown in Figure 23. For values of  $\bar{r}_0 > 2$ , therefore, one can reconstruct the midplane stress distribution without resorting to equations such as (30) or (31).

Another observation is that if one draws a tangent to the curve at  $\bar{r} = \bar{r}_0$  and then extends this tangent so that it intersects the abscissa, one has an estimate of the radius of contact for the actual case of two contacting disks which is close to that predicted by Gould [83]. The prediction is

$$\bar{r}_c = \bar{r}_0 + 0.65 \quad (32)$$



MIDPLANE STRESS OF DISK OF INFINITE  
RADIUS AND NO CENTER HOLE  
FIG. 22

which compares favorably to that obtained in [83],

$$\bar{r}_c = \bar{r}_0 + 0.50 \quad (19)$$

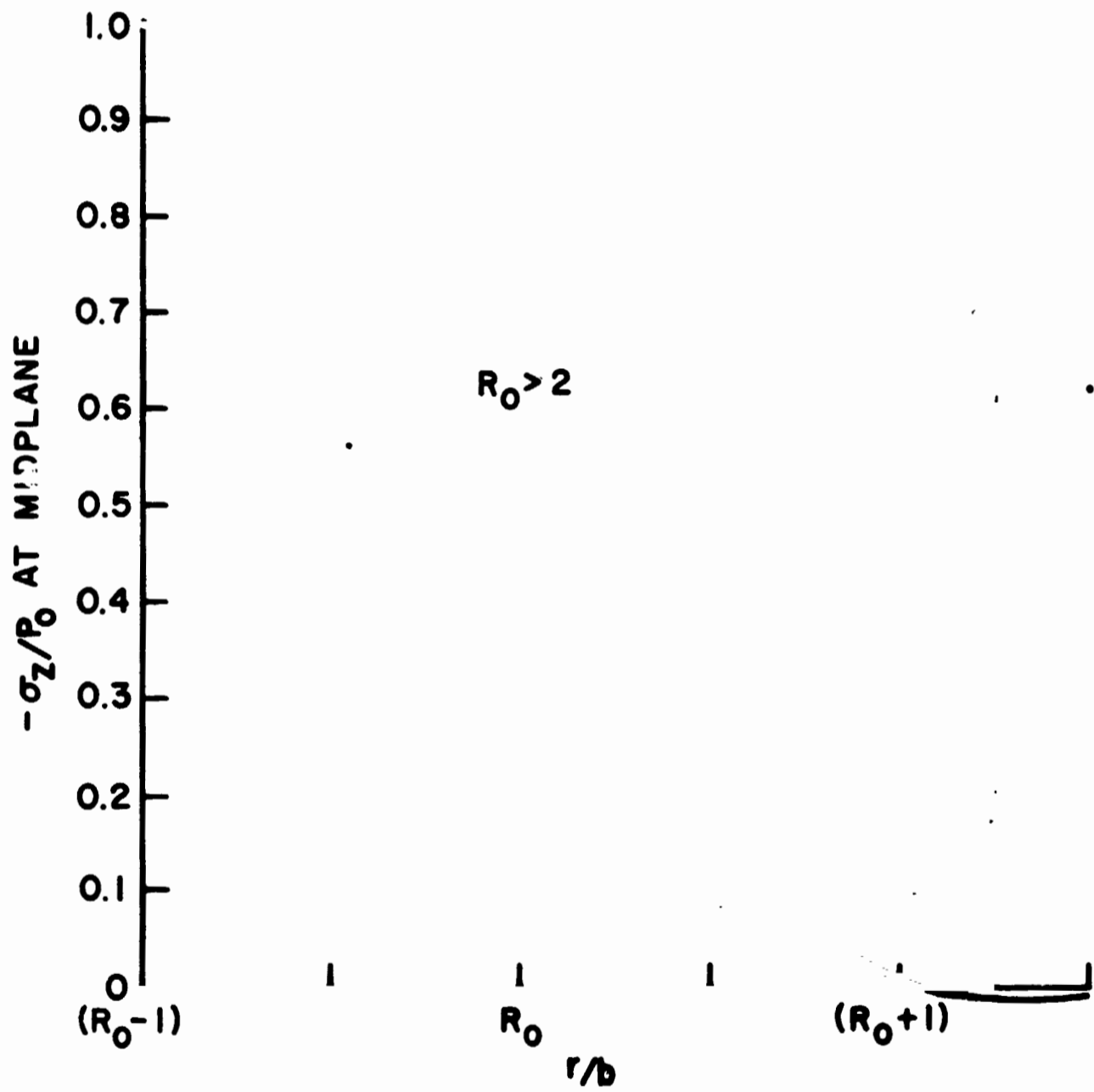
Thus an estimate can be made of the contact area from the midplane stress curve by not only neglecting the tensile stress zone but by also ignoring the flaring of the distribution immediately before this zone.

A question asked earlier was how much greater does  $\bar{a}$  have to be than  $\bar{r}_0$  for the disk to be considered to be of infinite radius? Or, stated in a different manner, for a fixed  $\bar{r}_0$ , how does  $\sigma_z/p_0$  change as  $\bar{a}$  increases? For  $\bar{a} = \bar{r}_0$  the pressure distribution is trivial:  $\sigma_z/p_0 = -1$ . For  $\bar{a} \gg \bar{r}_0$  the pressure distribution is like that shown in Figure 23. How the transition occurs from one to another is shown in Figure 24. It is assumed that any  $\bar{r}_0$  can be chosen to investigate the effect of changing  $\bar{a}$  and the results will be common to all values of  $\bar{r}_0$  (except possibly for very small ones which are not of much practical interest). The particular one used here for comparison is  $\bar{r}_0 = 1$ .

As is shown in Figure 24, when

$$\bar{a} > 4\bar{r}_0$$

no further change occurs to the midplane pressure distribution in the entire range. When



MIDPLANE STRESS OF DISK OF INFINITE RADIUS AND NO CENTER HOLE

FIG. 23

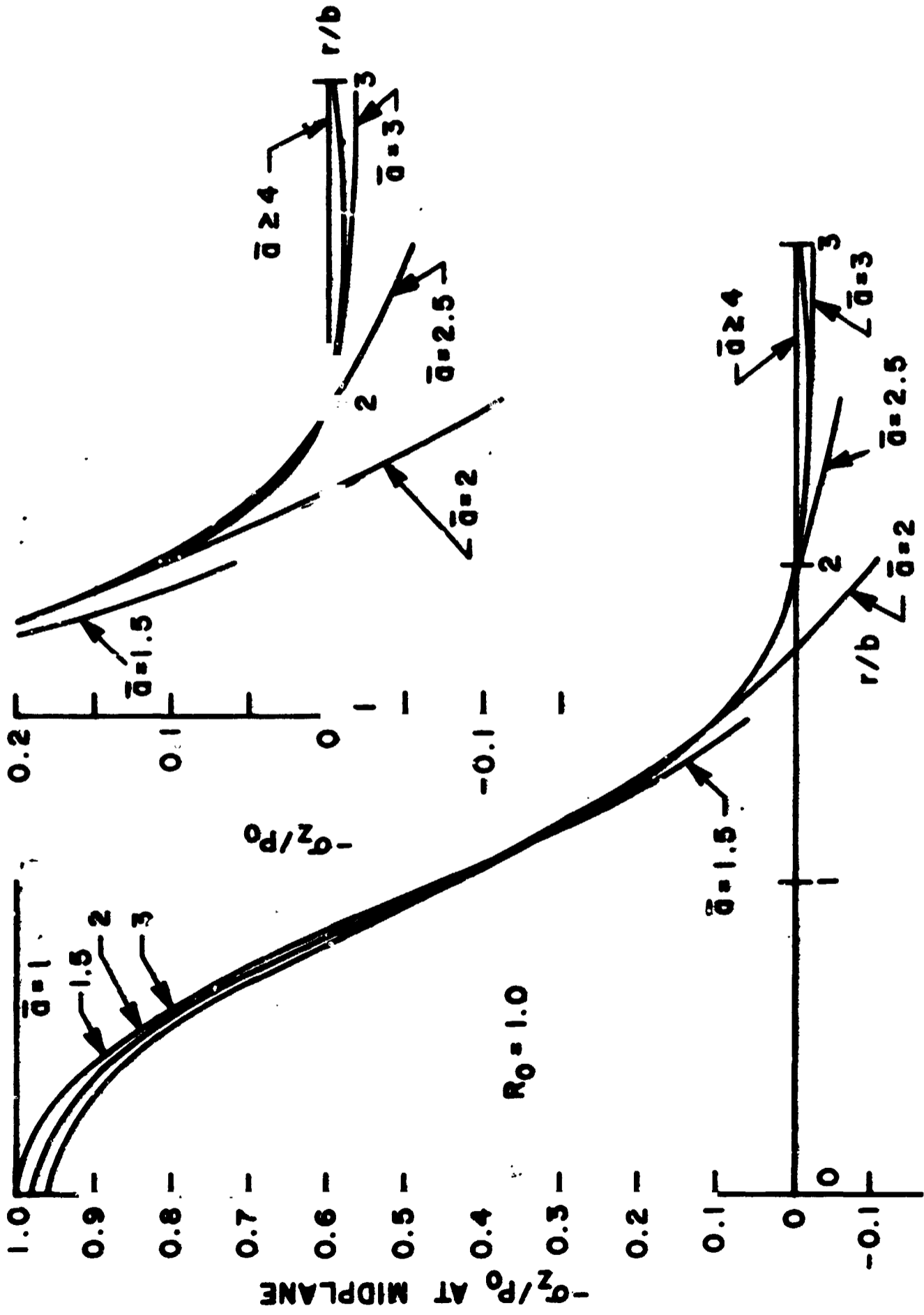


FIG. 24

1  
2  
3  
4  
5  
6  
7  
8  
9  
10  
11  
12  
13  
14  
15  
16  
17  
18  
19  
20  
21  
22  
23  
24  
25  
26  
27  
28  
29  
30  
31  
32  
33  
34  
35  
36  
37  
38  
39  
40  
41  
42  
43  
44  
45  
46  
47  
48  
49  
50  
51  
52  
53  
54  
55  
56  
57  
58  
59  
60  
61  
62  
63  
64  
65  
66  
67  
68  
69  
70  
71  
72  
73  
74  
75  
76  
77  
78  
79  
80  
81  
82  
83  
84  
85  
86  
87  
88  
89  
90  
91  
92  
93  
94  
95  
96  
97  
98  
99  
100

$$\bar{a} > 2.5\bar{r}_0$$

no further change occurs in the region where the stress is compressive: i.e., all differences between curves for different values of  $\bar{a}$  are in the region of tensile stress. Thus one can assume that if  $\bar{a} > 4\bar{r}_0$ , the disk may be considered to be of infinite extent and any boundary condition at the edge  $\bar{r} = \bar{a}$  can be ignored. If  $\bar{a}$  is large enough, therefore, one can use equation (31) in calculating the midplane stress rather than equation (30), which is the exact solution. Since equation (30) has two infinite series whose coefficients must be solved for simultaneously and since equation (31) has just one series with no need for simultaneous solution of coefficients, it is both more convenient and less expensive to use (31).

The last conclusion to be drawn from the work done on the midplane stress is that Poisson's ratio does not affect the stress distribution in any way. This can be seen from (30) and (31) which are not influenced at all by  $\nu$ .

The conclusions drawn, then, from the study of midplane stress distribution of a disk of thickness  $2b$  are:

- (a) the methods used here to solve the elastic deformation of a thick disk of finite radius are accurate;
- (b) an estimate of the contact area can be made by extending a tangent from the curve at  $\bar{r} = \bar{r}_0$  to the abscissa;

- (c) for  $\bar{r}_0 > 2$  and for large  $\bar{a}$ , midplane stress distributions for different  $\bar{r}_0$  are merely linear translations of each other;
- (d) if  $\bar{a} > 4\bar{r}_0$  the boundary conditions specified at  $\bar{r} = \bar{a}$  can be ignored without error and the simpler governing equation can be used;
- (e) Poisson's ratio,  $\nu$ , does not affect the midplane stress distribution.

Now that the classical single-body contact model has been examined, we shall return to the two-body model, Figure 6.

### 2.2.3 Solution

The solution to the contact of two disks where the roughness is allowed to alter the pressure distribution is achieved using the same procedure as was done for the spherical surfaces. The flow diagram given in Figure 15 can be used here with the substitution of equation numbers (27), (28), and (29) for (23), (24), and (25). The same algorithm is used to calculate  $\bar{y}_0$ .

Some difficulty is encountered, however, in the solution for the disks which is not found in the case of the spherical surfaces. In the latter there is an original curvature to the surfaces which rapidly enlarges the gap between the two bodies and quickly reduces the chances for asperity contact at any appreciable distance from the original radius of contact. In the former the gap is relatively

narrow with no original curvature to superimpose on the deflection. Thus the effect of the asperities is more pronounced than that found with the spheres, and any oscillations which occur during the solution take longer to die out. When iterating for the contact between the two disks, it becomes important to choose the proper initial stress distribution and the proper weighting parameter for subsequent estimates of pressure distributions.

Otherwise the procedure is the same as before: guess a  $\bar{p}(\bar{r})$  and substitute it into (27); take the subsequent deflection,  $\bar{w}(\bar{r})$ , and place that along with a guess for  $\bar{y}_0$  into (28); adjust the  $\bar{y}_0$  in (28) until the  $\bar{p}(\bar{r})$  it predicts satisfies (29); and finally, compare this  $\bar{p}(\bar{r})$  with the original and, if different, take the weighted average and start again. A computer program written in FORTRAN IV for the IBM 360/65 which will perform the above is listed in the Appendix.

#### 2.2.4 Results

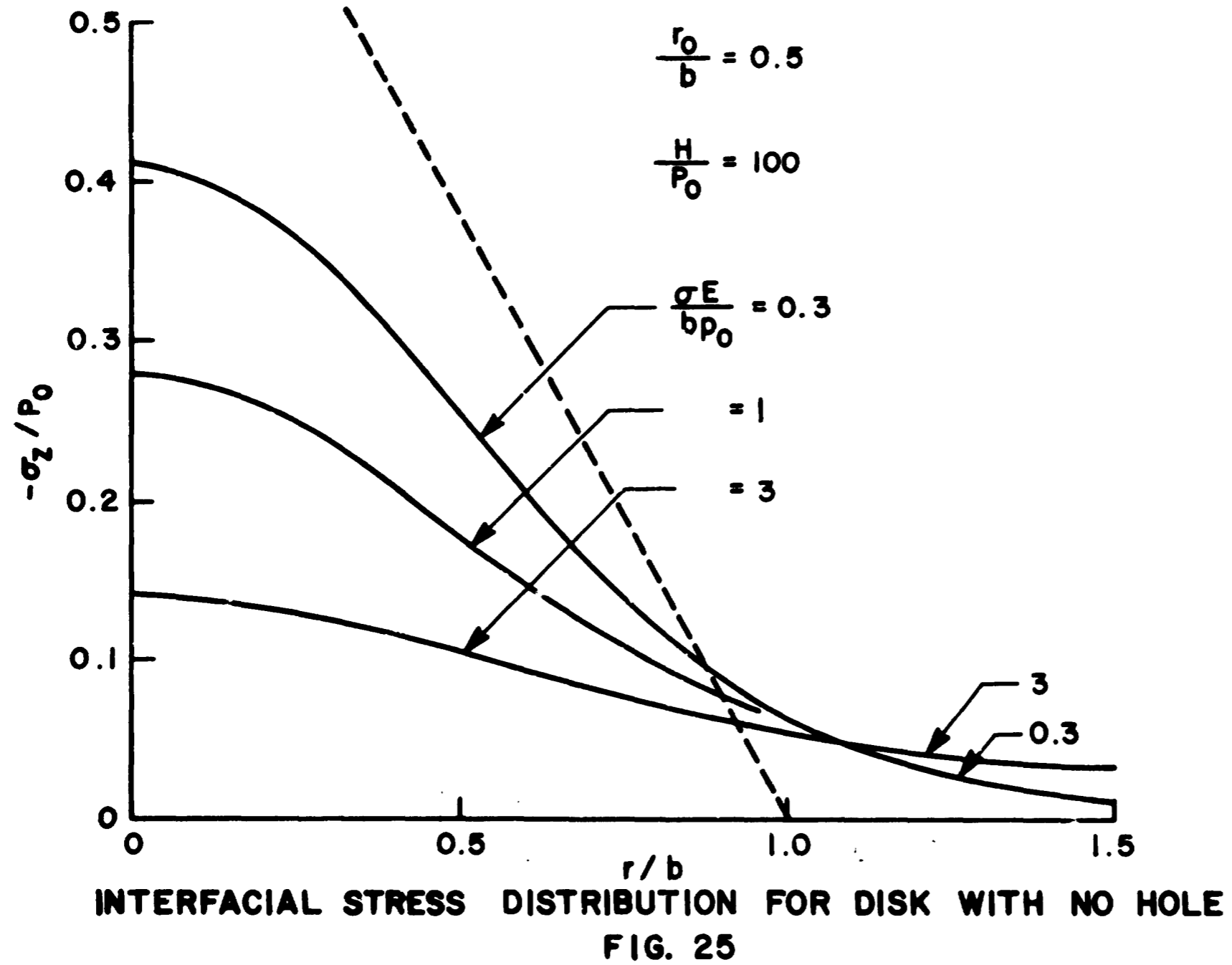
Unlike with spherical surfaces, all data concerning the contact problem of two disks cannot be expressed by one master graph. There are too many governing parameters:  $\bar{\sigma}$  and  $\bar{H}$  as before and now  $\bar{r}_0$  and  $\bar{a}$ . Physically, though, one can expect  $\bar{a}$  to be much greater than  $\bar{r}_0$ ; and, from the conclusions drawn in the previous section on midplane stress, one can treat the disk radius as infinite and no longer

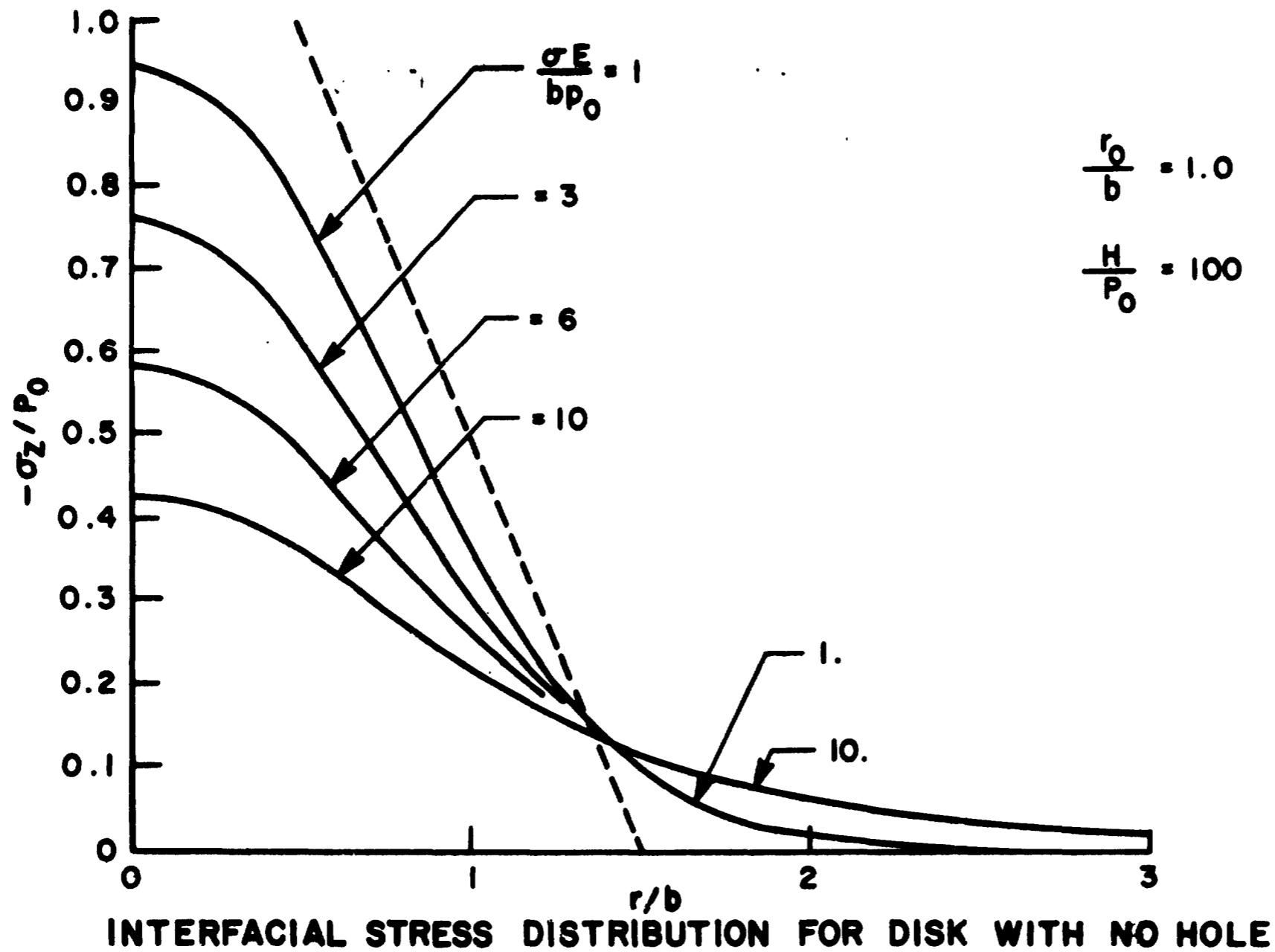
consider it a variable in the problem. This leaves  $\bar{\sigma}$ ,  $\bar{H}$ , and  $\bar{r}_0$ . Unfortunately no further reduction can be made.

For one particular  $\bar{r}_0$  one can plot the pressure distribution for various values of  $\bar{\sigma}$  at one  $\bar{H}$ . By changing  $\bar{H}$  and comparing two different distributions caused by different values of  $\bar{\sigma}$  and  $\bar{H}$  but having the same centerline pressure,  $\bar{p}(0)$ , one again sees that the distributions match. One can then plot  $\bar{p}(0)$  versus  $\bar{\sigma}$  for different values of  $\bar{H}$  and observe that  $\bar{p}(0)$  is, as before, a strong function of  $\bar{\sigma}$  and a weak function of  $\bar{H}$ . Since  $\bar{p}(\bar{r})$  is determined solely from  $\bar{p}(0)$ , one can plot  $\bar{r}_c$  versus  $\bar{p}(0)$  for different percentage levels. This is all the same as was done before except now it has to be repeated for each value of  $\bar{r}_0$ .

Data for three values of  $\bar{r}_0$  are shown in subsequent graphs:  $\bar{r}_0 = 0.5, 1.0, \text{ and } 2.0$ . In Figures 25, 26, and 27 the change in pressure distribution with changing  $\bar{\sigma}$  is shown at one value of  $\bar{H}$ . There is no data for the contact of two smooth disks without holes as there is for spherical surfaces or for disks with holes [83]. But estimates can be made using the conclusions drawn from the midplane stress curves given in section 2.2.2. These are shown in the figures as dashed lines and serve as a rough guide to the effect that roughness has on the distribution.

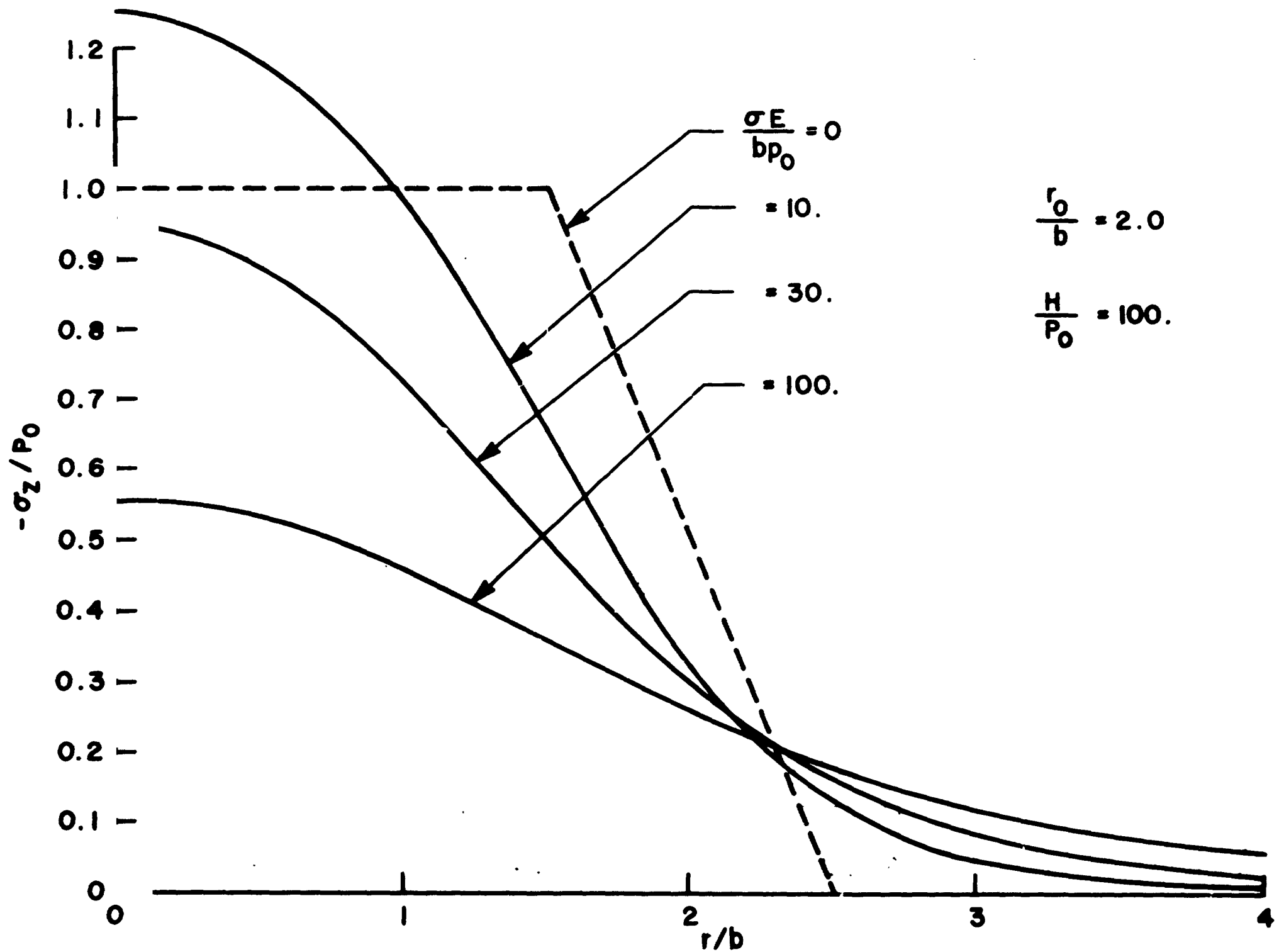
The immediate observation made is that the effect of roughness on disks is much more pronounced than that already shown for the spheres (Figure 16). This is to be





INTERFACIAL STRESS DISTRIBUTION FOR DISK WITH NO HOLE

FIG. 26



INTERFACIAL STRESS DISTRIBUTION FOR DISK WITH NO HOLE  
 FIG. 27

expected since the original curvature of the spheres draws the two surfaces apart quickly and removes any possibility for contact. It should also be noted that the range of  $\bar{\sigma}$  which influences the distribution changes markedly for each  $\bar{r}_0$ : for  $\bar{r}_0 = 0.5$  it is  $0.1 < \bar{\sigma} < 1.0$ ; for  $\bar{r}_0 = 1.0$  it is  $1.0 < \bar{\sigma} < 10$ ; and for  $\bar{r}_0 = 2.0$  it is  $10 < \bar{\sigma} < 100$ . Again this is not unexpected since a larger  $\bar{r}_0$  implies a thinner plate. A thinner plate has greater deformation and requires, therefore, a larger asperity height to cause the needed interference.

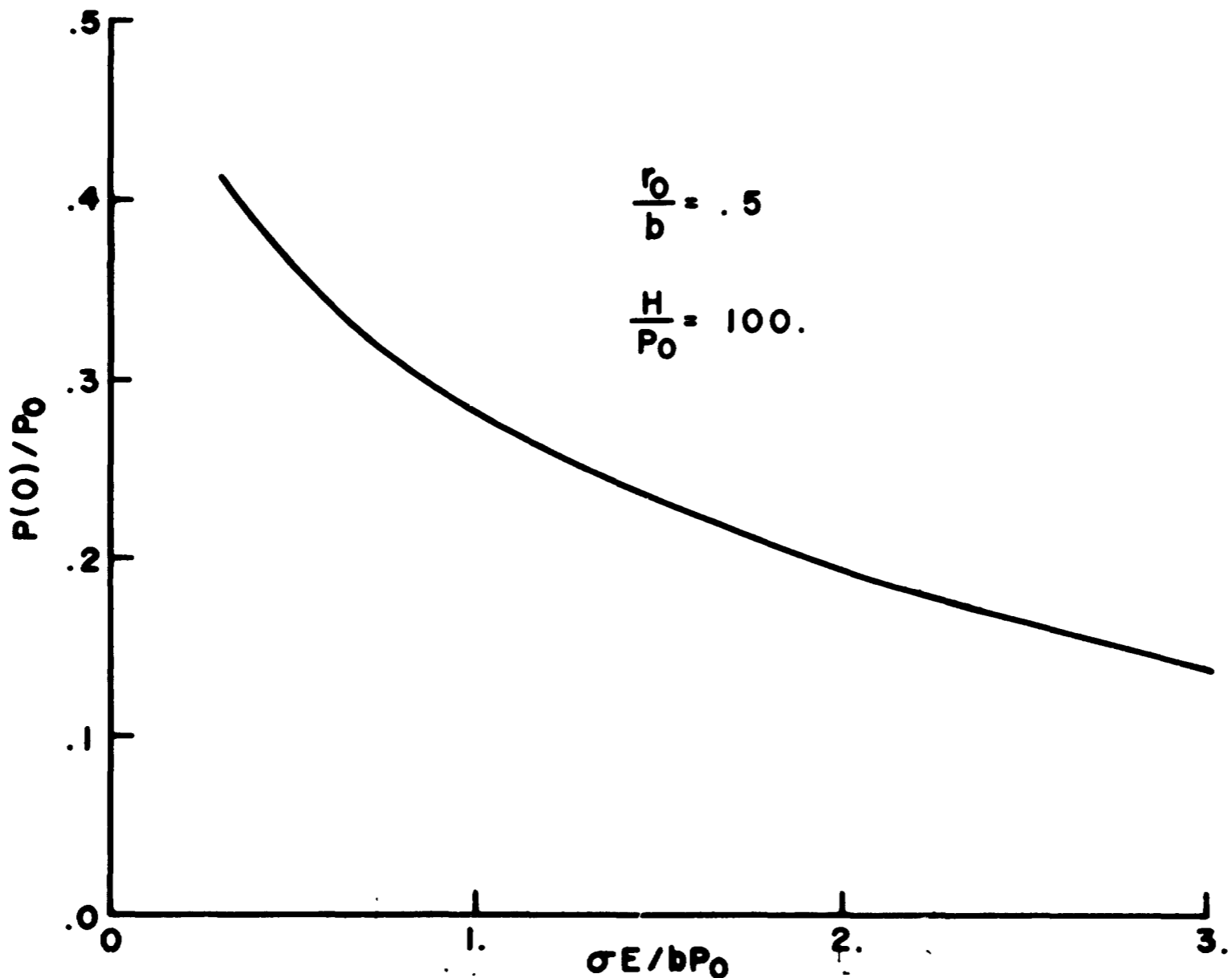
These three figures are all for a specific value of  $\bar{H}$ . If one recomputes the stress distributions for other values of  $\bar{H}$  and then compares two curves with the same value of centerline pressure,  $\bar{p}(0)$ , but not necessarily the same values of  $\bar{\sigma}$  and  $\bar{H}$ , one finds here as with the spherical surfaces that the distributions lie on each other. That is, if

$$\bar{p}_1(0) = \bar{p}_2(0)$$

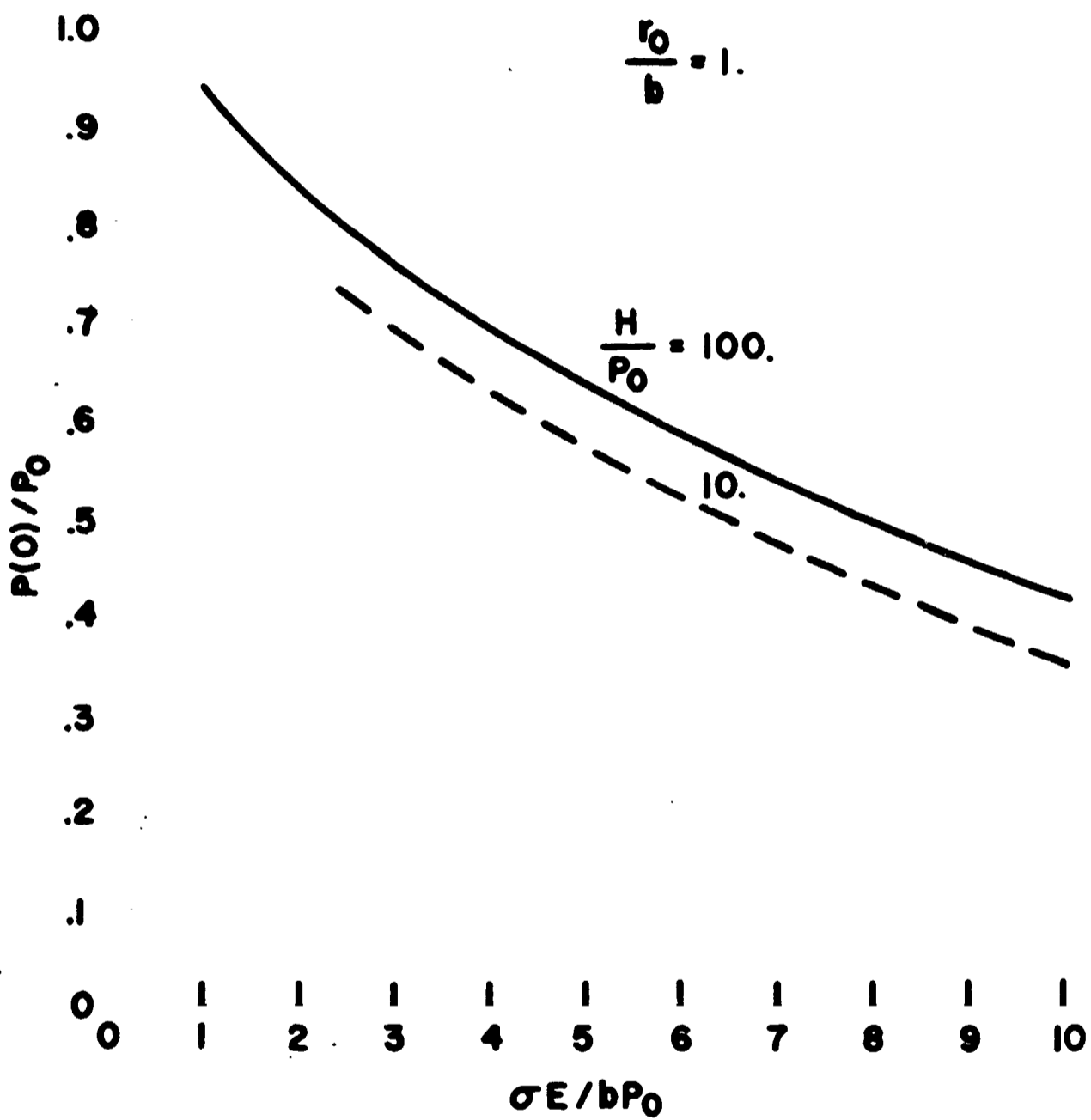
then for all  $\bar{r}$

$$\bar{p}_1(\bar{r}) \cong \bar{p}_2(\bar{r})$$

Following the same procedure as before, one can graphically illustrate the relationship between  $\bar{p}(0)$ ,  $\bar{\sigma}$ , and  $\bar{H}$ . This

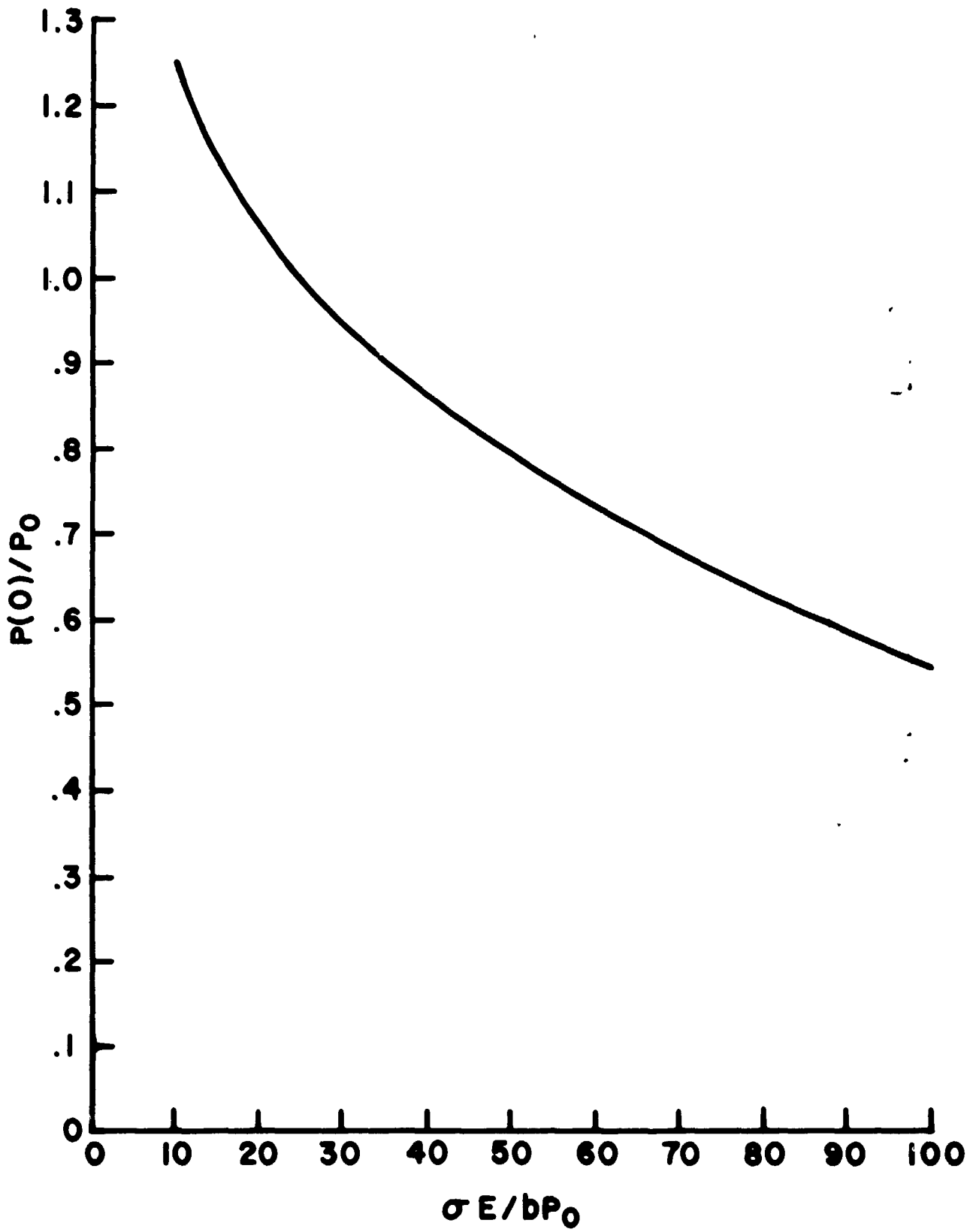


**CENTERLINE PRESSURE VERSUS ROUGHNESS FOR DISKS WITH NO HOLE**  
**FIG. 28**



CENTERLINE PRESSURE VERSUS ROUGHNESS  
FOR DISKS WITH NO HOLE

FIG. 29

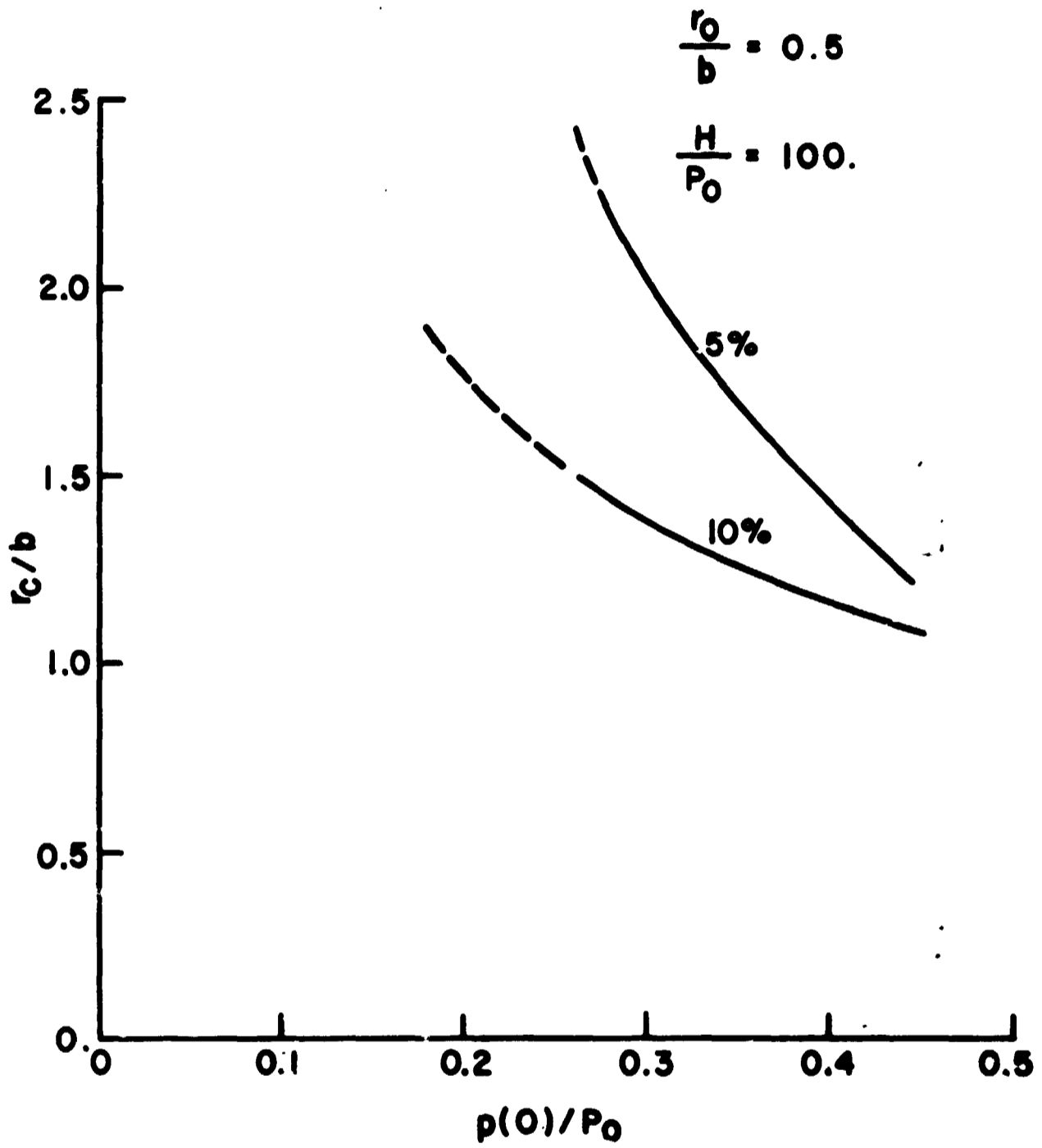


**CENTERLINE PRESSURE VERSUS ROUGHNESS  
FOR DISKS WITH NO HOLE  
FIG. 30**

relationship is shown in Figures 28, 29, and 30. Since it is found again that  $\bar{p}(0)$  is a strong function of  $\bar{\sigma}$  and a weak one of  $\bar{H}$ , only one representative value of  $\bar{H}$  is used in each figure,  $\bar{H} = 100$ . In Figure 29 (that for  $\bar{r}_0 = 1.0$ ), however, the  $\bar{p}(0) - \bar{\sigma}$  curve for  $\bar{H} = 10$  is also shown so as to demonstrate how the behavior here does parallel that shown in Figure 17 for the spherical surfaces.

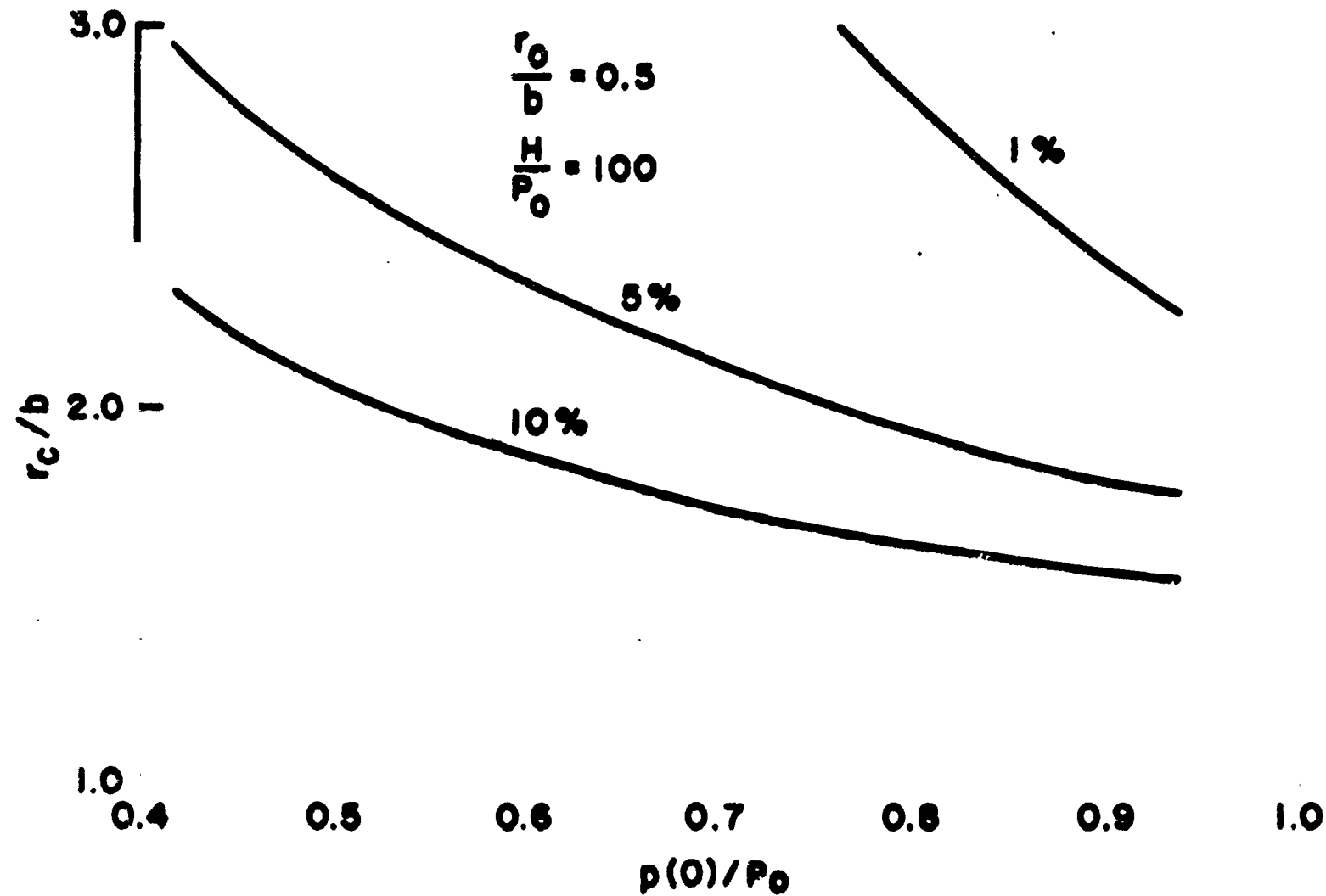
Since  $\bar{\sigma}$  and  $\bar{H}$  determine  $\bar{p}(0)$  uniquely and since  $\bar{p}(0)$  determines  $\bar{p}(\bar{r})$ , one can again plot the radius of contact,  $\bar{r}_c$ , versus  $\bar{p}(0)$  without any other parameters. For the same reasons as those discussed before, the contact radius is arbitrarily defined at three levels: where  $\bar{p}(\bar{r}_c)$  is 10% of  $\bar{p}(0)$ , 5% of  $\bar{p}(0)$ , and 1% of  $\bar{p}(0)$ . The results are shown in Figures 31, 32, and 33. The same general behavior is shown here as in Figure 19 for spherical surfaces except that in the case of two disks the curves separate from each other much more rapidly as  $\bar{p}(0)$  decreases than they did for spheres. This is, again, because of the greater influence that the asperities have in the gap between the disks than in the gap between the spherical surfaces.

In section 2.1.4 an example was given to demonstrate how the results there could be used. The procedure here is the same. If one had  $\bar{r}_0 = 1$  for example, one would calculate  $\bar{\sigma}$  and  $\bar{H}$  and go to Figure 29 to find the centerline pressure. With this value of  $\bar{p}(0)$ , one can go to Figure 32 for  $\bar{r}_c$  and to Figure 26 for  $\bar{p}(\bar{r})$ . The latter can be used as a master



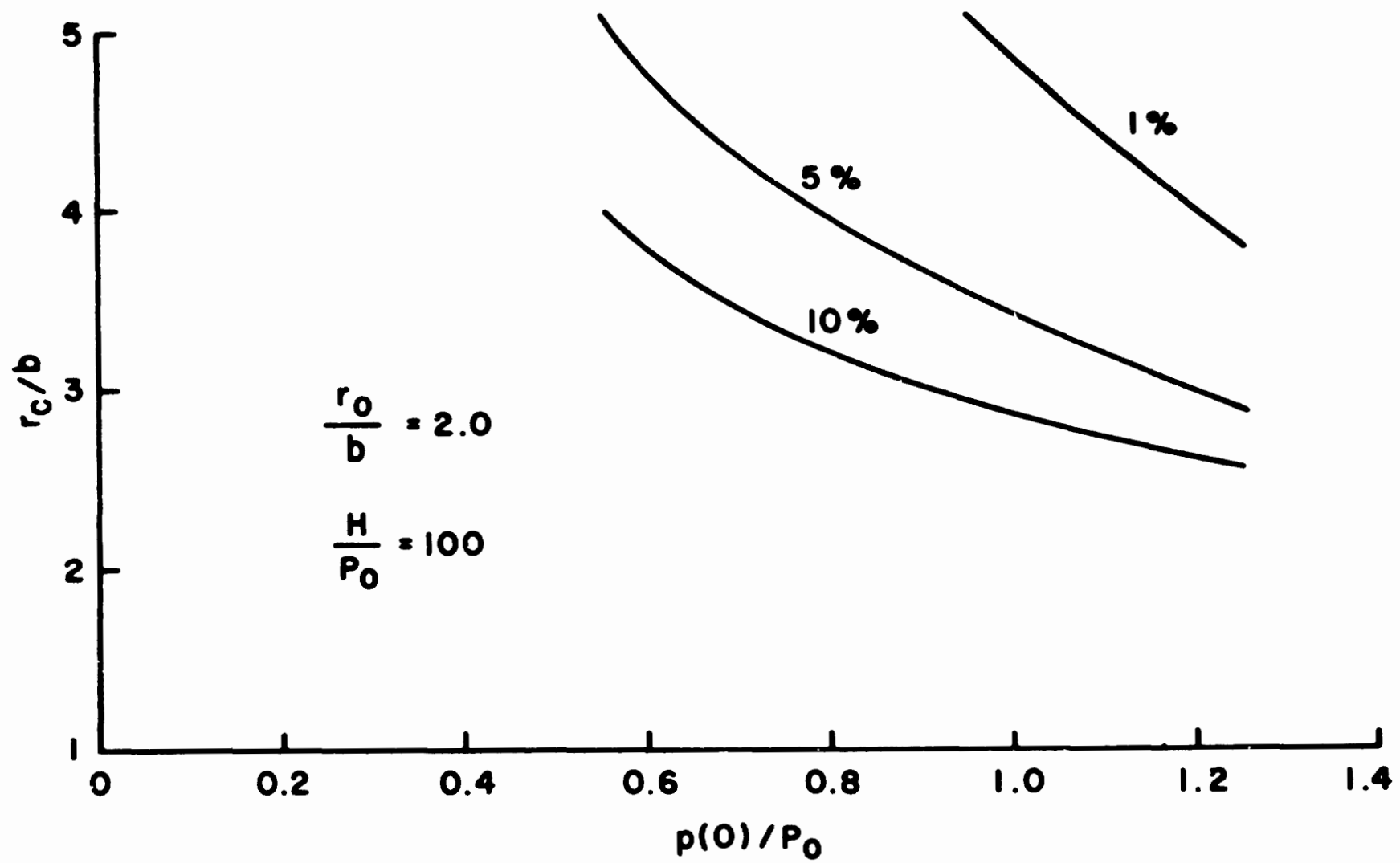
RADIUS OF CONTACT AT VARIOUS PRESSURE LEVELS FOR DISKS WITH NO HOLES

FIG.31



**RADIUS OF CONTACT AT VARIOUS PRESSURE LEVELS FOR DISKS WITH NO HOLES**

**FIG. 32**



**RADIUS OF CONTACT AT VARIOUS PRESSURE LEVELS FOR DISKS WITH NO HOLES**

**FIG.33**

graph regardless of the labels on the individual curves as long as the curve with the proper  $\bar{p}(0)$  is chosen.

### 2.2.5 Summary

These previous sections have shown that the effect of asperities on the contact of two disks without holes is similar to the effect on the contact of two spherical surfaces. In the former, however, it is much more pronounced and the radius of contact for the disks increases with increasing roughness at a greater rate than it would for the spheres. This, itself, has significance for the thermal contact problem for it is precisely this increase in  $\bar{r}_c$  which is of importance.

It was also shown how the elastic deformation solution used in this report can be considered as being accurate if it is compared to existing data in the literature and it was also shown how various parameters such as Poisson's ratio influence the final result.

One difference between the information presented here and that given earlier for spheres is that an extra parameter,  $\bar{r}_0$ , is needed. This leads to a family of curves rather than the single one used before. This is mostly just an inconvenience, however, and the basic behavior remains the same.

The next section will repeat the procedure followed for the spherical surfaces and for the disks without holes, but this time for the contact of two disks with center holes.

## 2.3 Contact of Two Plates with Center Holes

### 2.3.1 Model

The model used for the contact of two plates with a center hole is the contact of two disks (with center hole) of finite radius and finite thickness as shown in Figure 7. It is assumed that

- (a) the disks deform elastically;
- (b) asperities deform plastically;
- (c) asperity height distribution above a mean plane is Gaussian;
- (d) asperity contact is normal with no tangential component;
- (e) the contact (i.e., pressure distribution and deformation) will be symmetric about an axis through the center of the area in contact;
- (f) both disks have the same dimensions, material characteristics and loading distribution.

Again, no solution for the elastic deformation of the disks exists and the multiple infinite series technique described before is used. The boundary conditions are

$$\text{at } z = b \quad \sigma_z = -p_0 \quad c < r < r_0$$

$$\sigma_z = 0 \quad r_0 < r < a$$

$$\tau_{rz} = 0$$

$$\text{at } z = 0 \quad \sigma_z = -p(r)$$

$$\tau_{rz} = 0$$

$$\text{at } r = c \quad \sigma_r = 0$$

$$\tau_{rz} = 0$$

$$\text{at } r = a \quad \sigma_r = 0$$

$$\tau_{rz} = 0$$

The desired result is the deflection at  $z = 0$  due to the applied pressure,  $p(r)$ . As before, it will be assumed that  $a \gg r_0$  and that all boundary conditions at  $r = a$  can be ignored. It will also be assumed that the boundary condition

$$\text{at } r = c \quad \sigma_r = 0$$

can be ignored. This is done for expediency's sake and the error involved will be discussed later.

The governing equations are, then,

(a) deformation of solid disks

$$\bar{w}(\bar{r}) = \sum_{14} [\bar{r}, \bar{r}_0, \bar{c}, \bar{a}, \bar{p}(\bar{r})] - \sum_{15} [\bar{r}, \bar{r}_0, \bar{c}, \bar{a}, \bar{p}(\bar{r})] \quad (33)$$

(b) pressure distribution at asperities

$$\bar{p}(\bar{r}) = \frac{\bar{H}}{2} \operatorname{erfc} \left( \frac{\bar{y}_0 + 2\bar{w}(\bar{r})}{\sigma\sqrt{2}} \right) \quad (28)$$

(c) and for load

$$\int_{\bar{c}}^{\bar{a}} \bar{r} \bar{p}(\bar{r}) d\bar{r} = \frac{\bar{r}_0^2 - \bar{c}^2}{2} \quad (34)$$

The same non-dimensional variables are used here as were used in 2.2 with the addition of

$$\bar{c} = \frac{c}{b}$$

A digression will be made here, as was done previously, to study the midplane stress so as to gain insight into the overall problem.

### 2.3.2 Midplane Stress

Here we examine the midplane stress of a disk of thickness  $2b$ . As with the disks with no center holes, this stress has been used before as an estimate of the interfacial pressure distribution in smooth two-body contact problems. For the body shown in Figure 21b and the boundary conditions

$$\text{at } z = \pm b \quad \sigma_z = -p_0 \quad c < r < r_0$$

$$\sigma_z = 0 \quad r_0 < r < a$$

$$\tau_{rz} = 0$$

$$\text{at } r = c \quad \sigma_r = 0$$

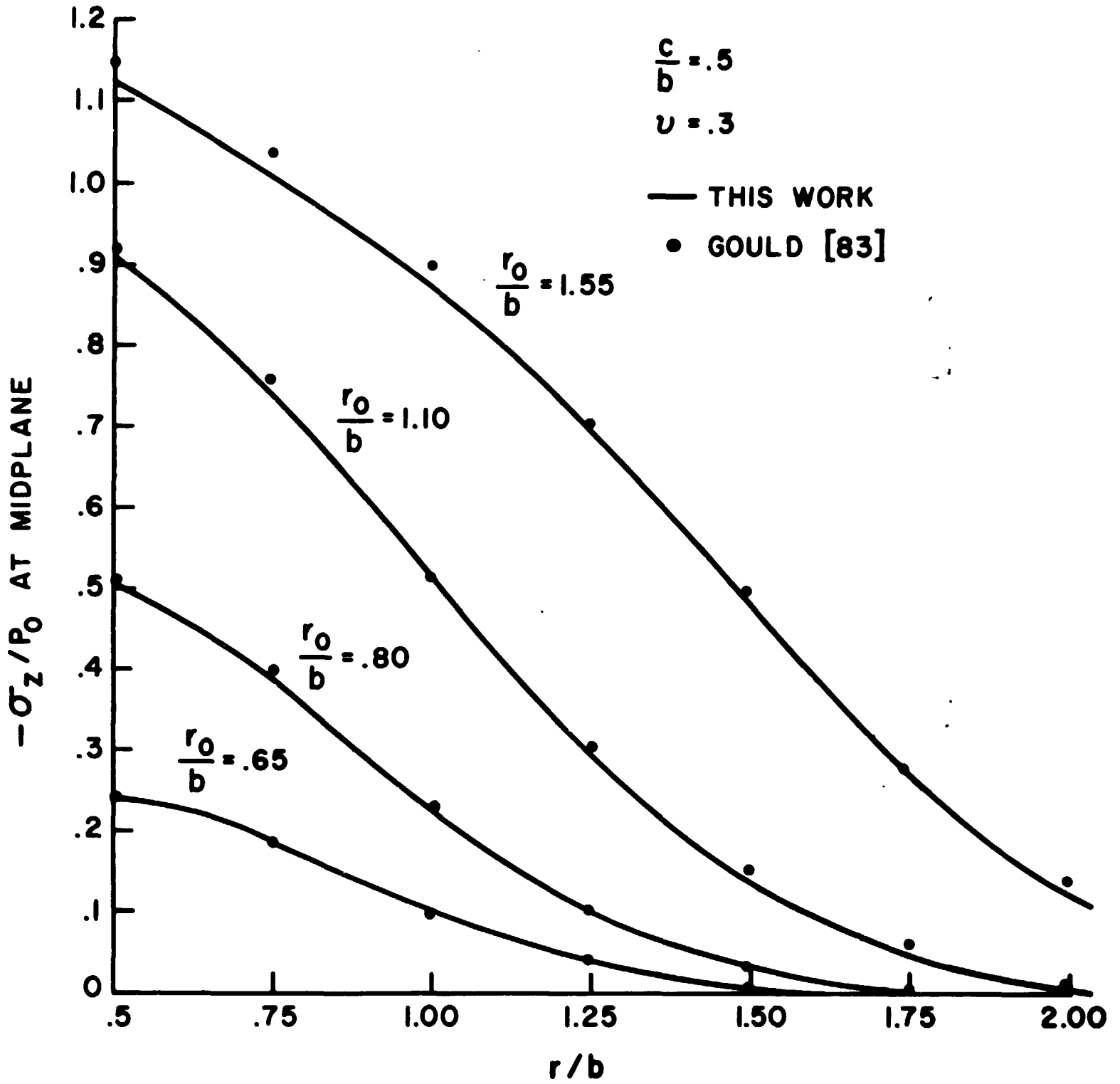
$$\tau_{rz} = 0$$

the midplane stress is

$$\left. \frac{\sigma_z}{p_0} \right|_{\bar{z}=0} = - \frac{\bar{r}_0^2 - \bar{c}^2}{\bar{a}^2 - \bar{c}^2} + \sum_{10} (\bar{r}, \bar{r}_0, \bar{c}, \bar{a}) - \sum_{11} (\bar{r}, \bar{r}_0, \bar{c}, \bar{a}) \quad (35)$$

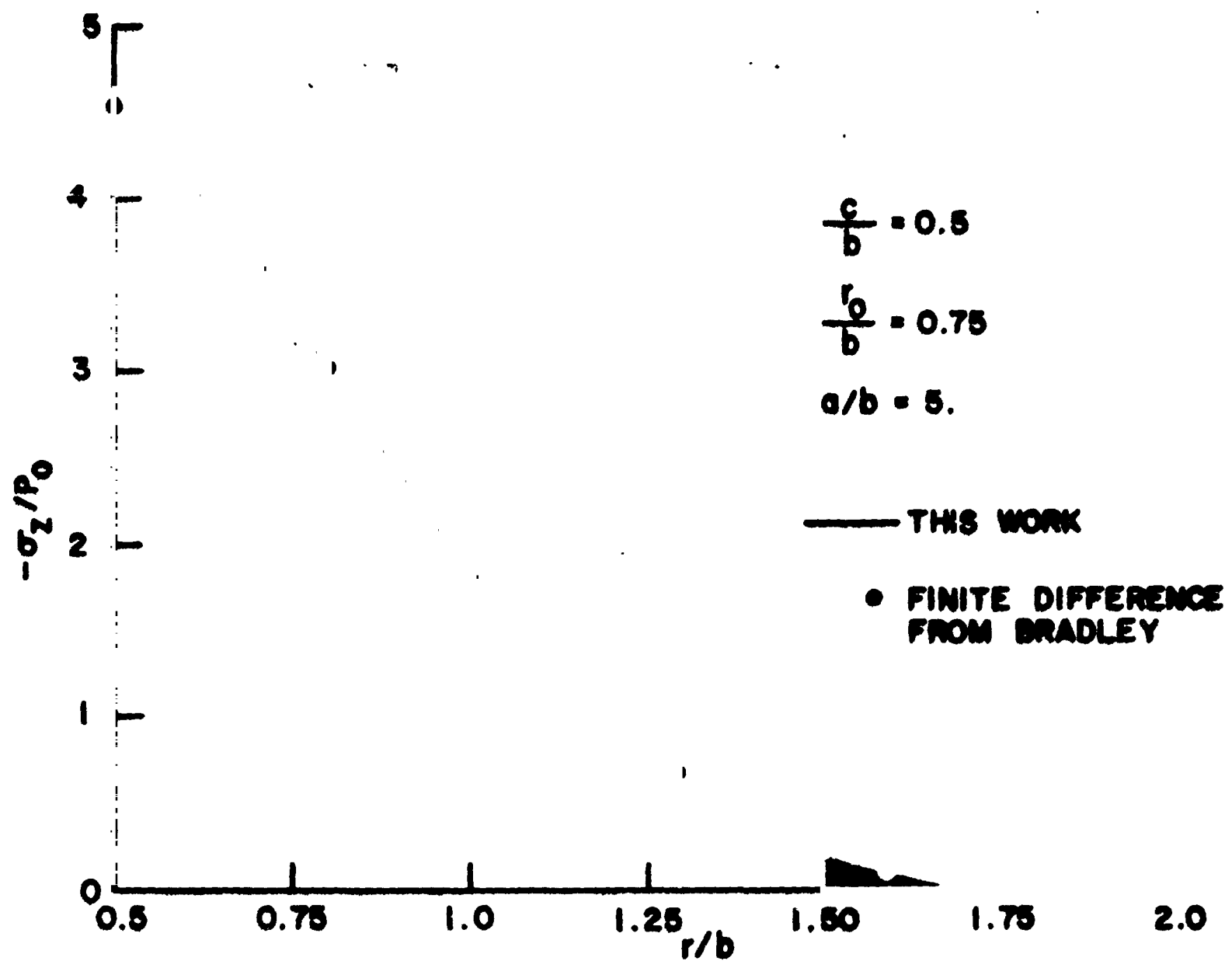
Note that the boundary conditions at  $r = a$  have not been used. It has been tacitly assumed that  $\bar{a}$  is sufficiently greater than  $\bar{r}_0$  (i.e.,  $\bar{a} > 4\bar{r}_0$ ) so that the outer edge may be assumed to be at infinity. This is physically reasonable.

Results from (35) are compared to data in the literature, notably the work of Gould [83], Bradley [84], and Fernlund [87]. The first two solve for the midplane stress using a finite element analysis; the latter uses a technique similar to that used here but somewhat less rigorous in application. Agreement between the results computed here from (35) and those from [83] and [84] are excellent (see Figures 34 and 35); agreement with that from [87] is poor. This is because the boundary conditions at  $r = c$  are ignored in [87] while they are satisfied in the others. More on this will be discussed later.



MIDPLANE STRESS OF DISK WITH HOLE

FIG. 34



MIDPLANE STRESS OF DISK WITH HOLE

FIG. 35

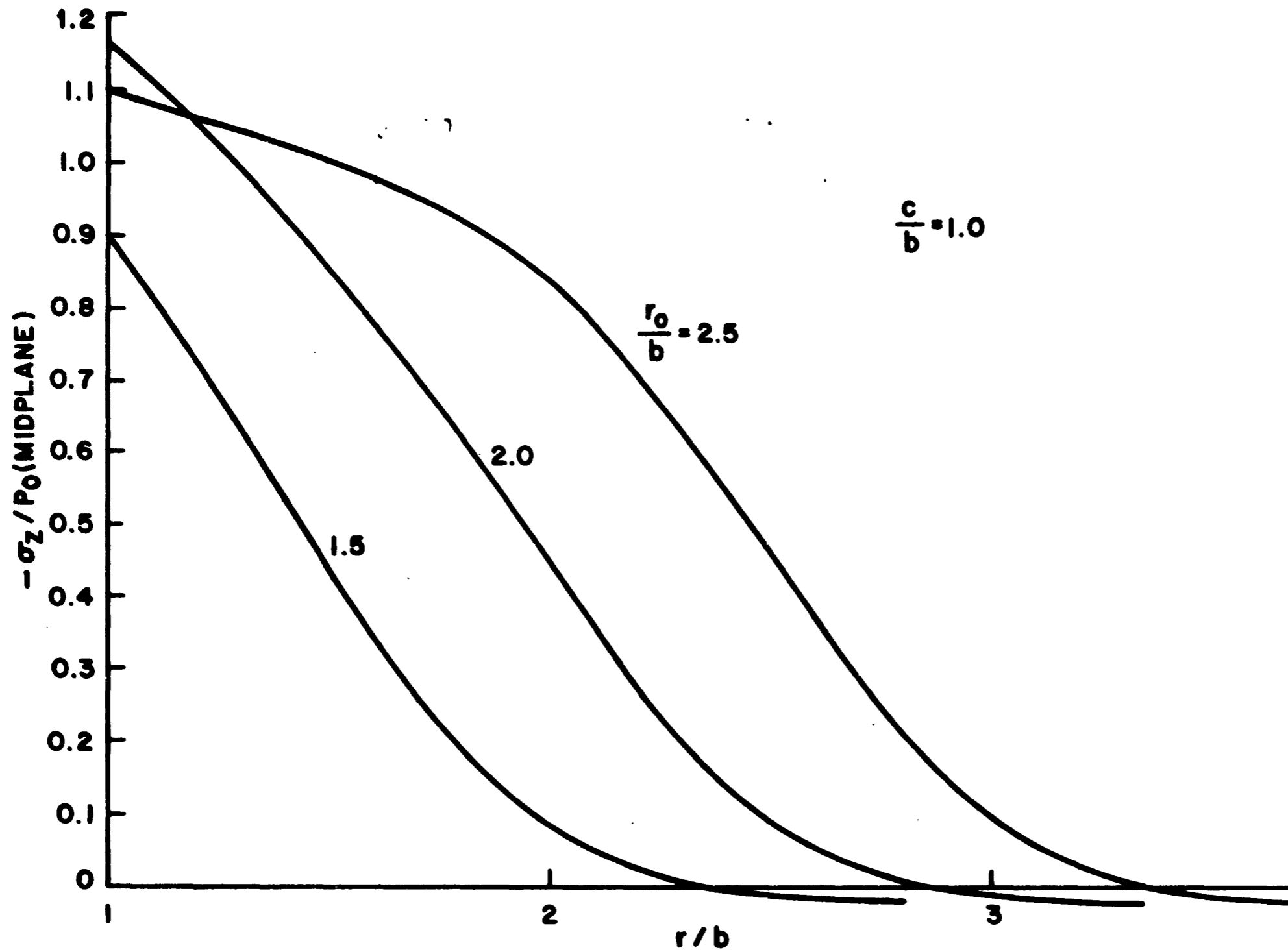
Another parameter, the hole radius, has been added to those used before. Rather than consider all possible combinations of hole radii and load radii, three specific values of  $\bar{c}$  are used:  $\bar{c} = 1.0, 0.5,$  and  $0.25$ . In Figures 36, 37, and 38 the midplane stress as calculated from (35) is shown for these values of  $\bar{c}$ . The general behavior is much like that shown in Figure 22 for disks with no holes.

If one extends the tangent to the curves at the load radius,  $\bar{r}_0$ , to the abscissa, one observes that the estimated radius of contact for values of  $\bar{r}_0 > 0.5$  is

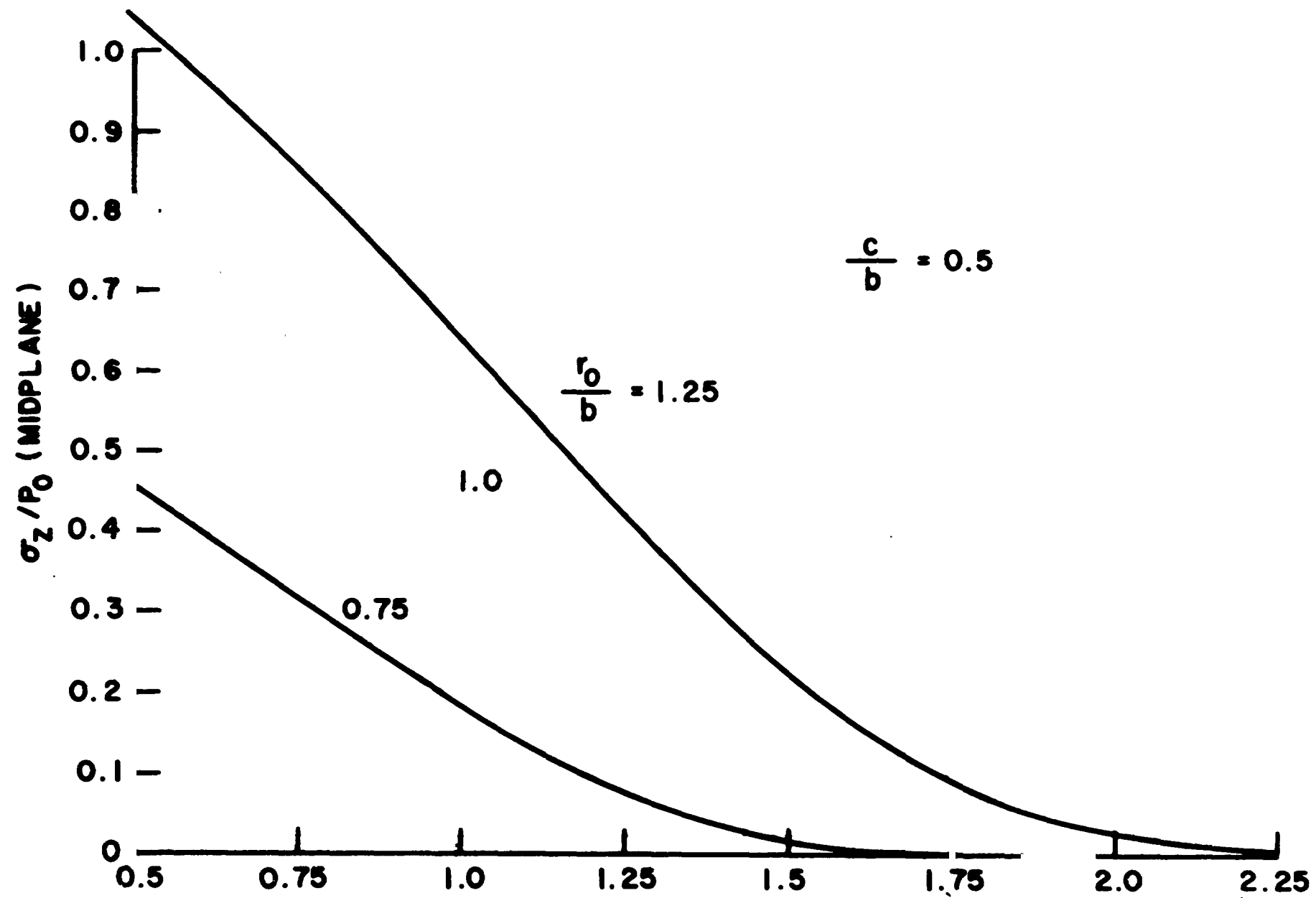
$$\bar{r}_c = \bar{r}_0 + 0.5 \quad (36)$$

which is exactly that predicted in [83] for smooth two-body contact. One can, therefore, use the modified midplane stress distribution as a rough guide to the pressure distribution in the two-body problem.

Another observation to be made is that for large  $\bar{r}_0$  the results for a disk with a center hole approach those for a disk without a center hole. This is not unreasonable since the effect of the presence of the hole will die out with increasing radius. The effect of the load is felt in the region immediately after its furthest extent,  $\bar{r}_0$ . If  $\bar{r}_0$  is far enough removed from  $\bar{c}$ , the two effects will not be superimposed upon each other. In that case the presence of the hole can be ignored.

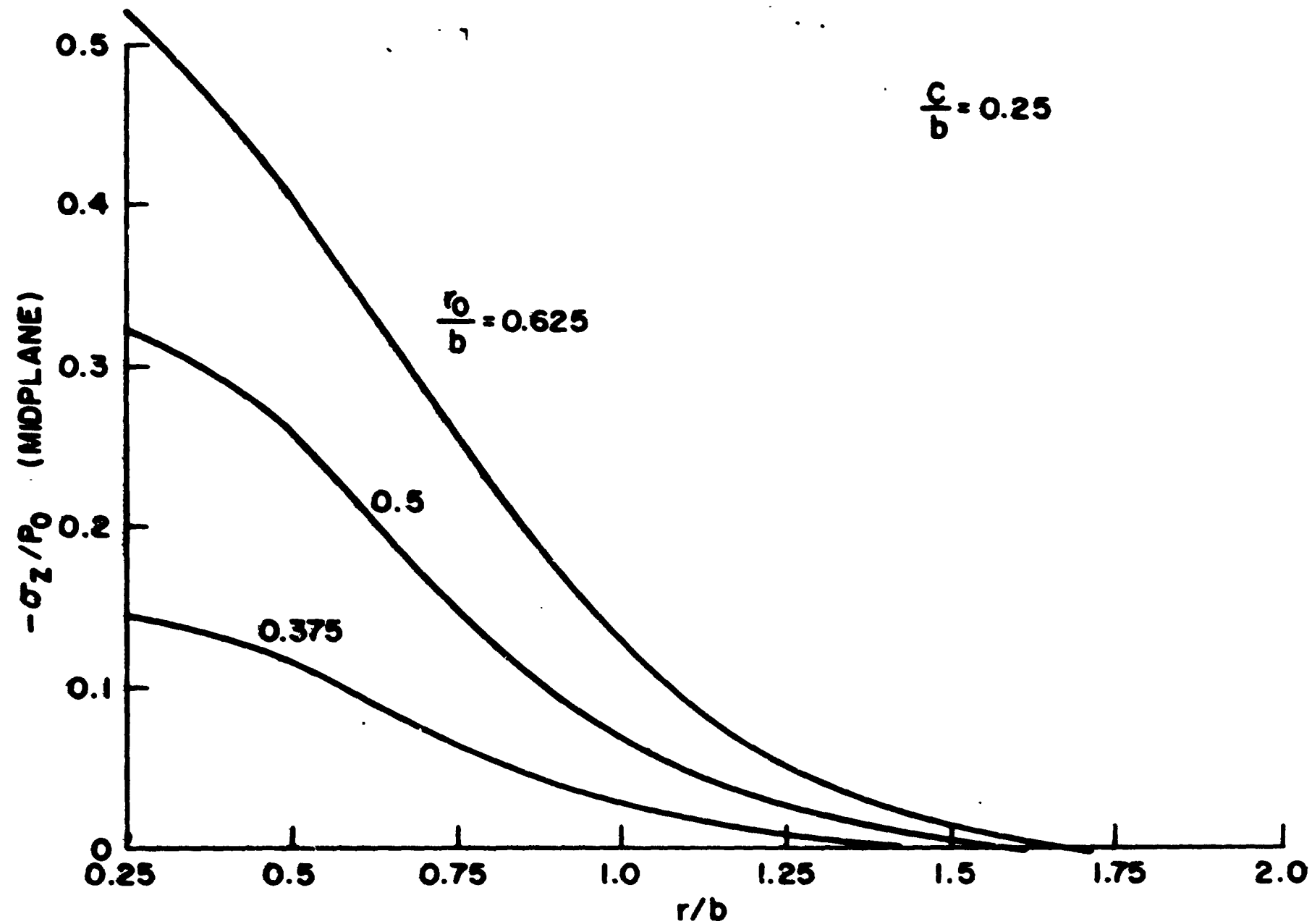


MIDPLANE STRESS—DISK WITH HOLE  
FIG. 36



MIDPLANE STRESS DISK WITH HOLE

FIG. 37



MIDPLANE STRESS DISK WITH HOLE  
 FIGURE 33

At the beginning of this section the boundary conditions which lead to (35) were listed. It was noted then that the conditions at  $r = a$  were ignored. If one also ignores the boundary condition

$$\text{at } r = c \quad \sigma_r = 0$$

one gets for the midplane stress, instead of (35),

$$\left. \frac{\sigma_z}{p_0} \right|_{\bar{z}=0} = - \frac{\bar{r}_0^2 - \bar{c}^2}{\bar{a}^2 - \bar{c}^2} + \sum_{10} (\bar{r}, \bar{r}_0, \bar{c}, a) \quad (37)$$

Since this has one infinite series, no simultaneous solution of equations is needed in order to find the Fourier-Bessel coefficients. One also sees that results from (37) agree closely with those from Fernlund [87] and disagree with those exact solutions presented earlier. As is expected the disagreement is in the region immediate to the hole. From (37)

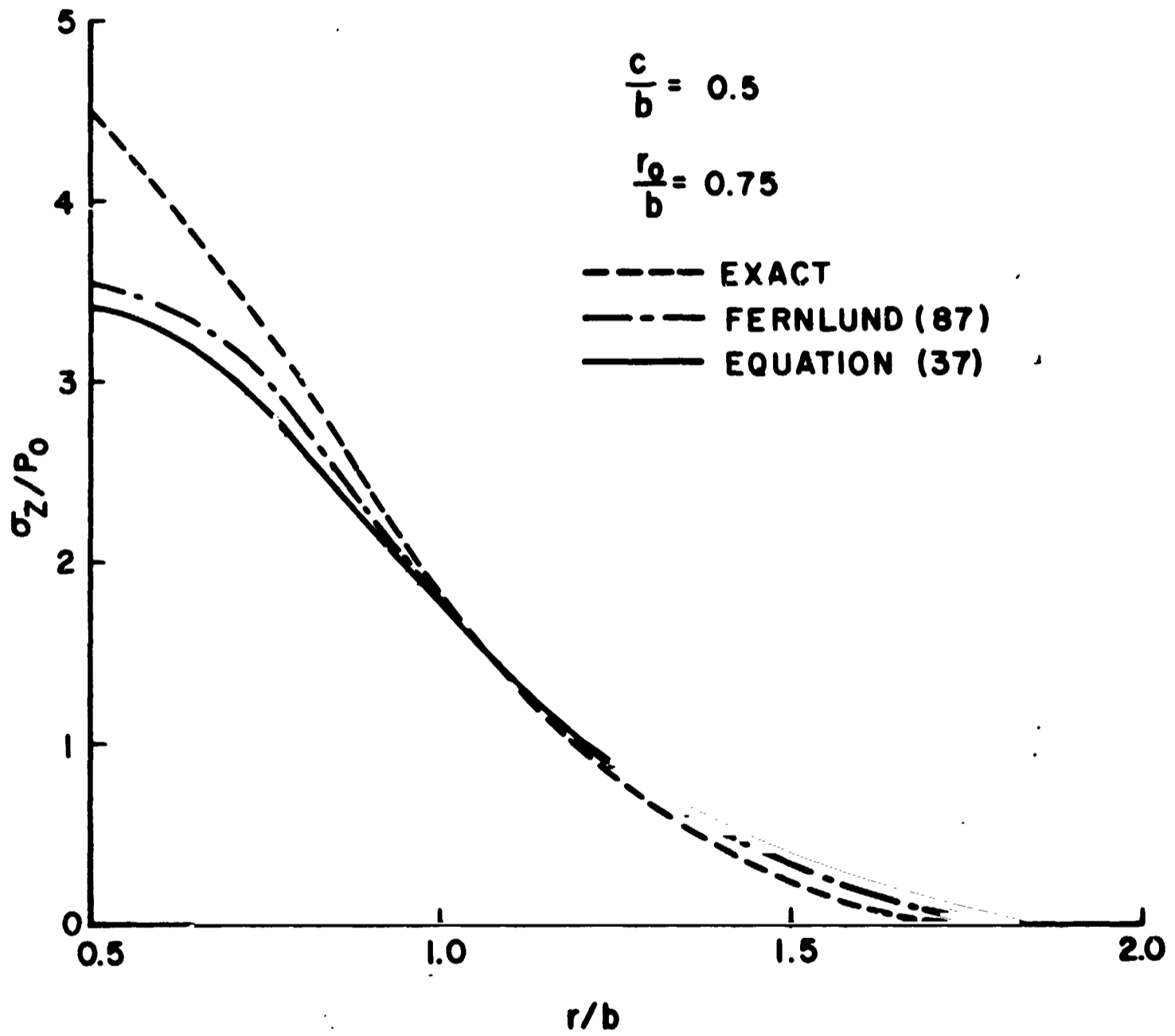
$$\left. \frac{d}{dr} (\sigma_z) \right|_{r=c} = 0$$

where from (35) one sees that

$$\left. \frac{d}{dr} (\sigma_z) \right|_{r=c} \neq 0$$

Thus the dropping of the boundary condition leads one to force the stress distribution to have a zero slope at the hole edge rather than its normal slope. Figure 39 shows an example as calculated from (37) and from [87] and the true distribution as given by (35).

The reason for introducing (37) is two-fold: first to explain the disagreement to Fernlund's data (which is done above) and secondly to justify the dropping of this particular boundary condition in further work. The ultimate goal in this report is to see how the pressure distribution changes with the presence of asperities and, in doing so, how the contact conductance changes. The most critical region for this purpose is the outermost one in the neighborhood of  $r_c$ . This is the region which goes from zero conductance to a finite conductance when asperities are considered. However small the conductance might be, in a typical case (Figure 53) it allows a short cut for the heat to travel to avoid the bulk material in the center. As can be seen from Figure 39, the disagreement in this region, between (36) and (37), the "exact" and "approximate", is not great. It is only near the center, which is relatively unimportant for our needs, that the difference is substantial. Therefore, for the purposes of this thesis, the dropping of the boundary condition at the hole is not critical even though it might be so in other circumstances: for example, in an investigation of the maximum stress point near the hole.



EFFECT OF NEGLECTING NORMAL HOLE STRESS  
ON MIDPLANE STRESS DISTRIBUTION

FIG. 39

One might also consider that the boundary condition of zero normal stress in the hole may not be an accurate description of the conditions in the hole in the first place since there may be shear or compressive forces due to the bolt, for example. This further reduces the importance of this particular boundary condition.

The work, then, on the midplane stress has shown the same general behavior evidenced previously and has demonstrated the effect of ignoring the normal stress in the hole when calculating interfacial pressure distributions. It was also shown that an estimate of contact radius for smooth two-body contact could be made using the midplane stress solutions and that this estimate agreed with that from [83].

### 2.3.3 Solution

The three governing equations for the contact of two disks with a center hole (Figure 7) are: (33), deformation of the disks; (28), pressure distribution at the asperities; and (34), total load. As mentioned before, (33) ignores the boundary condition of zero normal stress within the hole and assumes that  $\bar{a} \gg \bar{r}_0$  so that any boundary condition at the outer edge can be ignored. The justification for both assumptions has been discussed earlier.

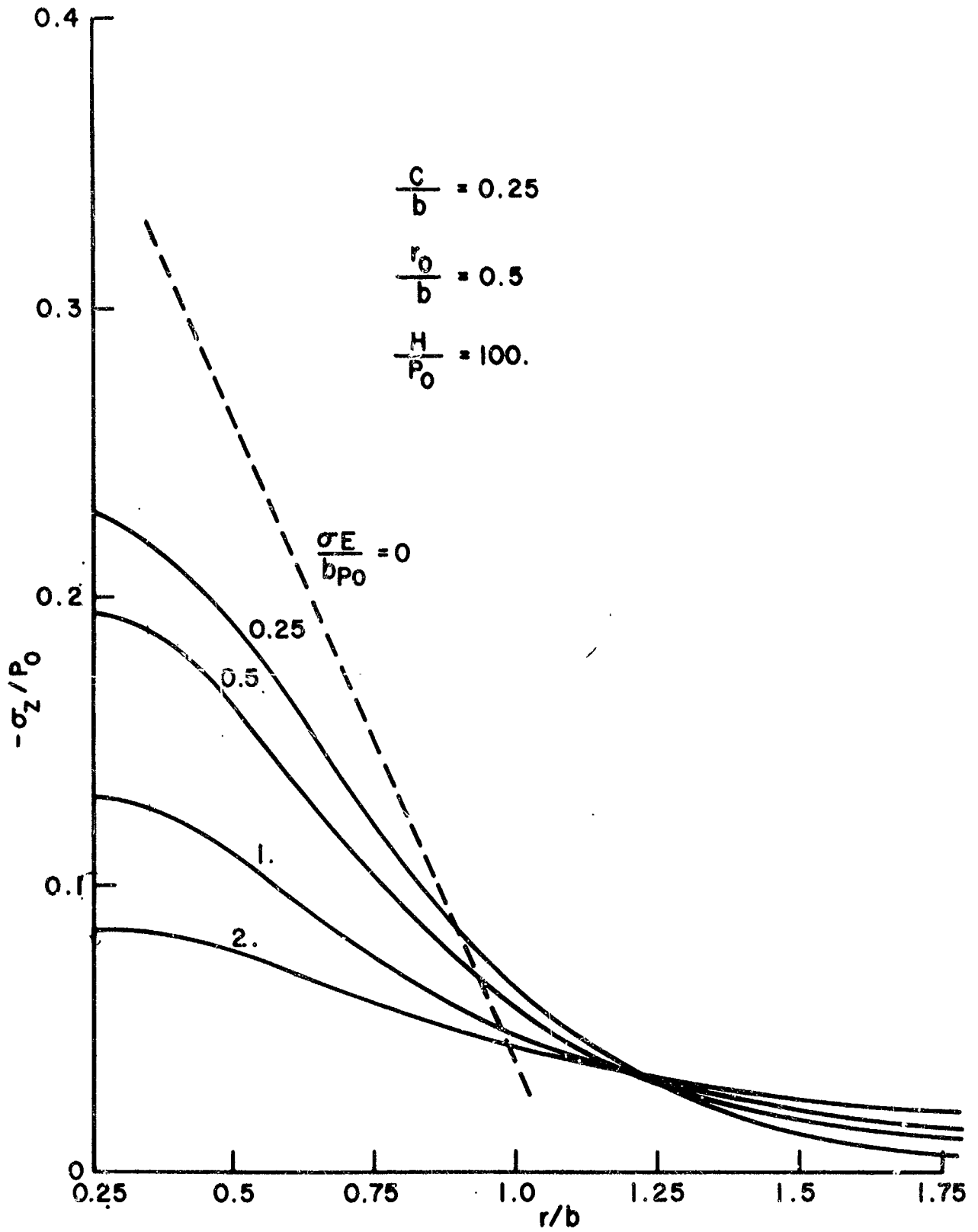
Again the flow diagram given in Figure 15 can be used to arrive at a compatible set of  $w(r)$ ,  $p(r)$ , and  $y_0$ . Equations (33), (28), and (34) are substituted for (23), (24), and (25) respectively. The same difficulties arise

in the solution as those discussed in section 2.2.3 for the disks with no center hole. A computer program which will perform the proper iteration sequence is listed in the Appendix.

#### 2.3.4 Results

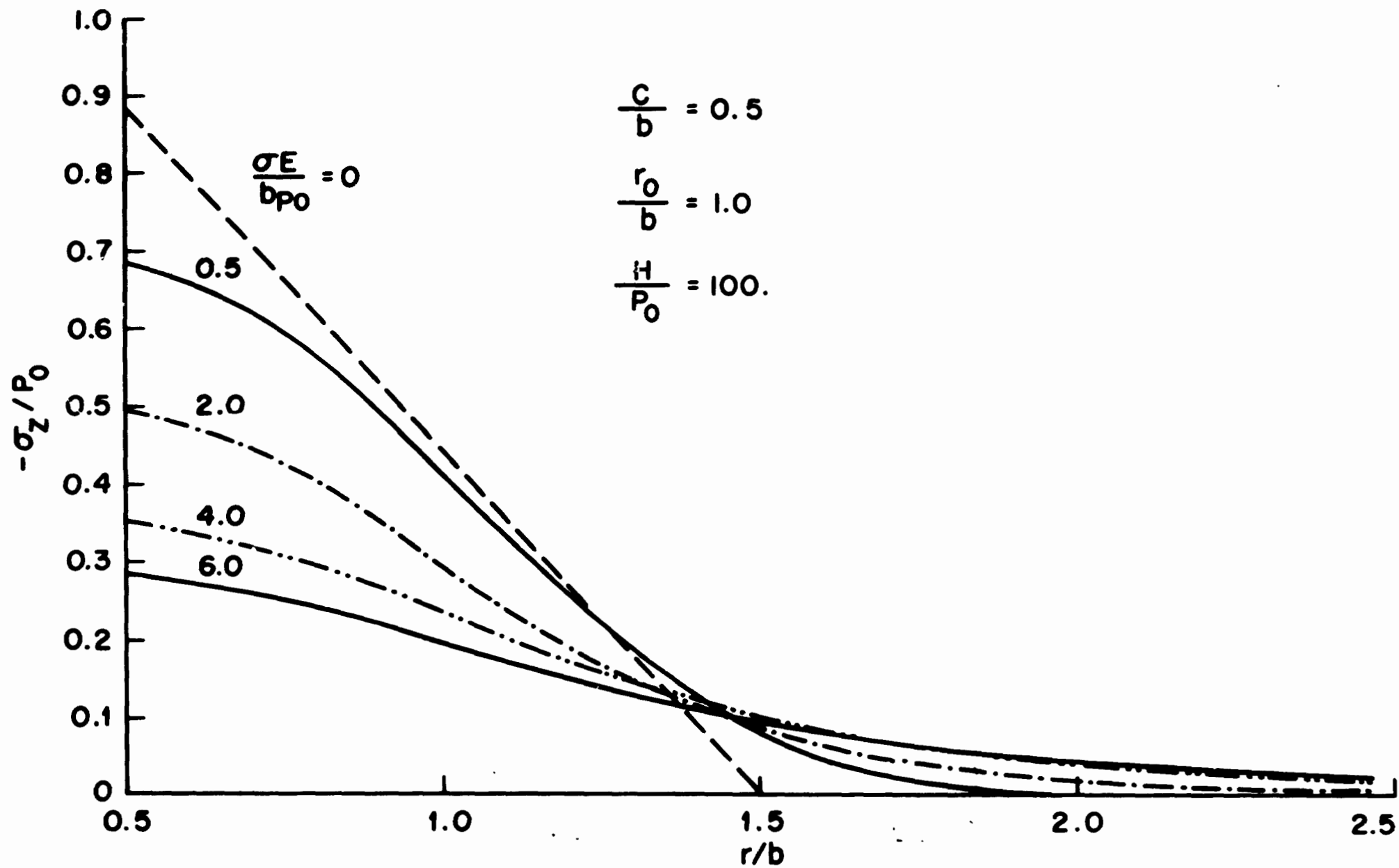
In order to describe the interfacial pressure distribution for spherical surfaces, one needs two parameters,  $\bar{\sigma}$  and  $\bar{H}$ ; for disks with no holes, three:  $\bar{\sigma}$ ,  $\bar{H}$ , and  $\bar{r}_0$  ( $\bar{a}$  being ignored). In the present case for disks with center holes one needs four parameters:  $\bar{\sigma}$ ,  $\bar{H}$ ,  $\bar{r}_0$ , and  $\bar{c}$ . As before, only one  $\bar{H}$  is considered since it has such a weak influence on the final result. Rather than attempting to present data for many combinations of  $\bar{\sigma}$ ,  $\bar{r}_0$ , and  $\bar{c}$ , only three sets of  $\bar{r}_0$  and  $\bar{c}$  are used. These are all physically reasonable values and lie within the range of practical interest. Results from Gould [83] are used for the zero-roughness distributions.

In Figures 40, 41, and 42 the same behavior as seen before is shown. As with the disks with no hole, different ranges of  $\bar{\sigma}$  affect the final distribution for different sets of  $\bar{r}_0$  and  $\bar{c}$ . The non-dimensional load is  $\bar{r}_0^2 - \bar{c}^2$  and as this value increases, the  $\bar{\sigma}$  needed to change the pressure distribution increases. Since the normal stress at the holes is not accounted for in the solution, all the  $p(r)$ -curves have zero slope at the hole wall. This is incorrect, of course, and a more exact estimate might be made by extending the linear portion of the curve (in the neighborhood of  $\bar{r}=\bar{r}_0$ ) directly back to the ordinate.

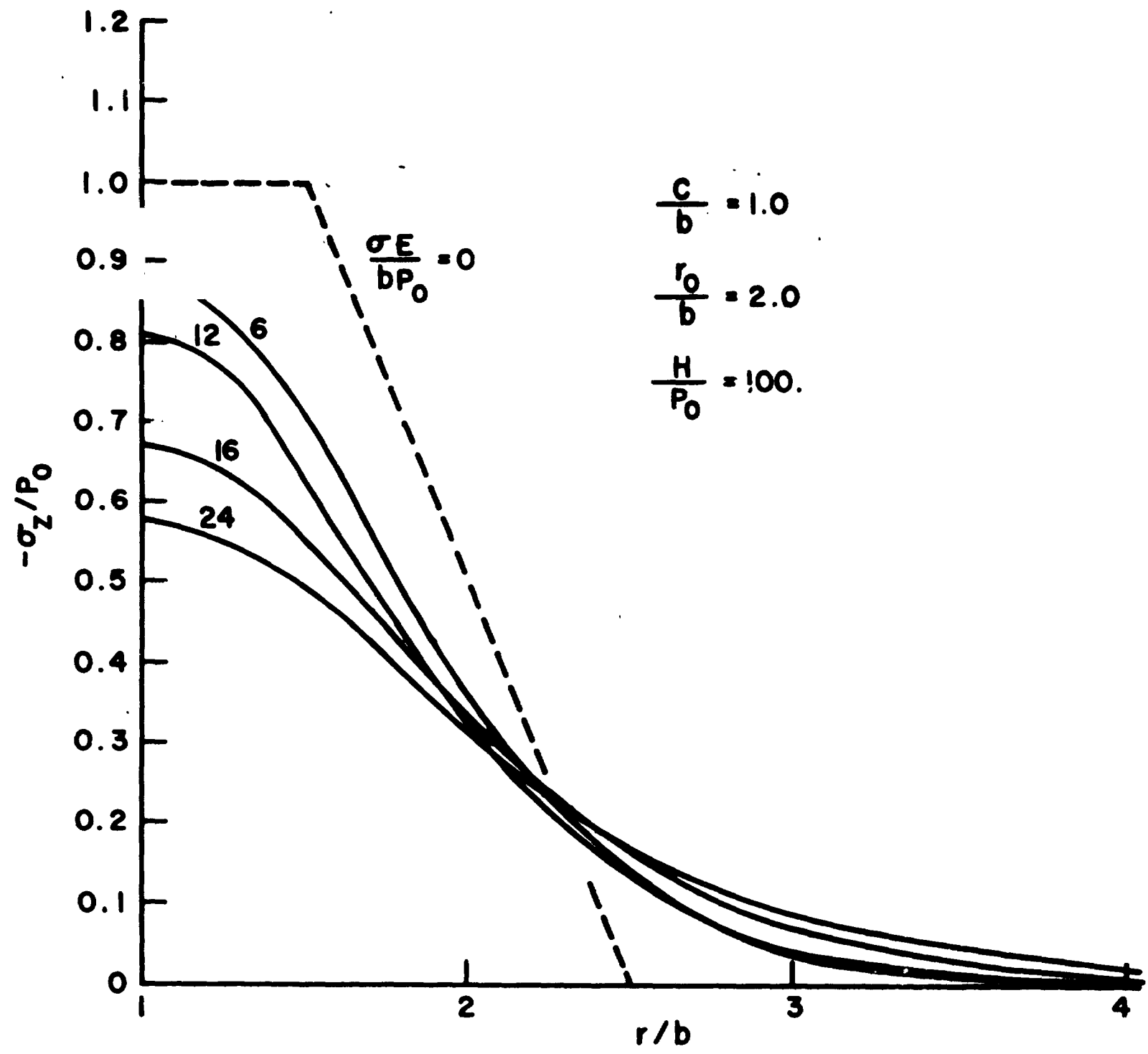


EFFECT OF ROUGHNESS ON INTERFACIAL STRESS DISTRIBUTION FOR DISKS

FIG. 40



EFFECT OF ROUGHNESS ON INTERFACIAL STRESS  
 DISTRIBUTION FOR DISKS  
 FIGURE 41

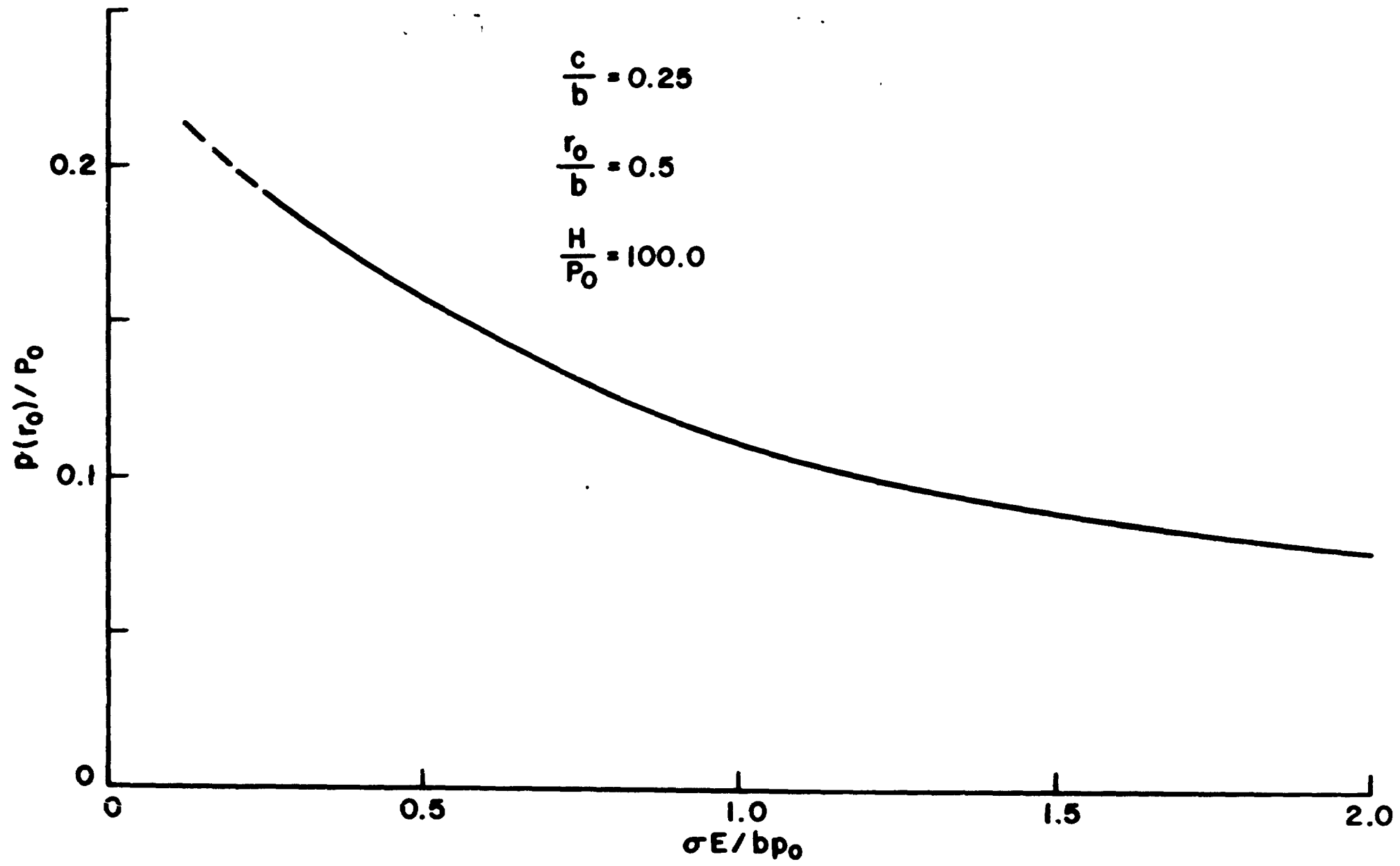


EFFECT OF ROUGHNESS ON INTERFACIAL STRESS DISTRIBUTION FOR DISKS

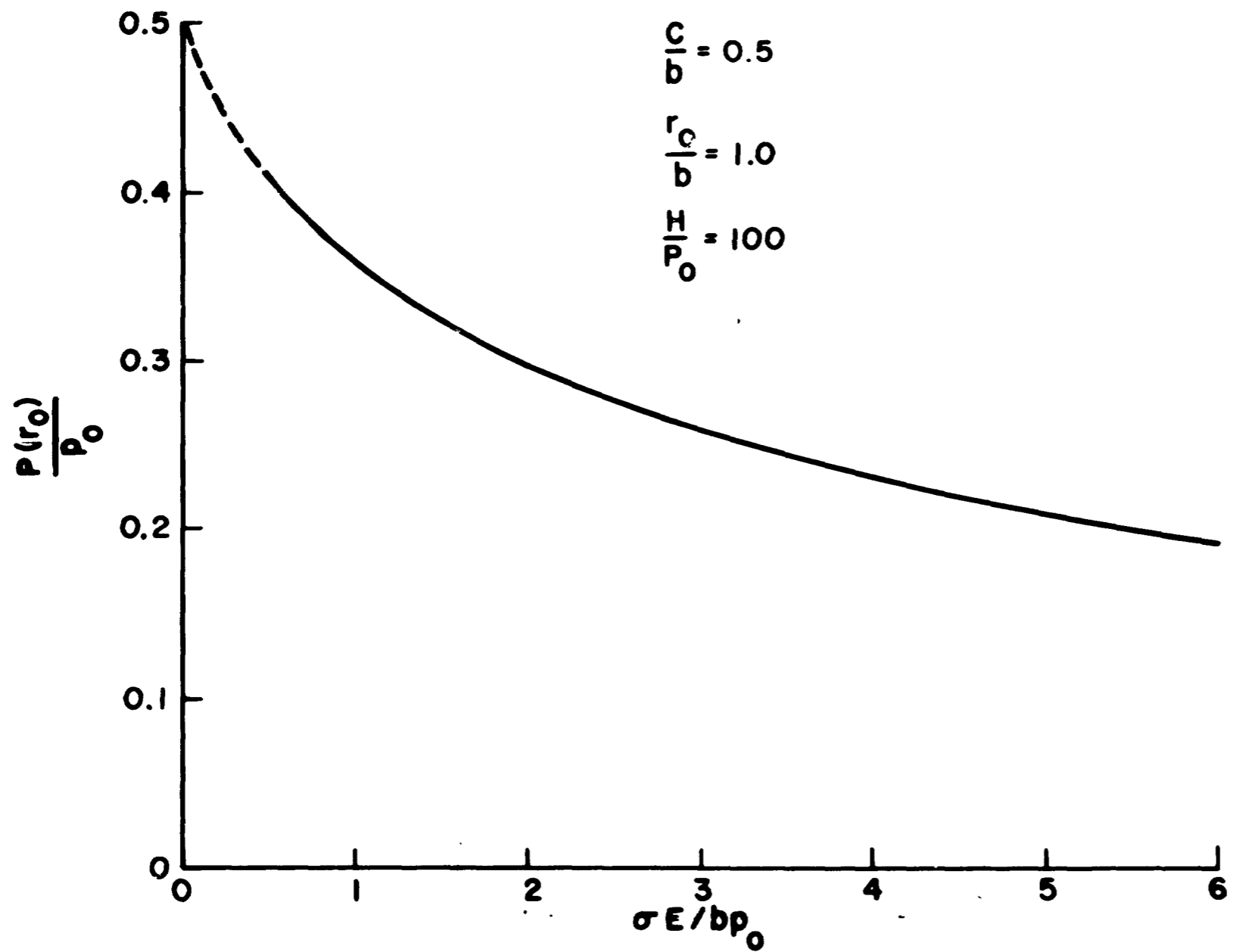
FIGURE 42

In the previous two models it was noted that the centerline pressure determines the rest of the curve: i.e., knowing  $\bar{p}(0)$ , one knew  $\bar{p}(r)$  for all  $\bar{r}$ . Here, of course, there is no "centerline" and one has to use another reference point. The first one that comes to mind is the hole edge,  $\bar{r} = \bar{c}$ , and one does find that for various values of  $\bar{\sigma}$  and  $\bar{H}$  the distributions will match if the pressure at the hole edge matches. Therefore if  $\bar{p}(\bar{c})$  is known,  $\bar{p}(\bar{r})$  is known. But since the solutions are developed with an assumption that causes an error in the curve in the region immediate to the hole, it would be better to choose another reference point. A logical one is the load radius,  $\bar{r}_0$ . At this distance from the hole the approximate profile has almost joined the exact one (see Figure 39). The disadvantage in using  $\bar{r}_0$  as the reference point is that the separation between curves is less here than at the hole edge and possibility of error is greater. Figures 43, 44, and 45 show  $\bar{p}(\bar{r}_0)$  versus  $\bar{\sigma}$ . While these curves strictly pertain to one  $\bar{H}$ , they can be extended over the range with little error.

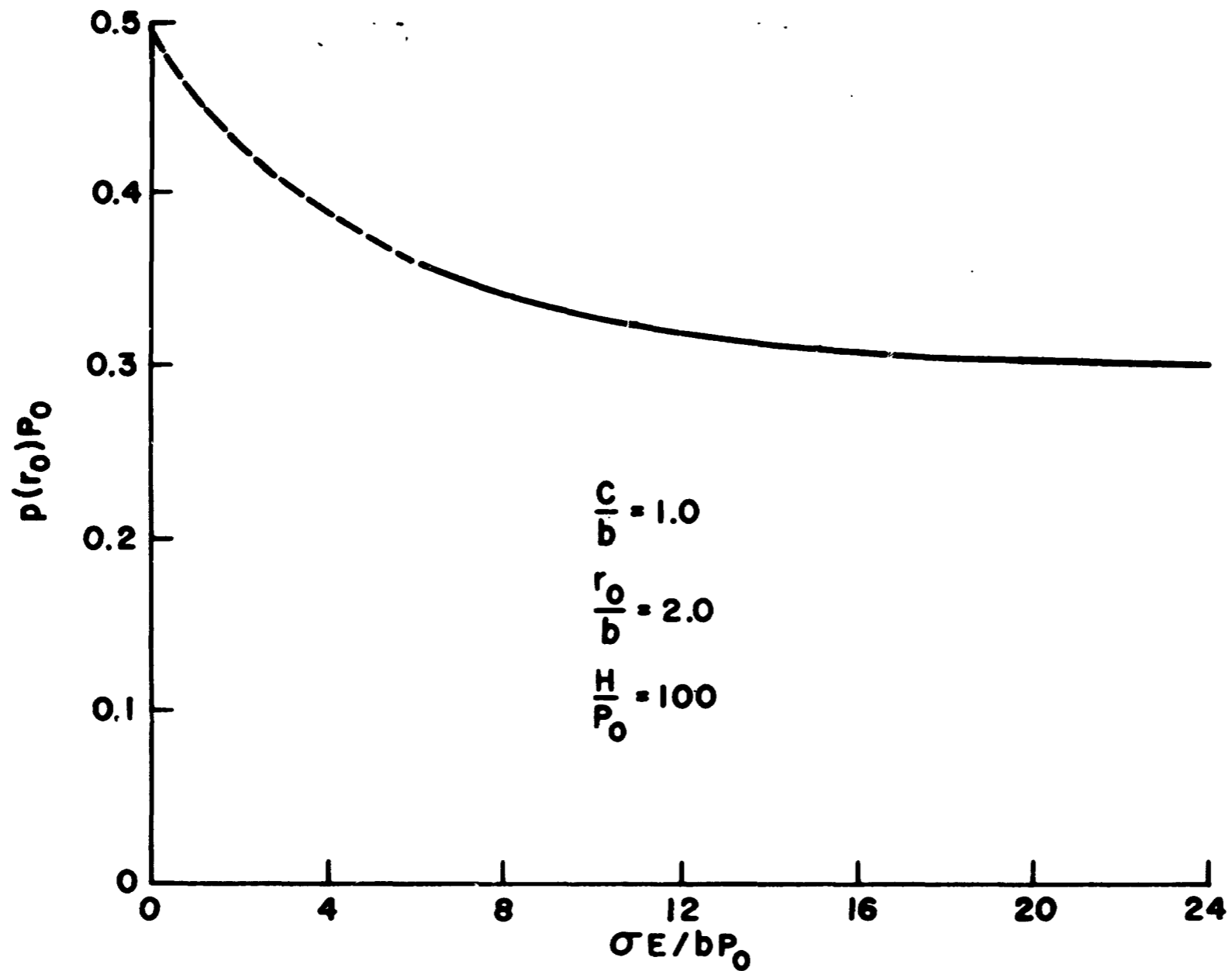
Here, as before, the radius of contact is a function only of one point on the pressure distribution,  $\bar{p}(\bar{r}_0)$ . By defining the contact radius at different levels, one can again show the change in contact radius with decreasing  $\bar{p}(\bar{r}_0)$  and, therefore, with increasing roughness. The curves shown in Figures 46, 47, and 48 behave much in the same



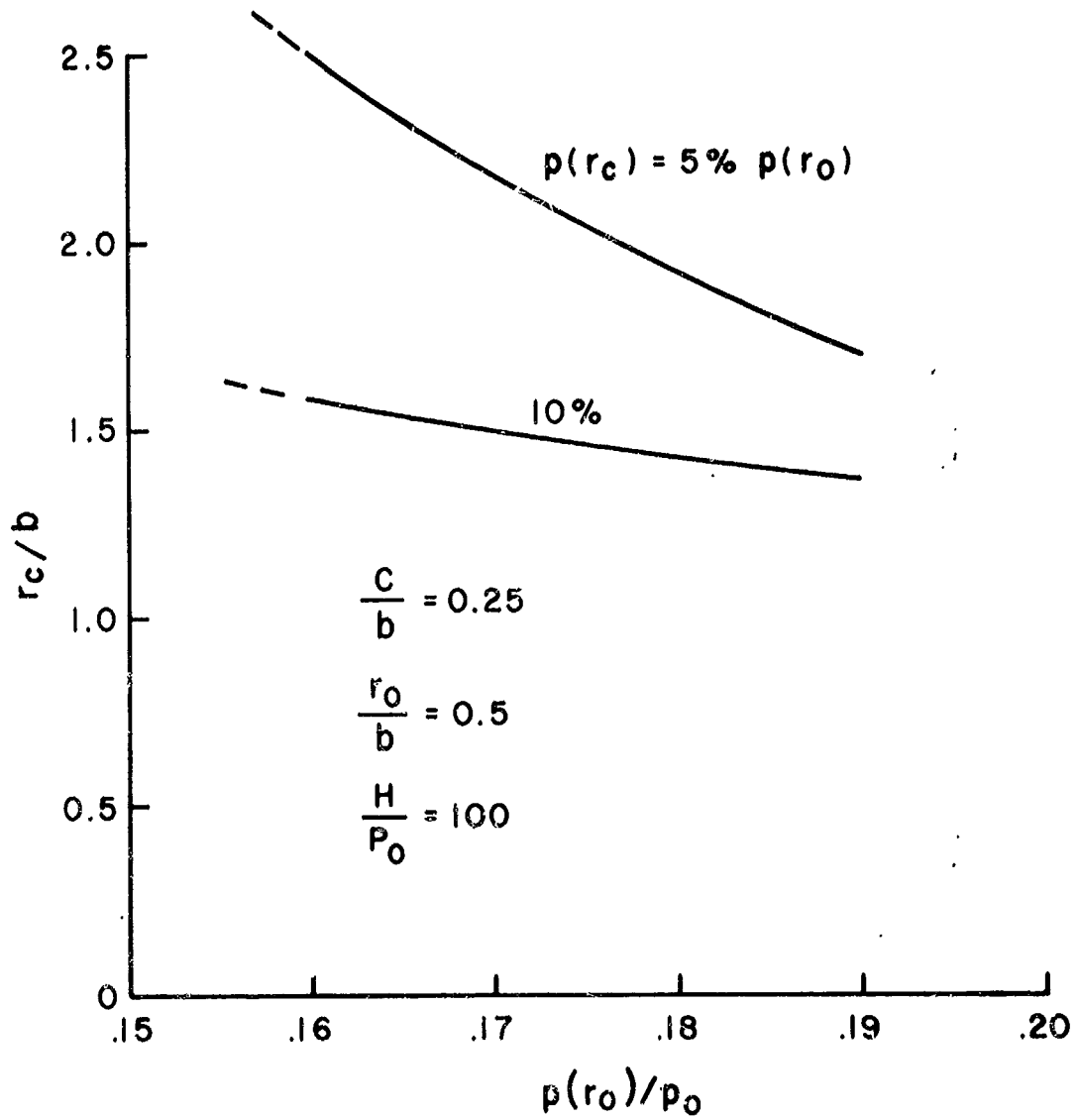
**PRESSURE AT LOAD RADIUS AS FUNCTION OF ROUGHNESS**  
**FIG. 43**



PRESSURE AT LOAD RADIUS AS FUNCTION OF ROUGHNESS  
 FIG. 44

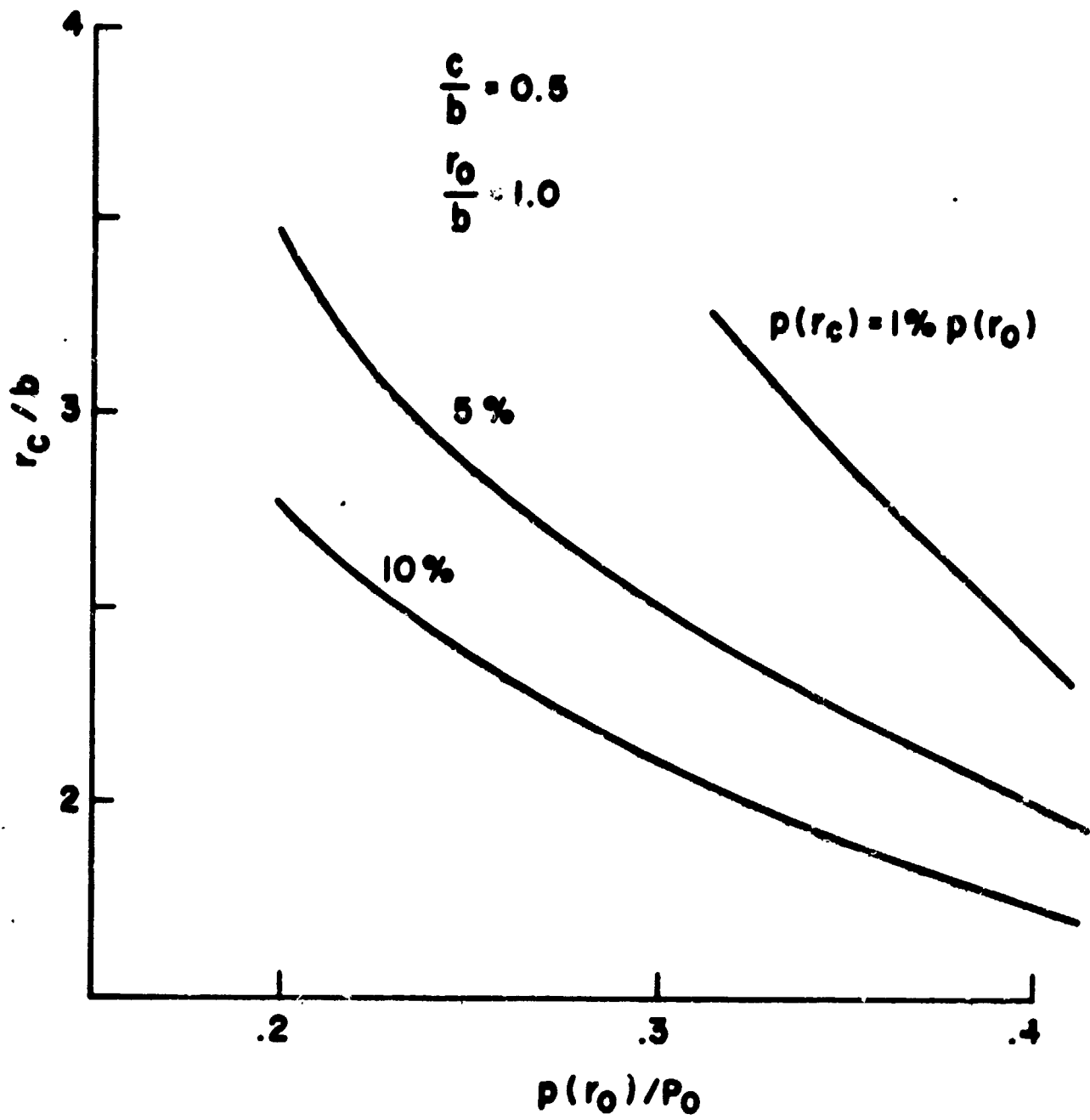


PRESSURE AT LOAD RADIUS AS FUNCTION OF ROUGHNESS  
 FIG. 45



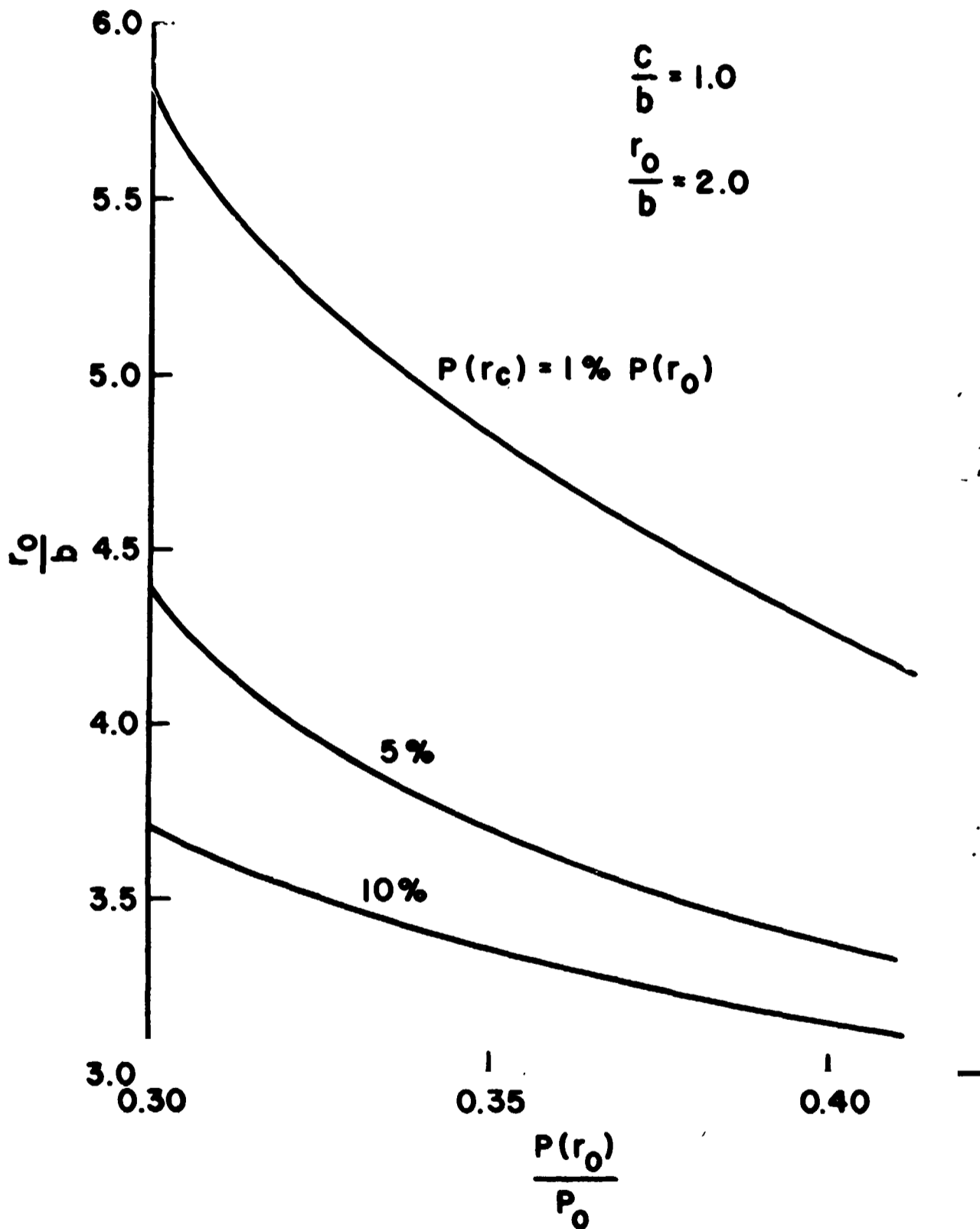
RADIUS OF CONTACT AS A FUNCTION  
OF REFERENCE PRESSURE FOR  
DIFFERENT LEVELS

FIG. 46



**RADIUS OF CONTACT AS A FUNCTION  
OF REFERENCE PRESSURE FOR  
DIFFERENT LEVELS**

**FIG. 47**



RADIUS OF CONTACT AS A FUNCTION  
OF REFERENCE PRESSURE FOR  
DIFFERENT LEVELS

FIG. 48

manner as those given for the previous two models. Unlike the previous two models, however, the reference point used is not the innermost one but the load radius,  $\bar{r}_0$ . This is consistent with the previous sets of data.

### 2.3.5 Summary

All the information developed in this section parallels that presented before. With the model described in 2.3.1 it was shown that increasing the roughness (here  $\bar{\sigma}$ ) does have a substantial effect on the pressure distribution and the radius of contact. The midplane stress for a disk with a center hole was investigated and results were found which agree with data in the literature developed with numerical techniques. An approximate solution was also presented which ignored the boundary condition of zero normal stress within the hole. The results from this solution fell below those from the exact one in the region immediate to the hole but at and beyond the load radius,  $r_0$ , the two solutions produced similar results. The midplane stress solutions also enabled one to predict  $r_c$  for the smooth two-body contact problem which agreed with that in the literature.

Specific values of  $\bar{r}_0$  and  $\bar{c}$  were chosen and the same type of curves were generated for these as was done before: the pressure distribution for different values of roughness; the reference point pressure,  $\bar{p}(\bar{r}_0)$ , for a particular value of  $\bar{H}$  at varying  $\bar{\sigma}$ ; and the contact radius at different reference pressures.

At the end of these three sections, then, one has the pressure distribution,  $p(r)$ , as a function of the various parameters governing each particular model. Using equation (3) one can now predict the local contact conductance at the interface. Knowing  $h_c(r)$  one can calculate the entire thermal resistance of the particular system. In section 3 this is what is done.

Before proceeding to that, however, some experimental observations corroborating the conclusions drawn in this chapter will be presented.

#### 2.4 Experimental Observations

This section describes the experimental work done on bolted disks. The basic difficulty in measuring the contact in a bolted joint is to avoid disturbing the contact with the measuring devices. Traditionally in smooth, two-body contact, there are two parameters of interest which are to be measured: the radius of contact,  $r_c$ , and the pressure distribution,  $p(r)$ . The most common way of measuring either of them is with penetrating oil with or without an intermediate substance to act as a capillary medium [53,59,87]. Agreement with theory using this method has been claimed to be good. The theories used, however, are approximate and in the best of the three [87], the agreement with the exact solution near the hole is not good. Thus one might conclude that these experiments with the oil would be useful in predicting the general trend of the distribution but not useful for calculating actual numerical values. There is, after all, the hydrostatic effect of the oil between the plates and no estimate of its influence on the pressure distribution has yet been made.

A better way, perhaps, to measure the interfacial pressure distribution is through photoelasticity. This guarantees that no foreign material which could influence

the distribution is placed in the interface. This method was used successfully in [84] but it was felt that the accuracy in determining the pressure distribution was no better than 10-15%. It was also found to be impossible to measure the radius of contact using this method. A further disadvantage is that only one type of material can be used in a photoelastic experiment .

Common to all techniques which attempt to measure the interfacial pressure distribution is the lack of knowledge of the load distribution in actual practice. All the theory presented in this paper (and others also) assumes that the load is constant up to a given radius and then zero afterwards. In an actual experiment, especially where a torqued bolt is used, it is doubtful that one can predict a priori what the distribution will be. And, to measure the load distribution involves the same problems as does measuring the interfacial one. Therefore with any of the techniques suggested to date, it would be difficult, if not impossible, to measure the interfacial pressure distribution with any precision.

In measuring the radius of contact one can avoid disturbing the original distribution even with the penetrating oil technique. But this is subject again to the vagaries of the actual load distribution, soak time, capillary flow in the narrow gap, etc. Another way of measuring the

radius of contact is to take the two disks in contact and rotate them (about the axis of the bolt) with respect to each other. Where they are in contact they will rub; where they are not in contact, they will not. The transition from one region to the other is the radius of contact. The worn area is visible and can be measured. Or, if one of the plates is made to be radioactive, the radioactive material transferred to the other plate by rubbing can be recorded photographically. In either case the radius of contact can be measured. This was done in [83] and the results were consistent with the theoretical work done there. Again, since the load distribution is not known exactly, one cannot expect to arrive at a precise value for  $r_c$  but just confirm the general behavior.

The experimental work done in this report uses the rubbing technique described in [83]. It is limited to demonstrating the overall effect on contact radius that the asperities have and not to arriving at a precise value of  $r_c$ . Since, theoretically, the pressure distribution in the presence of asperities never gets to zero, there is no radius of contact as such. Before, when dealing with the theoretical curves, one defined the radius of contact at different pressure levels: e.g.,  $r_c = r$  where  $p(r) = 10\%p(0)$ . In the rubbing experiment, then, one might expect to see wear marks on the entire surface of the

disks but with decreasing frequency as one got further out on the radius away from the center hole. This is in contrast to the sharply defined contact area for the disks when the surfaces were smooth.

The disks used in the rubbing tests are made from 304 stainless steel and are four inches in diameter. The hole radius is in the neighborhood of 1/8 inch and the thicknesses used are 0.117", 0.250", and 0.304". The actual disk dimensions in nondimensional terms are

disk pair number	$\bar{a}$	$\bar{c}$
1	17.1	1.128
2	8.0	0.512
3	6.6	0.424

The disks were first machined and then annealed. After annealing they were ground flat to 0.0002 inches and then lapped flat to better than  $10 \cdot 10^{-6}$  inches. After lapping it was found that the roughness as measured on a Talysurf was

$$\text{C.L.A.} = 5 \cdot 10^{-6} \text{ inches}$$

or, for each disk,

$$\sigma = 7.26 \cdot 10^{-6} \text{ inches}$$

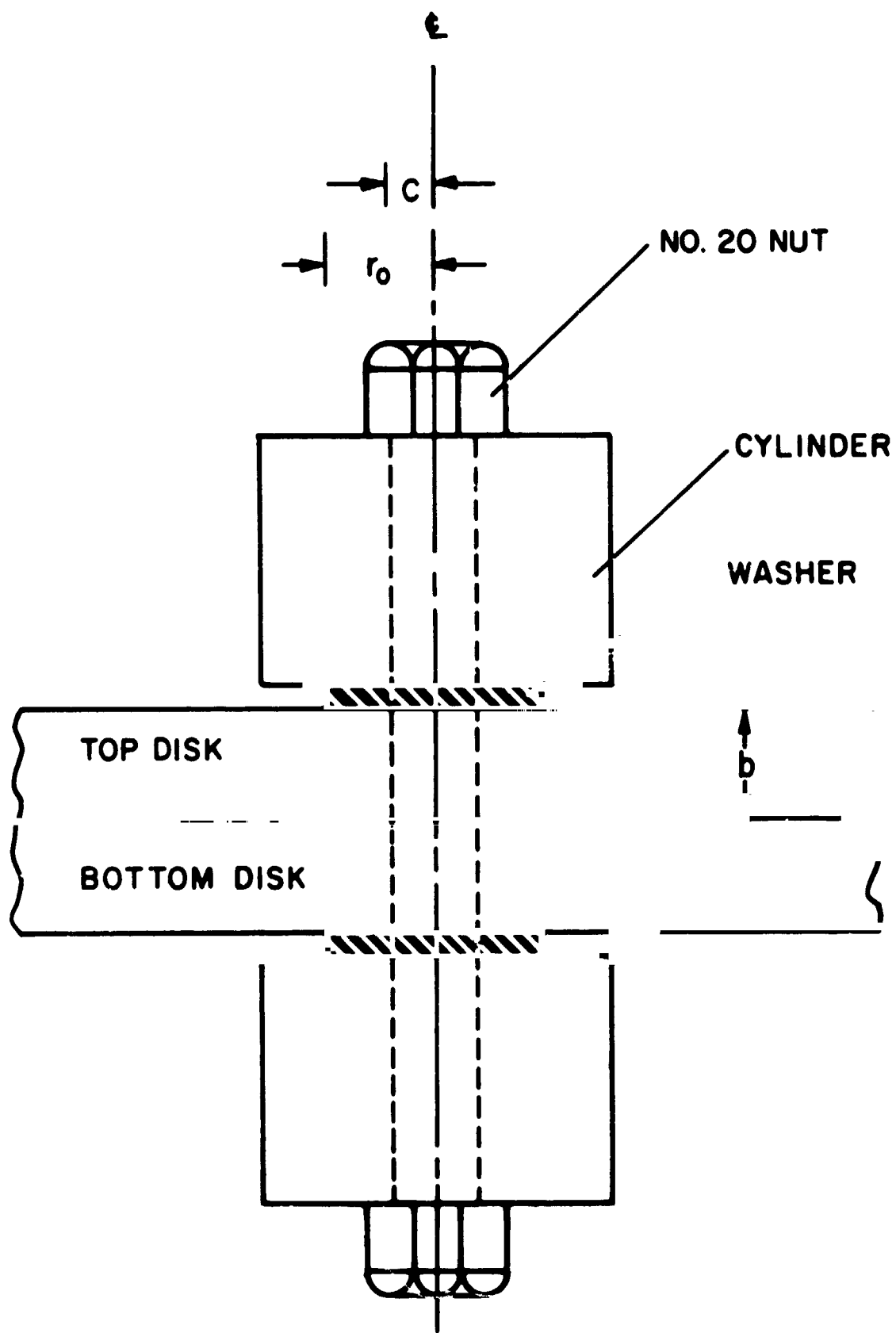
Material properties of the disks are

$$E = 29 \cdot 10^{+6} \text{ psi}$$

$$H = 26.7 \cdot 10^{+4} \text{ psi (Vickers)}$$

Each disk was fastened to its mate and joined through the hole by a 1/4-20 bolt. Cylinders were placed on the bolt on either side of the disks. These were of greater radius than the TEFLON<sup>®</sup> washers to insure as uniform a load over the washers as possible. Compliant washers were used so that any irregularities that might arise between cylinder and disks would die out. Figure 49 shows the experimental setup.

The apparatus described in [83] was used to insure that the disks do not turn with respect to each other while the nuts are tightened to a specified torque. The torque on the nut was translated into a load on the bolt by use of a chart developed with Belleville washers. A Belleville washer is a spring in the shape of a washer where the outer rim is in a different plane than the inner. Upon compression the washer flattens out. The force-deflection curve for a particular washer is known so if one measures the deflection caused by a particular torque, one knows the torque-force relationship. The particular washer used was Associated Spring Corporation Belleville washer #B1000-073. It was found in a series of experiments that the results were repeatable.

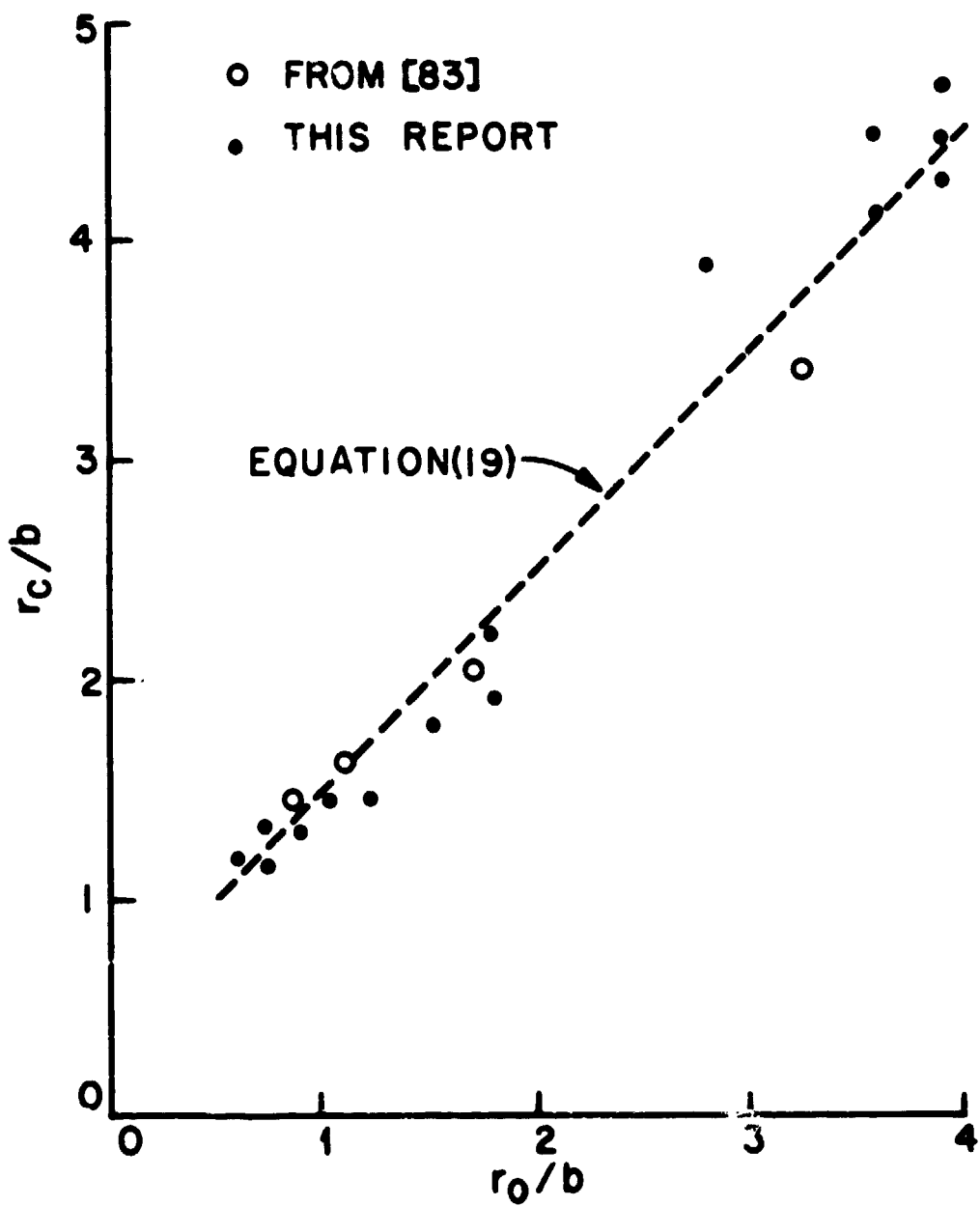


EXPERIMENTAL SETUP

FIG. 49

After turning the disks with respect to each other, the nuts were loosened and the interface was visually examined for the extent of wear. At first the experiments were done for the smooth, two-body contact problem to verify the general procedure. Afterward they were repeated for disks with roughened surfaces.

It was expected that for the case of roughened surfaces it would be difficult to see the wear marks on the disk surface and that some method of enhancing these traces would be needed. It was found that if one covered one of the two disks with a dye the traces would show even under the lightest of loads. The dye used was Dykem Steel Blue, the dye used by machinists for scribing. A very dilute solution was used so as to have as thin a film as possible. The problem to avoid, of course, is having the film interfere with the pressure distribution at the interface and altering the results. If the film is thin enough it is felt that the properties of the surface will indeed be those of the main body underneath. For this reason the rubbing experiments for the smooth disks were tried with and without the dye present. The results for both cases agreed with each other and with that given in [83]. Figure 50 gives the data found for  $\bar{r}_c$  versus  $\bar{r}_0$  and compares it to both the data and theory from [83]. There, it was claimed that



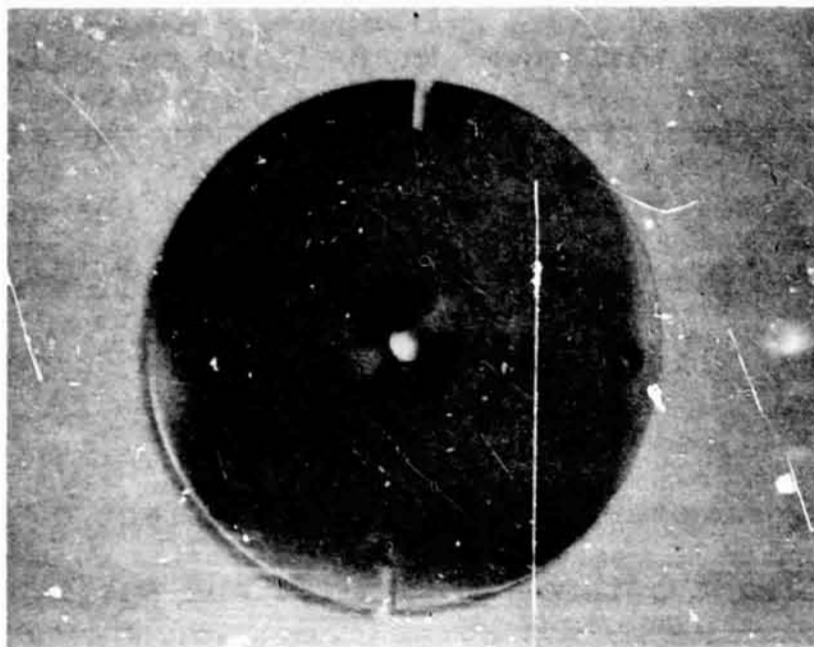
EXPERIMENTAL RESULTS FOR ZERO ROUGHNESS

FIG. 50

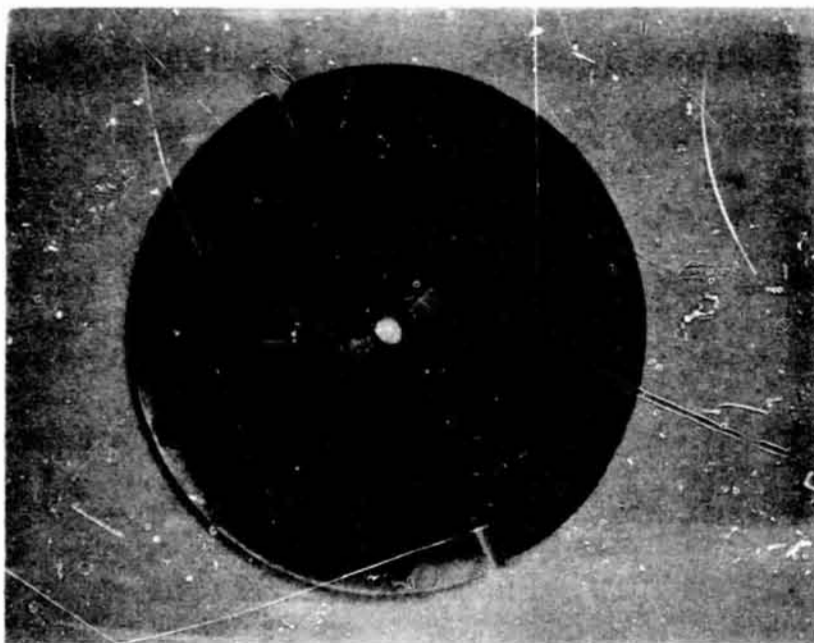
$$\bar{r}_c = \bar{r}_o + 0.5 \quad (19)$$

There is scatter, of course, in Figure 50 but the data does seem to correlate with (19) better than it would for other estimates such as that of Greenwood, for example, equation (18). Again, since it is difficult to control the load distribution, the data cannot be considered to be an absolute proof of (19).

Using the above technique it is possible to see the effect of asperities when either of the two disks are roughened. One of the two disks of a pair is subjected to a sandblaster until the required roughness is achieved. The other disk is coated with the dye. The two are then joined and rubbed together as before. When they are separated one sees that the imprint left behind is different than that when both disks were smooth. Before, the rubbed area was uniform and completely worn up to the radius of contact which was fairly well defined. Figure 51 shows such a pair both with and without the dye. With the rough disks the rubbed area consists of a series of scratches, the number of which decrease in density as one gets further from the center hole. In this case there is no specific radius of contact. This agrees, of course, with the conclusions drawn earlier. In sections 2.1, 2.2, and 2.3 it was recognized that in theory the interference between the



a) Smooth disk used in rubbing experiment - polished area  
in center is worn area



b) Smooth disk with dye used as mate to the above

## FIGURE 51

two surfaces would not stop at a particular point but would continue indefinitely. That is why the arbitrary percentage levels were used in defining the radius of contact when asperities were present. In the experimental work no attempt was made to correlate the number of scratches per unit area at a particular radius with the pressure level which caused it. Therefore no prediction of  $r_c$  at a particular level can be made.

One can, however, illustrate the effect of the asperities by taking the three disk pairs and subjecting them to the same load. If the parameters are chosen carefully one can achieve values of  $\bar{\sigma}$  which affect some pairs and do not affect the others. It was found that a torque of 60 in-lbs (equivalent load of 650 lbs) applied over an annular area of outer radius 0.455" and inner radius 0.125" would produce such an effect. The results are shown in Figure 52. The only difference between the three runs was the disk thicknesses, which were 0.117", 0.250", and 0.304". The average rms roughness averaged  $170 \cdot 10^{-6}$  in. which is, of course, an extremely rough plate. One expects that the thinnest plate will deflect more than the thicker; its gap will be wider and, therefore, less interference between asperities will occur. From Figure 52 one sees that for the thin disk,  $b=0.117$ ", the wear marks are concentrated tightly toward the center. For the other two they are



**FIGURE 52a**

Dyed disk where  $\tau$  too small  
to affect large-scale contact  
area

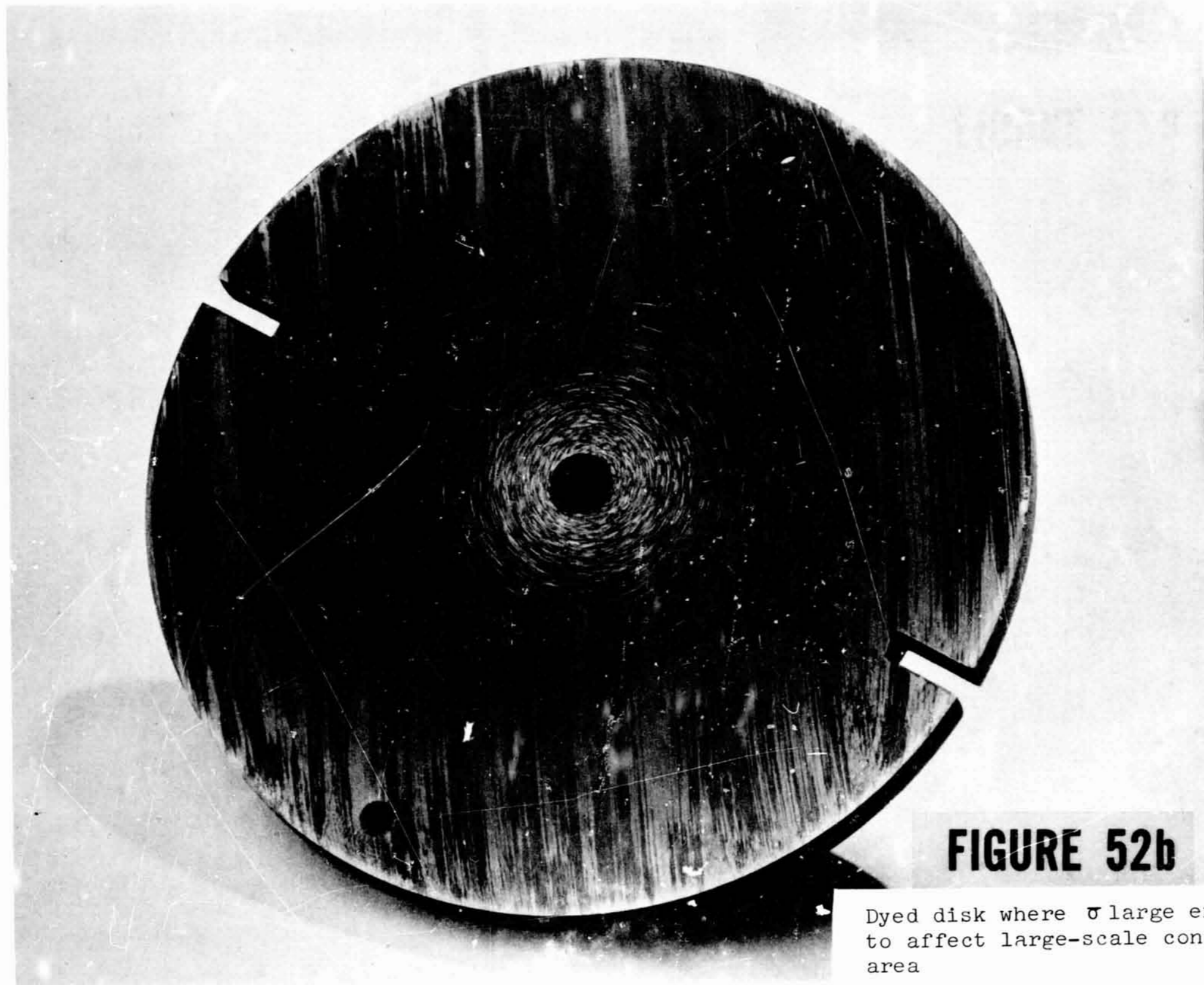


**FIGURE 52b**

Dyed disk where  $\sigma$  large enough  
to affect large-scale contact  
area

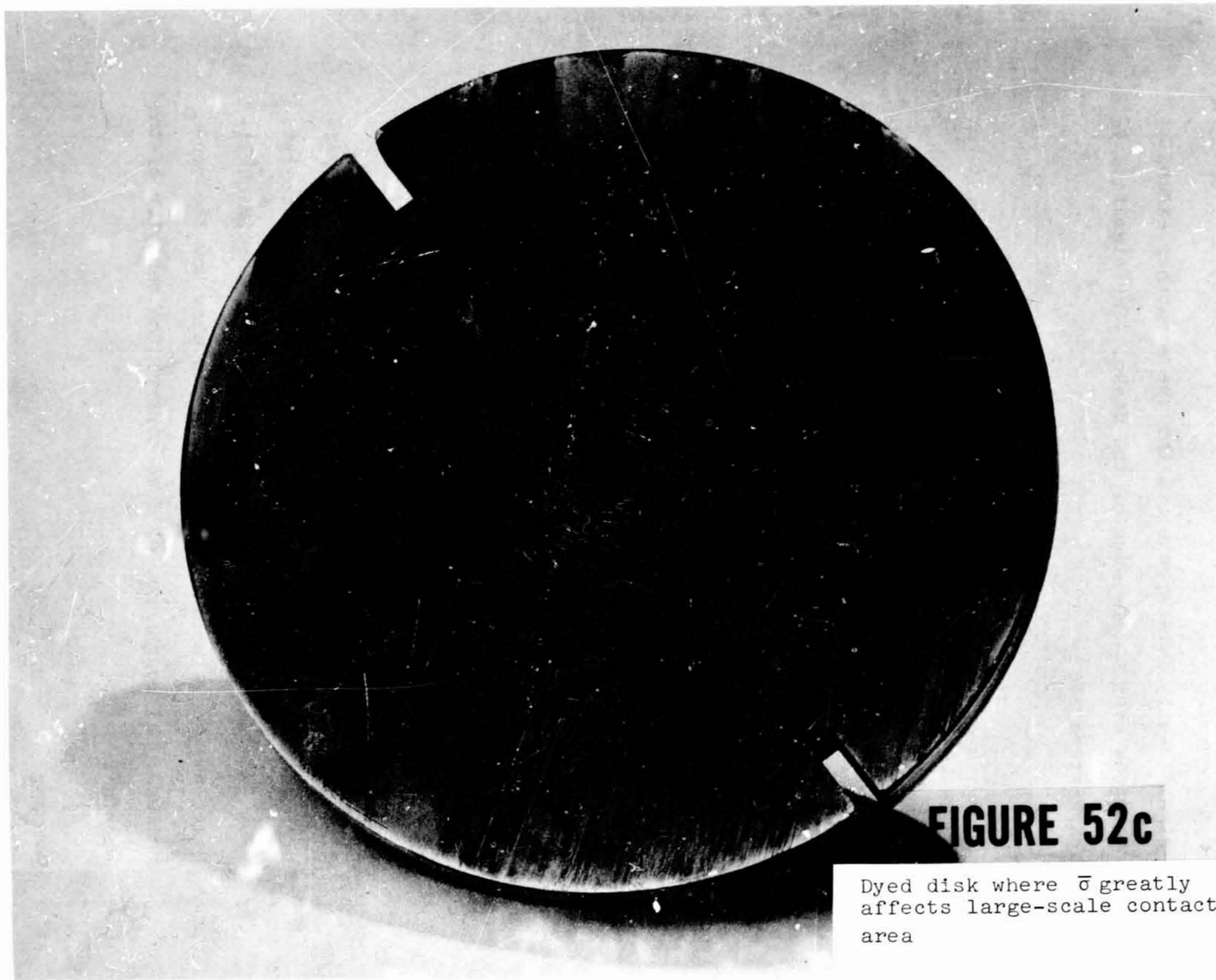


**FIGURE 52c**

Dyed disk where  $\bar{\sigma}$  greatly  
affects large-scale contact  
area

significantly more spread out and the scratches extend outwards even to the edge of the disks. The significant parameters are

disk pair number	$\bar{c}$	$\bar{r}_0$	$\bar{\sigma}$
1	1.128	3.89	40
2	0.512	1.82	16
3	0.425	1.50	17

No distributions were calculated for these specific values but for disk pairs #2 and #3 it can be seen from Figures 41 and 42 that a  $\bar{\sigma}$  in the neighborhood of 16 will lower the stress profile significantly. For disk pair #1, since  $\bar{r}_0$  is so much larger than  $\bar{c}$ , one might ignore the hole and examine the data given in Figures 25, 26, and 27 for disks with no hole. Even though curves for  $\bar{r}_0=4$  are not given it is not unreasonable to expect that the range of  $\bar{\sigma}$  necessary to affect the pressure distribution will lie above  $\bar{\sigma}=40$ .

In summary, therefore, although the experiments performed were not able to quantitatively verify the analytical predictions given earlier, they did corroborate qualitatively the expected behavior and did show how the non-dimensional roughness,  $\bar{\sigma}$ , does control the behavior of the contact.

### 3. HEAT TRANSFER EXAMPLE AND EXPERIMENTS

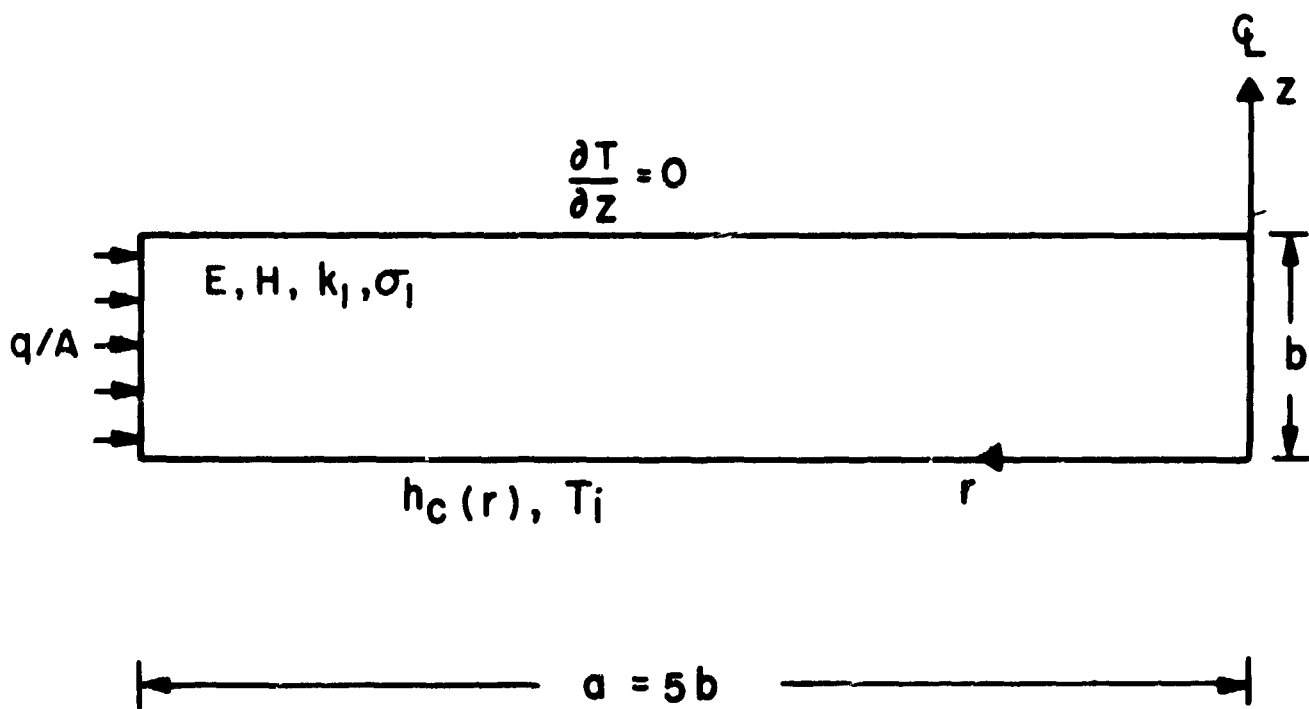
In the introduction it was mentioned that one cannot determine an overall contact resistance for an interface without describing the system of which the interface is a part. The best that one can do is present an equation such as (3)

$$h_c = 1.45 \frac{k \tan \theta}{\sigma} \left[ \frac{P}{H} \right]^{.985} \quad (3)$$

which will describe the conductance at a particular point. Any further consolidation of information is at the expense of generality. In this section the possible thermal effects of the phenomena investigated and discussed previously will be demonstrated by use of a specific example: the total thermal resistance of a disk like that shown in Figure 53. For this case the radius is five times the thickness, or  $\bar{a} = 5$ . The thermal boundary conditions are:

$$\begin{array}{ll} \text{at } z = 0 & k \frac{\partial T}{\partial z} = h_c(r)[T - T_1] \\ z = b & k \frac{\partial T}{\partial z} = 0 \\ r = 0 & k \frac{\partial T}{\partial r} = 0 \\ r = a & k \frac{\partial T}{\partial r} = q \end{array}$$

The particular value of  $h_c(r)$  used depends on the pressure distribution chosen from previous examples. The presence



MODEL USED IN THERMAL ANALYSIS

FIG. 53

of the hole can be included by allowing  $h_c(r) = 0$  for  $r < c$ . Three groups of  $p(r)$  at  $z = 0$  are examined: those for  $\bar{r}_0 = 0.5$ ,  $\bar{c} = 0.25$ ;  $\bar{r}_0 = 1.0$ ,  $\bar{c} = 0.5$ ; and  $\bar{r}_0 = 2.0$ ,  $\bar{c} = 1.0$ . For each of these groups the different interfacial stress distributions caused by different values of  $\bar{\sigma}$  are used. The desired result is the resistance of the system defined as

$$R_c = \frac{T(r = a, z = b/2) - T_1}{q/A}$$

Since the temperature level is unimportant,  $T_1$  is set arbitrarily to zero. It is also assumed that the exponent used in equation (3), 0.985, can be considered to be 1.0 with little error. If that is true then (3) can be rewritten as

$$\frac{h_c(r)b}{k} = 1.45 \left[ \frac{E}{H} \tan \theta \right] \frac{\left[ \frac{p(r)}{p_0} \right]}{\left[ \frac{\sigma E}{bp_0} \right]}$$

or

$$\bar{h}_c(\bar{r}) = 1.45 \left[ \frac{E}{H} \tan \theta \right] \frac{\bar{p}(\bar{r})}{\bar{\sigma}} \quad (38)$$

If one defines

$$\bar{R}_c = \frac{R_c k}{b} \quad Q = \frac{q/Ab}{k}$$

then

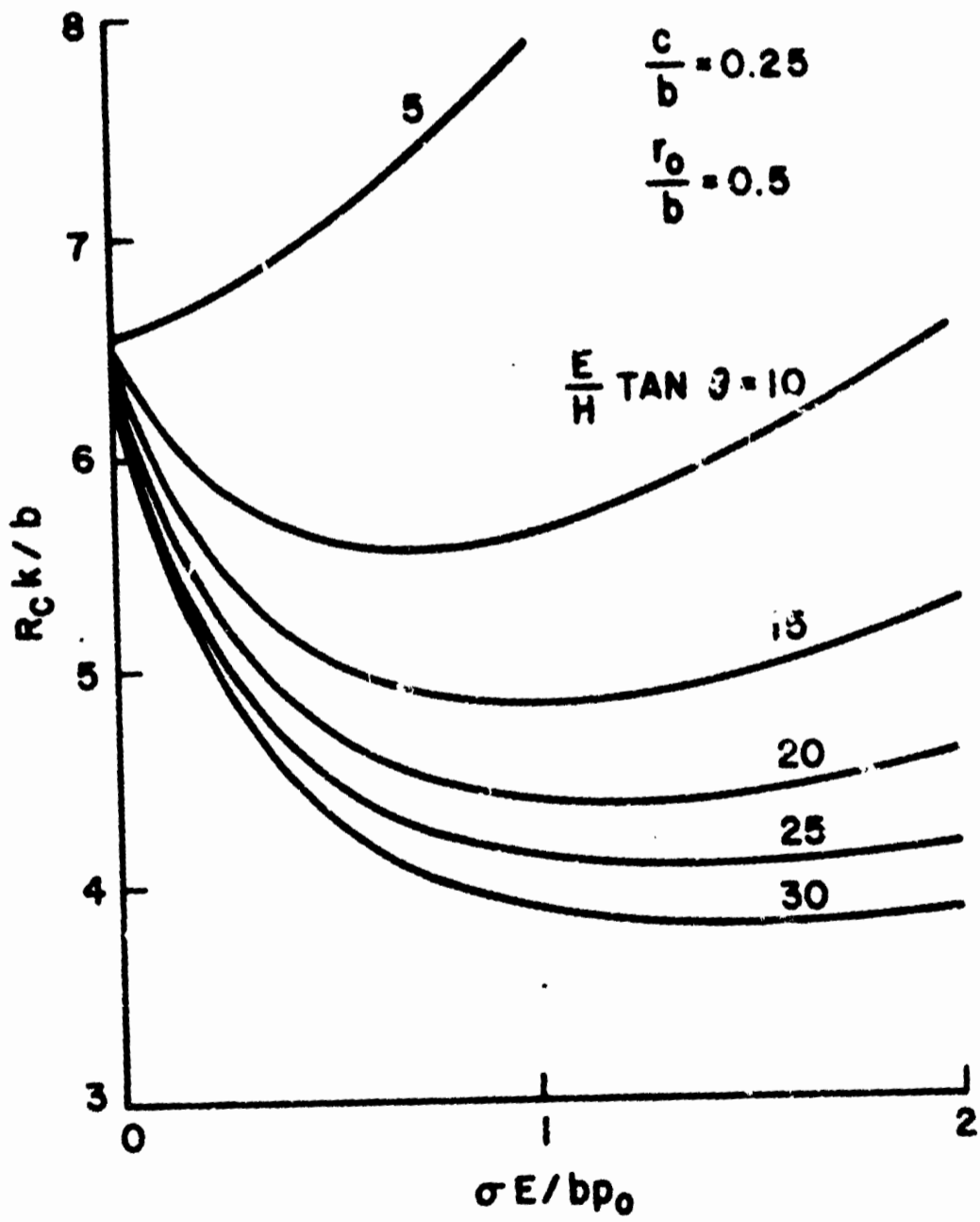
$$\bar{R}_c = \frac{T(\bar{r} = \bar{a}, \bar{z} = 0.5)}{Q} \quad (39)$$

The boundary conditions now are:

$$\begin{aligned} \text{at } \bar{z} = 0 & \quad \frac{\partial T}{\partial \bar{z}} = \bar{h}_c(r)T \\ \bar{z} = 1 & \quad \frac{\partial T}{\partial \bar{z}} = 0 \\ \bar{r} = 0 & \quad \frac{\partial T}{\partial \bar{r}} = 0 \\ \bar{r} = \bar{a} & \quad \frac{\partial T}{\partial \bar{r}} = Q \end{aligned}$$

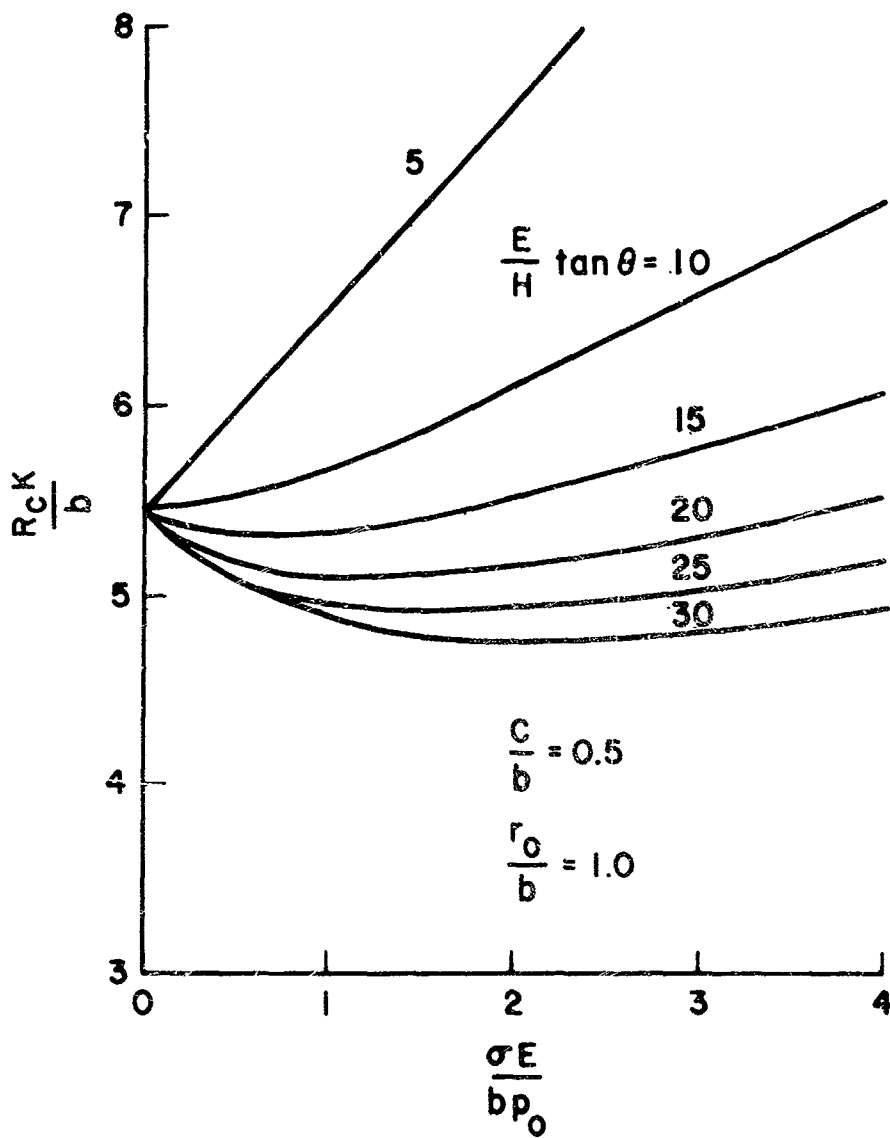
The governing equation is the Laplacian,  $\nabla^2 T = 0$ . Because of the varying  $h_c(r)$  no analytical solution is available, but the above is simple enough to solve numerically. The final result is a plot of  $\bar{R}_c$  versus  $\bar{\sigma}$  for various values of  $E \tan \theta/H$ . There is one such graph for each set of  $\bar{r}_0, \bar{c}$ . It should be noted that the resistance presented is for one disk only. In an assembly of two disks the total resistance would be double that shown here. Figures 54, 55, and 56 show the results.

It was mentioned earlier that the total resistance was the sum of that due to the bulk and that due to the resistance at the interface. As one varied the roughness one might expect that the total effect would decrease or



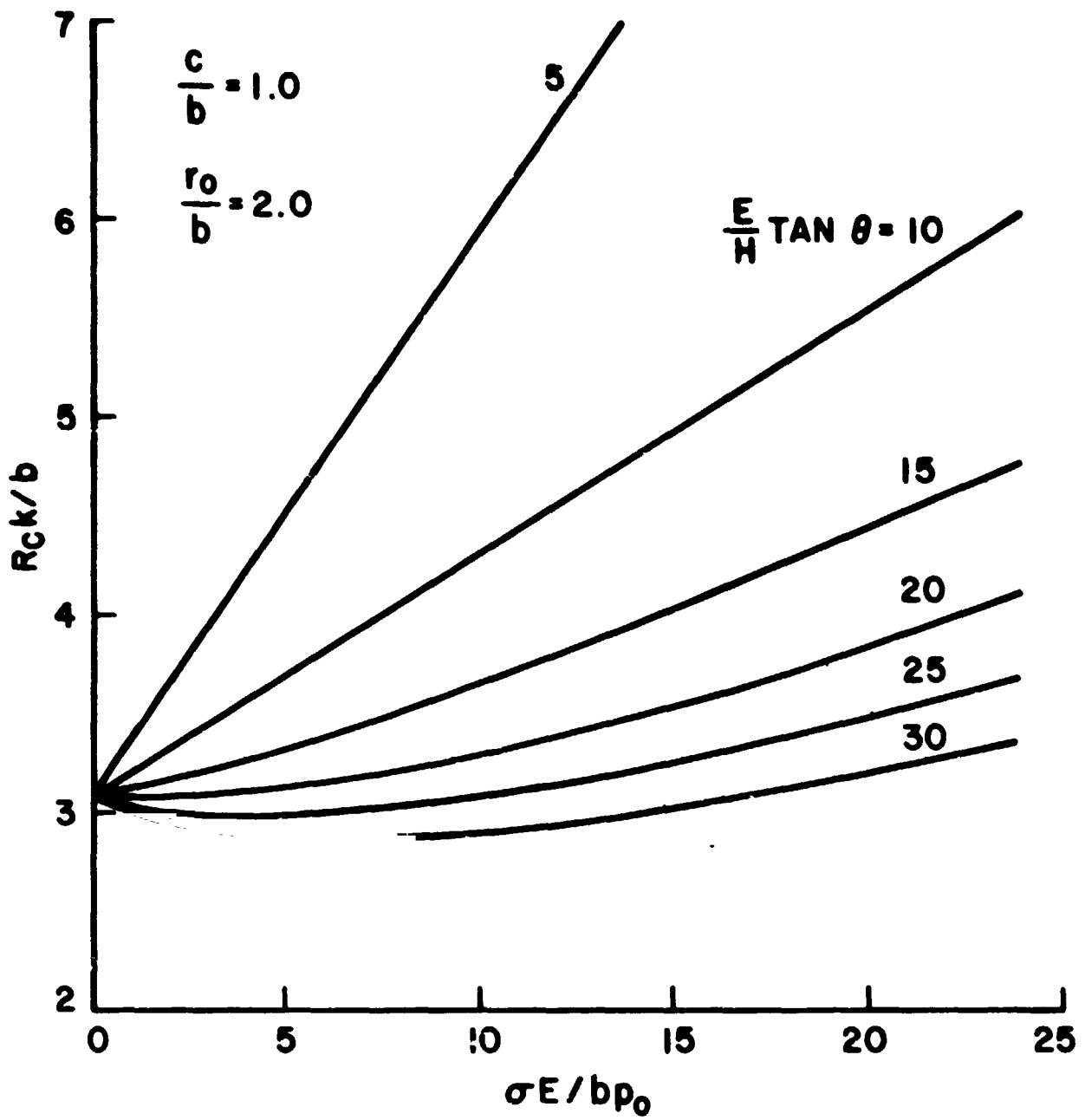
THERMAL RESISTANCE OF DISK WITH HOLE  
AS SHOWN IN FIGURE 53

FIG. 54



THERMAL RESISTANCE OF DISK WITH HOLE  
AS SHOWN IN FIGURE 53

FIG. 55



THERMAL RESISTANCE OF DISK WITH HOLE  
AS SHOWN IN FIGURE 53

FIG. 56

increase depending on the operating conditions. From the figures shown here it is obvious that this is true and that the quantity  $E \tan \theta/H$  is the critical variable. Depending on the value of  $\bar{r}_0$  and  $\bar{c}$ , there is a value of  $E \tan \theta/H$  below which one cannot lessen the resistance by altering the roughness. Conversely, for sufficiently large values of  $E \tan \theta/H$  one can decrease the resistance markedly by increasing the roughness. At intermediate values there is an optimum roughness at which to operate.

The entire effect seems to be strongly dependent on the particular value of  $\bar{r}_0$  and  $\bar{c}$  one is at. Compare, for example, Figures 54 and 56. The effect of roughness is much more pronounced for a small value of  $r_0$  than it is for a large one. This is mostly due to the particular example being used here. Since heat is forced in through the sides, the final resistance is strongly dependent on radius of contact, the first place where the heat can turn from one plate into the other. If  $r_c$  is large enough the majority of the heat flows through the area immediate to  $r_c$  and ignores the central area. A large  $r_0$  implies a large  $r_c$ . A large  $r_c$  means that less of the total resistance is due to the bulk and most is due to the contact resistance at the interface. Since an increase in roughness increases the resistance at the interface, then one would expect the total resistance to increase with greater  $\bar{\sigma}$  for large  $r_0$ . For a small  $r_0$  most of the resistance is due to

the bulk. Increasing  $\bar{\sigma}$  increases the radius of contact greatly. Therefore the greater part of the resistance is lessened. Thus, for small  $r_0$ , increasing  $\bar{\sigma}$  tends to decrease the total resistance.

Therefore the behavior exhibited in these figures is largely due to the configuration chosen for the example. If instead of having the heat enter the edges at  $r = a$  one had it enter at the top,  $z = b$ , one would arrive at a different set of curves. These would be more like those in Figure 56 rather than in Figure 54 since the bulk resistance would be a minor part of the total.

Actual experiments which measured the thermal resistance of two disks joined together by a bolt were performed by Joseph Pigott [89]. The following description of the experimental measurements is from Reference [89].

The experiments on contact resistance were done in the vacuum chamber shown in Figure 57. A vacuum of between 30 microns and 50 microns was maintained to minimize the effects of interstitial fluid.

The test pieces were made according to Figure 58. The only geometry investigated had dimensions:

$$\begin{aligned}c/b &= 0.5 \\r_0/b &= 1.0\end{aligned}$$

The radius of the plates may be anything greater than  $5b$ . This is well beyond the radius of contact.

All runs were made with the same applied pressure to the joint and the same power input to the system.

Five runs were made with the dimensionless roughness ( $\frac{\sigma E}{bP_0}$ ) ranging from 0.023 to 1.23, and the slope ( $E \tan \theta/H$ ) ranging from approximately zero to 16.2.

The resultant temperature profiles (Figures 59, 60, 61, 62, and 63) agree fairly well with the theoretical predictions. The deviations of isolated points are probably due to faulty thermocouple setup.

To find the contact resistance it was necessary to determine the actual heat rate passing through the test specimen and an appropriate temperature difference,  $\overline{\Delta T}$ , both of which appear in the resistance equation:

$$R = \frac{\overline{\Delta T}}{q/A}$$

It is known from the pressure distribution that the plates are not in contact beyond the fourth thermocouple position (see Figure 41; the values of  $r/b$  correspond to the thermocouple positions shown in Figure 58). Therefore, by knowing the temperatures at positions 5 and 6 and the corresponding radii, the heat rate passing through the test section can be calculated:

$$q = \frac{2\pi kb}{\ln(r_6/r_5)}(T_6 - T_5)$$

Since the plates are not in contact and radiation between the plates was found to be very small, the heat must flow in one direction: radially. However, it was found that there was not perfect symmetry across the interface. Therefore, the temperature difference in the above equation was found for both the top and bottom plates and the average of these values was used as the temperature difference.

The resistance equation actually involves a heat flux rather than a heat rate. Since the flux was calculated between points 5 and 6, the area chosen was that lateral area of the cylinder passing through the midpoint between positions 5 and 6.

The temperature difference,  $\overline{\Delta T}$ , may be chosen arbitrarily, depending on how the resistance is to be defined. In the present case the temperature difference between the top and bottom plates at the sixth thermocouple position was used in order to give the total resistance. The theoretical predictions were given as values of half the total resistance, so the experimental results were divided by two for comparison.

For convenience, the resistance equation has been non-dimensionalized in the following manner:

$$\frac{Rk}{b} = \frac{\overline{\Delta T}}{Q}$$

where

$$Q = \frac{qb}{Ak}$$

The resistances found for the various roughnesses tested were:

roughness (rms micrometer)	resistance ( $R_k/b$ )
7.05	9.95
112.6	10.20
132.7	9.80
270	10.40
303	9.60

These resistances are roughly constant. They correlate fairly well with the theoretical results in the same range of parameters (Figure 55). However, the values are approximately twice those predicted. It is believed that this was caused by an inevitable deviation from radial symmetry in the test, either in pressure distribution or, more likely, in heat transfer distribution.

The range of parameters investigated here covers the range of surface conditions ordinarily found for surfaces in thermal contact.

For the geometry used and the range of parameters tested, both the theoretical model and the experimental results suggest that the roughness has negligible effect on the resistance of the joint.

Furthermore, since the range of parameters used here covers most of the conditions of practical interest, one can extend the conclusions to a general statement that roughness

- 144D -

for the bolted joint geometry considered does not strongly affect the value of thermal contact resistance. Consequently, from a practical point of view, it is not necessary to demand great care in providing smooth surfaces for thermal contact.

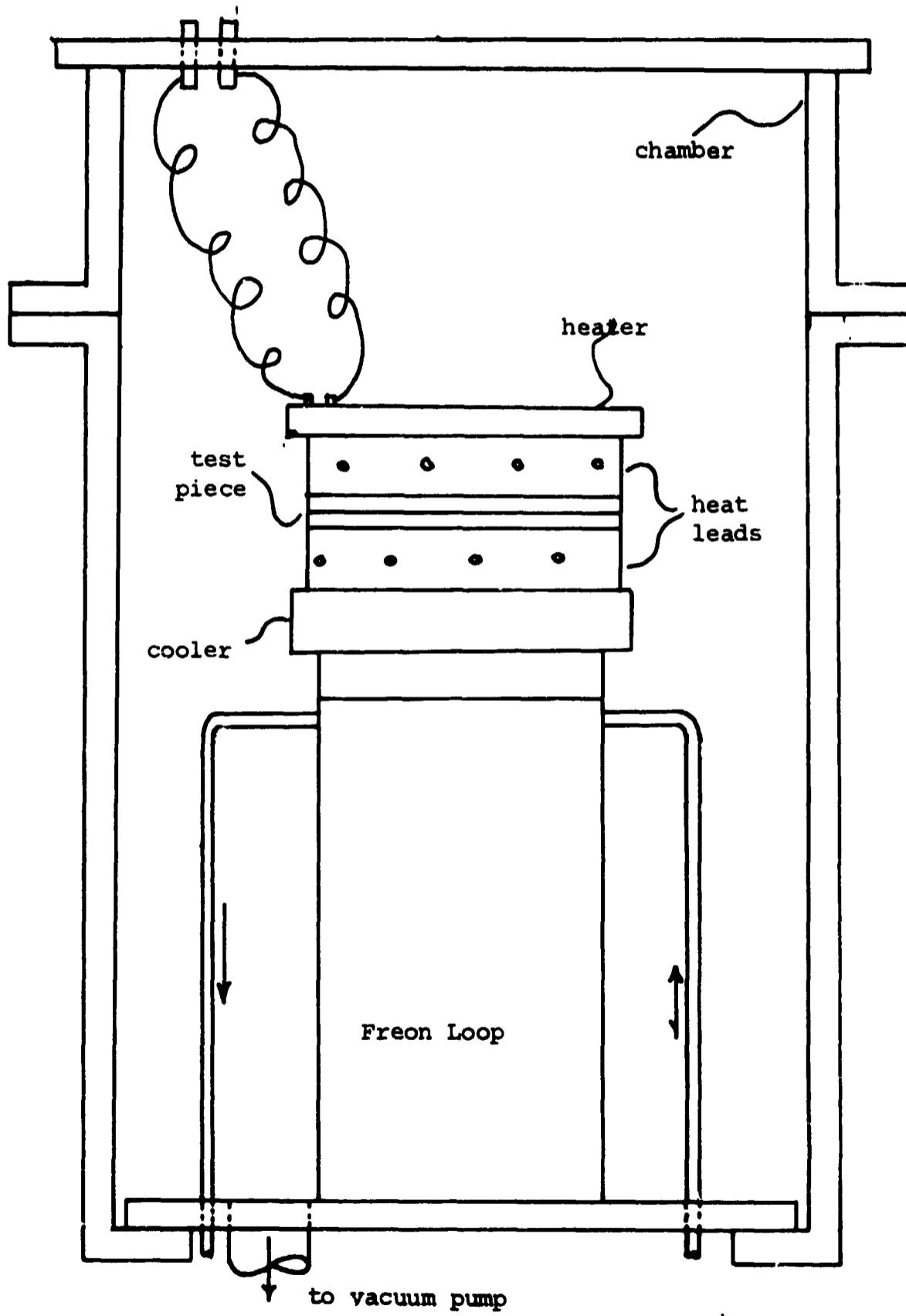


Figure 57

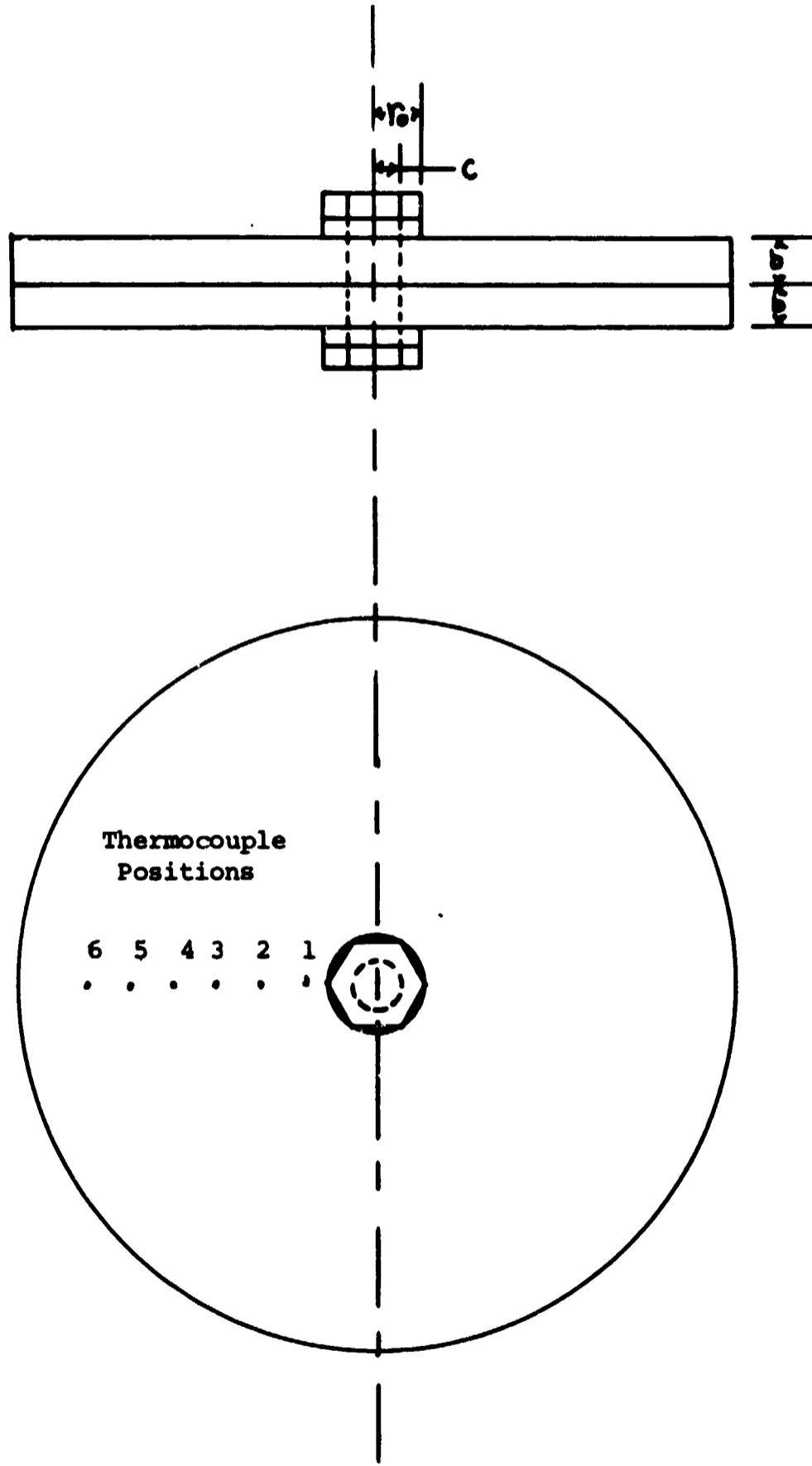


Figure 58

- 144G -

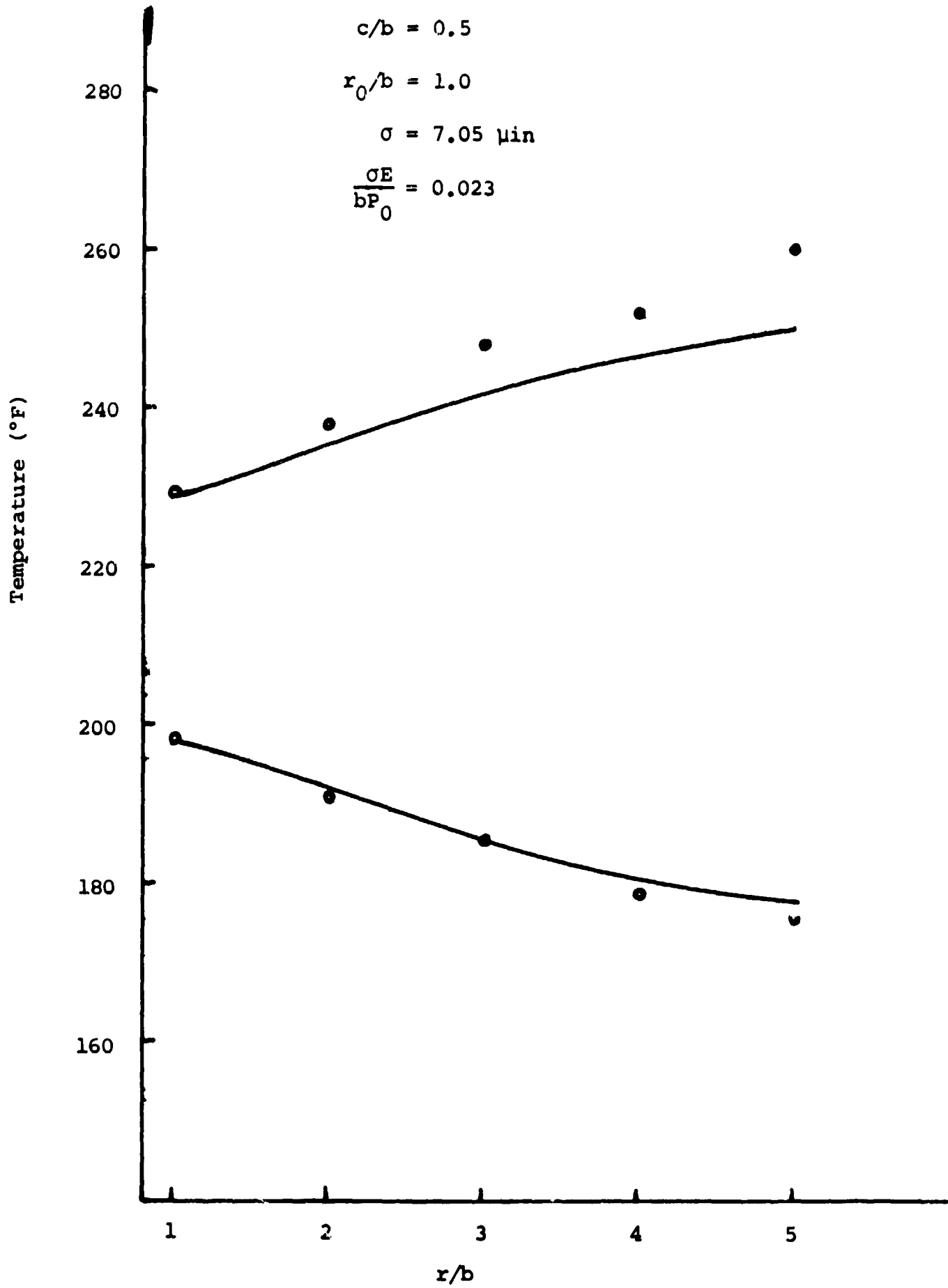


Figure 59

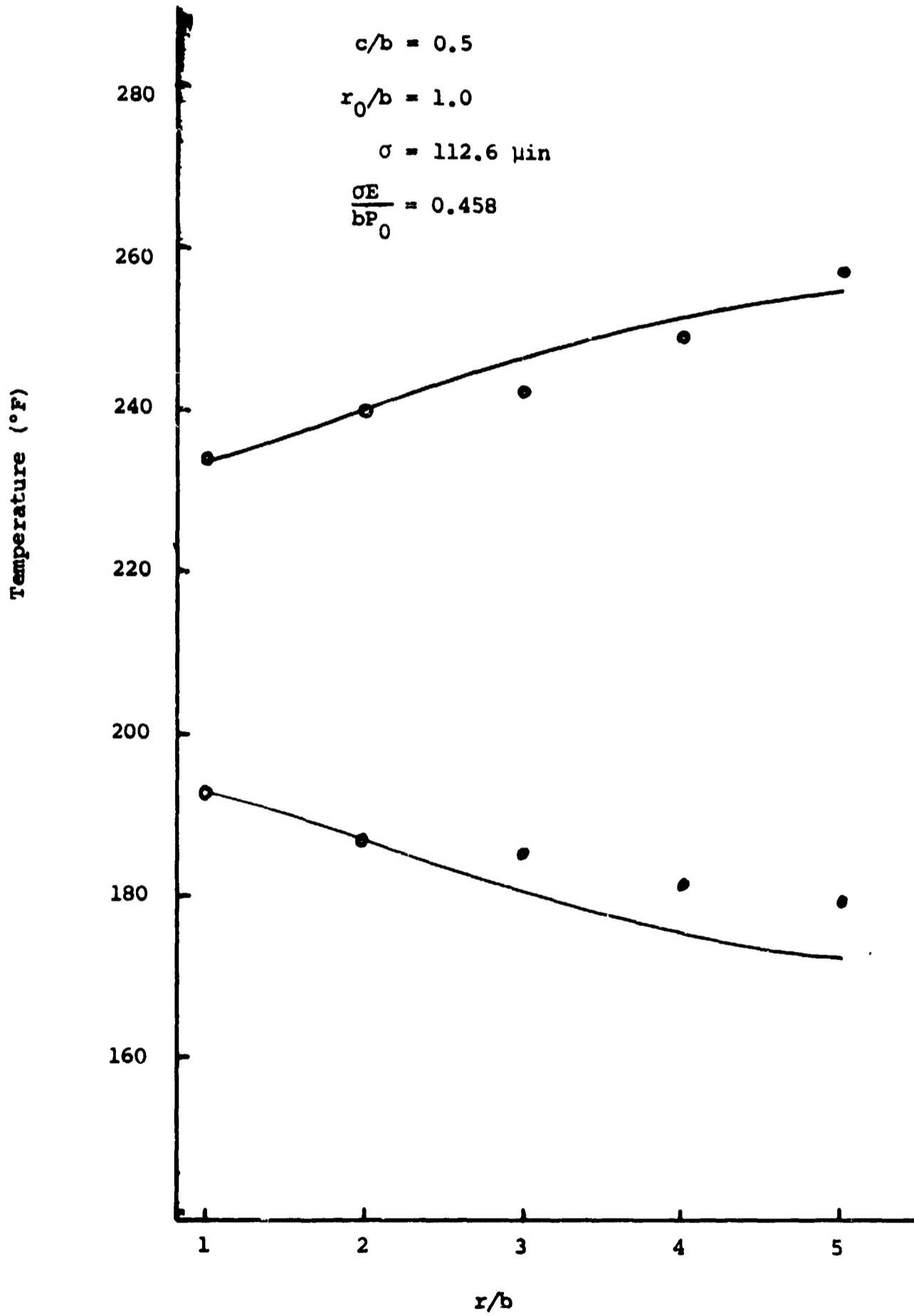


Figure 60

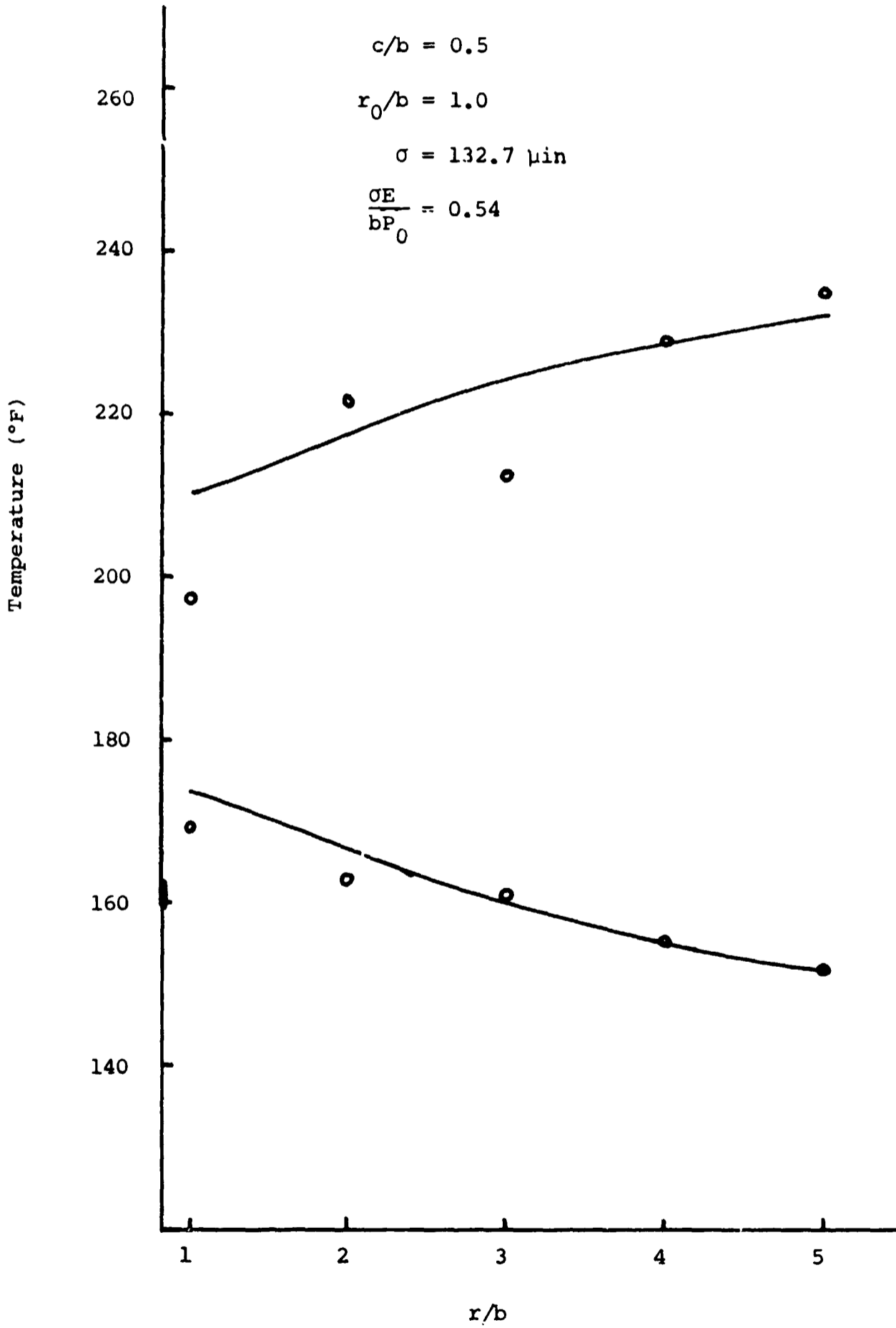


Figure 61

- 144J -

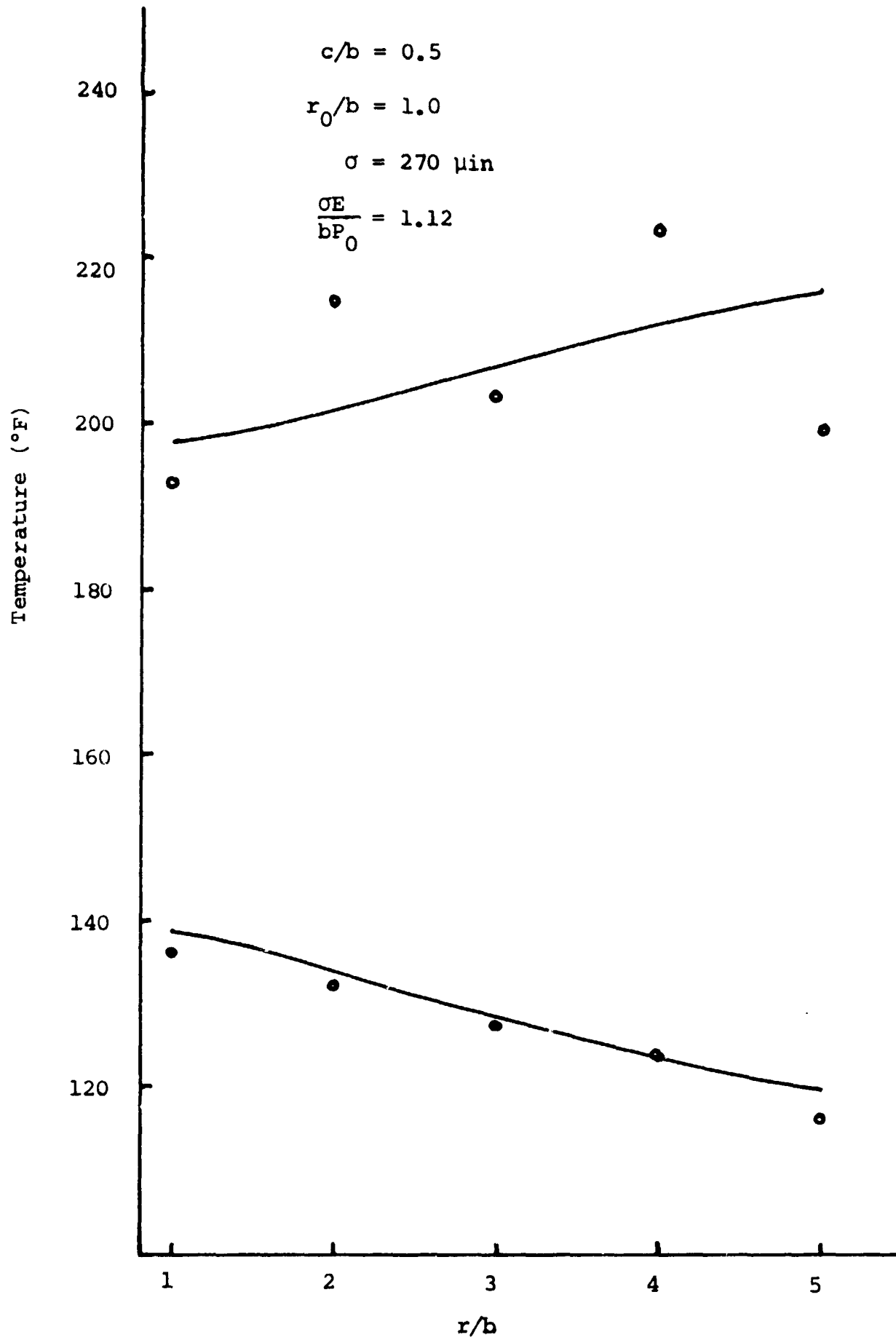


Figure 62

- 144K -

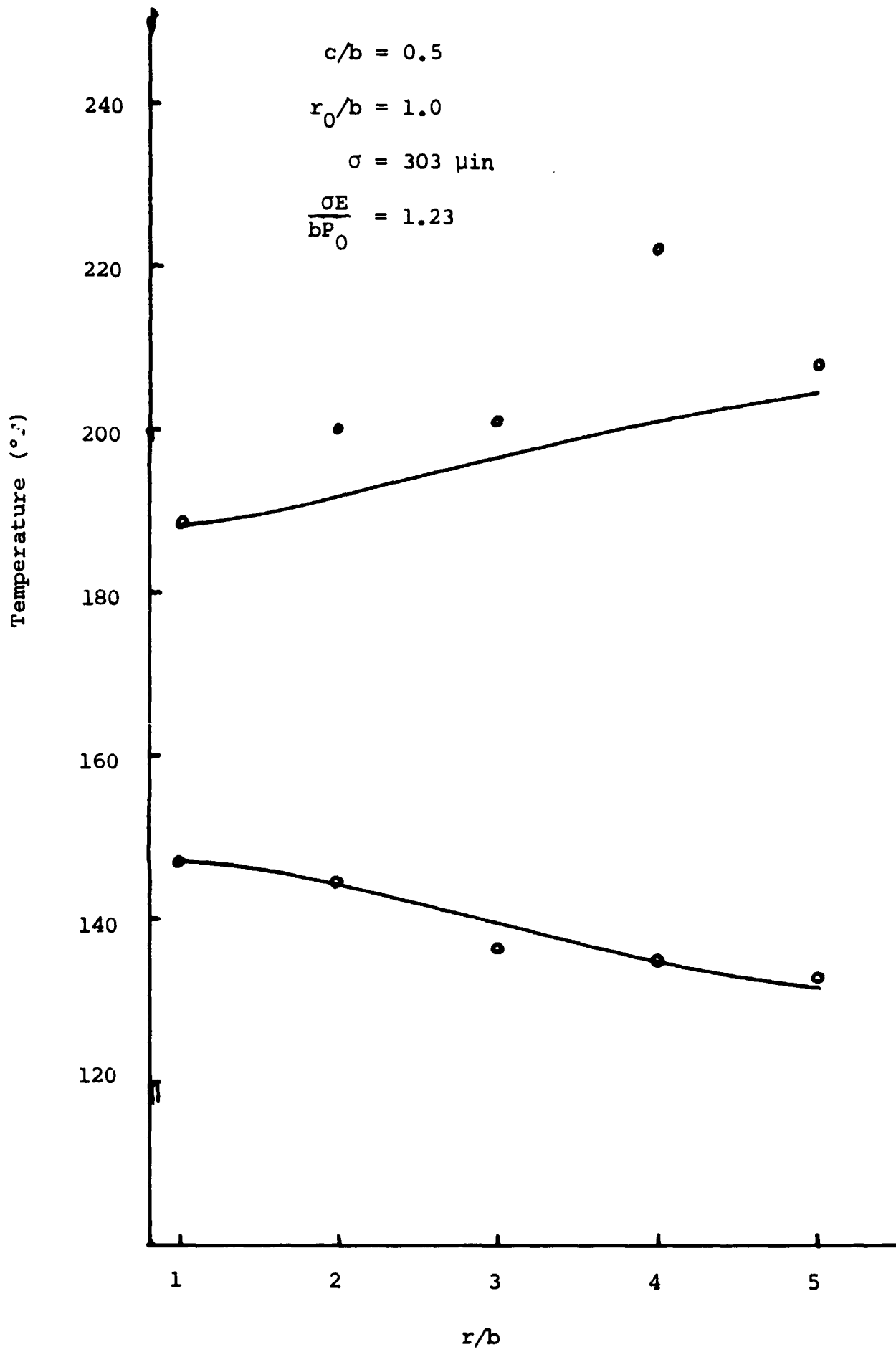


Figure 63

#### 4. SUMMARY AND CONCLUSIONS

It was noted at the beginning of this paper that the thermal resistance at a joint can be divided into two categories: that due to the large-scale constriction of the heat from the main body to the general contact area and that due to the constriction within this contact area at the asperities. Since an increase in surface roughness affects these two components in opposite directions - decreasing large-scale resistance, increasing small-scale resistance - it was postulated that one might be able to decrease the total resistance by increasing the roughness.

Three cases were considered: contact of two rough, wavy surfaces, contact of two rough but nominally flat plates with an applied load over a defined area, and contact of two rough but nominally flat plates joined together with bolts. The models for the above are, respectively: two spherical surfaces, two disks of finite radius, and two disks of finite radius with center holes. An iterative solution was used where the force and deflection of the bulk was matched to the force and deflection of the asperities. Solutions were to be generated for the cases of zero and nonzero roughness. It was found that to solve the overall problem one needed force-deflection relationships for asperities, spherical surfaces, and disks both with and without holes. Such relationships for the

asperities and special surfaces already existed in the literature. Those for disks with or without holes were developed in this report.

Nondimensional variables were chosen so as to minimize the information needed to explain the results. For the spherical surfaces it was found that all information could be expressed on one master graph of interfacial pressure distribution as a function of roughness. For the disks without holes one master was needed for each load radius; for the disks with holes one was needed for each set of hole radius and load radius. In addition to the geometrical variables needed to describe the model, it was found that two nondimensional surface variables were needed:  $\bar{\sigma}$  and  $\bar{H}$  where

$$\bar{\sigma} = \frac{\sigma \bar{E}}{a_h p_0} \quad (\text{for spherical surfaces})$$

$$\bar{\sigma} = \frac{\sigma E}{b p_0} \quad (\text{for disks})$$

$$\bar{H} = \frac{H}{p_0}$$

It was further found that the results were weakly dependent on  $\bar{H}$  and strongly dependent on  $\bar{\sigma}$ . Given a particular  $\bar{\sigma}$ ,  $\bar{H}$  pair, one could determine a pressure at an arbitrarily chosen reference point. This pressure would then be

matched with that on the master graph to arrive at the entire distribution. This could be done because all distributions which agreed at one point would agree at all points. One could also estimate the radius of contact for various values of  $\bar{\sigma}$  and  $\bar{H}$ . It was also found that different ranges of  $\bar{\sigma}$  influenced the contact for different values of geometric properties such as load radius. In general, the surface properties affected the behavior of the disks more strongly than that of the spheres.

In the process of developing the force-deflection relationships needed for the disks with and without holes, further work was done on the classical midplane stress problem as discussed by Sneddon, Greenwood, Lardner, et al. From this it was concluded that the multiple Fourier-Bessel series technique used to develop the required solutions to the various models is accurate.

The resulting pressure distributions were used in a heat transfer example to show that one could indeed lower the overall thermal resistance of a system with an interface by increasing the surface roughness. It was found that the resistance (in nondimensional terms) depends on  $\bar{\sigma}$  and on another quantity,  $E \tan \theta/H$ . The latter determines if it is at all possible to raise or lower the resistance by changing  $\bar{\sigma}$ . In brief, then, the behavior discussed at the beginning of the report was found to exist for all three models considered.

There are two general areas for which conclusions may be drawn: the overall problem itself and the techniques used to arrive at the solutions. Considering the value of  $E \tan \theta/H$  that one might find in practice ( $\sim 25$ ) the effect of playing the large-scale constriction off against the small-scale constriction in order to lessen the overall resistance is not as strong as hoped for. While it is obvious that in many cases it is not necessary to go through elaborate (and expensive) finishing procedures to decrease the overall resistance, it does not seem possible to decrease the resistance drastically by increasing the roughness except in those cases where the resistance is very sensitive to the outermost radius of contact.

The multiple series technique used to develop the various solutions has been proven successful and, although laborious to implement, straightforward in its application.

5. BIBLIOGRAPHY

1. Little, W. A. "The Transport of Heat Between Dissimilar Solids at Low Temperatures", Can. J. of Phys. Vol 37, 1959, pp 334-349.
2. Holt, V. E. "Quantized Energy Transport Across Interfaces at Low Temperatures", 4th Conference of Soc. for Eng. Science, Proc. Pergamon Press, Nov. 1966, pp 109-121.
3. Rechowicz, T. et al "Heat Transfer Across Pressed Contacts at Low Temperatures", Cryogenics, Dec. 1967, pp 369-370.
4. Brown, E. C. and Holt, V. E. "Thermal Conductance of Imperfect Contacts", 7th Conference on Thermal Conductivity, NBS Special Publication No. 302, April 1968, pp 761-768.
5. Baer, Y. "Resistance Thermique de Contact Entre Isolateurs", Phys. Kondens. Materie 8, 1968, pp 1-30.
6. Gale, E. H., Jr. "Effects of Surface Films on Thermal Contact Conductance", ASME 70-HT/SpT-26 1970, pp 1-8.
7. Boeschoten, F. and Van Der Held, E. F. M. "The Thermal Conductance of Contacts Between Aluminum and other Metals", Physica XXIII, 1957, pp 37-44.
8. Graff, W. J. "Thermal Conductance Across Joints", Machine Design Vol 32, Sept. 15, 1960, pp 166-172.
9. Cordier, H. and Maimi, R. "Etude Experimentale de L'Influence de la Pressian sur les Resistances Thermiques de Contact", Séance, April 25, 1960, pp 2853-2855.
10. Bory, Ch. and Cordier, H. "Resistances Thermiques de Contact", Institute Francais des Cambustibles et de L'Energie, Journees de la Transmission de la Chaleur, 1.08, pp 1-6.
11. Cordier, H. "Etude Experimentale des Resistances Thermiques de Contact Influence de la Pressian", Annoles de Physique, 1961, pp 5-19.
12. Fried, E. "The Thermal Conductance of Space Vehicle Interfaces - Experimental Results", General Engineering Laboratory Report No. 61GL65, March 1961, General Electric Company.

13. Fried, E. and Costello, F. A. "The Interface Thermal Contact Resistance Problem in Space Vehicles", American Rocket Society Structures, Materials and Design Conference, April 4-6, 1961, p 279.
14. Bernard, J. J. "The Thermal Resistance of Joints", Royal Aircraft Establishment Library Translation, No. 951, June 1961.
15. Stubstad, W. R. "Measurement of Thermal Contact Conductance in Vacuum", ASME paper 63-WA-150.
16. Petri, F. J. "An Experimental Investigation of Thermal Contact Resistance in a Vacuum", ASME paper 63-WA-156.
17. Fried, E. "Thermal Joint Conductance in a Vacuum", ASME paper 63-AHGT-18.
18. Atkins, H. L. and Fried, E. "Thermal Interface Conductance in a Vacuum", 1st AIAA Annual Meeting, June 1964.
19. "Thermal Contact Conductance in a Vacuum Environment", Douglass Aircraft Company, Missile and Space Systems Division Report No. SM-47700, Dec. 1964.
20. Stubstad, W. R. "Thermal Contact Resistance Between Thin Plates in Vacuum", ASME paper 65-HT-16.
21. Fried, E. and Kelley, M. J. "Thermal Conductance of Metallic Contacts in a Vacuum", AIAA Thermophysics Specialist Conference paper 65-661.
22. Fry, E. M. "Measurements of Contact Coefficients of Thermal Conductance", Bell Telephone Laboratories paper MM-66-6221-2, May 1966.
23. Clausing, A. M. "An Experimental and Theoretical Investigation of the Thermal Contact Resistance", U. of Ill. Eng. Exp. Station report no. ME-TN-242-3, July 1966.
24. Ozisik, M. N. and Hughes, D. "Thermal Contact Conductance of Smooth-to-Rough Contact Joints", ASME paper 66-WA/HT-54.

25. Veziroglu, T. N. "Correlation of Thermal Contact Conductance Experimental Results", AIAA Thermophysics Specialist Conf. April 1967. pp 879-907.
26. Jeng, D. R. "Thermal Contact Resistance in Vacuum," Journal of Heat Transfer, Aug. 1967, pp 275-276.
27. Fletcher, L. S. "Thermal Contact Resistance of Metallic Interfaces", PhD thesis, Arizona State U., Aug. 1968.
28. Minges, M. L. "The Temperature Dependence of the Thermal Contact Resistance Across Nonmetallic Interfaces", Air Force Mat. Lab. report AFML-TR-69-1, October 1969.
29. Cassidy, J. F. and Mark, H. "Thermal Contact Resistance Measurements at Ambient Pressures of One Atmosphere to  $3 \times 10^{-12}$  mm Hg and Comparison with Theoretical Predictions", NASA TM X-52566, 1969.
30. McKinzie, D. J., Jr. "Simplified Method for Calculating Thermal Conductance of Rough, Nominally Flat Surfaces in High Vacuum", NASA TN D-5627, Jan. 1970.
31. Centinkale, T. N. and Fishenden, M. "Thermal Conductance of Metal Surfaces in Contact", General Discussion on Heat Transfer, Conf. of Inst. of Mech. Eng. and ASME, London, 1951.
32. Fenech, H. and Rohsenow, W. M. "Prediction of Thermal Conductance of Metallic Surfaces in Contact", Journal of Heat Transfer, Feb. 1963, pp 15-24.
33. Henry, J. J. and Fenech, H. "The Use of Analog Computers for Determining Surface Parameters Required for Prediction of Thermal Contact Conductance", Journal of Heat Transfer, Nov. 1964, pp 543-551.
34. Clausing, A. M. and Chao, B. T. "Thermal Contact Resistance in a Vacuum Environment", Journal of Heat Transfer, May 1965, pp 243-251.
35. Shlykov, Yu. L. "Calculating Thermal Contact Resistance of Machined Metal Surfaces", Teploenergetika, Vol 12, 1965, pp 79-83, UDC 537.311.4.001.24, pp 102-107.
36. Mikic, B. B. "Thermal Contact Resistance", ScD thesis, MIT, Sept. 1966.

37. Rogers, G. F. C. "Heat Transfer at the Interface of Dissimilar Metals", Int. J. of Heat Mass Transfer Vol 2, 1961, pp 150-154.
38. Powell, R. W. et al. "Heat Transfer at the Interface of Dissimilar Materials", Int. J. Heat Mass Transfer Vol. 5, Pergamon Press, 1962, pp 897-902.
39. Moon, J. S. and Keeler, R. N. "A Theoretical Consideration of Directional Effects in Heat Flow at the Interface of Dissimilar Metals", Int. J. Heat Mass Transfer Vol. 5, Pergamon Press, 1962, pp. 967-971.
40. Clausing, A. M. "Heat Transfer at the Interface of Dissimilar Metals", Int. J. Heat Mass Transfer Vol. 9, Pergamon Press, 1966, pp 791-801.
41. Lewis, D. V. and Perkins H. C. "Heat Transfer at the Interface of Stainless Steel and Aluminum", Int. J. Heat Mass Transfer Vol 11, Pergamon Press, 1968, pp 1371-1383.
42. Veziroglu, T. N. and Chandra S. "Directional Effect in Thermal Contact Conductance", Fourth International Heat Transfer Conference, paper 68-IC-5, Aug.-Sept. 1970.
43. Thomas, T. R. and Probert, S. D. "Thermal Contact Resistance: The Directional Effect and Other Problems", Int. J. Heat Mass Transfer Vo. 13, Pergamon Press, 1970, pp 789-807.
44. Mikic, B. "Analytical Studies of Contact of Nominally Flat Surfaces; Effect of Previous Loading", ASME paper 71-Lub-M.
45. Mikic, B. and Carnasciali, G. "The Effect of Thermal Conductivity of Plating Material on Thermal Contact Resistance", ASME paper 69-WA/HT-9.
46. Smuda, P. A. and Gyrog, D. A. "Comparison of the Effective Thermal Insulation for Interstitial Materials Under Compressive Loads", Arizona State U. Mech. Eng. Dept. paper ME-TR-033-3, June 1968.
47. Gyrog, D. A. and Smuda, P. A. "Investigation of Thermal Isolation Materials and Their Application in Bolted Flange Joints", Arizona State U. Mech. Eng. Dept. paper ME-TR-033-5, Aug. 1968.

48. Clausing, A. M. "Thermal Contact Resistance in a Vacuum Environment", PhD thesis, U. Of Ill., 1963.
49. Yovanovich, M. M. "Thermal Contact Resistance Between Smooth Rigid Isothermal Planes Separated by Elastically Deformed Smooth Spheres", AIAA paper no. 66-461.
50. Yovanovich, M. M. and Rohsenow, W. M. "Influence of Surface Roughness and Waviness upon Thermal Contact Resistance", ScD thesis, M.I.T., June 1967.
51. Moore, C. ., Jr. "Heat Transfer Across Surfaces in Contact: Studies of Transients in One-Dimensional Composite Systems", PhD thesis, Southern Methodist U., March 1967.
52. Veziroglu, T. N. and Huerta, M. A. "Thermal Conductance of Two Dimensional Eccentric Constrictions", U. of Miami, Mech. Eng. Dept., NASA Grant NGR 10-007-010-SUB 3, Sept. 1968.
53. Lindh, K. G. et al "Studies in Heat Transfer in Aircraft Structure Joints", UCLA Dept. of Eng. Report 57-50, May 1957.
54. "A Study of the Thermal Conductance of Metallic Joints", Douglas Aircraft Co. Engineering Report No. LB-25705, AD 606479, Jan. 1958.
55. Aron, W. and Colombo, G. "Controlling Factors of Thermal Conductance Across Bolted Joints in a Vacuum Environment", ASME paper 63-WA-196.
56. Andrew, I. D. C. "An Investigation of the Thermal Conductance of Bolted Joints", Royal Aircraft Establishment Tech. Note No. WE. 46, AD 442270, Jan. 1964.
57. Elliott, D. H. "Thermal Conduction Across Aluminum Bolted Joints", ASME paper 65-HT-53.
58. Osborn, A. B. and Mair, W. N. "Thermal Conductance of Lap-Joints in Vacuum", Royal Aircraft Establishment Tech. Note No. 66034, AD 637770, Feb. 1966.
59. Fontenot, J. E. Jr. "The Thermal Conductance of Bolted Joints", PhD thesis, Louisiana State U. and Agr. and Mech. College, 1968.

60. Calimbas, A. T. "Long-Term Influence of Vacuum and Thermal Environment on the Thermal Resistance Across Filled, Bolted Joints", AIAA paper No. 69-628, June 1969.
61. Mikic, B. B. "Thermal Constriction Resistance Due to Non-Uniform Surface Conditions", Int. J. Heat Mass Transfer Vol. 13, Pergamon Press, 1970, pp 1497-1500.
62. McMillan, R. Jr. "Thermal Contact Resistance with Non-Uniform Interface Pressures", S. M. thesis, M.I.T., Feb. 1971.
63. "Thermal Contact Conductance", Bell Telephone Laboratories Bibliography No. 101, Dec. 1966.
64. Hsieh, C. K. and Davis, F. E. "Bibliography on Thermal Contact Conductance", Air Force Mat. Lab. Wright-Patterson, Report AFML-TR-69-24, March 1969.
65. Eckert, E. R. G. et al "Heat Transfer Bibliography", Int. J. Heat Mass Transfer Vol. 13, Pergamon Press, 1970, pp 617-630.
66. Thompson, W. G., Jr. Private communication to R. T. Roca, Nov. 1970.
67. Greenwood, J. A. "The Area of Contact Between Rough Surfaces and Flats", J. Lub. Technology, Jan. 1967, pp 81-91.
68. Flengas, S. "Thermal Contact Resistance in a Vacuum under Conditions of Nonuniform Interface Pressure", P. E. thesis, MIT, Feb. 1968.
69. Williamson, J. B. P. et al "Asperity Persistence and the Real Area of Contact Between Rough Surfaces"; "On the Plastic Contact of Rough Surfaces", Burndy Corporation Research Division Reports Nos. 78 add 79, Dec. 1969.
70. Greenwood, J. A. and Williamson, J. B. P. "Contact of Nominally Flat Surfaces", Proceedings of the Royal Society, London, Vol. 295, Series A, 1966, pp 300-318.
71. Greenwood, J. A. and Tripp, H. H. "The Contact of Two Nominally Flat Rough Surfaces", Proc. Instn. Mech. Engrs., Vol. 185 48/71, pp 625-633.
72. Mikic, B. "Analytical Studies of Contact of Nominally Flat Surfaces; Effect of Previous Loading", ASME paper No. 71-Lub-M.

73. Mikic, B. B. and Roca, R. T. "Behavior of Surfaces in Elastic Contact", to be published.
74. Timoshenko, S. and Goodier, J. N. Theory of Elasticity, 2nd Ed. McGraw-Hill, New York, 1951.
75. Greenwood, J. A. and Tripp, J. H. "The Elastic Contact of Rough Spheres", J. Appl. Mech., March 1967, pp 153-159.
76. Snedden, I. N. Fourier Transforms, McGraw-Hill, New York, 1951..
77. Snedden, I. N. "The Elastic Stresses Produced in a Thick Plate by the Application of Pressure to its Free Surfaces", Proc. Camb. Phil. Soc., Vol. 42, 1946, pp 260-271.
78. Nelson, C. W. "Further Consideration of the Thick-Plate Problem with Axially Symmetric Loading", J. Appl. Mech., March 1962, pp 91-98.
79. Greenwood, J. A. "The Elastic Stresses Produced in the Mid-Plane of a Slab by Pressures Applied Symmetrically at its Surface", Proc. Camb. Phil. Soc., Vol. 60, 1964, pp 159-169.
80. Lardner, T. J. "Stresses in a Thick Plate with Axially Symmetric Loading", J. Appl. Mech. June 1965, pp 458-459.
81. Lardner, T. J. "Thermal Joint Conductance: Midplane Stress Distributions", JPL Space Programs Summary No. 37-19, Vol. IV, N63-13582.
82. Pickett, G. "Application of the Fourier Method to the Solution of Certain Boundary Problems in the Theory of Elasticity", J. Appl. Mech., Vol. 11, Sept. 1944.
83. Gould, H. H. and Mikic, B. B. "Areas of Contact and Pressure Distribution in Bolted Joints", M.I.T. Heat Transfer Lab Report DSR 71821-68, June 1970.
84. Bradley, T. L. "Stress Analysis for Thermal Contact Resistance Across Bolted Joints", S. M. Thesis, Dept. Mech. Eng., M.I.T., Aug. 1968.
85. Love, A. H. Treatise on the Mathematical Theory of Elasticity, 4th Ed., Cambridge Univ. Press, 1927, reprinted Dover, N.Y., 1944.

86. Abramowitz, M. and Stegun, I. A. (ed) Handbook of Mathematical Functions, National Bureau of Standards Applied Math. Series, No. 55, 1965.
87. Fernlund, I. A Method to Calculate the Pressure Between Bolted or Riveted Plates, Trans. of Chalmers University of Technology Nr 245, Gothenburg, Sweden, 1961.
88. Lanczos, C. Lecture Course on Fourier Series, Oliver and Boyd, Edinburgh, 1966.
89. Pigott, J. G. "Thermal Contact Resistance in Bolted Joints", S. M. Thesis, MIT, Oct. 1971.

6. APPENDIX

6.1 Deformation of Disks with and without Center Holes

It can be shown [85] that the governing equations for the deformation of a disk of finite outer radius can be reduced to

$$\nabla^4 \chi = 0 \quad (A1)$$

where

$$\nabla^4 \phi = \frac{1}{r} \frac{\partial}{\partial r} \left\{ r \frac{\partial}{\partial r} \left[ \frac{1}{r} \frac{\partial}{\partial r} \left( r \frac{\partial \phi}{\partial r} \right) \right] \right\} \quad (A2)$$

The general solutions to (A1) are

$$[A \cosh(kz) + B \sinh(kz)][CJ_0(kr) + DY_0(kr)]$$

$$r[A \cosh(kz) + B \sinh(kz)][CJ_1(kr) + DY_1(kr)]$$

$$z[A \cosh(kz) + B \sinh(kz)][CJ_0(kr) + DY_0(kr)]$$

if the homogeneous direction is the r axis and

$$[A \cos(kz) + B \sin(kz)][CI_0(kr) + DK_0(kr)]$$

$$r[A \cos(kz) + B \sin(kz)][CI_1(kr) + DK_1(kr)]$$

$$z[A \cos(kz) + B \sin(kz)][CI_0(kr) + DK_0(kr)]$$

if the homogeneous direction is the z axis. A complete solution is any combination of the above, e.g.,

$$\chi = AC \cosh(kz)rJ_1(kr) + BDz \sinh(kz)Y_0(kr)$$

which satisfies the boundary equations. The constants A, B, C, D and k are constants to be evaluated and k is the eigenvalue. Stresses and deflections in terms of  $\chi$  are,

$$\tau_{rz} = \frac{\partial}{\partial r} \left[ (1-\nu)\nabla^2\chi - \frac{\partial^2\chi}{\partial z^2} \right] \quad (A3)$$

$$\sigma_r = \frac{\partial}{\partial z} \left[ \nu\nabla^2\chi - \frac{\partial^2\chi}{\partial r^2} \right] \quad (A4)$$

$$\sigma_z = \frac{\partial}{\partial z} \left[ (2-\nu)\nabla^2\chi - \frac{\partial^2\chi}{\partial z^2} \right] \quad (A5)$$

$$\sigma_\theta = \frac{\partial}{\partial z} \left[ \nu\nabla^2\chi - \frac{1}{r} \frac{\partial\chi}{\partial r} \right] \quad (A6)$$

$$u = - \frac{1+\nu}{E} \frac{\partial^2\chi}{\partial r\partial z} \quad (A7)$$

$$w = \frac{1+\nu}{E} \left[ (1-2\nu)\nabla^2\chi + \frac{\partial^2\chi}{\partial r^2} + \frac{1}{r} \frac{\partial\chi}{\partial r} \right] \quad (A8)$$

There are a total of eight boundary conditions to satisfy: two on each face of the disk, two at the outer edge and two at the inside of the hole wall if a hole is present or two at the centerline if a hole is not present. It is difficult, if not impossible, to proceed as is done in solving the Laplacian ( $\nabla^2 T=0$ ) and by sight pick the proper choices from the possible solutions. What follows here is a solution using simultaneous Fourier-Bessel series. The procedure used is straightforward but tedious and, therefore, only one complete solution is given from beginning to end. In the rest of the cases only the results are presented. More on this method of solution can be found in [81].

#### 6.1.1 Disk-No Hole-Midplane Stress

The problem to be solved is shown in Figure 21a.

Boundary conditions are

$$\begin{aligned} \text{at } z = \pm b \quad \sigma_z &= -p(r) \\ &\tau_{rz} = 0 \\ r = 0 \quad \text{stresses finite} & \quad (A9) \\ r = a \quad \sigma_r &= 0 \\ &\tau_{rz} = 0 \end{aligned}$$

The governing equation is (A1). From equations (A3) - (A8) one observes that since

$$\sigma_{\theta} \text{ is even in } z$$

$$\sigma_r \text{ is even in } z$$

$$\sigma_z \text{ is even in } z$$

$$\tau_{rz} \text{ is odd in } z$$

$$u \text{ is even in } z$$

$$w \text{ is odd in } z$$

then  $\chi$  must be odd in  $z$ . The original problem is broken into two separate parts, Figure A1, one homogeneous in  $z$  and satisfying

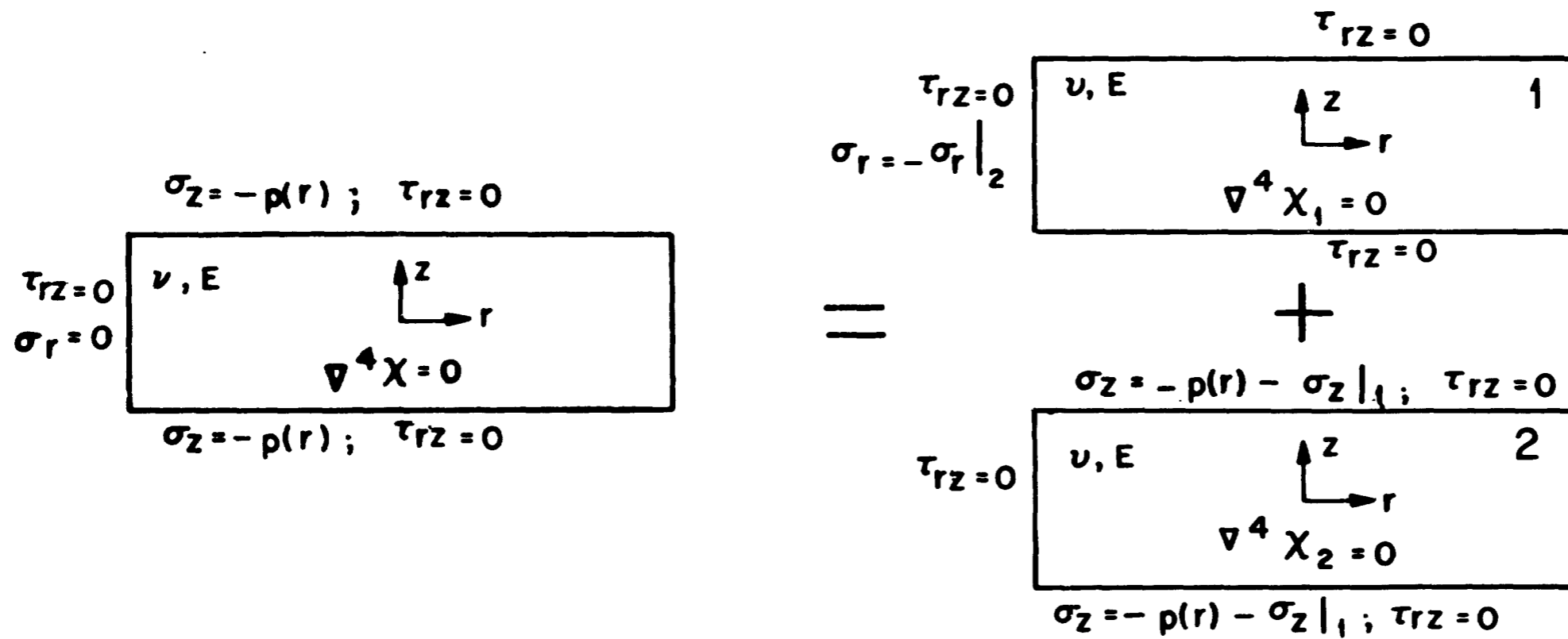
$$\nabla^4 \chi_1 = 0$$

$$\text{and at } z = \pm b \quad \tau_{rz} = 0$$

$$r = 0 \quad \text{stresses finite} \quad (A10)$$

$$r = a \quad \tau_{rz} = 0$$

$$\sigma_{r'} = -\sigma_r \text{ (as calculated from body 2)}$$



SPLITTING OF ORIGINAL PROBLEM INTO TWO SEPARATE PROBLEMS WHICH ARE SOLVABLE AND WHICH ADD UP TO THE ORIGINAL.

FIG. A1

and the other homogeneous in  $r$  and satisfying

$$\nabla^4 \chi_2 = 0$$

$$\text{and at } z = \pm b \quad \sigma_z = -p(r) - \sigma_z \text{ (as calculated from body 1)}$$

$$\tau_{rz} = 0 \quad (A11)$$

$$r = 0 \quad \text{stresses finite}$$

$$r = a \quad \tau_{rz} = 0$$

The final solution is

$$\chi = \chi_1 + \chi_2$$

Note that the boundary conditions as given in (A10) and (A11) add up to the original ones as given in (A9). In body 1 no restriction is made on  $\sigma_z$ . After all the other boundary conditions are met one can solve for  $\sigma_z$ . This value is then used in (A11) to calculate  $\chi_2$ . There is no restriction for body 2 on  $\sigma_r$ . The value of  $\sigma_r$  calculated for body 2 is used in calculating  $\chi_1$ .

One, then, iterates back and forth until the solutions are compatible. Another way is to solve them simultaneously. In any case one does arrive at a solution.

Observing that both  $\chi_1$  and  $\chi_2$  are odd in  $z$ , try

$$\chi_1 = \sin(\beta z) [A I_0(\beta r) + B r I_1(\beta r)] \quad (A12)$$

$$\chi_2 = J_0(\alpha r)[C \sinh(\alpha z) + Dz \cosh(\alpha z)] \quad (A13)$$

By omitting  $Y_0$ ,  $Y_1$ ,  $K_0$ , and  $K_1$  the stresses at  $r = 0$  remain finite. By substituting (A12) in (A3) one can show that for  $\tau_{rz} = 0$  at  $r = a$

$$A = -B \frac{\beta a I_0(\beta a) + 2(1-\nu)I_1(\beta a)}{\beta I_1(\beta a)} \quad (A14)$$

and for  $\tau_{rz} = 0$  at  $z = \pm b$

$$\beta_n = \frac{n\pi}{b} \quad n=0,1,2,\dots \quad (A15)$$

The zeroeth term is a constant term and can be carried along as the zeroeth term in an infinite series or as a constant outside the series. In this solution it is carried in the series until the very end. From (A14) and (A15), then,

$$\chi_1 = \sum_{n=0,1,2}^{\infty} \sin(\beta_n z) B_n a \left\{ \frac{\beta_n r}{\beta_n a} I_1(\beta_n r) - I_0(\beta_n r) \right. \\ \left. \cdot \left[ \frac{2(1-\nu)}{\beta_n a} + \frac{I_0(\beta_n a)}{I_1(\beta_n a)} \right] \right\} \quad (A16)$$

likewise for  $\chi_2$ ,

$$\chi_2 = \sum_{m=0,1,2}^{\infty} J_0(\alpha_m r) D_m b \left\{ \frac{\alpha_m z}{\alpha_m b} \cosh(\alpha_m z) - \frac{\sinh(\alpha_m z)}{\alpha_m b} \right. \\ \left. \cdot \left[ 2\nu + \frac{\alpha_m b}{\tanh(\alpha_m b)} \right] \right\} \quad (A17)$$

If one substitutes

$$B_n^* = \frac{B_n \beta_n^3 a}{\beta_n a I_1(\beta_n a)} \quad (A18)$$

and

$$D_m^* = \frac{D_m \alpha_m^3 b}{\alpha_m b \sinh(\alpha_m b)} \quad (A19)$$

one finds that for the original problem as shown in Figure 1A,

$$\begin{aligned} \chi = & \sum_{n=0}^{\infty} \frac{B_n^* \sin(\beta_n z)}{\beta_n^3} \left\{ \beta_n r I_1(\beta_n r) I_1(\beta_n a) - I_0(\beta_n r) \right. \\ & \left. \cdot [2(1-\nu) I_1(\beta_n a) + \beta_n a I_C(\beta_n a)] \right\} \\ & + \sum_{m=0}^{\infty} \frac{D_m^* J_0(\alpha_m r)}{\alpha_m^3} \left\{ \alpha_m z \cosh(\alpha_m z) \sinh(\alpha_m b) - \sinh(\alpha_m z) \right. \\ & \left. \cdot [2\nu \sinh(\alpha_m b) + \alpha_m b \cosh(\alpha_m b)] \right\} \quad (A20) \end{aligned}$$

and

$$\tau_{rz} = \sum_{n=0}^{\infty} B_n^* \sin(\beta_n z) [\beta_n r I_0(\beta_n r) I_1(\beta_n a) - \beta_n a I_1(\beta_n r) I_0(\beta_n a)]$$

$$+ \sum_{m=0}^{\infty} D_m^* J_1(\alpha_m r) [\alpha_m z \sinh(\alpha_m b) \cosh(\alpha_m z) - \alpha_m b \cdot \cosh(\alpha_m b) \sinh(\alpha_m z)] \quad (A21)$$

$$\sigma_z = \sum_{n=0}^{\infty} B_n^* \cos(\beta_n z) [\beta_n r I_1(\beta_n r) I_1(\beta_n a) + 2I_0(\beta_n r) I_1(\beta_n a) - \beta_n a I_0(\beta_n r) I_0(\beta_n a)] - \sum_{m=0}^{\infty} D_m^* J_0(\alpha_m r) [\alpha_m z \sinh(\alpha_m z) \sinh(\alpha_m b) - \cosh(\alpha_m z) \sinh(\alpha_m b) - \alpha_m b \cosh(\alpha_m z) \cosh(\alpha_m b)] \quad (A22)$$

$$\sigma_r = \sum_{n=0}^{\infty} B_n^* \cos(\beta_n z) \left[ \beta_n a I_0(\beta_n r) I_0(\beta_n a) + I_0(\beta_n r) I_1(\beta_n a) - \beta_n r I_1(\beta_n a) I_1(\beta_n r) - \frac{2(1-\nu)}{\beta_n r} I_1(\beta_n r) \cdot I_1(\beta_n a) - \frac{\beta_n a}{\beta_n r} I_0(\beta_n a) I_1(\beta_n r) \right] + \sum_{m=0}^{\infty} D_m^* \left\{ \alpha_m z \left[ 1 - \frac{J_1(\alpha_m r)}{\alpha_m r J_0(\alpha_m r)} \right] \sinh(\alpha_m z) \sinh(\alpha_m b) + \left[ 1 - \frac{J_1(\alpha_m r)}{\alpha_m r J_0(\alpha_m r)} \right] [\cosh(\alpha_m z) \sinh(\alpha_m b) - \alpha_m b \cosh(\alpha_m z) \cosh(\alpha_m b)] + 2\nu \left[ \frac{J_1(\alpha_m r)}{\alpha_m r J_0(\alpha_m r)} \right] \cdot \cosh(\alpha_m z) \sinh(\alpha_m b) \right\} \quad (A23)$$

There are now two sets of unknowns

$$B_n^* \quad n=0,1,2,\dots,\infty$$

$$D_m^* \quad m=0,1,2,\dots,\infty$$

They are found in the normal manner of Fourier-Bessel series, through orthogonality. The remaining boundary conditions are,

$$\text{at } z = \pm b \quad \sigma_z = -p(r)$$

$$r = a \quad \sigma_r = 0$$

It is now that the zeroeth terms are removed from the infinite series. Noting that

$$\beta_0 = 0$$

$$\alpha_0 = 0$$

and that

$$\lim_{\alpha_0 \rightarrow 0} \frac{J_1(\alpha_0 a)}{\alpha_0 a} = \frac{1}{2}$$

one finds from (A22) and (A23) upon substitution into the boundary conditions that

$$-p(r) = 2D_0^* \alpha_0 b + \sum_{m=1}^{\infty} D_m^* J_0(\alpha_m r) [ \quad ] + \sum_{n=1}^{\infty} B_n^* \cos(\beta_n b) [ \quad ]$$

(A24)

and

$$0 = B_0^* \beta_0 a \left[ 1 - \left( \frac{1-\nu}{2} \right) \right] + \nu D_0^* \alpha_0 b + \sum_{m=1}^{\infty} D_m^* J_0(\alpha_m a) [ \quad ]$$

$$+ \sum_{n=1}^{\infty} B_n^* \cos(\beta_n z) [ \quad ] \quad (A25)$$

Multiply (A24) by  $rJ_0(\alpha_0 r)$  and integrate from 0 to a and multiply (A25) by  $\cos(\beta_0 z)$  and integrate from 0 to +b to get

$$D_0^* \alpha_0 b = - \frac{F}{2\pi a^2} \quad (A26)$$

$$B_0^* \beta_0 a = \frac{F}{\pi a^2} \frac{\nu}{1+\nu} \quad (A27)$$

where F is the total load. If  $p_0$  is the average pressure then

$$p_0 = F/\pi a^2 \quad (A28)$$

Now repeating the orthogonalizing procedure one arrives at

$$B_n^* I_1^2(\beta_n a) = \sum_{m=1}^{\infty} 4D_m^* \sinh^2(\alpha_m b) \cdot \left[ \frac{J_0(\alpha_m a) \cos(\beta_n b)}{2(1-\nu^2) - (\beta_n a)^2 \left[ \frac{I_0^2(\beta_n a)}{I_1^2(\beta_n a)} - 1 \right]} \right]$$

$$\cdot \frac{\alpha_m a (\beta_n b)^3}{\left[ (\alpha_m b)^2 + (\beta_n b)^2 \right]^2} \quad (A29)$$

and

$$\begin{aligned}
 D_m^* \sinh^2(\alpha_m b) = & - \frac{2 \sinh^2(\alpha_m b) \int_0^a r p(r) J_0(\alpha_m r) dr}{a^2 J_0^2(\alpha_m a) [\alpha_m b + \cosh(\alpha_m b) \sinh(\alpha_m b)]} \\
 & - \sum_{n=1}^{\infty} \frac{4 B_n^* I_1^2(\beta_n a) \cos(\beta_n h)}{\left[ \frac{\alpha_m b}{\sinh^2(\alpha_m b)} + \frac{\cosh(\alpha_m b)}{\sinh(\alpha_m b)} \right]} \\
 & \cdot \frac{\left[ \frac{(\alpha_m a)^3 \beta_n a}{\left[ (\alpha_m a)^2 + (\beta_n a)^2 \right]^2} \right]}{\alpha_m a J_0(\alpha_m a)} \tag{A30}
 \end{aligned}$$

We now have the complete solution for a given  $p(r)$  when we combine (A29) and (A30) with (A21), (A22), and (A23).

For the particular loading as given in Figure 21a.

$$\begin{aligned}
 p(r) &= P_0 & 0 < r < r_0 \\
 &= 0 & r_0 < r < a
 \end{aligned}$$

and

$$\begin{aligned}
 \theta_m &= \alpha_m a \\
 \bar{a} &= a/b & \bar{r} &= r/b \\
 \bar{r}_0 &= r_0/b & \bar{z} &= z/b
 \end{aligned}$$

The mid plane stress is, then,

$$\frac{\sigma_z}{p_0} \Big|_{z=0} = - \frac{r_0^2}{a^2} + \sum_1 (\bar{a}, \bar{r}, \bar{r}_0) + \sum_2 (\bar{a}, \bar{r}, \bar{r}_0) \quad (A31)$$

where

$$\sum_1 ( ) = \sum_{n=1}^{\infty} \bar{A}_n \left\{ n\pi\bar{r} \frac{I_1(n\pi\bar{r})}{I_1(n\pi\bar{a})} + \frac{I_0(n\pi\bar{r})}{I_1(n\pi\bar{a})} \left[ 2 - n\pi\bar{a} \frac{I_0(n\pi\bar{a})}{I_1(n\pi\bar{a})} \right] \right\} \quad (A32)$$

$$\sum_2 ( ) = \sum_{m=1}^{\infty} \bar{B}_m J_0(\theta_m \bar{r}/\bar{a}) \cdot \left[ \frac{1}{\sinh(\theta_m/\bar{a})} + \frac{\theta_m \cosh(\theta_m/\bar{a})}{\bar{a} \sinh^2(\theta_m/\bar{a})} \right] \quad (A33)$$

$$\bar{A}_n = \sum_{m=1}^{\infty} 4\bar{B}_m \frac{J_0(\theta_m) \cos(n\pi)}{2(1-\nu) - \bar{a}^2 n^2 \pi^2 \left[ \frac{I_2^2(n\pi\bar{a})}{I_1^2(n\pi\bar{a})} - 1 \right]} \cdot \left\{ \frac{\theta_m n^3 \pi^3}{\left[ \frac{\theta_m^2}{\bar{a}^2} + n^2 \pi^2 \right]^2} \right\} \quad (A34)$$

$$\bar{B}_m = - \frac{\left[ \frac{\bar{r}_0}{\bar{a}} \frac{J_1(\theta_m \bar{r}_0 / \bar{a})}{J_0^2(\theta_m)} \right]}{\theta_m \left[ \frac{\theta_m / \bar{a}}{\sinh^2(\theta_m / \bar{a})} + \frac{\cosh(\theta_m / \bar{a})}{\sinh(\theta_m / \bar{a})} \right]}$$

$$- \sum_{n=1}^{\infty} 4\bar{A}_n \frac{\bar{a} \cos(\quad)}{\theta_m J_0(\theta_m) \left[ \frac{\theta_m / \bar{a}}{\sinh^2(\theta_m / \bar{a})} + \frac{\cosh(\theta_m / \bar{a})}{\sinh(\theta_m / \bar{a})} \right]}$$

$$\cdot \left\{ \frac{n\pi\theta_m^3}{\left[ \theta_m^3 + n^2\pi^2\bar{a}^2 \right]^2} \right\} \quad (A35)$$

### 6.1.2 Disk-No Hole-Midplane Stress-Approximate Solution

If the boundary condition

$$\sigma_r = 0 \quad \text{at} \quad r = a$$

is ignored then the solution to the midplane stress is greatly simplified. The justification for ignoring this condition lies in St. Venant's theorem. If  $a \gg r_0$  then any minor change in the boundary conditions at  $r = a$  will not affect the stress distribution in the neighborhood of

$r_0$ . Ignoring the boundary condition is equivalent to setting  $\bar{A}_n = 0$ . Therefore,

$$\frac{\sigma_z}{P_0} \Big|_{\bar{z}=0} = - \frac{r_0^2}{\bar{a}^2} + \sum_3 (\bar{r}, \bar{r}_0, \bar{a}) \quad (\text{A36})$$

where

$$\sum_3 (\bar{r}, \bar{r}_0, \bar{a}) = - \sum_{m=1}^{\infty} 2 \frac{\bar{r}_0}{\bar{a}} \frac{J_1(\theta_m \bar{r}_0 / \bar{a})}{J_0^2(\theta_m)} J_0(\theta_m \bar{r} / \bar{a})$$

$$\cdot \frac{\left[ \frac{1}{\sinh(\theta_m / \bar{a})} + \frac{\theta_m}{\bar{a}} \frac{\cosh(\theta_m / \bar{a})}{\sinh^2(\theta_m / \bar{a})} \right]}{\theta_m \left[ \frac{\theta_m / \bar{a}}{\sinh^2(\theta_m / \bar{a})} + \frac{\cosh(\theta_m / \bar{a})}{\sinh(\theta_m / \bar{a})} \right]} \quad (\text{A37})$$

Equation (A36) is another form of the equations given in [80,81]. This can be shown through the following. For large  $m$

$$\theta_m \cong m\pi + \pi/4$$

As  $\bar{a}$  approaches infinity (disk of infinite radius which is used as a model in [80,81]) define  $u_m$  such that

$$u_m = \frac{\theta_m}{\bar{a}}$$

Therefore from (A36) and (A37) with some trigonometric rearranging,

$$\frac{\sigma_z}{P_0} = \sum_{m=0}^{\infty} \frac{2\bar{r}_0}{\bar{a}} \frac{J_1(u_m \bar{r}_0) J_0(u_m \bar{r})}{u_m \bar{a} J_0^2(u_m \bar{a})}$$

$$\cdot 2 \frac{u_m \bar{z} \sinh(u_m z) \sinh(u_m) - \cosh(u_m z) [\sinh(u_m) + u_m \cosh(u_m)]}{2u_m + 2 \sinh(u_m) \cosh(u_m)}$$

where the zeroeth term has been returned into the infinite series. For large values of m

$$J_0^2(u_m \bar{a}) = J_0^2(\theta_m) = \frac{2}{\pi u_m \bar{a}}$$

Also

$$\begin{aligned} du &= \lim_{a \rightarrow \infty} (u_{m+1} - u_m) \\ &= \frac{1}{a} [\theta_{m+1} - \theta_m] \\ &= \frac{\pi}{a} \end{aligned}$$

Therefore

$$\lim_{a \rightarrow \infty} \frac{1}{u_m \bar{a} J_0^2(u_m \bar{a})} = \frac{du}{2}$$

The final expression for the midplane stress is, then

$$\frac{\sigma_z}{P_0} = -2\bar{r}_0 \int_0^{\infty} \{ \cosh(uz) [\sinh(u) + u \cosh(u)] - (uz) \sinh(uz) \sinh(u) \}$$

$$\cdot \frac{J_1(u\bar{r}_0) J_0(u\bar{r})}{2u + \sinh(2u)} du$$

which is equation (1) in [81].

### 6.1.3 Disk-No Hole-Variable Load

Since the pressure distribution on each face may be different (see Figure 6b) three infinite series are needed. Boundary conditions are

$$\text{at } z = b \quad \sigma_z = -p_1(r) = -p_0 \quad 0 < r < r_0$$

$$= 0 \quad r_0 < r < a$$

$$\tau_{rz} = 0$$

$$z = 0 \quad \sigma_z = -p_2(r)$$

$$\tau_{rz} = 0$$

$r = 0$  stresses finite

$r = a$   $\sigma_r = 0$

$\tau_{rz} = 0$

The solutions for  $\sigma_z$  and  $w$  are:

$$\begin{aligned} \frac{\sigma_z}{P_0} = & -\frac{\bar{r}_0^2}{a^2} + \sum_4 [\bar{z}, \bar{r}, \bar{a}, \bar{r}_0, \bar{p}_2(\bar{r})] - \sum_5 [\bar{z}, \bar{r}, \bar{a}, \bar{r}_0, \bar{p}_2(\bar{r})] \\ & + \sum_6 [\bar{z}, \bar{r}, \bar{a}, \bar{r}_0, \bar{p}_2(\bar{r})] \end{aligned} \quad (A38)$$

$$\begin{aligned} \frac{w}{b} \frac{E}{P_0} = & -\bar{z} \frac{\bar{r}_0^2}{a^2} + \sum_7 [\bar{z}, \bar{r}, \bar{a}, \bar{r}_0, \bar{p}_2(\bar{r}), \nu] - \sum_8 [\bar{z}, \bar{r}, \bar{a}, \bar{r}_0, \bar{p}_2(\bar{r}), \nu] \\ & - \sum_9 [\bar{z}, \bar{r}, \bar{a}, \bar{r}_0, \bar{p}_2(\bar{r}), \nu] \end{aligned} \quad (A39)$$

where

$$\begin{aligned} \sum_4 = \sum_{n=1}^{\infty} A_n \cos(n\pi\bar{z}) & \left\{ n\pi\bar{r} \frac{I_1(n\pi\bar{r})}{I_1(n\pi\bar{a})} + \frac{I_0(n\pi\bar{r})}{I_1(n\pi\bar{a})} \right. \\ & \left. \cdot \left[ 2 - n\pi\bar{a} \frac{I_0(n\pi\bar{a})}{I_1(n\pi\bar{a})} \right] \right\} \end{aligned} \quad (A40)$$

$$\sum_5 = \sum_{m=1}^5 B_m J_0 \left( \theta_m \frac{r}{a} \right) \left\{ \frac{\theta_m}{a} \bar{z} \frac{\sinh(\theta_m \bar{z}/a)}{\sinh(\theta_m/a)} - \frac{\cosh(\theta_m \bar{z}/a)}{\sinh(\theta_m/a)} \right. \\ \left. \cdot \left[ 1 + \frac{\theta_m \cosh(\theta_m/a)}{a \sinh(\theta_m/a)} \right] \right\} \quad (A41)$$

$$\sum_6 = \sum_{m=1}^{\infty} C_m J_0(\theta_m \bar{r}/a) \left\{ \frac{\theta_m}{a} (1-\bar{z}) \frac{\sinh[\theta_m (1-\bar{z})/a]}{\sinh(\theta_m/a)} - \frac{\cosh[\theta_m (1-\bar{z})/a]}{\sinh(\theta_m/a)} \right. \\ \left. \cdot \left[ 1 + \frac{\theta_m \cosh(\theta_m/a)}{a \sinh(\theta_m/a)} \right] \right\} \quad (A42)$$

$$\sum_7 = \sum_{n=1}^{\infty} (1+\nu) A_n \sin(n\pi \bar{z}) \left\{ \bar{r} \frac{I_1(n\pi \bar{r})}{I_1(n\pi a)} + \frac{I_0(n\pi \bar{r})}{I_1(n\pi a)} \right. \\ \left. \cdot \left[ 2(1+\nu) - \frac{I_0(n\pi a)}{I_1(n\pi a)} \right] \right\} \quad (A43)$$

$$\sum_8 = \sum_{m=1}^{\infty} (1+\nu) B_m J_0(\theta_m \bar{r}/\bar{a}) \left\{ \bar{z} \frac{\cosh(\theta_m \bar{z}/\bar{a})}{\sinh(\theta_m/\bar{a})} - \frac{\sinh(\theta_m \bar{z}/\bar{a})}{\sinh(\theta_m/\bar{a})} \right. \\ \left. \cdot \left[ \frac{2(1-\nu)}{\theta_m/\bar{a}} + \frac{\cosh(\theta_m/\bar{a})}{\sinh(\theta_m/\bar{a})} \right] \right\} \quad (A44)$$

$$\sum_9 = \sum_{m=1}^{\infty} (1+\nu) C_m J_0(\theta_m \bar{r}/\bar{a}) \left\{ (1-\bar{z}) \frac{\cosh[\theta_m (1-\bar{z})/\bar{a}]}{\sinh(\theta_m/\bar{a})} \right. \\ \left. - \frac{\sinh[\theta_m (1-\bar{z})/\bar{a}]}{\sinh(\theta_m/\bar{a})} \right. \\ \left. \cdot \left[ \frac{2(1-\nu)}{\theta_m/\bar{a}} + \frac{\cosh(\theta_m/\bar{a})}{\sinh(\theta_m/\bar{a})} \right] \right\} \quad (A45)$$

where

$$\theta_m = \alpha_m a = \text{zero of } J_1(\theta_m) = 0 \quad (A46)$$

and where

$$A_n = \frac{4n^2\pi^2\bar{a}^3}{2(1-\nu) - n^2\pi^2\bar{a}^2 \left[ \frac{I_0^2(n\pi\bar{a})}{I_1^2(n\pi\bar{a})} - 1 \right]} \sum_{m=1}^{\infty} [B_m - (-1)^n C_m]$$

$$\cdot \frac{(-1)^n J_0(\theta_m) \theta_m n \pi \bar{a}}{[\theta_m^2 + n^2 \pi^2 \bar{a}^2]^2} \quad (A47)$$

$$B_m = - \left\{ \frac{4 \sinh^2(\theta_m/\bar{a}) \theta_m}{J_0^2(\theta_m) [\cosh(\theta_m/\bar{a}) + 1] [\sinh(\theta_m/\bar{a}) + \theta_m/\bar{a}]} \right\}$$

$$\cdot \left\{ \sum_{n=1}^{\infty} A_n \frac{(-1)^n J_0(\theta_m) \theta_m n \pi \bar{a}}{[\theta_m^2 + n^2 \pi^2 \bar{a}^2]^2} + \frac{1}{4\theta_m} \int_0^1 [p_1(x) + p_2(x)] x J_0(\theta_m x) dx \right\}$$

$$+ \left\{ \frac{2 \sinh^2(\theta_m/\bar{a})}{J_0^2(\theta_m) [\cosh(\theta_m/\bar{a}) - 1] [\sinh(\theta_m/\bar{a}) - \theta_m/\bar{a}]} \right\}$$

$$\cdot \left\{ \int_0^1 [p_2(x) - p_1(x)] x J_0(\theta_m x) dx \right\} \quad (A48)$$

$$C_m = -B_m + \frac{4 \sinh^2(\theta_m/\bar{a})}{J_0^2(\theta_m)[\cosh(\theta_m/\bar{a}) - 1][\sinh(\theta_m/\bar{a}) - \theta_m/\bar{a}]}$$

$$\cdot \int_0^1 [p_2(x) - p_1(x)] x J_0(\theta_m x) dx \quad (A49)$$

#### 6.1.4 Disk-No Hole-Variable Load-Approximate Solution

As in section 6.1.2 if one ignores the boundary condition

$$\sigma_r = 0 \quad \text{at} \quad r = a$$

one has a somewhat simpler solution.

$$\frac{\sigma_z}{p_0} = -\frac{\bar{r}_0^2}{\bar{a}^2} - \sum_5 + \sum_6 \quad (A50)$$

$$\frac{w}{b} \frac{E}{p_0} = -\bar{z} \frac{\bar{r}_0^2}{\bar{a}^2} - \sum_8 - \sum_9 \quad (A51)$$

where  $\sum_5$  and  $\sum_6$  are given by (A41) and (A42);  $\sum_8$  and  $\sum_9$  are given by (A44) and (A45);  $B_m$  is given by (A48);  $C_m$  is given by (A49); and

$$\bar{A}_n = 0 \quad \text{all } n \quad (A52)$$

6.1.5 Disk-Hole-Midplane Stress

Define  $C_0(\lambda_n x)$  and  $C_1(\lambda_n x)$  such that

$$C_0(\lambda_n x) = Y_0(\lambda_n x)J_1(\lambda_n) - Y_1(\lambda_n)J_0(\lambda_n x) \quad (A53)$$

$$C_1(\lambda_n x) = Y_1(\lambda_n x)J_1(\lambda_n) - Y_1(\lambda_n)J_1(\lambda_n x) \quad (A54)$$

These cylinder functions are combinations of Bessel Functions and can be treated as a function alone when integrating or differentiating.  $\lambda_n$  is the eigenvalue.

$$\int_{x_1}^{x_2} x C_0(\lambda_n x) C_0(\lambda_m x) dx = 0 \quad m \neq n$$

$$= \frac{x^2}{2} C_0^2(\lambda_n x) \Big|_{x_1}^{x_2} \quad m=n$$

where  $\lambda_n$  is zero of

$$C_1(\lambda_n x_1) = 0$$

$$C_1(\lambda_n x_2) = 0$$

Also

$$\frac{d}{dx} [C_0(\lambda_n x)] = -\lambda_n C_1(\lambda_n x)$$

Therefore for the problem shown in Figure 21b where

$$\begin{aligned}
 \text{at } z = \pm b \quad \sigma_z &= -p_0 & c < r < r_0 \\
 &= 0 & r_0 < r < a \\
 \tau_{rz} &= 0 \\
 r = c \quad \sigma_r &= 0 & (A55) \\
 \tau_{rz} &= 0 \\
 r = a \quad \sigma_r &= 0 \\
 \tau_{rz} &= 0
 \end{aligned}$$

one can arrive at a solution for the midplane stress following the same procedure as before but using three simultaneous infinite series. By ignoring the boundary condition  $\sigma_r = 0$  at  $r = a$  (i.e., assuming that  $a \gg r_0$ ) this is reduced to two infinite series. The results are

$$\begin{aligned}
 \left. \frac{\sigma_z}{p_0} \right|_{z=0} &= - \frac{\bar{r}_0^2 - \bar{c}^2}{\bar{a}^2 - \bar{c}^2} + \sum_{10} (\bar{r}, \bar{r}_0, \bar{c}, \bar{a}) \\
 &- \sum_{11} (\bar{r}, \bar{r}_0, \bar{c}, \bar{a}) & (A56)
 \end{aligned}$$

$$\sum_{10} = \sum_{n=1}^{\infty} A_n \frac{C_0(\psi_n \bar{r}/\bar{c})}{\sinh^2(\psi_n/\bar{c})} \left[ \sinh(\psi_n/\bar{c}) + \frac{\psi_n}{\bar{c}} \cosh(\psi_n/\bar{c}) \right] \quad (\text{A57})$$

$$\sum_{11} = \sum_{m=1}^{\infty} \frac{B_m}{K_1^2(m\pi\bar{c})} [2K_0(m\pi\bar{r})K_1(m\pi\bar{c}) + m\pi\bar{c}K_0(m\pi\bar{c})K_0(m\pi\bar{r}) - m\pi\bar{r}K_1(m\pi\bar{c})K_1(m\pi\bar{r})] \quad (\text{A58})$$

and where

$$B_m = \sum_{n=1}^{\infty} 4A_n \frac{C_0(\psi_n) (-1)^m (m\pi)^3 \psi_n}{K_1^2(m\pi\bar{c}) \left[ \frac{\psi_n^2}{\bar{c}^2} + m^2 \pi^2 \right]^2} \cdot \left\{ \frac{1}{2(1-\nu) - m^2 \pi^2 \bar{c}^2 \left[ \frac{K_0^2(m\pi\bar{c})}{K_1^2(m\pi\bar{c})} - 1 \right]} \right\} \quad (\text{A59})$$

$$A_n = - \frac{2\bar{r}_0 C_1(\psi_n \bar{r}/\bar{c})}{\frac{\psi_n}{\bar{c}} \left[ \coth(\psi_n/\bar{c}) + \frac{\psi_n/\bar{c}}{\sinh^2(\psi_n/\bar{c})} \right] \left[ \bar{a}^2 C_0^2(\psi_n \bar{a}/\bar{c}) - \bar{c}^2 C_0^2(\psi_n) \right]} + \sum_{m=1}^{\infty} B_m (-1)^m \frac{1}{\left[ \coth(\psi_n/\bar{c}) + \frac{\psi_n/\bar{c}}{\sinh^2(\psi_n/\bar{c})} \right] \left[ \bar{a}^2 C_0^2(\psi_n \bar{a}/\bar{c}) - \bar{c}^2 C_0^2(\psi_n) \right]}$$

$$\left. \begin{aligned} & \left[ 4 m \pi \psi_n^2 \left[ c_0(\psi_n) - \frac{\bar{a}}{\bar{c}} \frac{K_1(m\pi\bar{a})}{K_1(m\pi\bar{c})} c_0(\psi_n \bar{a}/\bar{c}) \right] \right. \\ & \left. + \frac{2c_0(\psi_n \bar{a}/\bar{c})}{\left[ m^2 \pi^2 + \psi_n^2 / \bar{c}^2 \right]} \right. \\ & \left. \cdot \left[ m^2 \pi^2 \bar{a}^2 \frac{K_0(m\pi\bar{a})}{K_1(m\pi\bar{c})} - m^2 \pi^2 \bar{c} \bar{a} \frac{K_0(m\pi\bar{c}) K_1(m\pi\bar{a})}{K_1^2(m\pi\bar{c})} \right] \right\} \quad (A60) \end{aligned}$$

The eigenvalue,  $\psi_n$ , is defined as the eigenvalue which will produce

$$c_1(\psi_n) = 0$$

$$c_1(\psi_n \bar{a}/\bar{c}) = 0 \quad (A61)$$

Tables of these eigenvalues may be found in reference [86], Table 9.7, page 415. With the above formulae one can reproduce the midplane stress curves as calculated using a finite-element technique [83,84].

### 6.1.6 Disk-Hole-Midplane Stress-Approximate Solution

By ignoring the boundary conditions

$$\text{at } r = a \quad \sigma_r = 0$$

$$r = c \quad \sigma_r = 0$$

one reduces the problem to one infinite series. The first condition can be safely ignored as mentioned before. Ignoring the second causes one to underestimate the stress magnitude near the hole but gives an accurate estimate further out. The full effect of this assumption is discussed in the main body of the report. The final result is equivalent to the approximate technique used in [87].

$$\frac{\sigma_z}{p_0} \Big|_{\bar{z}=0} = - \frac{\bar{r}_0^2 - \bar{c}^2}{\bar{a}^2 - \bar{c}^2} + \sum_{10} (\bar{r}, \bar{r}_0, \bar{c}, \bar{a}) \quad (\text{A62})$$

where  $\sum_{10}$  is given by (A57). The Fourier coefficient for  $\sum_{10}$  is

$$A_n = \frac{-2\bar{r}_0 c_1(\psi_n \bar{r}_0 / \bar{c})}{\frac{\psi_n}{\bar{c}} \left[ \bar{a}^2 c_1^2(\psi_n \bar{a} / \bar{c}) - \bar{c} c_0^2(\psi_n) \right]}$$

$$\cdot \left\{ \frac{1}{\tanh(\psi_n / \bar{c}) + \frac{\psi_n}{\bar{c}} \left[ 1 - \tanh^2(\psi_n / \bar{c}) \right]} \right\} \quad (\text{A63})$$

which is (A60) rewritten with  $B_m = 0$ .

6.1.7 Disk-Hole-Variable Load-Approximate Solution

For the problem shown in Figure 6b and boundary conditions

$$\text{at } z = b \quad \sigma_z = -p_1(r) = -p_0 \quad c < r < r_0$$

$$\tau_{rz} = 0$$

$$z = 0 \quad \sigma_z = -p_2(r)$$

$$\tau_{rz} = 0$$

$$r = c \quad \tau_{rz} = 0$$

$$r = a \quad \tau_{rz} = 0$$

one needs two simultaneous equations. Note that the boundary condition  $\sigma_r = 0$  at  $r = c$  is not applied.

$$\frac{\sigma_z}{P_0} = - \frac{\bar{r}_0^2 - \bar{c}^2}{\bar{a}^2 - \bar{c}^2} + \sum_{12} [\bar{z}, \bar{r}, \bar{r}_0, \bar{c}, \bar{a}, \bar{p}_2(\bar{r})]$$

$$- \sum_{13} [\bar{z}, \bar{r}, \bar{r}_0, \bar{c}, \bar{a}, \bar{p}_2(\bar{r})] \tag{A64}$$

$$\frac{w}{b} \frac{E}{P_0} = -\bar{z} \frac{\bar{r}_0^2 - \bar{c}^2}{\bar{a}^2 - \bar{c}^2} + \sum_{14} [\bar{z}, \bar{r}, \bar{r}_0, \bar{c}, \bar{a}, \bar{p}_2(\bar{r}), \nu]$$

$$- \sum_{15} [\bar{z}, \bar{r}, \bar{r}_0, \bar{c}, \bar{a}, \bar{p}_2(\bar{r}), \nu] \quad (\text{A65})$$

where

$$\sum_{12} = \sum_{n=1}^{\infty} A_n C_0(\psi_n \bar{r}/\bar{c}) \left\{ -\psi_n \frac{\bar{z}}{\bar{c}} \frac{\sinh(\psi_n \bar{z}/\bar{c})}{\sinh(\psi_n/\bar{c})} + \frac{\cosh(\psi_n \bar{z}/\bar{c})}{\sinh(\psi_n/\bar{c})} \right. \\ \left. \left[ 1 + \frac{\psi_n \cosh(\psi_n/\bar{c})}{\bar{c} \sinh(\psi_n/\bar{c})} \right] \right\} \quad (\text{A66})$$

$$\sum_{13} = \sum_{n=1}^{\infty} B_n C_0(\psi_n \bar{r}/\bar{c}) \left\{ -\psi_n \frac{(1-\bar{z})}{\bar{c}} \frac{\sinh[\psi_n(1-\bar{z})/\bar{c}]}{\sinh(\psi_n/\bar{c})} \right. \\ \left. + \frac{\cosh[\psi_n(1-\bar{z})/\bar{c}]}{\sinh(\psi_n/\bar{c})} \left[ 1 + \frac{\psi_n \cosh(\psi_n/\bar{c})}{\bar{c} \sinh(\psi_n/\bar{c})} \right] \right\} \quad (\text{A67})$$

$$\sum_{14} = \sum_{n=1}^{\infty} A_n (1+\nu) \frac{C_0(\psi_n \bar{r}/\bar{c})}{\psi_n/\bar{c}} \left\{ -\frac{\psi_n \bar{z}}{\bar{c}} \frac{\cosh(\psi_n \bar{z}/\bar{c})}{\sinh(\psi_n/\bar{c})} + \frac{\sinh(\psi_n \bar{z}/\bar{c})}{\sinh(\psi_n/\bar{c})} \right. \\ \left. \cdot \left[ 2(1-\nu) + \frac{\psi_n \cosh(\psi_n/\bar{c})}{\bar{c} \sinh(\psi_n/\bar{c})} \right] \right\} \quad (\text{A68})$$

$$\sum_{15} = \sum_{n=1}^{\infty} \frac{B_n}{\psi_n/\bar{c}} \left\{ 2(1-\nu^2)C_0(\psi_n) - (1+\nu)C_0(\psi_n\bar{r}/\bar{c}) \right.$$

$$\cdot \left[ -\psi_n \frac{(1-\bar{z})}{\bar{c}} \frac{\cosh[\psi_n(1-\bar{z})/\bar{c}]}{\sinh(\psi_n/\bar{c})} + \frac{\sinh[\psi_n(1-\bar{z})/\bar{c}]}{\sinh(\psi_n/\bar{c})} \right.$$

$$\left. \left. \cdot \left[ 2(1-\nu) + \frac{\psi_n \cosh(\psi_n/\bar{c})}{\bar{c} \sinh(\psi_n/\bar{c})} \right] \right] \right\} \quad (A69)$$

$$A_n = \frac{\left[ \coth(\psi_n/\bar{c}) + \frac{\psi_n/\bar{c}}{\sinh^2(\psi_n/\bar{c})} \right] P_1 - \left[ \frac{1}{\sinh(\psi_n/\bar{c})} + \frac{\psi_n \coth(\psi_n/\bar{c})}{\bar{c} \sinh(\psi_n/\bar{c})} \right] P_2}{\left[ 1 - \frac{\psi_n^2/\bar{c}^2}{\sinh^2(\psi_n/\bar{c})} \right]} \quad (A70)$$

$$B_n = \frac{- \left[ \coth(\psi_n/\bar{c}) + \frac{\psi_n/\bar{c}}{\sinh^2(\psi_n/\bar{c})} \right] P_2 + \left[ \frac{1}{\sinh(\psi_n/\bar{c})} + \frac{\psi_n \coth(\psi_n/\bar{c})}{\bar{c} \sinh(\psi_n/\bar{c})} \right] P_2}{\left[ 1 - \frac{\psi_n^2/\bar{c}^2}{\sinh^2(\psi_n/\bar{c})} \right]} \quad (A71)$$

$$P_1 = \frac{-2\bar{r}_0 C_1(\psi_n \bar{r}_0 / \bar{c})}{\frac{\psi_n}{\bar{c}} \left[ \bar{a}^2 C_0^2(\psi_n \bar{a} / \bar{c}) - \bar{c}^2 C_0^2(\psi_n) \right]} \quad (A72)$$

$$P_2 = \frac{-2 \int_{\bar{c}}^{\bar{a}} \frac{P_2(\bar{r})}{P_0} \bar{r} C_0(\psi_n \bar{r} / \bar{c}) d\bar{r}}{\left[ \bar{a}^2 C_0^2(\psi_n \bar{a} / \bar{c}) - \bar{c}^2 C_0^2(\psi_n) \right]} \quad (A73)$$

### 6.1.8 Semi-Infinite Body-Finite Radius

Figure A2 shows the problem to be solved. The boundary conditions are

$$\text{at } z = 0 \quad \sigma_z = -p(r)$$

$$\tau_{rz} = 0$$

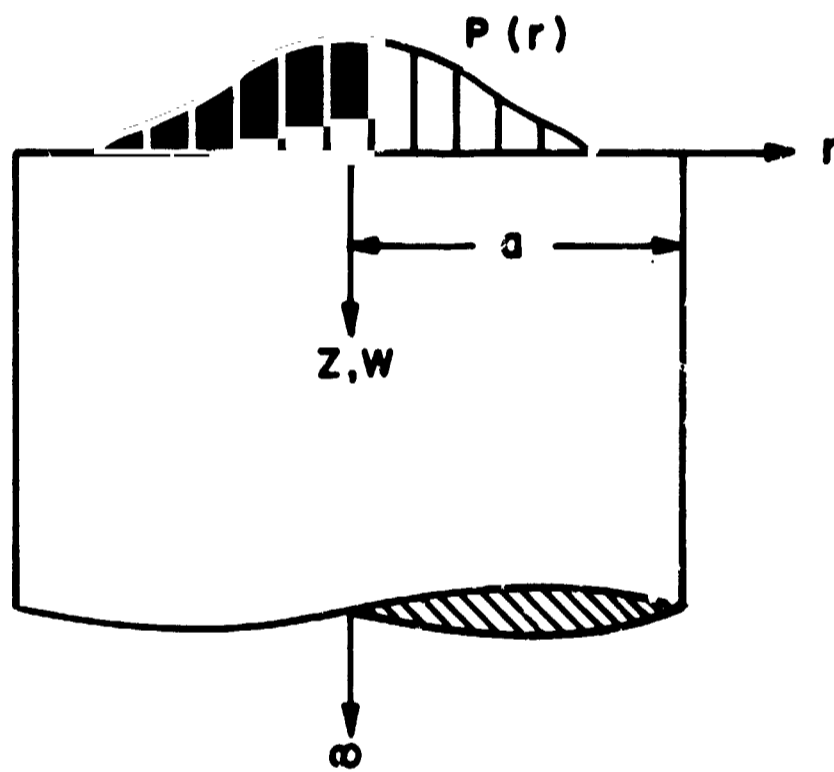
$$r = 0 \quad \text{stresses finite}$$

$$r = a \quad \tau_{rz} = 0$$

$$z = \infty \quad \text{stresses finite}$$

The governing equation is

$$\nabla^4 \chi = 0 \quad (A1)$$



MODEL FOR SEMI-INFINITE BODY  
WITH FINITE RADIUS

FIG. A2

Rather than using the general solutions given before the  $\cosh(kz)$  and  $\sinh(kz)$  will be split into  $\exp(+kz)$  and  $\exp(-kz)$ . Observing that for the stresses to be finite at  $z = \infty$  the terms containing  $\exp(+kz)$  cannot exist, one has for a solution to (A1)

$$\chi = J_0(kr)[Ae^{-kz} + Bze^{-kz}] \quad (A74)$$

Equation (A74) satisfies the boundary conditions

at  $r = 0$  stresses finite

$z = \infty$  stresses finite

The remaining three boundary conditions are met through the constants  $k$ ,  $A$ , and  $B$ . The results are:

$$\sigma_z = -\frac{F}{\pi a^2} - \sum_{n=1}^{\infty} B_n J_0(\alpha_n r) [1 + \alpha_n z] e^{-\alpha_n z} \quad (A75)$$

$$w = \frac{1+\nu}{E} \sum_{n=1}^{\infty} B_n \frac{J_0(\alpha_n r)}{\alpha_n} [\alpha_n z + 2(1-\nu)] e^{-\alpha_n z} \quad (A76)$$

$$B_n = \frac{2}{a^2} \frac{\int_0^a r p(r) J_0(\alpha_n r) dr}{J_0^2(\alpha_n a)} \quad (A77)$$

where

$$\alpha_n \text{ is zero of } J_1(\alpha_n a) = 0 \quad n=1,2,\dots \quad (\text{A78})$$

## 6.2 Relationships for Hyperbolic and Cylindrical Functions

Let

$$\nabla^2 \phi = \frac{1}{r} \frac{d}{dr} \left( r \frac{d\phi}{dr} \right)$$

then

$$\nabla^2 J_0(mr) = -m^2 J_0(mr)$$

$$\nabla^2 Y_0(mr) = -m^2 Y_0(mr)$$

$$\nabla^2 I_0(mr) = m^2 I_0(mr)$$

$$\nabla^2 K_0(mr) = m^2 K_0(mr)$$

$$\nabla^2 r J_1(mr) = 2m J_0(mr) - m^2 r J_1(mr)$$

$$\nabla^2 r Y_1(mr) = 2m Y_0(mr) - m^2 r Y_1(mr)$$

$$\nabla^2 r I_1(mr) = 2m I_0(mr) + m^2 r I_1(mr)$$

$$\nabla^2 r K_1(mr) = -2m K_0(mr) + m^2 r K_1(mr)$$

also

$$\int \cosh(az)\cos(bz)dz = \frac{a \sinh(az)\cos(bz) + b \cosh(az)\sin(bz)}{a^2+b^2}$$

$$\int z \sinh(az)\cos(bz)dz = \frac{z}{a^2+b^2} [a \cosh(az)\cos(bz) + b \sinh(az)\sin(bz)]$$
$$- \frac{(a^2-b^2)\sinh(az)\cos(bz) + 2ab \cosh(az)\sin(bz)}{(a^2+b^2)^2}$$

$$\int_0^r r J_n^2(ar) dr = \frac{r^2}{2} [J_n^2(ar) - J_{n-1}(ar)J_{n+1}(ar)]$$

$$\int_0^r r I_0(br)J_0(ar) dr = \frac{r}{a^2+b^2} [bJ_0(ar)I_1(br) + aI_0(br)J_1(ar)]$$

$$\int_0^r r^2 I_1(br)J_0(ar) dr = \frac{r^2}{a^2+b^2} [aI_1(br)J_1(ar) + bI_0(br)J_0(ar)]$$
$$- \frac{2br}{(a^2+b^2)^2} [bJ_0(ar)I_1(br) + aI_0(br)J_1(ar)]$$

$$\int rK_0(br)C_0(ar)dr = \frac{r}{a^2+b^2} [aK_0(br)C_1(ar) - bC_0(ar)K_1(br)]$$

$$\int r^2K_1(br)C_0(ar)dr = -\frac{r^2}{a^2+b^2} [bK_0(br)C_0(ar) - aK_1(br)C_1(ar)]$$

$$+ \frac{2br}{(a^2+b^2)^2} [aK_0(br)C_1(ar) - bC_0(ar)K_1(br)]$$

where  $C_0(ar)$  and  $C_1(ar)$  are defined in (A53) and (A54).

### 6.3 Truncation of Infinite Series

The problem is: given  $f(x)$  such that

$$f(x) = \sum_{n=0,1}^{\infty} A_n J_0(\theta_n x) \quad (\text{A79})$$

where  $\theta_n$  is eigenvalue and

$$J_1(\theta_n) = 0 \quad \text{for all } n$$

how can one truncate the infinite series to  $N$  terms and get an accurate result,  $\bar{f}(x)$ , where

$$f(x) \approx \bar{f}(x) = \sum_{n=0,1}^N B_n J_0(\theta_n x) \quad (\text{A80})$$

The solution is to use local smoothing where the average value of the function is used rather than the precise value at  $x$  [88]. That is, let

$$\bar{f}(x) = \frac{1}{2\epsilon} \int_{x-\epsilon}^{x+\epsilon} f(y) dy \quad (\text{A81})$$

One must now choose the interval  $2\epsilon$  over which to sample. To gain an insight into this try this method with an infinite series using circular functions, e.g.

$$g(x) = \sum_{k=1,2}^{\infty} C_k \sin(kx)$$

$$\bar{g}(x) = \sum_{k=1,2}^N D_k \sin(kx)$$

from (A81) one observes that

$$D_k = \frac{\sin(\epsilon k)}{\epsilon k} C_k$$

or

$$\bar{g}(x) = \sum_{k=1,2}^N \frac{\sin(\epsilon k)}{\epsilon k} C_k \sin(kx)$$

Thus the original series with the original coefficient returns but with a truncation term. If the interval  $\epsilon$  is chosen such that

$$\epsilon = \pi/N$$

then the last truncation term will be zero and the general form for the truncation term,  $t_k$ , will be;

$$t_k = \frac{\sin\left(\frac{k\pi}{N}\right)}{\frac{k\pi}{N}} \quad k=0,1,\dots \quad (\text{A82})$$

note

$$\lim_{\delta \rightarrow 0} \frac{\sin(\delta)}{\delta} = 1$$

The net result is to weight the lower frequencies against the higher ones. We can therefore expect to reproduce the function accurately in regions of slow change. The term  $t_k$  given by (A82) is the term used for all Fourier series using circular functions whether they are in terms of cos, sin, or a combination of the two.

To find the truncation term for Fourier-Bessel series once again applies (A81),

$$\bar{f}(x) = \frac{1}{2\epsilon} \int_{x-\epsilon}^{x+\epsilon} \left[ \sum_{n=0,1}^{\infty} A_n J_0(\theta_n y) \right] dy$$

or

$$\sum_{n=0,1}^N B_n J_0(\theta_n x) = \sum_{n=0,1}^N A_n \frac{1}{2\epsilon} \int_{x-\epsilon}^{x+\epsilon} J_0(\theta_n y) dy$$

where all terms after N in the original series are ignored. The integral is not available in closed form but if one notices that

$$J_0(z) \rightarrow \sqrt{\frac{2}{\pi z}} \cos(z - \pi/4)$$

as  $z \rightarrow \infty$  then it seems reasonable to try as a truncation term a form similar to (A82). By trial and error it was found that the best solution was

$$t_n = 1 \quad n=0$$

$$t_n = \frac{\sin \left[ \frac{\theta_n - 3\pi/4}{\theta_N - 3\pi/4} \pi \right]}{\left[ \frac{\theta_n - 3\pi/4}{\theta_N - 3\pi/4} \pi \right]} \quad n=1,2,\dots,N \quad (A83)$$

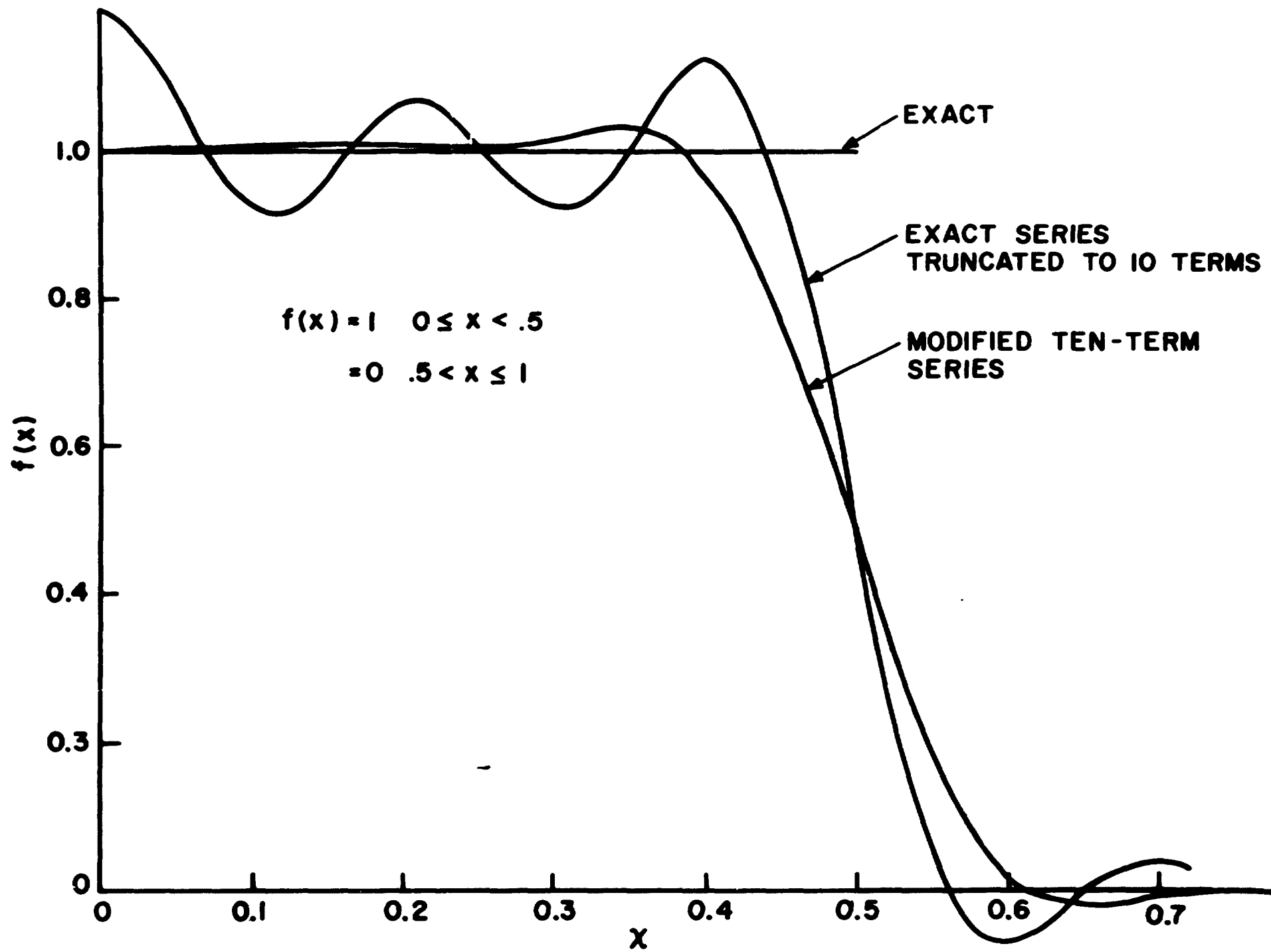
In any Fourier series, Bessel or circular, the zeroeth term gives the average value over the range or the level. In both (A82) and (A83) the truncation term  $t_0$ , is 1 so this average value is unchanged. Therefore, at worst, the truncated series will accurately predict the average behavior. It should be noted from (A83) that

$$\lim_{N \rightarrow \infty} t_n = 1$$

and we have back the original infinite series.

Figure A3 shows the advantage of the truncation term.

In this case



COMPARISON OF ORIGINAL AND MODIFIED SERIES  
EACH CARRIED TO TEN TERMS

FIG. A3

$$\begin{aligned} f(x) &= 1 \quad 0 < x < 1/2 \\ &= 0 \quad 1/2 < x < 1 \end{aligned} \tag{A84}$$

The solution (where  $x$  is a radial co-ordinate) is

$$f(x) = \frac{1}{4} + \sum_{n=1}^{\infty} \frac{J_1(\theta_n/2)}{\theta_n J_0^2(\theta_n)} J_0(\theta_n x) \tag{A85}$$

where  $\theta_n$  is a zero of

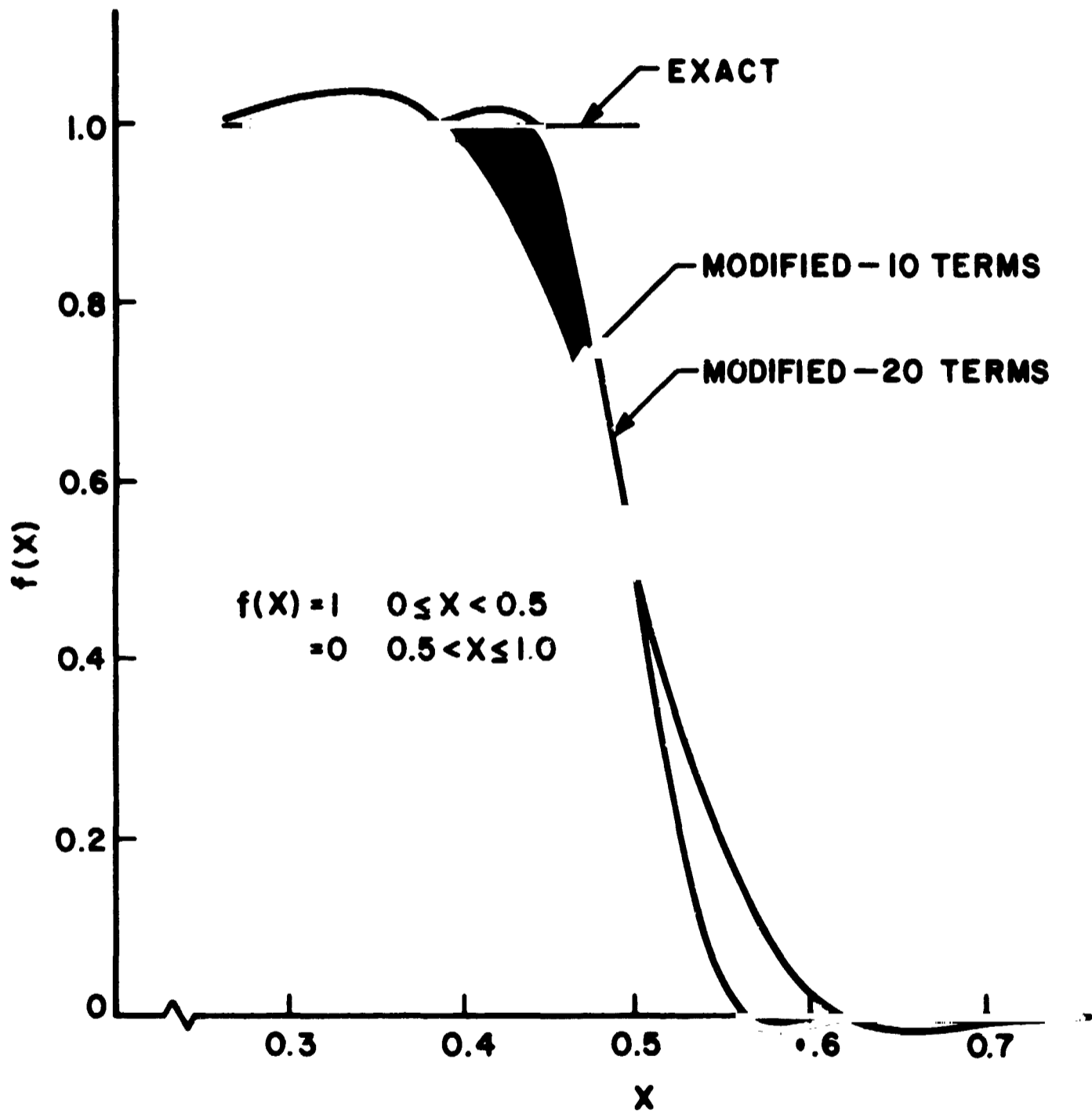
$$J_1(\theta_n) = 0$$

In Figure A3 the original function (A84) is shown along with the first ten terms of the infinite series solution (A85). By using the truncation term with  $N=10$ ,

$$t_n = \frac{\sin \left[ \frac{\theta_n - 3\pi/4}{\theta_{10} - 3\pi/4} \pi \right]}{\left[ \frac{\theta_n - 3\pi/4}{\theta_{10} - 3\pi/4} \pi \right]}$$

a more exact estimate is made of the original function. This new estimate removes the oscillations about the true value because it gives less and less weight to the higher frequency terms but it does not predict corner effects very well because

it does ignore the high frequencies. Adding more terms to the truncated series improves the estimate at the corners as shown in Figure A4.



TRUNCATED INFINITE SERIES  
FIG. A 4

#### 6.4 Computer Programs

In the following programs different nomenclature was used than that found in this report. Following is a list of the important changes.

<u>This Report</u>	<u>Computer Programs</u>
$\bar{a}$	RHO
$\bar{c}$	LAMBDA
$\bar{r}_0$	RO
$\bar{r}$	R
$\frac{y_0 E}{b p_0}$	YO
$\frac{\sigma E}{b p_0}$	S
$H/p_0$	H
$\frac{\sigma_z}{P_0} \Big _{z=0}$	SIGMAZ
$\frac{wE}{bP_0} \Big _{z=0}$	W
$\nu$	NU
$t_n$	SIG(N)

##### 6.4.1 Disk with No Hole

This program calculates the interfacial pressure distribution and deflection of two rough plates in contact.

The input data is  $\bar{r}_0$ ,  $\bar{a}$ ,  $\nu$ ,  $N$ ,  $\sigma E/bp_0$ ,  $H/P_0$ ,  $pp_0$ , and  $wt$ .  $N$  is the maximum number of terms to be used in the Fourier series. The first estimate of the pressure distribution is

$$\frac{\sigma_z}{P_0} = -pp_0 e^{-\frac{r^2}{r_0^2}}$$

and by inputting  $pp_0$  the user has an opportunity to start the iteration close to the final value. After an iteration is done the new stress distribution to be used is calculated from the original one,  $\sigma_z$ , and from the one as calculated from the deformation of the asperities,  $\sigma_z^*$  as

$$(\sigma_z)_{\text{new}} = wt \cdot \sigma_z + (1-wt) \cdot \sigma_z^*$$

Therefore the user can influence the speed of convergence of the procedure. Input format is as follows:

CARD 1  $\bar{r}_0$ ,  $\bar{a}$ ,  $\nu$ ,  $N$  (3F10.3,I10)

CARD 2  $S$ ,  $H$ ,  $pp_0$ ,  $wt$  (4F10.3)

CARD 3  $S$ ,  $H$ ,  $pp_0$ ,  $wt$  (new set)

⋮

LAST CARD BLANK

Example:

$$\bar{r}_0 = 1.1$$

$$\bar{a} = 7.3$$

$$v = .25$$

$$N = 40$$

and try two sets of S and H,

S = 10	S = 100
H = 100	H = 150
pp0 = 1.	pp0 = .8
wt = .5	wt = .25

the data cards are as follows:

1	10	20	30	40	
	1.100	7.300	.250	40	CARD 1
	10.000	100.000	1.000	.500	CARD 2
	100.000	150.000	.800	.250	CARD 3
	(blank)				CARD 4

The program is written in FORTRAN IV and was compiled and run on an IBM 360/65 computer system. CPU time for ten complete iterations is in the neighborhood of seven minutes. Without compiling, 94K of core is used. The program follows.

```

C
C MAIN PROGRAM
C
C THIS PROGRAM CALCULATES THE INTERFACIAL PRESSURE DISTRIBUTION AND
C DEFLECTION OF TWO ROUGH PLATES (NO HOLE) IN CONTACT. IT USES THE
C BESSEL FUNCTION PACKAGE AND SUBROUTINES--
C          STPNHL
C          QUADJO
C          OUTPUT
C THE FOLLOWING ARE VARIABLES--
C YO      SEPARATION OF PLATES
C S       ROUGHNESS
C H       HARDNESS
C SIGMAZ  LOAD AT Z=0
C W       DEFLECTION AT Z=0
C RO      LOAD RADIUS (AT Z=1)
C RHO     DISK RADIUS
C NU      POISSON'S RATIO
C NMAX    NUMBER OF TERMS IN INFINITE SERIES
C SIG(N)  TRUNCATION TERM FOR FOURIER SERIES
C IN      NUMBER OF INTERVALS ALONG RADIUS USED IN CALCULATION
C MMAX    NUMBER OF POINTS USED (=IN+1)
C DELR    SIZE OF INTERVAL
C ITER    NO. OF TIMES SUBROUTINE HAS BEEN CALLED
C
C DIMENSION ALPHA(40)
C COMMON/AAAA/P(40),D(40),E(40),SIG(40),THE TA(40),RBAR(40),CRAP(40)
C 1 ,PTOP(40),PBOT(40)
C COMMON SIGMAZ(201),W(201),SDATA(9)
C COMMON/RP/R/F(201),P1(201)
C REAL NU, LAMDA
C DATA ALPHA/3.83171,7.01559,10.17347,13.32369,16.47063,19.61586,
1 22.76008,25.90367,29.04683,32.18968,35.33231,38.47477,41.61709,
2 44.75932,47.90146,51.04354,54.18555,57.32753,60.46946,63.61136,
3 66.75323,69.89507,73.03690,76.17870,79.32049,82.46226,85.60402,
4 88.74577,91.88750,95.02923,98.17095,101.3127,104.4544,

```

```

MAIN0001
MAIN0002
MAIN0003
MAIN0004
MAIN0005
MAIN0006
MAIN0007
MAIN0008
MAIN0009
MAIN0010
MAIN0011
MAIN0012
MAIN0013
MAIN0014
MAIN0015
MAIN0016
MAIN0017
MAIN0018
MAIN0019
MAIN0020
MAIN0021
MAIN0022
MAIN0023
MAIN0024
MAIN0025
MAIN0026
MAIN0027
MAIN0028
MAIN0029
MAIN0030
MAIN0031
MAIN0032
MAIN0033
MAIN0034
MAIN0035
MAIN0036

```

```

5 107.5961 ,110.7378 ,113.8794 ,117.0211 ,
6 120.1628 ,122.3045 ,126.4461 /
DO F I=1,40
THETA(I)=ALPHA(I)
5 CONTINUE
PI=3.14159265
IN=100
C
C READ IN DISK DATA (ONCE PER RUN)
C
READ(5,10)PO,RHO,NU,NMAX
10 FORMAT(2F10.3,I10)
20 SDATA(1)=IN
SDATA(3)=0.
SDATA(4)=RHO
SDATA(5)=RO
SDATA(6)=NU
SDATA(7)=NMAX
MMAX=IN+1
DELP=RHO/IN
SDATA(2)=DELP
C
C CALCULATE TRUNCATION TERMS
C
DO 37 N=1,NMAX
R=(THETA(N)-.75*PI)/(THETA(NMAX)-.75*PI)*PI
SIG(N)=SIN(R)/R
37 CONTINUE
ITEP=0
C
C READ IN PUGHNESS DATA. MORE THAN ONE CASE MAY BE ENTERED.
C PROGRAM STOPS WHEN SUBMITTED "S" IS ZERO. PPO IS AN ESTIMATE OF
C THE VALUE OF P(0) AND WT IS A WEIGHTING FACTOR.
C
45 READ(5,40)S,H,PPO,WT
40 FORMAT(4F10.3)

```

```

MAIN0037
MAIN0038
MAIN0039
MAIN0040
MAIN0041
MAIN0042
MAIN0043
MAIN0044
MAIN0045
MAIN0046
MAIN0047
MAIN0048
MAIN0049
MAIN0050
MAIN0051
MAIN0052
MAIN0053
MAIN0054
MAIN0055
MAIN0056
MAIN0057
MAIN0058
MAIN0059
MAIN0060
MAIN0061
MAIN0062
MAIN0063
MAIN0064
MAIN0065
MAIN0066
MAIN0067
MAIN0068
MAIN0069
MAIN0070
MAIN0071
MAIN0072

```

```

      IF(S.LT..001) GO TO 998
C
C ESTIMATE Y0
C
      Y0=2.*S
      DO 50 J=1,MMAX
      R=(J-1)*DEL R
C
C FIRST ESTIMATE OF THE PRESSURE DISTRIBUTION
C
      SIGMA Z(J)=-PPO*EXP(-R*R*PPO/E0/R0)
      W(J)=0.
50 CONTINUE
      II=0
100 CONTINUE
C
C PERFORM THE FOLLOWING UP TO 10 TIMES
C
      II=II+1
      IF(II.GT.10) GO TO 45
C
C CALCULATE THE DEFLECTION GIVEN THE STRESS
C
      CALL STPNHL(ITER)
      ITER=ITER+1
      I=0
110 CONTINUE
      I=I+1
      IF(I.GT.20) GO TO 130
C
C FROM DEFORMATION OF ASPERITIES CALCULATE STRESS DISTRIBUTION.
C ITERATE UNTIL LOAD BALANCES.
C
      FORCE=0.
      DO 120 J=1,MMAX
      R=(J-1)*DEL R

```

```

MAIN0073
MAIN0074
MAIN0075
MAIN0076
MAIN0077
MAIN0078
MAIN0079
MAIN0080
MAIN0081
MAIN0082
MAIN0083
MAIN0084
MAIN0085
MAIN0086
MAIN0087
MAIN0088
MAIN0089
MAIN0090
MAIN0091
MAIN0092
MAIN0093
MAIN0094
MAIN0095
MAIN0096
MAIN0097
MAIN0098
MAIN0099
MAIN0100
MAIN0101
MAIN0102
MAIN0103
MAIN0104
MAIN0105
MAIN0106
MAIN0107
MAIN0108

```

```

IF(J.GT.1.OR.J.LT.MMAX) GO TO 112
IF(J.EQ.MMAX) GO TO 113
DA=PI*DELR*DELR/4.
GO TO 114
113 DA=2.*PI*P*DELR/2.
GO TO 114
112 DA=2.*PI*P*DELR
114 YY=(Y0+2.*W(J))/S/1.414214
IF(YY.GT.13.) GO TO 140
P1(J)=H/2.*EPRC(YY)
GO TO 145
140 P1(J)=0.
C
C SUM TO GET TOTAL LEAD
C
145 F(J)=FORCE+P1(J)*DA/P0/R0/PI
FORCE=F(J)
120 CONTINUE
C
C IF LOAD IS OFF BY 5 PERCENT REPEAT
C
IF(ABS(1.-FORCE).LT..05) GO TO 130
Y0=Y0+S/2.*ALOG(FORCE)
GO TO 110
130 CONTINUE
C
C PRINT OUTPUT FOR THIS ITERATION
C
CALL OUTPUT(Y0,II,S,H)
C
C ITERATE AROUND AGAIN UNLESS PRESSURES AGREE TO 2 PERCENT
C
CHK=ABS((-SIGMAZ(1)-P1(1))/P1(1))
IF(CHK.LT..02) GO TO 45
DO 100 J=1,MMAX
C

```

```

MAIN0109
MAIN0110
MAIN0111
MAIN0112
MAIN0113
MAIN0114
MAIN0115
MAIN0116
MAIN0117
MAIN0118
MAIN0119
MAIN0120
MAIN0121
MAIN0122
MAIN0123
MAIN0124
MAIN0125
MAIN0126
MAIN0127
MAIN0128
MAIN0129
MAIN0130
MAIN0131
MAIN0132
MAIN0133
MAIN0134
MAIN0135
MAIN0136
MAIN0137
MAIN0138
MAIN0139
MAIN0140
MAIN0141
MAIN0142
MAIN0143
MAIN0144

```

C NEW ESTIMATE OF STRESS DISTRIBUTION IS WEIGHTED COMBINATION OF  
C ELASTIC AND PLASTIC DISTRIBUTIONS  
C

160 SIGMA7(J)=WT\*SIGMAZ(J)-(1.-WT)\*P1(J)  
CONTINUE  
GO TO 100  
998 CALL EXIT  
END

MAIN0145  
MAIN0146  
MAIN0147  
MAIN0148  
MAIN0149  
MAIN0150  
MAIN0151  
MAIN0152

```

C
C   STPNHI
C
C   SUBROUTINE STPNHI (ITER)
C   THIS SUBROUTINE WILL CALCULATE THE STRESSES ON THE BOTTOM OF A DISK
C   WHEN THE NORMAL STRESS AT THE BOTTOM IS SPECIFIED AND THE LOAD ON THE
C   TOP IS UNIFORM OVER THE RADIUS R-SUB-ZERO
C   SIGMAZ IS THE NORMAL Z STRESS ON THE BOTTOM FACE AND W IS THE Z
C   DEFLECTION ON THE BOTTOM FACE
C   THE FOLLOWING ARE VARIABLES--
C   SIGMAZ   LOAD AT Z=0
C   W        DEFLECTION AT Z=0
C   RO       LOAD RADIUS (AT Z=1)
C   RHO      DISK RADIUS
C   NU       POISSON'S RATIO
C   NMAX     NUMBER OF TERMS IN INFINITE SERIES
C   SIG(N)   TRUNCATION TERM FOR FOURIER SERIES
C   IN       NUMBER OF INTERVALS ALONG RADIUS USED IN CALCULATION
C   MMAX     NUMBER OF POINTS USED (=IN+1)
C   DELP     SIZE OF INTERVAL
C   ITER     NO. OF TIMES SUBROUTINE HAS BEEN CALLED
C
C   COMMON SIGMAZ(201),W(201),SDATA(9)
C   COMMON/AAAA/B(40),D(40),E(40),SIG(40),THETA(40),RBAR(40),CRAR(40)
C   I ,PTOP(40),PBOT(40)
C   REAL NU,J0,J1
C   PI=3.14159265
C   IN=INT(SDATA(1)+.001)
C   MMAX=IN+1
C   DELP=SDATA(2)
C   RHO=SDATA(4)
C   RO=SDATA(5)
C   NU=SDATA(6)
C   NMAX=INT(SDATA(7)+.001)
C
C   IF THIS IS THE FIRST PASS GO THROUGH AND CALCULATE THE COEFFICIENTS

```

```

NOHL0001
NOHL0002
NOHL0003
NOHL0004
NOHL0005
NOHL0006
NOHL0007
NOHL0008
NOHL0009
NOHL0010
NOHL0011
NOHL0012
NOHL0013
NOHL0014
NOHL0015
NOHL0016
NOHL0017
NOHL0018
NOHL0019
NOHL0020
NOHL0021
NOHL0022
NOHL0023
NOHL0024
NOHL0025
NOHL0026
NOHL0027
NOHL0028
NOHL0029
NOHL0030
NOHL0031
NOHL0032
NOHL0033
NOHL0034
NOHL0035
NOHL0036

```

```

C USED IN THE SIMULTANEOUS EQUATIONS TO GET THE FOURIER COEFFICIENTS
C IF THIS IS NOT THE FIRST PASS SKIP TO STEP 20 SINCE THE FOLLOWING
C COEFFICIENTS HAVE NOT CHANGED

```

```

C
20 IF(ITER)20,20,30
CONTINUE
DO 40 N=1,NMAX
TT=THETA(N)/PHI
PN=N*PI*PHI

```

```

C FOR LARGE ARGUMENTS THE COSH AND SINH ARE INFINITE

```

```

C
23 IF(TT-40.)23,23,24
TS=TT/SINH(TT)
TSS=TT/SINH(TT)**2
SS=1./SINH(TT)**2
S=1./SINH(TT)
GO TO 25
24 TS=0.
TSS=0.
SS=0.
S=0.
25 R(N)=4.*N*N*PI*PI/(2.*(1.-NU)-PN*PN*(A10(PN)**2/A11(PN)**2-1.))
PTOP(N)=-R0/PHI*J1(TT*R0)/THETA(N)
D(N)=(1./TANH(TT)+TSS)/(1.-TS*TS)/JO(THETA(N))**2
E(N)=(S+TS/TANH(TT))/(1.-TS*TS)/JO(THETA(N))**2

```

```

40 CONTINUE
20 CONTINUE
DO 22 J=1,NMAX
CALL QUADJO(IP,THETA(J),SIGMAZ,PROT(J))
22 CONTINUE
DO 20 M=1,NMAX
PRAP(M)=2.*PTOP(M)*D(M)-2.*PROT(M)*E(M)
CRAP(M)=2.*PTOP(M)*E(M)-2.*PROT(M)*D(M)
20 CONTINUE

```

```

NOHL0037
NOHL0038
NOHL0039
NOHL0040
NOHL0041
NOHL0042
NOHL0043
NOHL0044
NOHL0045
NOHL0046
NOHL0047
NOHL0048
NOHL0049
NOHL0050
NOHL0051
NOHL0052
NOHL0053
NOHL0054
NOHL0055
NOHL0056
NOHL0057
NOHL0058
NOHL0059
NOHL0060
NOHL0061
NOHL0062
NOHL0063
NOHL0064
NOHL0065
NOHL0066
NOHL0067
NOHL0068
NOHL0069
NOHL0070
NOHL0071
NOHL0072

```

C THE NORMAL STRESS AND DEFLECTION ON THE BOTTOM ARE NOW CALCULATED  
 C FOR THE MMAX POSITIONS ALONG THE RADIUS

```

C
  DO 120 M=1,MMAX
  R=(M-1)*DELR
  SIGMAZ(M)=-P0*RO/RHO/RHC
  W(M)=0.
  DO 130 N=1,NMAX
  U=N*PI*R
  V=N*PI*RHC
  TT=THETA(N)/RHO
  IF(TT-40.)123,123,124
123  S=1./SINH(TT)
     TS=TT/SINH(TT)
     TSS=TT/SINH(TT)**2
     GO TO 125
124  S=0.
     TS=0.
     TSS=0.
125  SIGMAZ(M)=SIGMAZ(M)
     2  +SIG(N)*JO(TT*R)*(BRAR(N)*(S+TS/TANH(TT))-CRAR(N)*(1./TANH(TT)
     3  +TSS))
  W(M)=W(M)+2.*(1.-NU*NU)*CRAR(N)*SIG(N)*(JO(TT*R)-1.)/TT
130  CONTINUE
120  CONTINUE
  RETURN
  END
  
```

NOHL0073  
 NOHL0074  
 NOHL0075  
 NOHL0076  
 NOHL0077  
 NOHL0078  
 NOHL0079  
 NOHL0080  
 NOHL0081  
 NOHL0082  
 NOHL0083  
 NOHL0084  
 NOHL0085  
 NOHL0086  
 NOHL0087  
 NOHL0088  
 NOHL0089  
 NOHL0090  
 NOHL0091  
 NOHL0092  
 NOHL0093  
 NOHL0094  
 NOHL0095  
 NOHL0096  
 NOHL0097  
 NOHL0098  
 NOHL0099

6.4.2 Disk with Hole

The only modification to the previous program is that the radius of the center hole,  $\bar{c}$ , must be entered as data. This is done in card #1 at the beginning so that this card reads,

CARD 1  $\bar{c}$ ,  $\bar{r}_0$ ,  $\bar{a}$ ,  $v$ ,  $N$  (4F10.3,I10)

All other cards and instructions remain the same.

C		MAIN0001
C	MAIN PROGRAM	MAIN0002
C		MAIN0003
C	THIS PROGRAM CALCULATES THE INTERFACIAL PRESSURE DISTRIBUTION AND	MAIN0004
C	DEFLECTION OF TWO ROUGH PLATES (WITH HOLE) IN CONTACT. IT USES THE	MAIN0005
C	BESSEL FUNCTION PACKAGE AND SUBROUTINES--	MAIN0006
C	STRHOL	MAIN0007
C	CRSPRD	MAIN0008
C	QUADCO	MAIN0009
C	OUTPUT	MAIN0010
C	THE FOLLOWING ARE VARIABLES--	MAIN0011
C	YO        SEPARATION OF PLATES	MAIN0012
C	S         ROUGHNESS	MAIN0013
C	H         HARDNESS	MAIN0014
C	SIGMAZ    LOAD AT Z=0	MAIN0015
C	W         DEFLECTION AT Z=0	MAIN0016
C	LAMBDA    HOLE RADIUS	MAIN0017
C	R0        LOAD RADIUS (AT Z=1)	MAIN0018
C	RHO       DISK RADIUS	MAIN0019
C	NU        POISSON'S RATIO	MAIN0020
C	NMAX      NUMBER OF TERMS IN INFINITE SERIES	MAIN0021
C	SIG(N)    TRUNCATION TERM FOR FOURIER SERIES	MAIN0022
C	IN        NUMBER OF INTERVALS ALONG RADIUS USED IN CALCULATION	MAIN0023
C	MMAX      NUMBER OF POINTS USED (=IN+1)	MAIN0024
C	DELR      SIZE OF INTERVAL	MAIN0025
C	ITER      NO. OF TIMES SUBROUTINE HAS BEEN CALLED	MAIN0026
C		MAIN0027
	COMMON SIGMAZ(201),W(201),SDATA(9)	MAIN0028
	COMMON/AAA/A(40),C(40),PSI(40),PTOP(40),PBOT(40),E1(40),E2(40),	MAIN0029
	1 E3(40),SIG(40)	MAIN0030
	COMMON/BBB/F(201),P1(201)	MAIN0031
	REAL NU, LAMBDA	MAIN0032
	PI=3.14159265	MAIN0033
	IN=100	MAIN0034
C		MAIN0035
C	READ IN DISK DATA (ONCE PER RUN)	MAIN0036

```

C
10 READ(5,10) LAMBDA,RO,RHO,NU,NMAX
20 FORMAT(4F10.3,I10)
SDATA(1)=IN
SDATA(3)=LAMBDA
SDATA(4)=RHO
SDATA(5)=RC
SDATA(6)=NU
SDATA(7)=NMAX
MMAX=IN+1
DELR=(RHO-LAMBDA)/IN
SDATA(2)=DELR
X=RHO/LAMBDA

C
C CALCULATE EIGENVALUES
C
C CALL CRSPRD(NMAX,X,PSI)
C
C CALCULATE TRUNCATION TERMS
C
C DO 30 J=1,NMAX
C R=(PSI(J)-.75*PI)/(PSI(NMAX)-.75*PI)*PI
C SIG(J)=SIN(R)/R
30 CONTINUE
ITER=0

C
C READ IN ROUGHNESS DATA. MORE THAN ONE CASE MAY BE ENTERED.
C PROGRAM STOPS WHEN SUBMITTED "S" IS ZERO. PPO IS AN ESTIMATE OF
C THE VALUE OF P(0) AND WT IS A WEIGHTING FACTOR.
C
45 READ(5,40) S,H,PPO,WT
40 FORMAT(4F10.3)
IF(S.LT..001) GO TO 998

C
C ESTIMATE YG
C

```

```

MAIN0037
MAIN0038
MAIN0039
MAIN0040
MAIN0041
MAIN0042
MAIN0043
MAIN0044
MAIN0045
MAIN0046
MAIN0047
MAIN0048
MAIN0049
MAIN0050
MAIN0051
MAIN0052
MAIN0053
MAIN0054
MAIN0055
MAIN0056
MAIN0057
MAIN0058
MAIN0059
MAIN0060
MAIN0061
MAIN0062
MAIN0063
MAIN0064
MAIN0065
MAIN0066
MAIN0067
MAIN0068
MAIN0069
MAIN0070
MAIN0071
MAIN0072

```

```

        YO=2.*S
        DO 50 J=1,MMAX
        R=LAMBDA+(J-1)*DELR
C
C   FIRST ESTIMATE OF THE PRESSURE DISTRIBUTION
C
        SIGMAZ(J)=-PPO*EXP(-(R*R-LAMBDA**2)+PPO/(RO*RO-LAMBDA**2))
        W(J)=0.
50      CONTINUE
        II=0
100     CONTINUE
C
C   PERFORM THE FOLLOWING UP TO 10 TIMES
C
        II=II+1
        IF(II.GT.10) GO TO 45
C
C   CALCULATE THE DEFLECTION GIVEN THE STRESS
C
        CALL STRHOL(ITER)
        ITER=ITER+1
        I=0
110     CONTINUE
        I=I+1
        IF(I.GT.20) GO TO 130
C
C   FROM DEFORMATION OF ASPERITIES CALCULATE STRESS DISTRIBUTION.
C   ITERATE UNTIL LOAD BALANCES.
C
        FORCE=0.
        DO 120 J=1,MMAX
        R=LAMBDA+(J-1)*DELR
        IF(J.GT.1.OR.J.LT.MMAX) GO TO 112
        DA=2.*PI*R*DELR/2.
        GO TO 114
112     DA=2.*PI*R*DELR

```

```

MAIN0073
MAIN0074
MAIN0075
MAIN0076
MAIN0077
MAIN0078
MAIN0079
MAIN0080
MAIN0081
MAIN0082
MAIN0083
MAIN0084
MAIN0085
MAIN0086
MAIN0087
MAIN0088
MAIN0089
MAIN0090
MAIN0091
MAIN0092
MAIN0093
MAIN0094
MAIN0095
MAIN0096
MAIN0097
MAIN0098
MAIN0099
MAIN0100
MAIN0101
MAIN0102
MAIN0103
MAIN0104
MAIN0105
MAIN0106
MAIN0107
MAIN0108

```

```

114 YY=(Y0+2.*W(J))/S/1.414214
    IF(YY.GT.13.) GO TO 140
    P1(J)=H/2.*ERFC(YY)
    GO TO 145
140 P1(J)=0.
C
C SUM TO GET TOTAL LOAD
C
145 F(J)=FORCE+P1(J)*DA/(RO**2-LAMBDA**2)/PI
    FORCE=F(J)
120 CONTINUE
C
C IF LOAD IS OFF BY 5 PERCENT REPEAT
C
    IF(ABS(1.-FORCE).LT..05) GO TO 130
    Y0=Y0+S/2.*ALOG(FORCE)
    GO TO 110
130 CONTINUE
C
C PRINT OUPUT FOR THIS ITERATION
C
    CALL OUTPUT(Y0,II,S,H)
C
C ITERATE AROUND AGAIN UNLESS PRESSURES AGREE TO 2 PERCENT
C
    CHK=ABS((-SIGMAZ(1)-P1(1))/P1(1))
    IF(CHK.LT..02) GO TO 45
    DO 160 J=1,MMAX
C
C NEW ESTIMATE OF STRESS DISTRIBUTION IS WEIGHTED COMBINATION OF
C ELASTIC AND PLASTIC DISTRIBUTIONS
C
    SIGMAZ(J)=WT*SIGMAZ(J)-(1.-WT)*P1(J)
160 CONTINUE
    GO TO 100
998 CALL EXIT

```

```

MAIN0109
MAIN0110
MAIN0111
MAIN0112
MAIN0113
MAIN0114
MAIN0115
MAIN0116
MAIN0117
MAIN0118
MAIN0119
MAIN0120
MAIN0121
MAIN0122
MAIN0123
MAIN0124
MAIN0125
MAIN0126
MAIN0127
MAIN0128
MAIN0129
MAIN0130
MAIN0131
MAIN0132
MAIN0133
MAIN0134
MAIN0135
MAIN0136
MAIN0137
MAIN0138
MAIN0139
MAIN0140
MAIN0141
MAIN0142
MAIN0143
MAIN0144

```

END

MAIN0145

```

C
C STRHOL
C
C THIS SUBROUTINE CALCULATES THE DEFLECTION AT Z=0 (BOTTOM) OF A DISK
C WITH A HOLE WHICH HAS A LOAD AT Z=1 (TOP) WHICH IS UNIFORM BETWEEN
C LAMBDA AND RO AND ZERO ELSEWHERE--AND A LOAD AT Z=0 WHICH IS AN
C INPUT VARIABLE. VARIABLES ARE --
C SIGMAZ LOAD AT Z=0
C W DEFLECTION AT Z=0
C LAMBDA HOLE RADIUS
C RO LOAD RADIUS (AT Z=1)
C RHO DISK RADIUS
C NU POISSON'S RATIO
C NMAX NUMBER OF TERMS IN INFINITE SERIES
C SIG(N) TRUNCATION TERM FOR FOURIER SERIES
C IN NUMBER OF INTERVALS ALONG RADIUS USED IN CALCULATION
C MMAX NUMBER OF POINTS USED (=IN+1)
C DELR SIZE OF INTERVAL
C ITER NO. OF TIMES SUBROUTINE HAS BEEN CALLED

```

```

SUBROUTINE STRHOL(ITER)
COMMON SIGMAZ(201),W(201),SDATA(9)
COMMON/AAA/A(40),C(40),PSI(40),PTOP(40),PBOT(40),E1(40),E2(40),
1 E3(40),SIG(40)
REAL NU, LAMBDA
PI=3.14159265
IN=INT(SDATA(1)+.001)
DELR=SDATA(2)
LAMBDA=SDATA(3)
RHO=SDATA(4)
RO=SDATA(5)
NU=SDATA(6)
MMAX=IN+1
NMAX=INT(SDATA(7)+.0001)
IF(ITER) 20,20,60
20 CONTINUE

```

```

HOLE0001
HOLE0002
HOLE0003
HOLE0004
HOLE0005
HOLE0006
HOLE0007
HOLE0008
HOLE0009
HOLE0010
HOLE0011
HOLE0012
HOLE0013
HOLE0014
HOLE0015
HOLE0016
HOLE0017
HOLE0018
HOLE0019
HOLE0020
HOLE0021
HOLE0022
HOLE0023
HOLE0024
HOLE0025
HOLE0026
HOLE0027
HOLE0028
HOLE0029
HOLE0030
HOLE0031
HOLE0032
HOLE0033
HOLE0034
HOLE0035
HOLE0036

```

```

DO 50 N=1,NMAX
PTOP(N)=-2.*R0*C1(PSI(N),R0/LAMBDA)/PSI(N)*LAMBDA/(RHO**2*CO(PSI
1 (N),RHO/LAMBDA)**2-LAMBDA**2*CO(PSI(N),1.))**2)
X=PSI(N)/LAMBDA
IF(X-40.)30,30,40
30 E1(N)=1./TANH(X)+X/SINH(X)**2
E2(N)=(1.+X/TANH(X))/SINH(X)
E3(N)=1.-X*X/SINH(X)**2
GO TO 50
40 E1(N)=1.
E2(N)=0.
E3(N)=1.
50 CONTINUE
60 DO 70 J=1,NMAX
CALL QUADCO(SIGMAZ,LAMBDA,RHO,IN,PSI(J),VALUE)
PBOT(J)= 2.*VALUE/(RHO**2*CO(PSI(J),RHO/LAMBDA)**2-LAMBDA**2*
1 CO(PSI(J),1.))**2)
A(J)=(PTOP(J)*E1(J)-PBOT(J)*E2(J))/E3(J)
C(J)=(PTOP(J)*E2(J)-PBOT(J)*E1(J))/E3(J)
70 CONTINUE
DO 80 M=1,MMAX
R=LAMBDA+(M-1)*DELR
SIGMAZ(M)=- (R0**2-LAMBDA**2)/(RHO**2-LAMBDA**2)
W(M)=0.
DO 80 N=1,NMAX
SIGMAZ(M)=SIGMAZ(M)+SIG(N)*CO(PSI(N),R/LAMBDA)*
1 (A(N)*E2(N)-C(N)*E1(N))
W(M)=W(M)+2.*(1.-NU*NU)*SIG(N)*C(N)*
1 (CO(PSI(N),R/LAMBDA)-CO(PSI(N),1.))/PSI(N)*LAMBDA
80 CONTINUE
RETURN
END

```

```

HOLE0037
HOLE0038
HOLE0039
HOLE0040
HOLE0041
HOLE0042
HOLE0043
HOLE0044
HOLE0045
HOLE0046
HOLE0047
HOLE0048
HOLE0049
HOLE0050
HOLE0051
HOLE0052
HOLE0053
HOLE0054
HOLE0055
HOLE0056
HOLE0057
HOLE0058
HOLE0059
HOLE0060
HOLE0061
HOLE0062
HOLE0063
HOLE0064
HOLE0065
HOLE0066
HOLE0067
HOLE0068

```

### 6.4.3 Auxiliary Programs

Each of the previous sections listed the main calling program and the subroutine which would calculate the stress for the particular disk. This section gives the listings for the miscellaneous programs needed for integrating, calculating zeroes of Bessel Functions, calculating values of Bessel Functions, giving output, etc. These programs are self-explanatory. The beginning of each main program lists the subroutines needed for that program.

C		OPUT0001
C	OUTPUT	OPUT0002
C		OPUT0003
C	THIS SUBROUTINE PRINTS THE RESULTING OUTPUT	OPUT0004
C	VARIABLES USED ARE--	OPUT0005
C	YO SEPARATION OF PLATES	OPUT0006
C	S ROUGHNESS	OPUT0007
C	H HARDNESS	OPUT0008
C	SIGMAZ LOAD AT Z=0	OPUT0009
C	W DEFLECTION AT Z=0	OPUT0010
C	LAMBDA HOLE RADIUS	OPUT0011
C	RO LOAD RADIUS (AT Z=1)	OPUT0012
C	RHO DISK RADIUS	OPUT0013
C	NU POISSON'S RATIO	OPUT0014
C	NMAX NUMBER OF TERMS IN INFINITE SERIES	OPUT0015
C	SIG(N) TRUNCATION TERM FOR FOURIER SERIES	OPUT0016
C	IN NUMBER OF INTERVALS ALONG RADIUS USED IN CALCULATION	OPUT0017
C	MMAX NUMBER OF POINTS USED (=IN+1)	OPUT0018
C	DELR SIZE OF INTERVAL	OPUT0019
C		OPUT0020
	SUBROUTINE OUTPUT(YO,II,S,H)	OPUT0021
	COMMON/BBB/F(201),P1(201)	OPUT0022
	COMMON SIGMAZ(201),W(201),SDATA(9)	OPUT0023
	REAL NU,LAMBDA	OPUT0024
	IN=INT(SDATA(1)+.001)	OPUT0025
	DELR=SDATA(2)	OPUT0026
	LAMBDA=SDATA(3)	OPUT0027
	RHO=SDATA(4)	OPUT0028
	RO=SDATA(5)	OPUT0029
	NU=SDATA(6)	OPUT0030
	NMAX=INT(SDATA(7)+.0001)	OPUT0031
	MMAX=IN+1	OPUT0032
	WRITE(6,10)II	OPUT0033
10	FORMAT(1H1,' A1 ITERATION NUMBER',I3)	OPUT0034
	WRITE(6,20) YO,S,H	OPUT0035
20	FORMAT(' YO IS',F10.6,' S IS',F7.3,' H IS',F8.3)	OPUT0036

```

30  WRITE(6,30)LAMBDA,RO,RHO,NU,NMAX
    FORMAT(' AND LAMBDA IS',F6.3,' RO IS',F6.3,' RHO IS',
1F6.3,' NU IS',F6.3,' NMAX IS', I6)
    WRITE(6,40)
40  FORMAT(1H)
    WRITE(6,50)
50  FORMAT(' STRESS PRES
    ISURE CUMULATIVE')
    WRITE(6,60)
60  FORMAT(' RADIUS ELASTIC DEFLECTION PLAS
    ITIC LOAD')
    WRITE(6,70)
70  FORMAT(1H )
    DO 80 J=1,MMAX,2
    R=LAMBDA+(J-1)*DELR
    WRITE(6,90)R,SIGMAZ(J),W(J),P1(J),F(J),J
90  FORMAT(F15.3,3F15.6,F15.3,I10)
80  CONTINUE
    RETURN
    END

```

```

OPUT0037
OPUT0038
OPUT0039
OPUT0040
OPUT0041
OPUT0042
OPUT0043
OPUT0044
OPUT0045
OPUT0046
OPUT0047
OPUT0048
OPUT0049
OPUT0050
OPUT0051
OPUT0052
OPUT0053
OPUT0054
OPUT0055
OPUT0056

```

C  
C  
C  
C  
C  
C  
C  
C  
C  
C

QUADJO

THIS SUBROUTINE SOLVES THE FOLLOWING INTEGRAL USING "N" INTERVALS --

$$\text{VALUE} = \int_{C.}^{! .} x * F(x) * JO(\text{THETAJ} * x) * dx$$

SUBROUTINE QUADJO(N, THETAJ, F, VALUE)

DIMENSION F(201)

REAL JO

H=1./N

VALUE=H/3.\*F(N+1)\*JO(THETAJ)

DO 5 K=2, N

VALUE=VALUE+H/3.\*(2.+(1+(-1)\*\*K))\*F(K)\*JO(THETAJ/N\*(K-1))

5 \*(K-1)/N

CONTINUE

RETURN

END

QDJ00001  
QDJ00002  
QDJ00003  
QDJ00004  
QDJ00005  
QDJ00006  
QDJ00007  
QDJ00008  
QDJ00009  
QDJ00010  
QDJ00011  
QDJ00012  
QDJ00013  
QDJ00014  
QDJ00015  
QDJ00016  
QDJ00017  
QDJ00018  
QDJ00019  
QDJ00020  
QDJ00021  
QDJ00022

C  
C  
C  
C  
C  
C  
C  
C  
C  
C  
C  
C

QUADCO

THIS SUBROUTINE CALCULATES THE FOLLOWING INTEGRAL USING SIMPSON'S  
RULE WITH "N" INTERVALS--

$$\text{VALUE} = \int_A^B x * F(x) * CO(\text{PSI}, x/A) * dx$$

```
SUBROUTINE QUADCO(F,A,B,N,PSI,VALUE)
DIMENSION F(201)
H=(B-A)/N
VALUE=H/3.*(F(1)*A*CO(PSI,1.)+F(N+1)*B*CO(PSI,B/A))
DO 5 K=2,N
X=A+(K-1)*H
VALUE=VALUE+H/3.*(3.+(-1)**K)*F(K)*X*CO(PSI,X/A)
5 CONTINUE
RETURN
END
```

QDC00001  
QDC00002  
QDC00003  
QDC00004  
QDC00005  
QDC00006  
QDC00007  
QDC00008  
QDC00009  
QDC00010  
QDC00011  
QDC00012  
QDC00013  
QDC00014  
QDC00015  
QDC00016  
QDC00017  
QDC00018  
QDC00019  
QDC00020  
QDC00021  
QDC00022

C  
 C BESSEL FUNCTION PACKAGE  
 C  
 C THIS FUNCTION PACKAGE CALCULATES THE BESSEL FUNCTIONS OF A REAL  
 C ARGUMENT "X" USING EQUATIONS GIVEN IN "HANDBOOK OF MATHEMATICAL  
 C FUNCTIONS", ED. ABRAMOWITZ AND STEGUN, CHAPTER 9. REFERENCES  
 C GIVE EQUATIONS USED. NOMENCLATURE-- JO(X) IS BESSEL FUNCTION OF  
 C FIRST KIND OF ORDER 0 - Y1(X) IS BESSEL FUNCTION OF SECOND KIND OF  
 C ORDER 1 - ETC. AIO(X) IS EXP(-X)\*I0(X) AND BKO(X) IS EXP(X)\*K0(X).

BESL0001  
 BESL0002  
 BESL0003  
 BESL0004  
 BESL0005  
 BESL0006  
 BESL0007  
 BESL0008  
 BESL0009  
 BESL0010  
 BESL0011  
 BESL0012  
 BESL0013  
 BESL0014  
 BESL0015  
 BESL0016  
 BESL0017  
 BESL0018  
 BESL0019  
 BESL0020  
 BESL0021  
 BESL0022  
 BESL0023  
 BESL0024  
 BESL0025  
 BESL0026  
 BESL0027  
 BESL0028  
 BESL0029  
 BESL0030  
 BESL0031  
 BESL0032  
 BESL0033  
 BESL0034  
 BESL0035  
 BESL0036

C  
 C JO(X) EQUATIONS 9.4.1 - 9.4.3

C  
 C FUNCTION JO(X)  
 C REAL JO  
 C IF(X-3)110,120,120  
 110 JO=1.-2.2499997\*(X/3)\*\*2+1.2656208\*(X/3)\*\*4-.3163866\*(X/3)\*\*6+  
 1 .0444479\*(X/3)\*\*8-.0039444\*(X/3)\*\*10+.0002100\*(X/3)\*\*12  
 C RETURN  
 120 JO=1./SQRT(X)\*(.79788456-.00000077\*(3/X)-.00552740\*(3/X)\*\*2  
 1 -.00009512\*(3/X)\*\*3+.00137237\*(3/X)\*\*4-.00072805\*(3/X)\*\*5  
 2 +.00014476\*(3/X)\*\*6)\*COS(X-.7853982 -.0416640 \*(3/X)-.0000395  
 3 \*(3/X)\*\*2+.0026257 \*(3/X)\*\*3-.0005413 \*(3/X)\*\*4-.0002933 \*(3/X)  
 4 \*\*5+.0001356 \*(3/X)\*\*6)  
 C RETURN  
 C END

C  
 C J1(X) EQUATIONS 9.4.4 - 9.4.6

C  
 C FUNCTION J1(X)  
 C REAL J1  
 C IF(X-3)130,140,140  
 130 J1=X\*(.5-.56249985\*(X/3)\*\*2+.21093573\*(X/3)\*\*4-.03954289\*(X/3)\*\*6  
 1 +.00443319\*(X/3)\*\*8-.00031761\*(X/3)\*\*10+.00001109\*(X/3)\*\*12)  
 C RETURN  
 140 J1=1./SQRT(X)\*(.79788456+.00000156\*(3/X)+.01659667\*(3/X)\*\*2  
 1 +.00017105\*(3/X)\*\*3-.00249511\*(3/X)\*\*4+.00113653\*(3/X)\*\*5

```

2  -.00020033*(3/X)**6)*COS(X-2.356194  +.1249961 *(3/X)
3  +.0000565 *(3/X)**2-.0063788 *(3/X)**3+.0007435 *(3/X)**4
4  +.0007982 *(3/X)**5-.0002917 *(3/X)**6)
RETURN
END

```

```

BESL0037
BESL0038
BESL0039
BESL0040
BESL0041
BESL0042
BESL0043
BESL0044
BESL0045
BESL0046
BESL0047
BESL0048
BESL0049
BESL0050
BESL0051
BESL0052
BESL0053
BESL0054
BESL0055
BESL0056
BESL0057
BESL0058
BESL0059
BESL0060
BESL0061
BESL0062
BESL0063
BESL0064
BESL0065
BESL0066
BESL0067
BESL0068
BESL0069
BESL0070
BESL0071
BESL0072

```

```

C
C AIO(X) EQUATIONS 9.8.1 - 9.8.2
C

```

```

FUNCTION AIO(X)
IF(X-3.75)150,160,160
150 Y=X/3.75
AIO=EXP(-X)*(1.+3.5156229*Y**2+3.0899424*Y**4+1.2067492*Y**6
1 +.2659732*Y**8+.0360768*Y**10+.0045813*Y**12)
RETURN
160 Y=3.75/X
AIO=1./SQRT(X)*(.39894228+.01328592*Y+.00225319*Y**2
1 -.00157565*Y**3+.00916281*Y**4-.0205770*Y**5+.02635537*Y**6
2 -.01647633*Y**7+.00392377*Y**8)
RETURN
END

```

```

C
C AII(X) EQUATIONS 9.8.3 - 9.8.4
C

```

```

FUNCTION AII(X)
IF(X-3.75)170,180,180
170 Y=X/3.75
AII=EXP(-X)*X*(.5+.8789059*Y**2+.51498869*Y**4+.15084934*Y**6
1 +.02658733*Y**8+.00301532*Y**10+.00032411*Y**12)
RETURN
180 Y=3.75/X
AII=1./SQRT(X)*(.39894228-.03988024*Y-.0036201*Y**2
1 +.00163801*Y**3-.01031555*Y**4+.02282967*Y**5-.02895312*Y**6
2 +.0178765*Y**7-.00420059*Y**8)
RETURN
END

```

C Y0(X) EQUATIONS 9.4.2 - 9.4.3

C

FUNCTION Y0(X)

REAL J0

IF(X-3)110,120,120

110 Y0=2./3.141593\*ALOG(X/2.)\*J0(X)+.3674669 +

1 .6055937\*(X/3.)\*\*2-.7435038\*(X/3.)\*\*4+.2530012\*(X/3.)\*\*6-

2 .0426121\*(X/3.)\*\*8+.0042792\*(X/3.)\*\*10-.0002485\*(X/3.)\*\*12

RETURN

120 Y0=1./SQRT(X)\*(.79788456-.00000077\*(3/X)-.00552740\*(3/X)\*\*2

1 -.00009512\*(3/X)\*\*3+.00137237\*(3/X)\*\*4-.00072805\*(3/X)\*\*5

2 +.00014476\*(3/X)\*\*6)\*SIN(X-.7853982 -.0416640 \*(3/X)-.0000395

3 \*(3/X)\*\*2+.0026257 \*(3/X)\*\*3-.0005413 \*(3/X)\*\*4-.0002933 \*(3/X)

4 \*\*5+.0001356 \*(3/X)\*\*6)

RETURN

END

C

C Y1(X) EQUATIONS 9.4.5 - 9.4.6

C

FUNCTION Y1(X)

REAL J1

IF(X-3)110,120,120

110 XY1=2./3.141593\*X\*ALOG(X/2.)\*J1(X)-.6366198+

1 .2212091\*(X/3.)\*\*2+2.168271\*(X/3.)\*\*4-1.316483\*(X/3.)\*\*6+

1 .3123951\*(X/3.)\*\*8-.0400976\*(X/3.)\*\*10+.0027873\*(X/3.)\*\*12

Y1=XY1/X

RETURN

120 Y1=1./SQRT(X)\*(.79788456+.00000156\*(3/X)+.01659667\*(3/X)\*\*2

1 +.00017105\*(3/X)\*\*3-.00249511\*(3/X)\*\*4+.00113653\*(3/X)\*\*5

2 -.00020033\*(3/X)\*\*6)\*SIN(X-2.356194 +.1249961 \*(3/X)

3 +.0000565 \*(3/X)\*\*2-.0063788 \*(3/X)\*\*3+.0007435 \*(3/X)\*\*4

4 +.0007982 \*(3/X)\*\*5-.0002917 \*(3/X)\*\*6)

RETURN

END

C

C BK0(X) EQUATIONS 9.8.5 - 9.8.6

BESL0073

BESL0074

BESL0075

BESL0076

BESL0077

BESL0078

BESL0079

BESL0080

BESL0081

BESL0082

BESL0083

BESL0084

BESL0085

BESL0086

BESL0087

BESL0088

BESL0089

BESL0090

BESL0091

BESL0092

BESL0093

BESL0094

BESL0095

BESL0096

BESL0097

BESL0098

BESL0099

BESL0100

BESL0101

BESL0102

BESL0103

BESL0104

BESL0105

BESL0106

BESL0107

BESL0108

```

C
FUNCTION BK0(X)
IF(X-2)110,120,120
110 BK0=-ALOG(X/2.)*EXP(2.*X)*A10(X)+EXP(X)*(-.5772157+
1 .4227842*(X/2.)**2+.2306976*(X/2.)**4+.0348859*(X/2.)**6+
2 .0026270*(X/2.)**8+.0001075*(X/2.)**10+.0000074*(X/2.)**12)
RETURN
120 BK0=1./SQRT(X)*( 1.2533141-.0783236*(2./X)**1+.0218957*(2./X)**2-
1 .0106245*(2./X)**3+.0058787*(2./X)**4-.0025154*(2./X)**5+
2 .0005321*(2./X)**6)
RETURN
END

C
C BK1(X) EQUATIONS 9.8.7 - 9.8.8
C
FUNCTION BK1(X)
IF(X-2)110,120,120
110 BK1=ALOG(X/2.)*EXP(2.*X)*A11(X)+EXP(X)/X*(1.+
1 .1544314*(X/2.)**2-.6727858*(X/2.)**4-.1815690*(X/2.)**6-
2 .0191940*(X/2.)**8-.0011040*(X/2.)**10-.0000469*(X/2.)**12)
RETURN
120 BK1=1./SQRT(X)*(1.253314+.2349862*(2./X)-
1 .0365562*(2./X)**2+.0150427*(2./X)**3-.0078035*(2./X)**4+
2 .0032561*(2./X)**5-.0006825*(2./X)**6)
RETURN
END

C
C CO(P,R) (P IS EIGENVALUE)
C
FUNCTION CO(P,R)
REAL JO,J1
CO=Y0(P*R)*J1(P)-Y1(P)*JO(P*R)
RETURN
END

C
C C1(P,R) (P IS EIGENVALUE)

```

```

BESL0109
BESL0110
BESL0111
BESL0112
BESL0113
BESL0114
BESL0115
BESL0116
BESL0117
BESL0118
BESL0119
BESL0120
BESL0121
BESL0122
BESL0123
BESL0124
BESL0125
BESL0126
BESL0127
BESL0128
BESL0129
BESL0130
BESL0131
BESL0132
BESL0133
BESL0134
BESL0135
BESL0136
BESL0137
BESL0138
BESL0139
BESL0140
BESL0141
BESL0142
BESL0143
BESL0144

```

C

```
FUNCTION C1(P,R)
REAL J1
C1=Y1(P*R)*J1(P)-Y1(P)*J1(P*R)
RETURN
END
```

```
BESL0145
BESL0146
BESL0147
BESL0148
BESL0149
BESL0150
```

```

C
C CRSPRD
C
C THIS SUBROUTINE CALCULATES THE EIGENVALUES, PSI, FOR--
C   C1(PHI,1.)=0 AND C1(PHI,RHO/LAMBDA)=0
C   LAMBDA HOLE RADIUS
C   RHO DISK RADIUS
C SEE "HANDBOOK OF MATHEMATICAL FUNCTIONS", ED. ABRAMOWITZ AND STEGUN,
C SECTION 9.5, EQUATIONS 9.5.27, 9.5.28, AND 9.5.29
C

```

```

SUBROUTINE CRSPRD(N,L,ZERO)
REAL L
INTEGER S
DIMENSION ZERO(40)
U=4.
P=(U-1.)/8./L
Q=(U-1.)*(U-25.)*(L**3-1.)/6./4.**3/L**3/(L-1.)
R=(U-1.)*(U*U-114.*U+1073.)*(L**5-1.)/5./4.**5/L**5/(L-1.)
DO 10 S=1,N
B=S*3.141593/(L-1.)
ZERO(S)=B+P/B+(Q-P*P)/B**3+(R-4.*P*Q+2.*P**3)/B**5
10 CONTINUE

```

```

C
C FOR GREATER ACCURACY USE TABULATED VALUES FOR FIRST 5 EIGENVALUES
C (HERE FOR RHO/LAMBDA=10.) SEE A + S, TABLE 9.7, PAGE 415
C

```

```

ZERO(1)=.39409
ZERO(2)=.73306
ZERO(3)=1.07483
ZERO(4)=1.41886
ZERO(5)=1.76433
RETURN
END

```

```

CRSP0001
CRSP0002
CRSP0003
CRSP0004
CRSP0005
CRSP0006
CRSP0007
CRSP0008
CRSP0009
CRSP0010
CRSP0011
CRSP0012
CRSP0013
CRSP0014
CRSP0015
CRSP0016
CRSP0017
CRSP0018
CRSP0019
CRSP0020
CRSP0021
CRSP0022
CRSP0023
CRSP0024
CRSP0025
CRSP0026
CRSP0027
CRSP0028
CRSP0029
CRSP0030
CRSP0031
CRSP0032
CRSP0033

```

VITA

The author was [REDACTED]

[REDACTED] [REDACTED] [REDACTED] He received his preliminary education in the Upper Darby Township school system and entered Lehigh University in 1962. After graduating with honors in 1966 with a Bachelor of Science degree in Mechanical Engineering he joined Bell Telephone Laboratories.

He received his Master of Science degree in 1967 from the Massachusetts Institute of Technology under the sponsorship of Bell Laboratories. His Master's thesis was entitled: "Information Flow in Fluid Lines." In 1969 he returned to M.I.T. under Bell Laboratories' Doctoral Support Program and completed his study in 1971. He is currently in the BTL Data Communications Technology Laboratory in Holmdel, New Jersey.

While with Bell Laboratories he has worked on various material and thermal problems dealing with micro-electronics including the design of hybrid integrated circuits. He is married and the father of two children.